

**ENHANCEMENT OF THERMAL,
ELECTRICAL AND OPTICAL PROPERTIES OF
ZINC OXIDE FILLED POLYMER MATRIX NANO
COMPOSITES**

**A Thesis Submitted to
the Graduate School of Engineering and Sciences of
İzmir Institute of Technology
in Partial Fulfillment of the Requirements for the Degree of**

DOCTOR OF PHILOSOPHY

in Chemical Engineering

**by
Filiz ÖZMIHÇI ÖMÜRLÜ**

**July 2009
İZMİR**

dedicated to
my son; Başar ÖMÜRLÜ

ACKNOWLEDGEMENT

Sincere gratitude is expressed to my advisor, Dr. Devrim BALKÖSE, for providing the opportunity to research on composite and powder world, continued involvement added greatly to my educational experience and her support and guidance throughout my Ph..D. project.

Special thanks are also given to my comitee member of Dr. Salih OKUR, Dr. Funda TIHMINLIOĞLU, Dr. Sevgi ULUTAN and Dr. Günseli ÖZDEMİR for their prescious contribution. Additionally I would like to thank to allow for using their laboratory any time.

I would like to express my appreciation to Prof. Dr. Muhsin ÇİFTÇİOĞLU for his great help kind and also my thanks for his generosity for letting me use his graduate laboratories anytime. I would like to thank to Dr. Serdar ÖZÇELİK for giving permission to use Fluorescence spectrometer.

My absolute thank to Yelda AKDENİZ, Berna TOPUZ, Özlem DUVARCI and Deniz ŞİMŞEK for their grateful advices, help and sincere friendship. Without them, I'm sure my thesis would not have been completed in such an enjoyable or efficient manner. I would like to thank to Ahmet KURUL and Tülin BURHANOĞLU for their precious contributions through UV and polymer processing. I ought to thank to Burcu ALP for her understanding and help in thermal analysis.

I would like to express my gratitude to all members of my family, for their patient devotion, understanding, and support all throughout the study. My special thanks to my sister, Dr. Serpil ÖZMIHÇI, my dear husband Turgay ÖMÜRLÜ and my son Başar ÖMÜRLÜ.

ABSTRACT

ENHANCEMENT OF THERMAL, ELECTRICAL AND OPTICAL PROPERTIES OF ZINC OXIDE FILLED POLYMER MATRIX NANO COMPOSITES

The purpose of this study is to enhance the electrical, thermal and optical properties of polyethylene and polypropylene by the addition of zinc oxide (ZnO) filler. Embedding ZnO in a polymeric matrix could make an economic, weight saving, chemically resistive, optical, flexible and conductive materials which possesses the properties of zinc oxide.

Composites with higher electrical and thermal conductivity having luminescence properties were prepared using commercial and hydrothermally synthesized ZnO powders with different particle size and conductivity. Effect of ZnO loading and surface treatment on composite properties was investigated. Luminescence effects in green and blue regions were detected in all powders due to the defects on the structure of ZnO. The powders were found to be moderately conductive materials, as well.

Un-homogenously dispersed composites were prepared using rheomixer since especially nano powders tended to be agglomerated in the composite. On the other hand, different surface properties of powder and polymer caused adhesion and wetting problems. Microvoids were detected in the interphase, as well.

Composites can be used as an electrostatic dissipation and moderate electrical conductive applications in the field of electrical conductivity, as a heat sink in the field of thermal conductivity and as a solid state lamp due to luminescence properties. Stiffness of the composites was very high compared to neat polymer and can be properly used as an engineering material.

ÖZET

ÇİNKO OKSİT KATKILI POLİMER MATRİSLİ NANO KOMPOZİTLERİN TERMAL, ELEKTRİK, VE OPTİK ÖZELLİKLERİNİN GELİŞTİRİLMESİ

Bu çalışmada, farklı tane boyutuna sahip çinko oksit (ZnO) katkılı polietilen ve polipropilen kompozitlerde elektrik iletkenliği, termal iletkenlik ve optik özelliklerin geliştirilmesi amaçlanmıştır. Polimer matris içine ZnO tozu katılarak elde edilen kompozit malzemeler, ekonomik, hafif, dayanıklı, optik özellikleri gelişmiş, esnek ve iletken olabilir aynı zamanda ZnO özelliklerini de taşıyabilir.

Farklı parçacık boyutunda ve iletkenlikte, ticari ve hidrotermal yöntem ile sentezlenmiş ZnO tozlarından polimer kompozit hazırlanmıştır. Kompozitlerin yüksek elektrik ve termal iletkenlikle birlikte lüminesans özelliğine sahip olduğu gözlenmiştir. Ayrıca polimere ZnO oranları ve ZnO tozuna yapılan yüzey işlemlerinin kompozit üzerindeki etkisi incelenmiştir. Yeşil ve mavi bölgede lüminesans etkisi ZnO tozların yapısındaki hatalar nedeniyle gözlenmiştir. Bütün tozlar aynı zamanda orta düzeyde iletken malzeme olarak tanımlanmıştır.

İyi dağıtılamamış kompozitler, reomikser kullanılarak hazırlanmış, ancak özellikle nano boyuttaki tozlar topaklanma eğilimi göstermiştir. Aynı zamanda, polimerlerde yapışma ve ıslanma problemi iki farklı malzemenin yüzey özelliklerine dayandırılıp, ayrıca ara yüzeyde mikro boşlukların olduğu gözlenmiştir.

Hazırlanan kompozitler, elektrostatik yük boşaltımında, orta düzeyde iletken malzeme olarak elektrik iletkenliğinde, ayrıca ısı soğutucu ve lüminesant malzeme olarak kullanım alanı bulabilecektir. Kompozitlerin sertliği, katkısız polimere göre daha fazla olmuştur ve bu kompozitler mühendislik malzemesi olarak kullanılabilirler.

TABLE OF CONTENTS

LIST OF TABLES	x
LIST OF FIGURES	xii
CHAPTER 1. INTRODUCTION	1
CHAPTER 2. POLYMER COMPOSITE	4
2.1. Polymer Matrix	5
2.1.1 Polyethylene	6
2.1.2 Polypropylene	10
2.2. Filler	12
2.2.1. Zinc Oxide.....	12
2.2.1.1. Synthesis of Zinc Oxide	13
2.2.1.2. Growth.....	16
2.2.1.3. Properties of Zinc Oxide	20
2.2.1.4 Surface Modification of Zinc Oxide.....	22
CHAPTER 3. ELECTRICAL AND THERMAL CONDUCTIVITY.....	28
3.1. Electrical Conductivity	28
3.1.1. Static Electricity	30
3.1.2. Electrical Conductivity in Polymer Composites and Percolation Theory.....	31
3.1.3. Factors Affecting the Electrical Conductivity of the Composites	40
3.1.4. Electrical Conductivity Models.....	42
3.2. Thermal Conductivity and Thermal Conductivity in Polymer Composites.....	46
3.2.1. Thermal Conductivity Models	50

CHAPTER 4. OPTICAL PROPERTIES OF ZINC OXIDE AND POLYMER COMPOSITES	54
4.1 Optical Properties of Zinc Oxide	56
4.2 Optical Properties of Zinc Oxide-Polymer Composites	62
CHAPTER 5. MATERIALS and METHOD	67
5.1 ZnO Powder Preparation.....	67
5.1.1. Al-doped ZnO Powder Preparation.....	67
5.1.2. Specifications of Materials.....	68
5.1.3. Characterization of Synthesized ZnO Powders.....	69
5.2. Surface Modification of ZnO Powders	70
5.3. Preparation of Composites	71
5.3.1 Characterization of Composites	71
CHAPTER 6. RESULTS AND DISCUSSION.....	77
6.1. Characterization of ZnO Powders.....	77
6.1.1. Characterization of Prepared ZnO Powder	81
6.1.2. Characterization of Al-doped ZnO Powder	85
6.1.3. Surface Modification of ZnO	92
6.1.4. Electrical Properties of ZnO Powder	95
6.1.5. Optical Properties of ZnO Powders	98
6.2. Characterization of Polymer Composites	105
6.2.1. Structural and Morphological Characterization of Polymer Composite	105
6.2.2. Thermal Characterization of Polymer Composites	114
6.2.3. Morphological Characterization of Surface Modified Composites	121
6.2.4. Density of the Polymer Composites.....	122
6.3. Electrical Conductivity of Polymer Composites.....	126
6.4. Thermal Conductivity of Polymer Composites	136
6.5. Optical Properties of Polymer Composites.....	144
6.6. Mechanical Characterization of Polymer Composites.....	154

6.7. Properties of ZnO Powders and Composites	160
CHAPTER 7. CONCLUSION and RECOMMENDATION	164
REFERENCES	170
APPENDICES	182
APPENDIX A. FTIR SPECTRA OF PEG4000 AND AMPTES MODIFIED ZnO.....	182
APPENDIX B. I-V CURVES OF POWDERS	184
APPENDIX C. SEM MICROGRAPHS AND MAPS OF THE COMPOSITES.....	186
APPENDIX D. VOLUME RESISTIVITY OF THE COMPOSITES	191

LIST OF TABLES

<u>Table</u>	<u>Page</u>
Table 4.1. The luminescence effect of Zinc oxide from literature.....	61
Table 5.1. The general and technical specifications of Zinc Oxide Powders	69
Table 5.2. Specifications of Polypropylene and Polyethylene.....	69
Table 6.1. The absorption and emission spectrum results of zinc oxide powders	105
Table 6.2. % crystallinity of eZnO-PP/PE composites calculated from XRD...	112
Table 6.3. % crystallinity of sZnO-PP/PE composites calculated from XRD ...	113
Table 6.4. eZnO-PP composites thermal analysis results	117
Table 6.5. eZnO-PE composites thermal analysis results	117
Table 6.6. sZnO-PP composites thermal analysis results	118
Table 6.7. sZnO-PE composites thermal analysis results	119
Table 6.8. Density of eZnO-PE composites.....	123
Table 6.9. Density of sZnO-PE composites	124
Table 6.10. Density of nZnO-PE composites.....	124
Table 6.11. Density of synZnO-PE composites	125
Table 6.12. Density of AlZnO-PE composites.....	125
Table 6.13. Volume resistivity of modified composites	130
Table 6.14. Interparticle distance for the PE-ZnO composites	131
Table 6.15. Thermal conductivity (W/mK) values of the PE composites.....	138
Table 6.16. Thermal conductivity values of the PP composites	138
Table 6.17. Fluorescence Spectrum results of PE composites.....	153
Table 6.18. Fluorescence Spectrum results of PP composites	153
Table 6.19. eZnO-PE composites mechanical behavior	155
Table 6.20. 15 vol% Modified eZnO loaded PE composites mechanical behavior.....	155

Table 6.21.	eZnO-PP composites mechanical behavior.....	157
Table 6.22.	nZnO-PE composites mechanical behavior	157
Table 6.23.	15 vol% modified nZnO loaded PE composites mechanical behavior.....	158
Table 6.24.	Properties of ZnO Powders	161
Table 6.25.	15 vol% loaded-PE composites properties.....	162

LIST OF FIGURES

<u>Figure</u>	<u>Page</u>
Figure 2.1. Chemical structure of pure polyethylene.....	6
Figure 2.2. Wurtzite structure of ZnO	13
Figure 2.3. a) SEM Micrograph of ZHC sheets b) XRD pattern of the ZHC sheet from obtained from 1 M ZnCl ₂ solution (pH ≈ 6) by quick cooling from 220 °C.....	17
Figure 2.4. Bonding mechanism in thermoplastic polymers	25
Figure 2.5. Grafting of MPS onto the ZnO nanoparticles.....	26
Figure 3.1. Electrical conductivity values of different materials	30
Figure 3.2. Schematic sketch of the resistivity of a composite as a function of filler	32
Figure 3.3. SEM micrograph of ZnO	35
Figure 3.4. DC volume resistivity of nanocomposites measured at 10 kV/cm as a function of ZnO content	37
Figure 3.5. Conduction mechanism for composites a-Homogenous distribution of fillers b-Un-homogenous distribution of filler.....	39
Figure 3.6. Diagram of filler in the polymer matrix with different aspect Ratio A: high aspect ratio B: Low aspect ratio.....	40
Figure 3.7. One dimensional composite model	50
Figure 4.1. A continuum of photon energies exists from radio waves through to γ –rays	54
Figure 4.2. A photoluminescence spectrum of ZnO fibres calcined at 600 °C	59
Figure 4.3. Photoluminescence of ZnO rods with different dopants.	60
Figure 4.4. Optical absorption and photoluminescence spectra of non modified ZnO and poly(vinylpyrrolidone) capped ZnO nanoparticle	64

Figure 5.1.	Experimental set-up of zinc oxide synthesis	68
Figure 5.2.	Haake Polydrive Rheomixer R600/610	72
Figure 5.3.	Carver hot press	72
Figure 5.4.	Hot wire probe	73
Figure 5.5.	Volume resistivity measurement technique.	74
Figure 5.6.	High resistivity test data sheet taken from Keithley 6517-A a) Current-time b) Volume Resistivity-Number of Reading	75
Figure 6.1.	SEM micrographs of Zinc oxide powders a) eZnO powder b) sZnO powder c) nZnO powder.....	78
Figure 6.2.	Particle size distribution of eZnO powder	79
Figure 6.3.	XRD pattern of commercial zinc oxide powders	79
Figure 6.4.	FTIR spectra of commercial zinc oxides.....	80
Figure 6.5.	X-Ray diffraction pattern of synZnO	81
Figure 6.6.	SEM micrographs of the zinc oxide powder of different magnifications a) 25000X b) 65000X and c) 100000X	82
Figure 6.7.	FTIR spectrum of the ZnO powder	83
Figure 6.8.	TGA curve of synZnO dried at 50 °C.....	84
Figure 6.9.	DTA curve of synZnO dried at 50 °C.....	84
Figure 6.10.	Particle size distribution of zinc oxide powder dried at 200 °C	85
Figure 6.11.	XRD pattern of the Al-doped ZnO powder dried at room temperature	87
Figure 6.12.	SEM micrographs of Al-doped ZnO powder for different magnifications dried at room temperature a) 120000X b) 100000X.	87
Figure 6.13.	FTIR spectrum of Al doped ZnO powder	88
Figure 6.14.	Particle size distribution of AlZnO.....	89
Figure 6.15.	TGA curve AlZnO powder.....	89

Figure 6.16.	DTA curves of Al doped-zinc oxide dried at room temperature.....	90
Figure 6.17.	XRD pattern of Al doped annealed ZnO powder	91
Figure 6.18.	SEM micrographs of Al-doped annealed ZnO powder for different magnifications annealed at 900 °C a) 6500X b) 20000X c) 50000X d) BSE 20000X	92
Figure 6.19.	FTIR spectra of PEG 4000 modified nano ZnO.....	94
Figure 6.20.	FTIR spectra of AMPTES modified nano ZnO.....	94
Figure 6.21.	Sweeping voltage versus current values for synZnO	96
Figure 6.22.	Typical diode curve	96
Figure 6.23.	Sweeping voltage versus current values for annealed Al-doped ZnO.....	97
Figure 6.24.	Creation of free electrons b- formation of vacancies	97
Figure 6.25.	Reflection spectra of zinc oxide powders.....	99
Figure 6.26.	Absorption spectra of commercial powders	100
Figure 6.27.	Absorption spectra of prepared powders	101
Figure 6.28.	Fluorescence spectrum of eZnO	101
Figure 6.29.	Fluorescence spectrum of sZnO	102
Figure 6.30.	Fluorescence spectrum of nZnO.....	103
Figure 6.31.	Fluorescence spectrum of SynZnO.....	103
Figure 6.32.	Fluorescence spectrum of AlZnO.....	104
Figure 6.33.	sZnO –PE composite SEM micrographs a-5vol% sZnO-PE, b-10 vol% sZnO-PE, c-15vol% sZnO-PE, d-20vol% sZnO-PE	106
Figure 6.34.	sZnO –PE composite SEM micrographs a-5vol% sZnO-PE, b-10 vol% sZnO-PE, c-15vol% sZnO-PE, d-20vol% sZnO-PE	107
Figure 6.35.	SEM micrograph of composites a) 20 vol%eZnO-PE, b) 15 vol% nZnO PE, c)15 vol% synZnO-PE, d)15 vol%AlZnO-PE	108

Figure 6.36.	Map of elemental Zinc in EDX a- 20 vol% eZnO-PE b- 20 vol% 10 eZnO-PP c- 20 vol% sZnO-PE d- 20vol% sZnO-PP e- 15 vol% nZnO-PE f- 15 vol% nZnO-PP. Red colors indicate zinc, black color indicates polymer matrix.....	109
Figure 6.37.	XRD pattern of eZnO-PP composites	111
Figure 6.38.	XRD pattern of eZnO-PE composites	112
Figure 6.39.	TGA curve of eZnO-PP composites	114
Figure 6.40.	DSC curve of eZnO-PP composites	115
Figure 6.41.	Weight loss at 1000°C versus weight % of ZnO in composites	116
Figure 6.42.	Crystallinity values found from XRD and DSC for PP composites.	119
Figure 6.43.	Crystallinity values found from XRD and DSC for PE composites	120
Figure 6.44.	SEM micrograph of a-1%PEG4000 b-1% AMPTES c-2% PEG4000 d2% AMPTES modified, 20vol % sZnO-PE composites	122
Figure 6.45.	Volume resistivity values of PP composites.....	127
Figure 6.46.	Volume resistivity values of PE composites	128
Figure 6.47.	Effect of critical exponent (McLachlan model) on volume resistivity of nZnO-PE composites.	133
Figure 6.48.	Experimental resistivity values of eZnO-PE and McLachlan model	134
Figure 6.49.	Experimental resistivity values of sZnO-PE and McLachlan model .	134
Figure 6.50.	Experimental resistivity values of nZnO-PE and McLachlan model	135
Figure 6.51.	Experimental resistivity values of synZnO-PE and McLachlan model	135
Figure 6.52.	Thermal conductivity values of PP composites (“0” corresponds t to Pure PP)	136

Figure 6.53.	Thermal conductivity values of PE composites	137
Figure 6.54.	Comparison of the experimental and predicted thermal conductivity values for eZnO-PE composite from theoretical models	140
Figure 6.55.	Comparison of the experimental and predicted thermal conductivity values for sZnO-PE composite from theoretical models.....	140
Figure 6.56.	Comparison of the experimental and predicted thermal conductivity values for sZnO-PP composite from theoretical models.....	141
Figure 6.57.	Comparison of the experimental and predicted thermal conductivity values for nZnO-PE composite from theoretical models.....	142
Figure 6.58.	Comparison of the experimental and predicted thermal conductivity values for nZnO-PP composite from theoretical models.....	142
Figure 6.59.	Comparison of the experimental and predicted thermal conductivity values for synZnO-PE composite from theoretical models.....	143
Figure 6.60.	Comparison of the experimental and predicted thermal conductivity values for AlZnO-PE composite from theoretical models.....	144
Figure 6.61.	Fluorescence spectra of PE and PP matrix	145
Figure 6.62.	Fluorescence spectra of eZnO loaded PE composites.....	146
Figure 6.63.	Fluorescence spectra of eZnO loaded PP composites	147
Figure 6.64.	Fluorescence spectra of sZnO loaded PE composites	148
Figure 6.65.	Fluorescence spectra of sZnO loaded PP composites	148
Figure 6.66.	Fluorescence spectra of nZnO loaded PE composites.....	149
Figure 6.67.	Fluorescence spectra of nZnO loaded PP composites.....	150

Figure 6.68.	Fluorescence spectra of synZnO loaded PE composites	151
Figure 6.69.	Fluorescence spectra of AlZnO loaded PE composites.....	151
Figure 6.70.	Fluorescence spectra of modified sZnO loaded PE composites and unmodified composite.....	152
Figure 6.71.	Force-Stroke diagram for eZnO loaded PE	154
Figure 6.72.	Youngs modulus of eZnO and nZnO-PE composites	159
Figure 6.73.	Yield stress of eZnO and nZnO-PE composites.....	159
Figure 6.74.	Electrical resistivities of 15 vol% ZnO-PE composites prepared from unmodified and modified zinc oxide powders.....	163

CHAPTER 1

INTRODUCTION

Polymeric materials are generally insulating or nonconductive materials in nature and normally used in electric and electronic applications as insulators, but likely to accumulate the electrostatic discharge (Sethi and Goosey, 1995). The increasing demand for lighter, economic, chemically resistive, conductive materials created a need for new materials. Often composites are used to fill these needs. Composites are a mixture of two or more types of materials (polymer, metal, ceramic, etc.) that form a new material with properties that are a combination of the constituents.

Electrostatic discharge can lead damage of highly sensitive electronic components or cause materials to ignite or gases to explode. In the polymeric industry the static electricity problem is generally obtained; during production; extrusion or fibre spinning, in packaging industry; problems with the loading of bags with dry materials, transportation problems; powders through plastic tubes or by accumulation of dusts on plastic objects. In order to overcome these problems lowering the resistivity of the polymer was a practical solution. For avoiding static electricity adding antistatic agents is one of the method but the soap like molecules of antistatic agents diffuse to the surface of the material and only the surface resistivity drops. For lowering the electrical resistivity addition of conductive filler (metal or metals oxide) was proposed in the literature as an alternative. The application of conductive particles/nanoparticles to an insulating polymer matrix is expected to induce an electrical conductivity and at the same time for using in multifunctional applications enhance the thermal properties of the composites. (Grop and Minder, 1999; Gojny et al., 2006; Gubin, 2002)

Zinc Oxide (ZnO), is an important electronic and photonic material which possesses semiconducting and piezoelectric properties. Can used as a proper filling material to improve the electrical, thermal and optical properties of polymer matrix. ZnO has important characteristics. It is a semiconductor, with a direct bandgap of 3.37 eV and a large excitation binding energy (60 meV) and exhibits near-UV emission and

transparent conductivity. This band gap value is equivalent to ultraviolet (UV) light energy, which means that ZnO has ability to absorb UV light (Tsuiji, 2003). Nano sized ZnO has recently draw attention in the industries of material science, chemical, and electronic engineering (Bangal et al., 2005).

When an electrically conducting phase was dispersed in sufficient quantity in a polymeric resin, and if a conductive path is observed a conductive composite was formed. The properties of such a composite make them technologically superior or more cost effective than alternative materials (Struempler and Glatz-Reihenbach, 1999). Adding conductive fillers to polymer matrix materials could be envisaged with specific properties to proper applications. Possible applications for electrical conductive resins are electromagnetic interference, housing (conductive paints), coatings, adhesives, electronic devices and electrostatic dissipation (Clingerman, 2001; Weber, 2001).

There are contradictory reports on the electrical properties of ZnO-Polyethylene composites. On the other hand, while Hong et al. (2003) reported neat polyethylene electrical resistivity, as at the order of 10^{19} ohm-cm, Tjong and Liang (2006) reported as 10^{13} ohm-cm. Generally nanosized and micron sized ZnO addition on electrical were compared in these studies. The percolation threshold value for ZnO-polyethylene composites was found approximately at 30 vol% and addition of 40 vol% ZnO decreases the resistivity to 10^{11} ohm-cm (Hong et al., 2003). Tjong and Liang (2006) found the lowest electrical resistivity as at the order of 10^{13} ohm-cm after the addition of 60 vol% ZnO. Hong et al. (2006) found the lowest resistivity as 10^9 ohm-cm upon the addition of 30 vol%.

Thermal conductive property of composites was investigated since thermal conductivity increase could make the composites multifunctional. An effective way of increasing thermal conductivity of polymer composites is adding conductive fillers. The main application for thermally conductive polymers was heat sinks. Several conductive fibers such as carbon fibers, nickel-coated graphite fibers, copper fibers, brass fibers, stainless steel fibers, metal oxides etc. have been used to make thermally conductive composites (Clingerman, 1998; Krueger, 2002).

Transition metal oxides like ZnO are highly photoactive materials. The high exciton binding energy of ZnO allows efficient excitonic emission and electroluminescence generates under UV light from ZnO (Lima et al., 2007; Ammala et al., 2002). Optical properties of ZnO differ by changing particle size and including nanostructures can be studied to understand the UV emission, defects and impurities.

Two emission bands are usually found. A relatively weak and narrow UV emission band is observed around 380 nm (3.25 eV), just below the onset of absorption. A much stronger and broader emission band is situated in the green part of the visible spectrum, with a maximum between 500 and 530 nm (2.50 eV) (Dijken et. al, 2000). ZnO/polymer composite films were prepared to have the potential to be used as UV absorbing and luminescent films in the design of optical coatings, solid lamps and photodetectors (Lü et al., 2007).

In this PhD dissertation five different type of ZnO having different particle size were used. It was aimed to prepare well dispersed composites which possesses static dissipative properties (electrically conductive), high thermal conductivity as well as enhanced optical properties of polymers. Three commercial and two synthesized ZnO powders were used to prepare the composites. Particle size difference was the main parameter to investigate in the electrical conductivity, thermal conductivity and optical properties. Polypropylene and polyethylene were chosen as a matrix material because they were widely used polymers in the industry. To enhance the surface properties of polymer and filler, due to the problem of adhesion and wetting modifiers (PEG 4000 and aminopropyltriethoxysilane) were used as well. The polymer-ZnO plates were prepared by mixing ingredients in torque rheometer and pressing the mixture in hot press. Tensile strength, elongation at break and modulus of elasticity, electrical and thermal conductivities of the composites were measured. Absorption and luminescence spectra were taken to optimize optical properties. The fit between experimental and theoretical thermal and electrical conductivities were also investigated.

CHAPTER 2

POLYMER COMPOSITE

Composite materials are composed of at least two different materials, called a matrix and a filler, and possess different properties than their components. Polymer composites generally have two components, a polymer matrix and a filler. The matrix is the continuous phase and the filler can be continuous or discrete fibers or particulate powders. Synthetic polymers were first developed early in the 1900's. Since polymers had low density, were easily shaped, could resist corrosion, and were materials having low toughness and strength compared to metals; to take these parameters as an advantage, researchers began to study to improve the mechanical properties of polymers by the addition of filler materials. This was the origin of the polymer composites. Nowadays, polymer composites are used for mechanical, thermal, electrical, or optical purposes. Generally, polymeric composites have advantages over metals due to their flexibility, durability, mechanical strength, stiffness, and chemical resistance. They have reproducible conductivity, reduced density, increased corrosion resistance, and they are cost- and weight-saving materials as well. Thermal instability, limited processability, and creep were the disadvantages of the composite materials (Mallick, 2007).

Commercial and industrial applications of polymer composites are so varied that it is impossible to list them all. Only the major structural application areas are highlighted, which include packaging industry, oil industry, aircraft, space, automotive, furniture (e.g., chair springs), sporting goods, marine, infrastructure, electronics (e.g., printed circuit boards), building construction (e.g., floor beams, covering), power industry (e.g., transformer housing), medical industry (e.g., bone plates, implants, and prosthetics), and in many industrial products, such as step ladders, oxygen tanks, and power transmission shafts.

In polymer composite materials, the role of the matrix should be keeping the filler in place, or providing a barrier against a harsh environment, such as chemicals and

moisture, to protect the filler surface from abrasion, chemical and mechanical degradation. The interaction between filler and matrix is important in designing damage-tolerant structures as well. Generally coupling agents were applied on the filler material to improve their wetting with the matrix as well as promote bonding across the fiber-matrix interface. The processing and defects in a composite material depend strongly on the processing characteristics of the matrix (Friedrich et al., 2005; Monk, 2004).

2.1. Polymer Matrix

Polymers are long chained molecules, containing one or more repeating units of atoms which are bonded covalently. “In the solid state, these molecules are frozen in space, either in a random manner for amorphous polymers or in a random manner and ordered chains in semicrystalline polymers” (Mallick, 2007).

Polymers can be thermoset or thermoplastic, the typical thermoset polymers are polyesters, epoxies, polyimides, phenolic compounds, thermoplastic polymers; polypropylene, polyvinylchloride (PVC), polyethylene, nylons, thermoplastic polyesters (PET, PBT), polycarbonate, and polyvinylacetate.

In a thermoplastic polymer, molecules are not chemically joined together they are individual and they are held in place by weak secondary bonds or intermolecular forces, such as van der Waals bonds and hydrogen bonds. “When heat is applied, these secondary bonds in a solid thermoplastic polymer can be broken and the molecules can move relative to each other or flow to a new configuration if pressure is applied on them. On cooling, the molecules can be frozen in their new configuration and the secondary bonds are restored, resulting in a new solid shape”. Thus, a thermoplastic polymer can be heat-softened, melted, and reshaped many times if it is desired. However, in thermoset polymers, a three-dimensional network structure is formed by chemically joining of the molecules and once these cross-links are formed during the polymerization reaction (also called the curing reaction), the thermoset polymer cannot be melted by the application of heat. However, if the number of crosslinks is low, it may

still be possible to soften them at elevated temperatures (Mallick, 2007; Friedrich, 2005).

In conductive semicrystalline thermoplastic composites, the breakdown of the conductive path occurs during melting of the crystalline phases, it can be attempted in thermoset conductive composites that the glass transition temperature will govern the process (Boiteux et al., 1999).

2.1.1. Polyethylene

Polyethylene consist of alkanes with the formula $C_{2n}H_{4n+2}$, where n is the degree of polymerization. The degree of polymerization could be as small as 100 and can be as high as 250,000 or more, equating to molecular weights varying from 1400 to more than 3,500,000. There are many type of polyethylene and the widely known polyethylenes are low density polyethylene, linear low density polyethylene, and high density polyethylene. The chemical structure of pure polyethylene is given in Figure 2.1. When the monomers are forced into close affinity by high pressure then the free radicals initiate the polymerization. Termination of chain growth occurs when the free radical on a growing chain is transferred to another chain or is quenched by another radical. In practice, numerous competing side reactions occur that result in branching and premature chain termination. The nature of the product is controlled by the initiator concentration, temperature, pressure, availability of vinyl comonomers, and the presence of chain transfer agents. Using Ziegler Natta catalyst is the one of the common method for the production of polyethylene (Peacock, 2000; Junior, 2007).

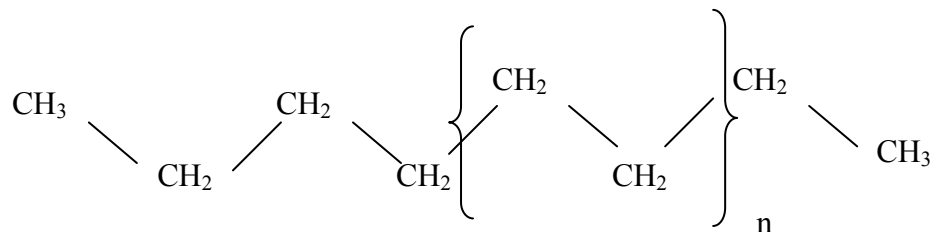


Figure 2.1. Chemical structure of pure polyethylene (Source: Peacock, 2000).

All types of polyethylene have covalently linked carbon atoms with pendant hydrogens; variation of polyethylene types are obtained due to branches, ranging from alkyl groups to acid and ester functionalities. Chain defects can occur due to polymer backbone and affect the degree of crystallinity. The more defect lowers the crystallinity of the polymer. Low density polyethylene (LDPE) is produced by high pressure polymerization and the crystallization process resulting in relatively low density. The branches primarily consist of ethyl and butyl groups together with some long chain branches. LDPE resin has densities in the range of 0.90-0.92 g/cm³. High density polyethylene (HDPE) has little branching stronger, harder and more opaque than LDPE. The density of the resin ranges between 0.96-0.97 g/cm³ (Peacock, 2000).

Polyethylene finds an application area in the markets due to low tensile strength, its flexibility, and low softening temperature. However creeping under sustained load is a serious problem. Polyethylene is used as an insulator in electric field and finds an application area in packaging, bottle blowing, piping, storage (tanks), plastic bags, chairs and fabric industry (Peacock, 2000).

Semicrystalline polymers consist of two or more solid phases, “at least one of which molecular main segments are organized into a regular three dimensional array, and in one or more other phases chain are disordered”. All commercial polyethylene’s are semicrystalline materials. The aspect of semicrystallinity is important since, polyethylene can be disordered to be a composite of crystalline and noncrystalline regions. Polyethylene that consisted only of crystalline matrices it would be easily broken into small peaces “friable material” and a totally amorphous sample would be highly viscous fluid. In practice “degree of crystallinity” defines the nature of semicrystalline polyethylene sample. Using the degree of crysatlinity many of the physical properties of polyethylene can be inferred such as density and stiffness of the polymeric material (Fontana et al., 2007; Junior, 2007; Werf, 1991).

Polyethylene exhibits three types of unit cells: orthorhombic, monoclinic, and hexagonal. In the XRD pattern of LDPE one dominant fairly sharp peak at 21.4 and a weak broad peak at 23.6, and a weak broad third peak centered on 19.5 occur. The two dominant peaks and the small broad peak arise from crystalline and amorphous regions in LDPE. It is clear from the relative areas under these peaks that the polymer sample produced in plate form after solidification from the melt becomes highly crystalline. The crystallinity of the polymeric material can be found by using these characteristic peaks. (Fontana et al., 2007). Polyethylene crystallizes from the molten state or solution

when generally conditions make the crystalline state more stable than the disordered one. The processes by which polyethylene crystallizes the properties of the disordered state reflect from which the ordered phase condenses and thus, levels of chain entanglement, molecular dimensions, and viscosity all play important roles. The formation of polyethylene semicrystalline morphologies involves two distinct processes: crystallite initiation and crystallite development. Primary nucleation, crystal growth, and secondary nucleation can all occur simultaneously. The factors affecting the the disordered state of the structure are both intrinsic to the molecules and extrinsic to the surrounding conditions. The factors influencing the system are the molecular weight, molecular weight distribution, and concentration, type and distribution of branches. External factors include temperature, pressure, shear, concentration of solution, and polymer–solvent interactions (Karian, 1999; Peacock, 2000; Junior, 2007).

Polyethylene molecules are largely resistant to chemical attack and little affected by electrical fields. Polyethylene melting behavior exhibits at temperatures from as low as room temperature up to 140°C. Polyethylene undergoes a transition from the semicrystalline to the molten state that takes place over a temperature range that can span from less than 10°C up to 70°C. As it passes through this transition the semicrystalline morphology gradually takes on more of the characteristics of the amorphous state at the expense of the crystalline regions. The glass transition of polyethylene has been assigned the β or γ transition at temperatures ranging from -20°C to -140°C (Sofian, 2001).

Heating behavior of the thermoplastics depend on the degree of order in molecular packing and the degree of crystallinity. Generally thermoplastic materials can melt without any chemical reaction. Firstly they form a viscous state however they often decompose thermally before melting. This melt decompose into smaller liquid or gaseous fragments, and then the liquid decompose further until they are sufficiently to vaporize (Beyler and Hirschler, 2002). PE begins to crosslink at 202 °C under inert atmosphere and reduction in the molecular weight starts at 292 °C the weight loss in PE observed below 372 °C. Branching of polyethylene causes enhanced intermolecular hydrogen transfer and results in thermal stability. The major products of decomposition are propane, propene, ethane, butane, hexane-1 and butane-1 (Beyler and Hirschler, 2002).

Polyethylene has no free electrons that can readily conduct thermal energy. Therefore it conducts heat only by the transmission of vibrational or rotational energy

from one chain segment to another by phonon transferring, either inter- or intramolecularly. The transmission of thermal energy is more efficient in high crystallites of polyethylene. Thus high density polyethylene is a better conductor of heat than low density polyethylene (Werff, 1991; Peacock, 2000).

The electrical properties of neat polyethylene materials are controlled by the negligible polar component of the carbon-carbon and carbon-hydrogen bonds that connect its constituent atoms. The absence of free electrons in polyethylene structure results as the material become an excellent insulator, and the lack of polarizability on bonds endow it with a general inertness to the effects of electrical fields. For these reasons polyethylene finds extensive use as an insulator, generally in the wire and cable industry. Despite, its intrinsically desirable electrical properties, polyethylene is not totally immune to the effects of electrical fields and currents. Under the influence of high electrical stresses, trace amounts of polar molecules, such as catalyst residues and water, and polarizable bonds, such as those contained in carbonyl and vinyl groups, reduce polyethylene's electrical inertness. Under the influence of high electrical stress, polyethylene gradually deteriorates, both chemically and physically, reducing its effectiveness as an insulator. In common with the majority of synthetic polymers, polyethylene has no free electrons with which to conduct electricity. It is therefore a good electrical insulator. Another desirable characteristic of polyethylene is that its carbon-carbon and carbon-hydrogen bonds exhibit negligible polar character, thus making them essentially inert to electrical fields (Peacock, 2000).

Polyethylene is permeable to some degree to most liquids, gases, and vapors. The surface contacts properties of polyethylene are important since the surface arising from its contact with other material, the two principal consequences of contact are wear and friction. There are three properties that define the principal optical characteristics of a polyethylene sample: its haze, transparency, and gloss. Haze is a function of light scattering; transparency is a function of unscattered light transmission, and gloss is dependent upon reflectivity. In general, unpigmented thin films of low density polyethylene are quite transparent and relatively free from haze, while thin high density polyethylene films and thicker low density polyethylene films are translucent, that is, they transmit a certain amount of light but preclude a clear view of objects on the far side. Samples more than 3mm thick, made from all but the very lowest density polyethylene resins, are opaque, blocking the transmission of virtually all light, even if they are unpigmented. The optical properties of polyethylene are important in both thin

and thick samples. Optical transmission properties are especially important for films, while reflective and coloration properties are of greater relevance to thick samples. Depending on the end use, polyethylene films may be used to either block or transmit light. As polyethylene crystallizes, spherulites and other supermolecular structures form that have an average density greater than that of the surrounding material (Junior, 2007; Taşdemir, 2008; Peacock, 2000).

2.1.2. Polypropylene

Polypropylene (PP) is a semicrystalline thermoplastic material produced by propylene monomer generally by using Ziegler Natta catalyst, by polymerization very long polymer molecules or chains obtained. At structural point, there are number of ways to link monomers together. PP has three types of form they are isotactic, syndiotactic and atactic PP. Polymer scientists discuss the stereochemical properties of PP, they usually discuss it in terms of tacticity of PP and the high tacticity, means high isotactic content. The isotactic PP materials have desirable physical, mechanical, and thermal properties in the solid state. Atactic material is a soft, sticky, gummy material that is mainly used in sealants, chaulks, and other applications where its stickiness is desirable. Syndiotactic PP, not a large volume commercial material, is far less crystalline than isotactic PP (Karian, 1999).

PP contains both crystalline and amorphous phases and the amount of phases depends on structural and stereochemical characteristics of the polymer chains. “Isotactic polypropylene (IPP) has three crystalline phases (α , β , and γ) and a mesomorphic smectic phase. The chain conformation of each crystalline phase is a 3 helix. The polymorphism of PP is surfacing from different packing of the helix into the unit cell, as observed by wide angle X-ray scattering.” The noncrystallizable, gummy, atactic PP phase has small amounts of a low molecular weight oily material at a level of 1% and lower. Typical crystallinity levels of extruded PP pellets are in the range of 60–70%. In the crystalline phase, the alpha or monoclinic phase is the dominant crystal form of PP with a melting point of about 160°C. The beta or hexagonal phase is less common and less stable (Chipara et al., 2008; Karian, 1999). The decomposition mechanism of PP

was investigated by Beyler and Hirschler (2002). For PP the reduction of molecular weight first observed at 227 to 247 °C and volatilization becomes above 302 °C. In PP chain scission and chain transfer reactions are very important during decomposition. In polypropylene, every other carbon atom is a tertiary carbon, which is prone to attack. This lowers the stability of polypropylene as compared to polyethylene. Major products are, pentane, 2 methyl-1-pentene, 2-4 dimethyl-1-heptene.

Polymeric products are sustain both to oxygen and to solar ultraviolet radiation (UV) when used in outdoor applications and the resulting photodegradation can significantly effect negatively their useful life. The degradation may result from direct photolysis or from photooxidation, but both mechanisms require absorption of UV and for solar wavelengths at “terrestrial sites” this means wavelengths above 290 nm. Neither pure PP nor pure PE absorb at wavelengths longer than 290 nm, radical-based oxidative processes may be initiated by the absorption of sunlight (Fernando et al., 2008; Sharma and Nayak, 2009; Avella et al., 2004).

The mechanical properties of PP changes by changing the level of crystallinity in the polymeric material when the flexural modulus or stiffness typically increases as the level of crystallinity increases in a PP product, but it also depends on the type of crystal morphology. Thus, stiffness generally decreases as the crystallizability (tacticity) decreases or, in random copolymers, as the ethylene content increases because this tends to decrease crystallizability. PP has a brittle behaviour at either low temperature or high loading rates, improvement in the fracture toughness of PP can be achieved by either modifying the crystalline structure, or addition of a second phase material. (Orange and Bomal, 2003; Han et al., 2009).

Polypropylene is a trading widely used thermoplastic polymer, which offers best price/performance characteristics among all thermoplastics. Its useful properties include high thermal stability and good mechanical properties, dimensional stability, low density, better process ability, high water permeation resistance, and resistance to corrosion. A great volume percent of PP blends used in fibers and fabrics technology and composites find wide application in automotive parts, extruded profiles, cable insulation, footwear, medical (syringes) and packaging industry. Nanocomposites offer great technological and economical benefits in the polymeric materials usage (Chow and Tham, 2009; Han et al., 2009; Sharma and Nayak, 2009).

2.2. Filler

Filler is very important in the properties of polymer composites since, the proper selection of the filler type, filler volume fraction, and aspect ratio of the filler influences the properties of composites. The filler can be an inorganic powder such as a metal or a ceramic, or an organic material such as carbon or a metallic powder or a conducting polymer. The factors that affect the conductive network of the composite include at least the type of metallic filler, filler size, hardness, shape, filler particle distribution. For very low filler fractions, the mean distance between conducting particles is large and the conductance is limited by the polymer matrix. Particulate mineral fillers generally enhance the stiffness but reduce the fracture strength and toughness (Taya, 2005; Tchoudakov et al., 1996; Lux, 1993).

2.2.1. Zinc Oxide

Nanocrystalline materials have found an increasing research area during the past years. This new class of material has several application areas for example; optical, electrical and mechanical properties of devices comprising nanocrystallite semiconductors and oxides have been demonstrated in photovoltaic solar cells, light-emitting diodes, varistor, and ceramics.

ZnO has a hexagonal structure with lattice parameters $a=0.3296$ and $c=0.5207$ nm as shown in Figure 2.2. The structure of ZnO is composed of tetrahedrally coordinated O^{2-} and Zn^{2+} ions, stacked along the c-axis and ZnO has partial ionic characteristics. “The non-centrosymmetric structure and there by piezoelectric behavior result from the tetrahedral coordination” (Wang et al., 2004).

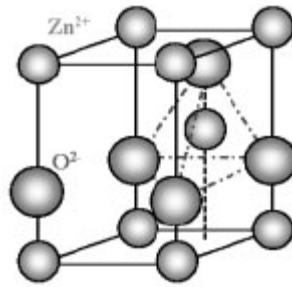


Figure 2.2. Wurtzite structure of ZnO
(Source: Wang. et al., 2004).

2.2.1.1. Synthesis of Zinc Oxide

ZnO powder can be synthesized easily by French process from the combustion of vapors coming from the distillation of metallic zinc. American process is the other mostly known method uses “active zinc oxide” where zinc ash was precipitated with alkali, other methods are chemical vapor deposition, sol–gel, magnetron sputtering, spray pyrolysis, pulsed laser deposition (PLD), hydrothermal, and microemulsion. According to the method followed, ZnO particles with different particle sizes (from several micrometers to nanometers), and shapes (rods, spheres, nanowires, etc.) can be obtained (Andres-Verges et al., 2005; Triboulet et al, 2005).

Hydrothermal precipitation synthesis method is preferred in this study because of the low growth temperature and good potential for scale-up. Hydrothermal precipitation has large advantages for preparing highly crystallized particles with narrow size distribution and high purity without further treatment and higher temperature as well. Size and morphology can be controlled by controlling reaction temperature, reaction time and additives in hydrothermal precipitation method (Sue et al., 2004; Loh and Chua, 2007).

In a typical hydrothermal reaction a precursor (hydrothermal fluid) consists of only water gets concentrated with time. At a certain level of supersaturation, spontaneous crystallization will occur, leading to a decrease of the concentration in the hydrothermal fluid. Most of the nanomaterials synthesized using hydrothermal methods and dispersed in solution. The product is collected by washing and centrifuging processes.

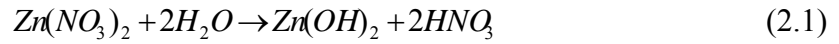
According to Loh and Chua (2007); in an aqueous system crystal nucleation will be influenced when the solution is supersaturated. Initial nucleation can occur either in solution or on the surface of the solid phases, depending on the net interfacial energy of the system. If the interaction between the growing nucleus and a substrate surface represents a lower net interfacial energy, heterogeneous nucleation is favored over homogenous nucleation.

In hydrothermal precipitation synthesis, aqueous solutions by dissolving precise amount of zinc salt ($\text{Zn}(\text{Ac})_2$, ZnCl_2 , ZnSO_4 , $\text{Zn}(\text{NO}_3)_2$) and alkali metal hydroxide (LiOH , KOH) in water were mixed.

Yu and Yu (2008) prepared ZnO hollow spheres using ZnCl_2 as a precursor by hydrothermal precipitation treatment. Glucose and varying amounts of ZnCl_2 were dissolved in water under stirring. The pH of the solution was about 5.5. Then the solution was put into to autoclave, and following by treatment at $180\text{ }^\circ\text{C}$ for 24 h. After hydrothermal reaction the precipitate was centrifuged and washed with water and alcohol several times. Finally the powder was calcined at $500\text{ }^\circ\text{C}$ for 4 h. The synthesized powders X-ray diffraction pattern is taken and the diffraction patterns were in good agreement with the hexagonal wurtzite structure of ZnO. With increasing precursor concentration the intensities of diffraction peaks decrease, indicating that crystallite size decreases or crystallization becomes weak. These also suggest that glucose inhibits the crystallization of ZnO. In the SEM images of the powder before calcination was spherical and had $1\text{ }\mu\text{m}$ size. After calcination diameter of the spheres drastically decreased to about 800 nm.

Wei and Chang (2008), synthesized nano ZnO particles containing different surfactants at room temperature and $50\text{ }^\circ\text{C}$ under ultrasonic condition by hydrothermal method. The reactants used are aqueous solutions of zinc chloride and potassium hydroxide, and the surfactants are cetyltrimethylammonium bromide (CTAB) and triethanolamine (TEA). All synthesized ZnO samples were in the form of zincite. The particle size of the nano ZnO powders synthesized at room temperature is approximately 46–61nm (i.e., corresponding to BET surface areas $17.5\text{--}23.0\text{ m}^2/\text{g}$). ZnO particle size can be effectively reduced to approximately 28–39nm (i.e., corresponding to BET surface areas $27.4\text{--}38.9\text{ m}^2/\text{g}$) if the synthesis processes in the ultrasonic water bath are kept at $50\text{ }^\circ\text{C}$. Moreover, the ZnO powder dispersion is considerably improved when the synthesis is carried out at $50\text{ }^\circ\text{C}$.

Hydrothermal synthesis of ZnO particles was done by Ohara et al. (2004) under supercritical conditions from zinc nitrate aqueous solution. The synthesized zinc oxide was in hexagonal wurtzite crystal structure without another phase. The reaction taking place in the reactor is considered to be as given in Equation 2.1 and Equation 2.2.



The first step is the hydrolysis of a metal salt to produce metal hydrous oxide, and the second step is dehydration of the hydrous oxide to produce metal oxide. Nine peaks appear at 2θ ($^\circ$) = 31.7, 34.4, 36.3, 47.5, 56.6, 62.3, 66.5, 67.9, and 69.1 $^\circ$, which correspond to (100), (002), (101), (102), (110), (103), (200), (112) and (201) planes respectively. From the XRD pattern of ZnO: ZnO particles possessed a high crystallinity, since all peaks were very sharp (Ohara et al., 2004).

Deng et al. (2001) studied synthesis of ultrafine zinc oxide powder using the combination of precipitation and mechanical milling followed by subsequent heat treatment. Zinc hydroxide/oxidehydrate precursor was precipitated from zinc chloride in ammonia solution, and then the precipitate was dried in a freeze-dryer. Precursor powder and sodium chloride powder was milled at 300 rpm for 12 hours, milled powders were annealed in air in alumina crucibles for one hour at a temperature between 140 and 600 $^\circ\text{C}$. Mechanical milling may lead to reduction of particle size from 170 nm to approximately 40 nm. This work has shown that a sufficient amount of NaCl can result in 10–20 nm precursor particles embedded in the NaCl matrix. The dehydration through annealing did not lead to formation of larger particles (Deng et al., 2001).

Xiao et al. (2008) synthesized ZnO nanosheets by sonochemical method. ZnCl_2 and NaOH precursors were dissolved together in water under constant stirring and pH was adjusted to 13 by using NaOH solution. After stirring, the mixture was irradiated with high density ultrasound for 2 h. Sonochemical synthesis were used which has become a routine method for preparing a wide variety of nanostructured material. Different shapes of ZnO powders including nanorod, trigonal, dendritic have been prepared with sonochemical synthesis.

Exhibiting well-crystallized zinc oxide powders with different morphology, crystallinity, and particle size have been successfully prepared by controlling the process temperature and molarity of precursor. With increasing process temperature and precursor molarity during synthesis, the morphology of ZnO powders changes from flowerlike agglomeration to a well-developed rodlike shape. The band gap of ZnO powders increases with a decrease in the molarity of NH_4OH during synthesis. However, the formation of the bonds of Zn–O–Zn among nanoparticles due to the existence of water molecules results in hard agglomerates. Therefore, removal of water in precursors is a key process for reducing hard agglomerates. (Hong et al., 2006a)

Zhang and Yanagisawa (2007) studied metal hydroxide salts (MHS) with layered structures. The metal hydroxide salts have a general formula of $\text{Ma}(\text{OH})_b(\text{X}_c)(2a-b)/c \cdot n\text{H}_2\text{O}$ where M corresponds to Zn^{2+} , Co^{2+} , Ni^{2+} , Mn^{2+} etc. They structurally consist of positively charged metal hydroxides that require the presence of interlayer anions to maintain overall charge neutrality. These interlayer anions (X) can be Cl^- , NO_3^- , CO_3^{2-} , CH_3COO^- , and SO_4^{2-} . The common synthesis methods of the metal hydroxide salts include co-precipitation method and hydrothermal method, and the obtained products usually have the lamellar morphologies such as films, sheets, and plates. In this paper, zinc hydroxide chloride (ZHC) sheets were synthesized by a simple hydrothermal precipitation method without using surfactant. The SEM photo and the XRD pattern of the ZHC sheet are given in Figure 2.3. ZnO usually has c-axis oriented growth habits, which make the tabular ZnO particles difficult to be obtained. The intercalated Cl^- in ZHC is smaller than other anions such as NO_3^- , CO_3^{2-} , CH_3COO^- , and SO_4^{2-} , which is favorable to producing dense structure after thermal decomposition. After thermal treatments, the ZHC sheets were transformed to sheetlike dense ZnO.

2.2.1.2. Growth of Zinc Oxide

Different shapes of ZnO powders including wires, tubes, nails, tower-, star-, dendrite- and flower-like structures have been prepared via different synthesis methods or under different preparation conditions. Control of the particle morphology is a

concern for material synthesis because electrical and optical properties of materials depend sensitively on both size and shape of the particles (Andres-Verges et al., 2005).

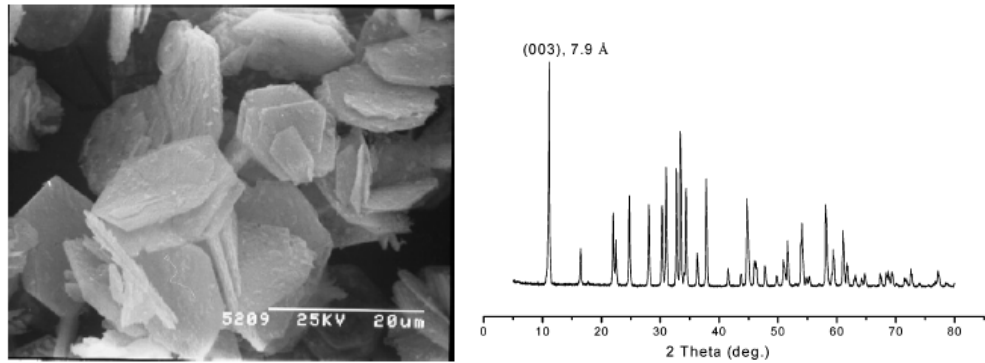
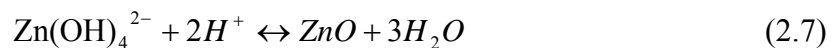
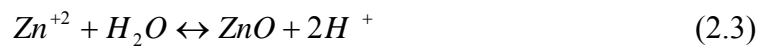


Figure 2.3. a) SEM micrographs of ZHC sheets b) XRD pattern of the ZHC sheet obtained from 1 M ZnCl₂ solution (pH ≈ 6) by quick cooling from 220 °C (Source: Zhang and Yanagisawa, 2007).

From the hydrothermal precipitation the synthesis condition of the aqueous solution can be controlled by adjusting the reactant concentration, growth temperature, and the pH. The crystal phase of the deposits was mainly determined by the pH of the aqueous solutions. If the pH is in the range 6 to 9, the Zn(OH)₂ is predominantly formed. The wurtzite ZnO crystal is formed at pH 9–13. During the progress of the formation of ZnO, the complex ion Zn(NH₃)₄⁺² or Zn(OH)₄⁻² was formed first. The equations expressing the thermal equilibrium of the ZnO–H₂O system are given in Equation 2.3 to Equation 2.7 below.



With an increase in temperature, these complexes will be dehydrated. The ZnO crystal forms a heterogeneous nucleus at the interface between substrate and solution. After that, the crystals begin to grow into the nanorods (Loh and Chua, 2007).

ZnO is a polar crystal, who has positive polar face [0001] rich in Zn and negative polar face [0001⁻] rich in O. According to the rule on ZnO crystal growth mechanism the growth rate in [0001] direction is the fast, and the velocities of crystal growth in the different directions are as follows: [0001]-[011⁻1⁻]-[011⁻0]-[011⁻1]-[0001⁻]. The different size and shape of ZnO crystals result from different growth rates along the c-axis in different reaction media. The growth rate of a face will be controlled by the external factors (supersaturation, temperature, solvent and impurity), besides the internal growth habit of the crystal (Xie et al., 2008).

Particle growth in colloidal systems can viewed from two standpoints. The first one corresponds to a decrease of the surface free energy at a constant total volume. This process is known as Ostwald ripening: “large particles grow at the expense of smaller particles, which have a higher solubility. The other one describes growth by the addition of reactive precursors available in solution to already existing particles. For the case of silica extensive investigations have shown that growth proceeds by a surface reaction limited condensation of precursors”. Nucleation process of a particle is more complicated process, and aggregation of building units appears to occur. The rate of particle growth is controlled by the concentration of precursors or dissolved species and their reactivity, which depends on the number of particle surface atoms, and the solution composition (Meulenkamp, 1998).

In order to obtain nanosized ZnO particles, crystalline growth should be controlled after the formation of nuclei. Anionic surfactant was added into the system to prevent the crystalline growth and agglomeration. Surfactant molecules are absorbed onto the surface of the precursor of ZnO in the medium. These organic molecules would “stericly hinder” the further growth of precipitate or interfere with the aggregation of ZnO nanoparticles during calcinations (Tang et al, 2008).

The pH conditions must have large effects on the morphology and the phase stability of Zinc hydroxide because it includes hydroxide ions. The addition of NaOH can increase the amount of the zinc hydroxide precipitates in the starting solution and the yield after hydrothermal reaction Zn^{2+} exists in different forms in the solution with different pH condition such as in acid or neutral condition $ZnCl_n(OH)_{6-n}$ and

(Zn(OH)_4^{2-}) in basic solution was obtained (Zhang and Yanagisawa, 2007; Klingshirn, 2007).

If growth process takes place in the presence of surfactant, wetting agents allowing easier spreading and lower interfacial tension between two liquids. Sun et al. (2002) studied effect of cetyltrimethylammonium bromide (CTAB). The growth process of ZnO in the presence of CTAB is different. Because of the existence of surfactant, the surface tension of solution is reduced, which lower the energy needed to form a new phase, and ZnO crystal, therefore, could form in a lower supersaturation. On the other hand, CTAB could also be considered to influence the erosion process of zinc and the growth process of ZnO by the electrostatic and stereochemical effects. CTAB is an ionic compound, which ionizes completely in water. The resulted cation is a positively charged tetrahedron with a long hydrophobic tail while the growth unit of ZnO crystal considered Zn(OH)_4^{2-} and it is negatively charged. The zinc particles are negatively charged and so CTAB is adsorbed on the surface. In the crystallization process, surfactant molecules may serve as a growth controller, as well as agglomeration inhibitor, by forming a covering film on the ZnO crystal. When ZnO crystal grew, a surfactant film could form at the interface between solution and ZnO crystal reducing the interface energy. The film is floating, and surfactant molecules carrying the growing units will release them at the surface of ZnO single crystal. (Sun et al., 2002; Wei and Chang, 2008).

In another study which was done by Usui (2007); single-crystalline ZnO nanorods of radial-shaped needles and single needle were prepared by chemical synthesis in aqueous solutions with surfactant sodium dodecyl sulfate (SDS). In an aqueous solution of SDS, aggregates of dodecyl sulfate ion form spherical micelles above the critical micelle concentration, and the spherical micelles have a property of encapsulating various salts generated in the solution. It is well-known that the spherical structure can change to one dimensional rod structure when the size and electrochemical properties of the salts are changed. Thus, an interior of the spherical micelles can be a space for nucleation and crystal growth of ZnO nanorod. Oxygen in the hydrophilic group of dodecyl sulfate ions is negatively charged. Consequently, a chemical reaction occurs due to an electrostatic interaction between the hydrophilic group and a positive polar plane of zinc-rich surface on growing the ZnO crystal. It is suggested that chemically active sites are randomly generated on the surface of the nucleated ZnO crystal by the chemical reaction and that new nanorods are nucleated at the active sites

and grow in another [0001] direction. This is supported by the morphology of the radial-shaped nanorods obtained in the SDS solution.

2.2.1.3. Properties of Zinc Oxide and Aluminum Doping

Zinc oxide (ZnO) occurs as zincite mineral in nature. Zinc Oxide is a white or yellowish powder called as zinc white as well. It is insoluble in water and alcohol but soluble in acid and alkali. ZnO has a hexagonal wurtzite type structure and due to the native structure of ZnO the material is an n-type semiconductor. The particle shape is important for maximizing physical properties of the powder. Zinc oxide particles may be spherical, acicular or nodular depending on the manufacturing process. It is known that conductive ZnO has a lower heat resistance since exposed to oxygen atmosphere for a long time (Tsuiji, 2003). The thermal conductivity of the zinc oxide is 1-1.2 W/mK. The ZnO conductivity is well-known mechanism and it is due to the ionization of zinc interstitials and oxygen vacancies. Since there are some deviations observed due to the native stoichiometry of the compound and the deviations could be due to presence of intrinsic defects such as oxygen vacancy and zinc interstitials. Undoped ZnO shows n-type conductivity with very high electron densities of 10^{21} 1/cm³ (Manouni et al., 2006; Wöll, 2007, Özgür et al, 2005).

Zinc oxide (ZnO), is a new kind of material, and is rather common material which is used for a quite large variety of different applications such as semi conductivity, wear resistance, vibration insulation, microwave absorption and antibacterial effect. Probably the most “visible” use in every day’s life is that, as a white pigment (zincwhite) in painting and coloring of e.g. paper. A completely different area is medicine, where zinc oxide is used e.g. in wound-treatment making use of its antiseptic properties. One example are transparent conducting oxide layers which are suitable to be used as front electrodes in thin film solar cells. ZnO has also been used as a sensor for hydrogen and carbon hydrides since the conductivity of thin zinc oxide films varies considerably with hydrogen gas pressure. Zinc oxide can found application area due to piezoelectric properties, varistor properties and thermochromic properties of the material. With regard to chemical processes one of the oldest applications is in

connection with rubber vulcanisation. ZnO has been used to accelerate sulphur-induced vulcanisation and to improve the properties of rubber. Today, in terms of industrial added value, the chemical properties of ZnO surfaces are the most important ones. Many different chemicals are produced using zinc oxide or zinc oxide based compounds as a heterogeneous catalyst (Tsuiji, 2003; Miller, 1941).

Zinc oxide is a material having a band gap of 3.2 eV. This band gap value is equivalent to ultraviolet (UV) light energy, that is why the zinc oxide material has ability to absorb UV light and has no absorption in the visible range and a low refractive index of 1.9 ~ 2.0 as well. Since the excitons of ZnO have a binding energy about 60 meV it is a brighter emitter. Especially nano-particles of zinc oxide exhibit characteristics of transmitting visible light and absorbing UV light, by taking advantage of these characteristics, nano-particle could be used in various fields such as an UV-absorbing or anti-fading film for fluorescent lamps, photo detector or as a sunscreen material (Tsuiji, 2003, Look et al., 2003b).

The ZnO could be doped with group III elements such as barium, gallium and indium, aluminum to have a lowest electrical resistivity and a good optical transmission in the visible and near-infrared regions

In order to improve the antistatic property of the composites, one important method was to reduce the resistivity of the ZnO whisker. Producing conductive ZnO could be possible by doping typical dopant element of F, B, Al, Ga, In, Sn. Replacing Zn⁺² atom with atoms of elements higher valence such as Al⁺³ is worthy to mention all the III group element. Aluminum is the common dopant for the preparation of doped zinc oxide since it is cheap and non toxic material (Çağlar et al., 2008).

The resistivity of zinc oxide is lowered by the doping of metal ions under heat treatment at reduced atmospheres. Al-doped ZnO resistivity were determined by various essential parameters such as temperature, dopant concentration and doping sources. Many papers reported that the conductivity of ZnO thin films could be improved by doping Al³⁺, and several preparation techniques were applied, such as spray pyrolysis, pulsed laser deposition, chemical spray process, sol-gel and sputtering method (Wan et al., 2008; Lin and Tsai, 2007; Tai and Oh, 2002; Hammer et al., 2008). Li et al. (2008) studied ZnO nanorods which were fabricated by hydrothermal method. Transition metals Co, Mn, and Cr was doped to ZnO nanorods again by hydrothermal method. Since hydrothermal synthesise is environmentally friendly, low temperature and low

cost method for doping, could be used as an appropriate method in the preparation of the doping system.

According to structural characterization of Al-doped ZnO which was studied by Çağlar et al.(2008) “the Al-doped ZnO films crystallized with the hexagonal wurtzite structure and a preferred orientation of (002).” In the Al-doped ZnO films the presence of a strong diffraction peak of (002) indicates that films have a (002) preferred orientation. The doping of the Al³⁺ could be in oxide form or metallic form. The doping mechanism does not change the replacement of zinc atoms with aluminum in the hexagonal structure and in the XRD pattern as well.

Wan et al. (2008) studied on tetra needle like zinc oxide with a resistivity of 10⁸ ohm-cm. The whiskers were doped with Al³⁺ by a solid state method. First Al salt was dissolved in ethanol and subjected to ultrasonic treatment for 1 hour until complete sol formation. Then the whisker was added into the sol and stirred for 5 hour at room temperature. The slurry was dried at 100 °C and then calcined at temperature ranging from 500-900 °C heating rate of 20 °C/min for 3 hours in air to obtain precursor and finally the obtained precursor was annealed at temperature ranging from 500-700 °C in N₂ atmosphere. The Al content was varied from 1 to 10 at.%. Three different Al source was used in this study the chemical formulas and the resistivity values were given as C₉H₂₁AlO₃, Al₂(SO₄)₂.18H₂O and AlCl₃.6H₂O, 912, 1307, and 3768 ohm-cm respectively. Increasing the Al content generally decreases the resistivity in the range of 1-10 at. %. Further increase in the Al content lead increasing in the resistivity value of ZnO whisker. The minimum resistivity value was reached when Al content is 7.0 at.%.

2.2.1.4. Surface Modification of Zinc Oxide

During the mixing process of zinc oxide with polypropylene and polyethylene; agglomerations and adhesion problems are observed. Inorganic particles tend to aggregate in an organic matrix due to their high surface energy. Sometimes the dispersion of particles determines the composite materials structure and properties. Generally, it is very difficult to achieve a homogeneous dispersion of particles in a

polymer matrix. Therefore, the enhancement of dispersion of particles in a matrix should be a significant characteristic of composites. Surface modification provides an effective way to increase particle dispersion and to improve its compatibility with the polymer matrix and change the chemical affinity of the materials to each other.

To describe the surface of a material hydrophobic and hydrophilic terms are frequently used. A surface is hydrophobic, if it tends not to adsorb water or be wetted by water. If it is hydrophilic, it tends to adsorb water or be wetted by water. In the same manner, the terms describe the interaction of the boundary layer of a solid phase with liquid or water vapor. To learn if the surface of the material hydrophilic or hydrophobic contact angle measurement is used. The surface free energy of the material can be estimated from the known surface tensions of probing liquids and the contact angles of the liquid to a given material (Metin, 2002). Generally polymers are hydrophobic materials; they have low surface energy and quite weak inorganic/polymer interfacial adhesion. Changing the chemical nature of the surface or the surface topography or removing a weak boundary layer can alter the properties of surface region in polymers or inorganic fillers.

Traditional fillers were in several microns, not on nanoscale in particle size. However, nowadays the primary particles size is below 100 nm, and they tend to make complex aggregates as well. Due to the high surface area in nanocomposites, the surface energy is an important parameter. For stabilizing the energy, several surface functionalization and stabilizing techniques have been developed. “Anchor groups are needed for adsorption or covalent binding of the modifier on the particle surface, while other parts interact with the polymer and therefore decrease the interface energy” (Althues et al., 2007).

When organic polymers are reinforced with fibers or minerals, the interface, or interphase region, between the polymer and the inorganic substrate is involved in a complex interplay of physical and chemical factors. These factors are related to adhesion, physical strength, and coefficient of expansion, concentration gradients and retention of product properties. The force affecting adhesion is, migration of water to the hydrophilic surface of the inorganic reinforcement. A “true” coupling agent creates a water-resistant bond at the interface between the inorganic and organic materials (Ge, 2003).

Adsorption of polymeric coupling agents onto surface of a metal oxide can be described by combination of chemical and electrostatic interaction, hydrogen bonding

and Van der Waals forces. For non ionic polymeric coupling agents hydrogen bonding is the primary adsorption mechanism (Liufu et al., 2004). Liufu et al. (2004) studied on polyethylene glycol (PEG) to improve the dispersion of zinc oxide. PEG macromolecules bond with the solid surface of ZnO via the –OH group with hydrogen bonding. When PEG added to the solution it was adsorbed onto the particle surface and then gets a gradual attainment. IR spectroscopy gives qualitative information about ZnO and PEG molecules. The peaks at 1509 cm^{-1} and 1355 cm^{-1} show the adsorption of PEG on the surface of ZnO particles.

Silane coupling agents have a general formula of $(\text{RO})_3\text{SiCH}_2\text{CH}_2\text{CH}_2\text{-X}$, RO is hydralisable group such as methoxy, ethoxy, or acetoxy, and X is non-hydrolysable and an organofunctional group, such as amino, methacryloxy, epoxy, etc. Silane coupling agents are silicon based materials and generally contains inorganic and organic tails in the same molecule. Silane coupling agents are reactive additives which modify the surface of inorganic fillers. A silane coupling agent will act at an interface between an inorganic substrate (such as glass, metal or mineral) and an organic material (such as an organic polymer, coating or adhesive) to bond, or couple, the two dissimilar materials. Surface treatment of silane coupling agents on filler material was carried out into two steps by following hydrolysis and condensation reactions. After hydrolysis reaction with hydroxyl group which was found on the surface of the filler the silanol group formed. After condensation reaction takes place siloxane bonds are formed (Metin et al., 2004; Tang et al., 2008).

In a composite it is important to choose the right silane coupling agent. Concentration of surface hydroxyl groups, type of surface hydroxyl groups, hydrolytic stability of the bond formed, physical dimensions of the substrate or substrate features, surface modification is maximized when silanes react with the substrate surface and present the maximum number of accessible sites with appropriate surface energies. The silane coupling agent treatment on the filler can provide: better bonding of the pigment or filler to the resin, improved mixing, increased matrix strength, reduced viscosity of the uncured sealant or adhesive. To measure the adhesion of metals to polymers have focused on techniques such as the scotch tape test, 90° peel test and stud pull test. Even though the peel test is simple to execute, peel strength represents the combination effect of adhesion and mechanical forces and is very sensitive to variation in test parameters (e.g., angle, rate, etc.) (Tang et al., 2008; Dowcorning, 2009).

Zhao and Li (2006) studied on phodegradation of polypropylene matrix-zinc oxide filler. They surface treated the zinc oxide with organasilane coupling agent. It was seen that most of the nanoparticles are uniformly dispersed in the PP matrix. The uniform dispersion of the ZnO nanoparticles in the PP matrix was obtained. Organic nature of nanoparticle surfaces was a key factor. Therefore, the presence of the organic surface treatment on the ZnO particles, which changes the surface properties from inorganic into organic, reduces the particle surface tension.

In the thermoplastic polymers such as polypropylene and polyethylene bonding using silane coupling agent can be explained by inter-diffusion and inter-penetrating network formation in the interphase region as given in Figure 2.4. To optimize inter-penetrating network formation it is important that the silane and the resin be compatible (Dowcorning, 2009).

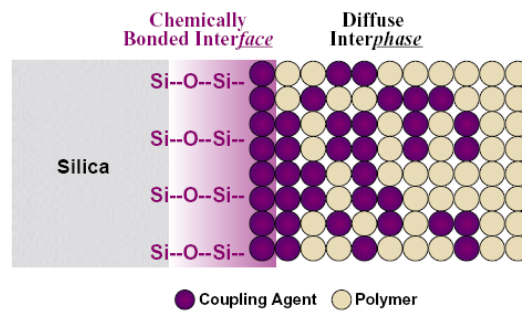


Figure 2.4. Bonding mechanism in thermoplastic polymers (Source: Dowcorning, 2009).

Grase et al. (2003) studied grafting aminopropyltriethoxysilane (APTES) on to commercial ZnO nanoparticles and determine the properties of coated and non-coated powders. They found that after grafting the ZnO specific surface area decreased immediately. The decrease may be due to the mechanism of condensation of aminosilane in basic media. Using ZnO which was coated with APTES in the case of UV sunblock is non convenient. Silanes are to sensitive to UV radiation, the problems should be adhesion between silane and oxide surface. Generally metal oxides will hydrolysis in the presence of water and zinc hydroxide buil up. However the found that, silane related ZnO is desirable in UVA/UVB sunblock applications.

Organic-inorganic nanocomposites are integrating important advantages in recent years. However to ensure the small size of the inorganic particles homogenous dispersion in the matrix is important since these nanoparticles tends to aggregate due to their high surface energies. Tang et al. (2008) studied on PVC- ZnO nanocomposites with 3-methacryloxypropyltrimethoxysilane (MPS) for modification of nano ZnO. MPS is an organic molecule chain, which can fulfill steric hindrance between inorganic nanoparticles and prevent their aggregation. Moreover, the nano-ZnO surface possesses a close affinity with the polymer matrix and can improve the properties of nanocomposites. The ZnO nanoparticles mixed with ethanol solution of MPS under ultrasonic mixing at room temperature and the mixture was heated to reflux for 4h. Then the mixture was cooled down and diluted with 2-propanol and centrifuged. The slurry dried at 40 °C in vacuum. Figure 2.5 shows the hydrolysis of MPS onto ZnO surface.

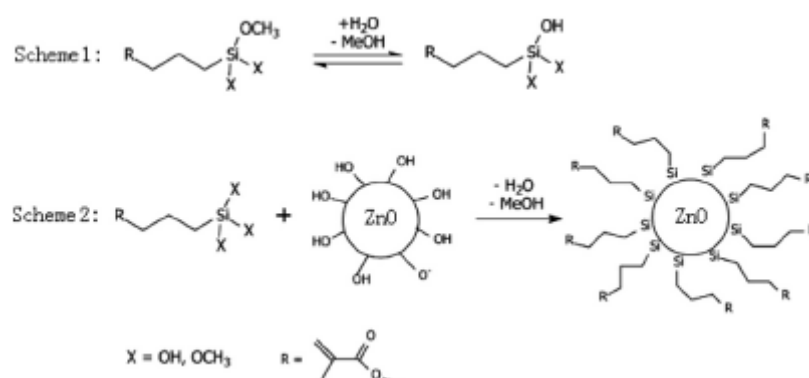


Figure 2.5. Grafting of MPS onto the ZnO nanoparticles (Source: Tang et al., 2008).

Scheme 1 shows the hydrolysis of MPS. Scheme 2 shows that MPS is grafted onto the surface of nano-ZnO. “The end group of MPS is an organic molecule, which can fulfill steric hindrance between inorganic nanoparticles and prevent their aggregation”. The grafting characterization was done using FTIR spectroscopy the peak at 1100 cm⁻¹ is assigned to the Si-O groups. The absorption peaks in the range 2800–3000 cm⁻¹ correspond to the CH₂ and CH₃ group of MPS. This demonstrates that MPS molecules are grafted on the surface of zinc oxide nanoparticles. The surface of nano-ZnO was treated with silane coupling agent (MPS) to obtain perfect compatibility with

organic polymer. FE-SEM analysis results showed that, ZnO nanoparticles could be homogeneously dispersed into PVC matrices. MPS molecules make ZnO nanoparticles integrate with PVC matrices (Tang et al., 2008).

Multiwalled carbon nanotube (MWCNT) polyimide (PI) composites were studied by modification MWCNT using (3-aminopropyl)triethoxysilane. The surface electrical resistivity of the MWCNT-PI composites drops 10^{15} ohm/cm² to 10^6 ohm/cm² after addition of 7 vol% MWCNT. APTES modified composite increases the surface resistivity of composite to the order of 10^{10} after 7 vol% MWCNT addition. TEM micrographs shows that MWCNTs may connect to each other in the PI matrix, MWCNT network and PI molecules may interpenetrate the crosslinked MWCNT network.

CHAPTER 3

ELECTRICAL AND THERMAL CONDUCTIVITY

3.1. Electrical Conductivity

Electrical conductivity was ability of a material to conduct electric current. An electrical potential difference was applied in a material and its movable charges tend to flow and cause a raise in the electric current. Electrical conduction requires that, electrons be able to gain energy in an electric field. In materials, like metals the current is carried by electrons (electronic conduction). In ionic crystals, the charge carriers are ions (ionic conductivity). The electrical conductivity is defined as the inverse of the resistivity.

According to their conductivity, materials may be classified into three broad categories; insulators, semiconductors and conductors. The electrons within the ground state have unfilled energy levels (in the upper part of the conduction band) in response to an electrical or other field can move into upper conduction level and give rise to conduction. This is the situation in conductors such as metals. The semiconductor band structure of conducting polymers allows electronic excitation or electron removal/addition from the valence to the conduction band (Ceylan, 2003).

Conductivity was the product of two important factors. The first is the number of carrier electrons or holes and second the carrier mobility, and defined as the ease with which a carrier moves through a material. The conducting fillers have a distribution within the polymer matrix. If the mean distance between conducting particles was large, for very low filler fractions the polymer matrix limits the conductivity. When the filler concentration becomes greater than a critical concentration, the resulting composites become conductors. At this point an electron can travel through the disordered network of fillers. A sharp transition in conductivity with the filler content had been observed, which means a sudden change in the dispersal

state of the conducting particles. When sufficient amount of filler was loaded to the system, the filler particles undergo aggregation or coagulation to form linkages (or conducting networks), which electrical conduction can travel throughout the composites. Higher mobilities would come with more crystalline, better oriented, defect free materials/polymers (Sethi and Goosey, 1995; Flandin et al., 2001).

The electrical conduction in composite systems contains a complicated network of conducting and insulating phases. The arrangement of filler particles and electrical conductivity could be determined either by, percolation in a continuous conducting network or by effective medium theories (Toker et al., 2003; Tang et al., 2004). Polymer composites filled with conductive filler particles were of interest for many researchers due to the characteristic of composites arises to electrical characteristics close to the fillers. The primary application area of conductive composites includes conductive coatings, electrostatic dissipation, electromagnetic shielding and housing for business machines. The composites should have an electrical conductivity in the range of 10^{-12} and 10^{-8} S/cm for electrostatic dissipation applications, 10^{-8} and 10^{-2} S/cm for moderately conductive applications 10^{-2} S/cm and higher for shielding applications if the composites were aimed to used of conductive applications (Clingerman, 2001; Weber, 2001; Struempfer and Glatz-Reihenbach, 1999).

In the many fields of engineering polymeric composites filled with conductive particles are of interest. This interest arises from the electrical characteristics of such polymeric composites were close to the properties of metals/semiconductors (filler) and the mechanical properties, processing methods were behave like for polymer. Electrical conductivity values for some of the materials were given in Figure 3.1. The factors that affect the electrical conductivity of filler (metal/semiconductor)-polymer composites include type of fillers, the particle shape, size, content (concentration) of the filler particles, pretreatment of conductive material, crystallinity of the polymer matrix, processing techniques, mixing rate and the thickness of the conductive film (Xue, 2005; Flandin et al., 2001, Mamunya et al., 2002a).

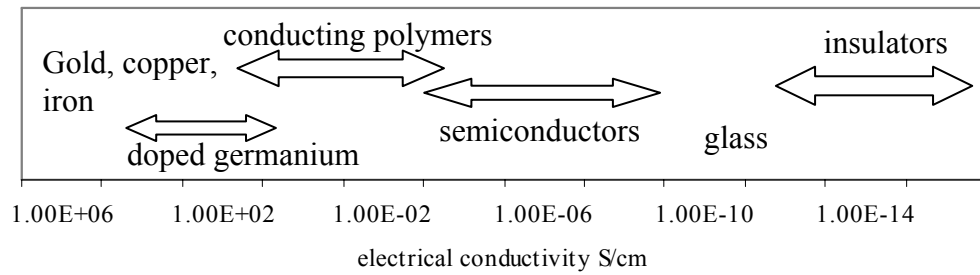


Figure 3.1. Electrical conductivity values of different materials (Source: Ceylan, 2003).

3.1.1. Static Electricity

Static electricity was defined as imbalance of positive and negative charges. These inequalities can be generated by separation or friction of two materials or through induction processes due to contact with ionized air. Static electricity could generate by touching two objects and then separating them, because of contact electrification effect. Usually, substances that didn't conduct electricity (insulators) were good at holding a surface charge and friction between two objects generates a great amount of static electric effect because of the many instances of contact and separation. The charge that was transferred in static electricity is stored on the surface of each object. Electrostatic charge; occur whenever positive and negative electric charges were held apart from each other. "Static electricity" was not charges at rest; it was opposite charges which were separated, or imbalanced (Maki et al., 2004; Grob and Minder, 1999).

To avoid the static electricity there are a lot of method. Adding an antistatic agent, loading conductive filler (carbon black, metal powder, metal oxide, or inorganic salt), mixing with a hydrophilic polymer or conductive polymer, coating of an antistatic agent on the surface of polymeric material, plasma, flame or corona treatment to the composite, and conductive coatings or metal deposition are some of the methods increased the antistatic ability of the material (Zhou and Pengsheng, 2003). Once the static electric charge had built up dissipation of the charge was depend on the nature of the materials that involved and the surrounding conditions. Polymers are strongly affected by the static electricity phenomenon, mainly due to the fact that they have very high volume resistivities in the range of 10^{14} - 10^{18} Ω -cm and therefore they are good

insulators. In industrial applications the static electricity problem could cause serious problems for example; If a combustible fluid was flowing through a polymeric pipe, and due to the frictions (increasing static electricity) fire or explosion could be obtain. (Maki et al., 2004; Grob and Minder, 1999).

The classical antistatic agents were in general “soap like” molecules with a hydrophobic and a hydrophilic part (fatty acid esters, ethoxylated amines, phosphate esters, etc.), they tend to migrate to the surface by attracting a layer of water, enhance the only the surface conductivity. Such products were easy to apply but have some important drawbacks: they give no volume conduction (only surface conduction), and generally after a while the antistatic agent easily removed and washed out, consequently limiting their effect over time. Permanency was an essential property in many applications for polymer composites as well. When it was required, addition of conductive fillers (carbon blacks, metallic fillers or carbon fibers) can be a good choice. (Li et al., 2004).

3.1.2. Electrical Conductivity in Polymer Composites and Percolation Theory

To describe the electrical resistivity in composite materials generally effective media and percolation theories were used. The percolation theory was firstly mentioned by Hammershley and Broadbent. They show “how the random properties of a medium influence the spread of fluid through it” (Clingermann, 2001).

In the polymeric environment, when the concentration of conductive fillers exceeds to a certain critical value, the conductive particles can connect each other to form conductive paths. At low conductive filler concentrations, when the conductive filler particles were "no contact" between them, the composite remains an insulator although its dielectric properties may change significantly. The increase of the conductive filler concentration and the conductive filler particles, in the polymeric matrix results electrons to travel in the polymeric gap in between the conductive particles (allowing current to flow) i.e., "hopping or tunneling effect". The ability of an electron to jump a gap, under a given voltage field, increases exponentially with decreasing distance of separation between

particles this is called interparticle distance as well. As depicted in Figure 3.2 the conductive filler concentration was increased further, the conductive particles start to contact physically each other, and a continuous network was obtained. The sharp drop in resistivity was achieved through the generation of a continuous network, which was defined as a "percolation" condition. This was called the critical volume fraction for that filler in the system or percolation value. At this point the resistivity will decrease dramatically; and this phenomenon can be explained by the percolation threshold (Xue, 2005; Flandin et al., 2001; Lo et al., 2001).

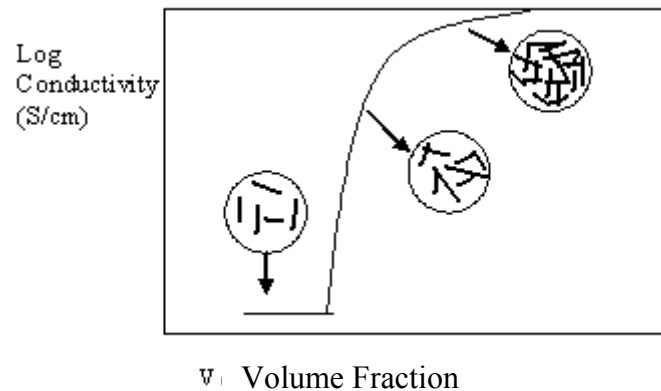


Figure 3.2. Schematic sketch of the resistivity of a composite as a function of filler (Source: Clingermann, 2001).

Generally two types of percolation are taken into consideration and they are site or bond percolation. Site percolation was assumed that the lattice sites were randomly filled until a continuous path was formed; continuity was assumed when neighboring sites were filled. In the bond percolation, lattice sites were filled but all sites in a lattice were occupied but are either disconnected or not. In real systems, it is thought that both site and bond percolation is observed. Percolation theory is often limited to the cases in which the insulating medium has zero conductance or the conducting filler has zero resistance (Struempfer and Glatz-Reihenbach, 1999; Weber and Kamal, 1997).

Effective media theory was studied in a spherical or ellipsoidal grain enclosed by a mixture which has conductivity of the composite medium. This theory generally applied to composite system which was predict and explain large volume average values of electrical thermal and diffusion properties. For effective media there were

symmetric and asymmetric cases. The symmetric case assumes that all space was filled by a random mixture of spherical (or ellipsoidal) particles of two or more components. When one component was a perfect insulator, the symmetric media theory contains a conductor-insulator transition. In the asymmetric case, the surface of the particles of one component was always completely covered by the other component. The modern effective medium theory was limited to the dilute cases (Weber and Kamal, 1997; McLachlan, 1987; Cai et al., 2006).

When the ratio of the conductivities of two components of binary disordered mixture (conductor-insulator) was not very small (conductivity of insulator/conductivity of filler) the conductivity of continuum media can be described by an effective media theory. But, when this ratio was very small ($\sigma_i/\sigma_c \leq 1$), conductor-insulator systems, especially near critical percolation threshold, were described by percolation theory. Thus, the percolation theory has been applied for describing the conducting behavior of percolating systems. But the percolation theory has two deficiencies; the first one is the theory which is applicable when the property difference of components is fairly significant. Second one is no clear correlation was found due to the real features of microstructure. McLachlan and co-workers developed the general effective media theory in order to describe the conductivity of conductor-insulator composites. Generalized effective media (GEM) equation was derived as an interpolation between the symmetric and asymmetric effective media theories and had the mathematical form of a percolation equation within the appropriate limits $\sigma_i/\sigma_c \neq 0$ as a function of volume fraction and critical percolation threshold (McLachlan, 1987; Bhargava, 2006; Struempfer and Glatz-Reichenbach, 1999; Wu and McLachlan, 1997).

The process of charge carrier transport can be divided into two steps in percolation process, charge carriers transport through the material could be obtained by hopping, tunneling, ballistic transport, diffusion, or metallic conduction. While charge carrier transport could take place, conduction in the polymer matrix, filler material, adjacent filler particles and from the filler into the matrix and vice versa these four different types of parameters were taken into consideration. The conditions is true for very low filler loading, below the percolation threshold value, the interparticle distance between the filler particles was large and no conduction phase was observed. And the mean separation distance of next adjacent particle was large and also tunneling could not observe. Therefore the loading has at low fields little effect on the electrical conductivity of the composite. For the conditions, if the interparticle distance between

the filler particles were still separated, but below the certain threshold value, the electric field transport by tunneling between neighboring filler. The conductivity was thus determined by the properties of the polymer, filler material, interface between two materials and, of course, by the dispersion of the filler material in the polymer. At sufficiently high loading, the conducting particles were in close contact, touching each other so charge carrier occurs through the continuous structure of the filler particles in the polymer matrix. The conductivity was determined by the filler material (Struempfer and Glatz-Reichenbach, 1999; Liang and Yang, 2007; Clingermann, 2001).

The percolation theory was originally developed for spherical particles, thus having limited validity for rod-like fillers. This critical filler content has been predicted to be 16 vol% for randomly oriented spherical particles. Rod-shaped particles (e.g. chopped carbon fibres, carbon nanofibres and nanotubes), having high aspect ratio, l/d greater than 1. An advanced percolation theory has been developed by Celzard et al. (1995, 1996 and 1997), which includes the aspect ratio of particles in determining the critical volume fraction which requires to achieve a conducting, percolated network. The percolation threshold of rod-like particles with aspect ratios of >100 , was calculated to be 0.24–1.35 vol% (Celzard et al., 1995; Celzard et al., 1996; Celzard et al., 1997).

Most composite conductors were made up conducting particles suspended in an insulating matrix. Particle contact requires 10 to 30 vol% conductor at the percolation threshold when the metal and insulator grains were comparable in size. But when the metal grains were much smaller, they are forced into interstitial regions between the insulating particles and into contact with one another, which results in a lower percolation threshold (3 to 10 vol%) (Mc Lachlan et al., 1990).

Psarass et al. (2003) studied on bisphenol type epoxy resin as a matrix and various amounts of iron powder were added for the production of composite. They reported that; polymer systems were essentially insulating materials and thus can be polarized as a response to an applied electrical field. Near the glass transition temperature the segmental mobility of the polymer was enhanced and the orientation of large parts of the molecular chains was facilitated. At lower temperatures, relaxations occur due to the orientation of smaller polar groups such as side groups or local segments of chains. However, the presence of conductive inclusions was critically changing the situation. Pinto and Martin (2001) investigated aluminum filled nylon 6 composites conductivity. The electrical conductivity was determined since the resistance values that were measured using a two point arrangement. In order to

decrease the contact resistance, the sample surfaces were coated with silver paint. The percolation threshold value increased with a decrease in aspect ratio of the filler and the electrical conductivity of the composites increases eleven orders of magnitude as it's compared with pure polymer. Zhou et al. (2003) studied on zinc oxide whisker (ZnO_w) shown in Figure 3.3. ZnO_w is a new kind of micro-fiber with single crystal, tetra-needle shaped; possesses good comprehensive properties such as high strength, semi conductivity, wear resistance, vibration insulation, microwave absorption and antibacterial effect The zinc oxide whisker was mixed with polyurethane and PVC to prepare composites.



Figure 3.3 SEM picture of ZnO
(Source: Zhou et al., 2003).

The authors found that; the tetrapod-shaped ZnO whisker was an effective additive for lowering the electrical resistivity of polymer materials. A formula of critical volume fraction of ZnO whisker for the formation of conducting paths of the polymer/ZnO_w composites has been put forward, and the critical volume fraction is mainly determined by the aspect ratio of whisker, and the effects of overlapping, covering and breaking also play important roles in actual situation. The charge concentrating effect at the pinpoint of the whisker and the tunnel effect may exist and cause the result in lowering electrical resistivity of the composites (Zhou et al., 2003).

Zhou et al. (1999) find that ZnO whisker that appeared to have excellent advantage of decreasing the reflection of microwaves. Vibration damping was absorbed by transmitting the energy of vibrations through a material as heat energy using deformation of that material.

Lü et al. (2007) prepared nano-ZnO/polymer composite films with different concentration of ZnO. Nano ZnO was put into monomer mixtures of urethane-methacrylate oligomer and 2-hydroxyethyl methacrylate, followed by ultraviolet (UV) radiation-initiated polymerization. The colloidal ZnO nanoparticles with a diameter of 3–5nm were synthesized from zinc acetate and lithium hydroxide in ethanol via a wet chemical method. The ZnO nanoparticles were uniformly dispersed in the polymer matrix no aggregation was observed, which contributed to the high transparency of the nanocomposites. The researchers found that, these composite film materials have the potential to be used as UV absorbance and luminescence films in the design of optical coatings.

ZnO and low density polyethylene (LDPE) nanocomposites were prepared to determine the effect of filler particle size on permittivity of the composites. The small particle size of ZnO nano particles did not affect the permittivity of the composite. The interfaces between ZnO and LDPE do not appear to contribute dielectric properties and permittivity as well. When the filler homogenously distributed in the composite, the ZnO/ZnO interface formed by touching neighboring particles, which possessed dipole moment to increase the permittivity (Hong et al., 2006b).

Hong et al. (2003) studied the electrical resistivity of LDPE composites. They studied with nanosized and micron sized ZnO. The measured dc resistivity of the nano composite was given in Figure 3.4 and resistivity began to decrease after 14 vol% additions of ZnO and the percolation threshold value is obtained when the concentration reached to 30 vol%. The neat polymers electrical resistivity was given as 10^{19} ohm-cm. At 40 vol% ZnO concentration the measured volume resistivity was found as 10^{11} ohm-cm for nanopowder, and as 10^{17} ohm-cm for micron sized powder. As a consequence they found that the electrical conduction is due to tunneling between ZnO-ZnO filler particles.

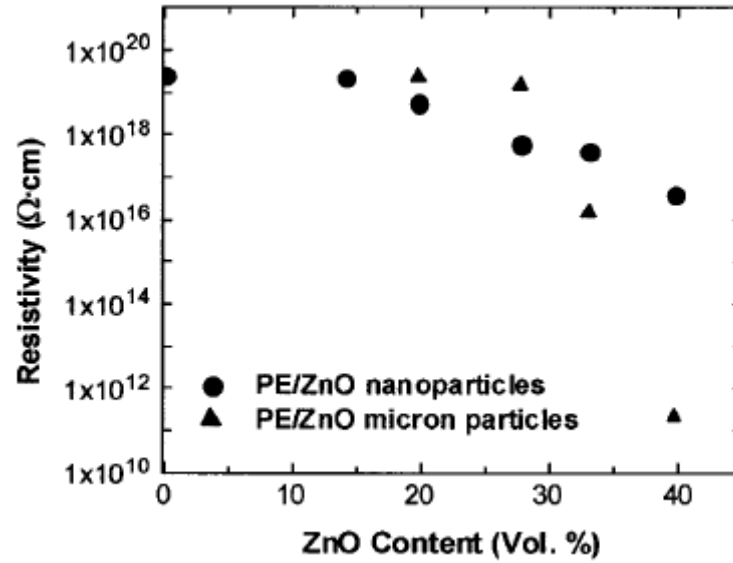


Figure 3.4. DC volume resistivity of nanocomposites measured at 10 kV/cm. as a function of ZnO content (Source: Hong et al., 2003).

Hong et al. (2003) discussed the interparticle distance as given in Equation 3.1. In Equation 3.1 the assumption is, spherical shape particles with a uniform size distribution and dispersion.

$$l = r \left[\frac{4\pi}{3\nu} \right]^{1/3} - 2 \quad (3.1)$$

Using the Equation 3.1 calculations was done and found that, the interparticle distance for the nanocomposite which was loaded 30 vol% of micron size particles was approximately 40 nm. When the average interparticle distance becomes less than a certain critical value, the conduction between particles can be observed and resistivity decreases. When the particle size of the filler decreases, the interparticle distance will be smaller at that volume fraction.

Fleming et al. (2008) studied on conductivity of ZnO-LDPE composites for nano and micron sized ZnO particles. The ZnO powders were pretreated with a hyperdispersant based on carboxylic acid functionality. The dc conductivity measurements were done by applying 10 and 20 kV/mm potential voltage. According to Fleming et al. (2008), the crystalline PE has a negative electron affinity, and electron transport will occur mainly through amorphous region. The influence of nano ZnO on

conductivity would be exerted only in amorphous region as well. Micron sized ZnO particles has little effect on DC conductivity and nanosized particles increase it by 1-2 orders of magnitude. This decrease is probably due to reduction carrier mobility in the amorphous regions of the sample.

Fleming et al. (2008) compare their results with Hong et al. (2003). Beyond threshold value a rapid increase was expected in conductivity and found at the study of Hong et al. paper and the authors suggested the increasing conductivity is due to tunneling between ZnO particles. Possible reason for the difference between results of two different study should be the current increase rather than nano particle addition or much larger electric field were applied to the system by Fleming et al. (2008).

Hong et al. (2006b) studied again ZnO particles and LDPE composites. For comparing the particle size affect three different powders, micron sized (300 nm) and nanosized (49 and 24 nm) were used as filler. For comparing the polymer matrix effect powder and granule formed matrix were used. The percolation limit decreases as the particle size decreases. When the interparticle distance decreases below 40 nm tunneling begins to occur. Due to decrease in interparticle spacing at a given volume fraction, the percolation onset should occur at a lower volume fraction as particle size was decreased. The neat polymer volume resistivity was 10^{19} ohm-cm and the lowest volume resistivity found was 10^9 ohm-cm for 24 nm powder at above 30 vol%. The difference between two sets of samples was given in Figure 3.5.

If a composite has a homogeneous distribution of filler particles, the electrons can tunnel between particles and through the insulating matrix. The tunneling does not decrease the resistivity significantly. As the concentration increases, conduction paths composed of touching ZnO particles and extending through the entire composite, and the resistivity drops rapidly. In the composites with inhomogeneous filler distributions, electron paths were obtained by touching particles. However resistivity of the composite was determined by the combination of these two competing effects. At high enough filler concentration, all of the samples exhibited the same sharp drop in resistivity with filler concentration, which was indicative of a conduction mechanism through touching ZnO particles (Hong et al. 2006b).

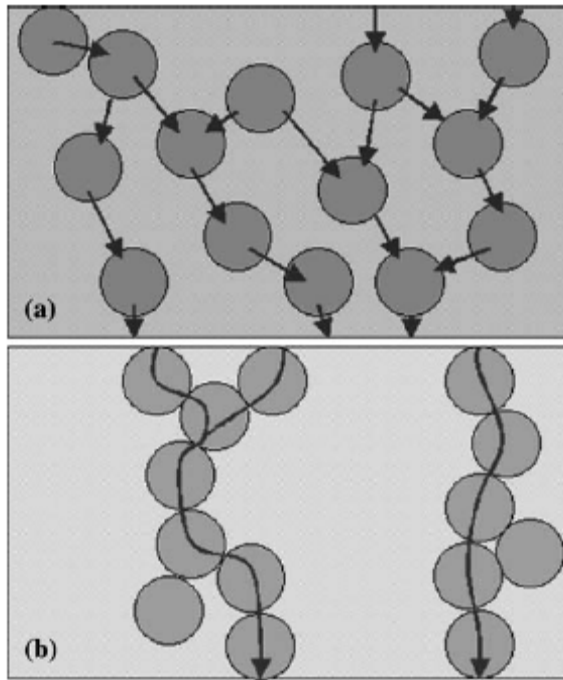


Figure 3.5. Conduction mechanism for composites a) Homogenous distribution of fillers b) Un-homogenous distribution of filler (Source: Hong et al., 2006b).

Using melt mixing process LDPE/ZnO composites were prepared by Tjong and Liang (2006). ZnO powders were 200 nm and 2 micron in particle size. The resistivity of neat LDPE was found $2.5 \cdot 10^{11}$ ohm-m and with 60 vol% nano ZnO addition the resistivity reduces to $0.3 \cdot 10^{11}$ ohm-m. On the other hand, the resistivity of LDPE/ZnO micro composites decreases slightly with the addition of 18 vol%. Above this concentration the resistivity decreases sharply so can be explained by percolation threshold value. The difference in percolation threshold was described by interparticle distance and assumed that filler particles were dispersed uniformly and arranged in a cubic lattice. The interparticle distance calculated was in the range of 75-842 nm when the interparticle distance between particles was lower than the critical value conduction occurs with tunneling and cause to decrease resistivity value.

3.1.3. Factors Affecting the Electrical Conductivity of the Composites

Normally the composite property was expected to fall between those of the matrix and filler and highly depends on the properties of the matrix and filler. Zinc oxide when used as filler it's a semiconductive material with a electrical resistivity of 10^9 - 10^2 ohm-cm. There were many crystal shapes of zinc oxide obtained for many application area given in the literature some of them are rod shaped some of them fiber shaped and they possesses different properties. The value for the filler electrical conductivity would be the upper limit for the electrical conductivity of the composite.

Another important parameter affecting the electrical conductivity of the composite was the particle shape and the particle size of the filler. To have a lower percolation threshold value it was expected to lower the particle size will increasing the surface area and probability of conductive network will increase. The same result was true for the aspect ratio the greater the aspect ratio the smaller the percolation the schematic presentation of this phenomenon was given in Figure 3.6. It was important to choose the right filler for the appropriate properties of application (Bigg, 1977; Taya, 2005; Krueger, 2002).

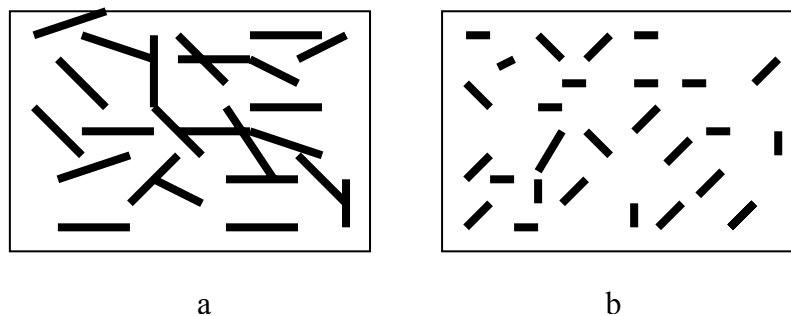


Figure 3.6. Diagram of filler in the polymer matrix with different aspect ratio a) high aspect ratio b) Low aspect ratio (Source: Krueger, 2002).

Conductivity depends on particle/particle contact, which was largely a particle surface phenomenon. For example, spherical particles have a geometric shape which allows for single points of contact between particles. Thus, high concentrations of

spheres were required to ensure continuous contacts between particles. Rod-shaped particles possess a geometric shape which allows for inter-particle contacts of the rods. Thus, conductive polymers of the invention provide a large surface area and require relatively less zinc oxide by weight for equivalent or better conductivity (Taya, 2005; Tchoudakov et al., 1996).

For higher conductivity the properties of polymer should be more crystalline, better oriented and defect free. The important parameters for the polymer was; the rheology of the polymer during mixing process, the crystallinity of the thermoplastic matrix, the wettability of the filler particles for the polymer, the cooling process of the melt polymer matrix. (Lux, 1993).

Processing conditions was another important parameter for the conductivity of the composites. For example during extrusion and injection molding of a composite can align fillers that have an aspect ratio greater than one due to the flow throughout the machine or mold. This alignment will produce anisotropic conductivity within the sample, this means conductivity will be greater in one direction over another (Lux, 1993; Tang et al., 2004).

The surface properties of the filler have a significant effect on the conductivity value. Surface free energy between filler and matrix will influence the interaction between two materials and how well the polymer wets the surface of the filler can be quantified by difference in surface energies. Smaller difference in surface energies leads better wetting between polymers and the filler and also better wetting improve well dispersion in the matrix (Clingermann, 2001).

Tang et al., (2004) described how zinc oxide nanoparticles coated with organic nucleating agents affect the morphology and crystallization temperature of isotactic polypropylene. Individual nanoscale-size particles of zinc oxide were approximately 40 nm, whereas agglomerated nanoparticles were 150 nm in length. The crystal structure of the isotactic polypropylene was unaffected by zinc oxide (Tang et al., 2004).

3.1.4. Electrical Conductivity Models

For the production of optimized conductive mixture; compounds showing sharp increase in conductivity at the smallest amount of conductive filler possible for mixture were the physical and chemical factors.

To understand the network formation there were lots of scientific models given in the literature. Lux (1993), classified the conductivity models in a four different systems. Statistical percolation model, thermodynamic percolation model, structure oriented percolation model, and geometrical percolation models.

Statistical percolation threshold model predicts the conductivity based on the probability of particle contacts within the composite. By computer simulation it was possible to predict the points and bands in a cluster. McLachlan (1990), proposed the model which was takes probability of connection. In this model general effective media theory was used for analyzing the electrical resistivity of the composite. McLachlan suggests this model for conductive particles in an insulating matrix. The goals of the modeling study for McLachlan to determine what factors were critical in controlling conductivity values and to be able to accurately predict and explain the results. The model equation was given in Equation 3.2 and it describes the conductivity (resistivity) of a wide variety of binary mixtures as a function of the conductivities of the component, the volume fraction of each parameters.

$$\frac{(1-\Phi)(\rho_m^{1/t} - \rho_h^{1/t})}{\rho_m^{1/t} + A\rho_h^{1/t}} + \frac{\Phi((\rho_m^{1/t} - \rho_l^{1/t}))}{\rho_m^{1/t} + A\rho_l^{1/t}} = 0 \quad (3.2)$$

In Equation 3.2, Φ was the volume fraction of the filler, A found from the critical percolation threshold value from $A=(1- \Phi_c)/ \Phi_c$, ρ_m , ρ_l , and ρ_h was given as resistivity of component, polymer and filler respectively and t was the critical exponent. The equation, was valid for all volume fractions, and is shown to fit a large variety of experimental data very well. The critical exponent ranges between 1.5 and 3.1. The value of t was varied within these ranges to obtain and determine the sensitivity of the model calculations with changing parameter (McLachlan,1987; McLachlan; 1990).

As t is increased, the calculated conductivity was decreased by up to several orders of magnitude. In order to accurately predict the conductivity using this model, it was important to pick the correct value for t unless this will lead to significant difference between expected conductivity values and experimental values (Clingerman, 2001).

In this model the conducting particle shape and spatial distribution and their connectivity and percolation was characterized by the volume fraction and exponent t as well. According to McLachlan, to have a more realistic model to finding the critical volume fraction (percolation threshold) should be in a function of pressure (McLachlan, 1990).

Thermodynamic model predicts the conductivity value, based on interactions between the polymer and filler material, using interfacial tension and the surface energies of each species. This model emphasizes the importance of interactions between polymer and the filler for the network formation and interprets the percolation as a phase separation process. Mamunya et al. (1995; 2002b), studied the percolation theory, used extensively predicts a conductivity (σ) dependence of the form of Equation 3.3.

$$\sigma = \sigma_0 \cdot (P - P_c)^t \quad (3.3)$$

where, σ is the electrical conductivity of the composite, σ_0 is the electrical conductivity of the conductive filler particles, P is the volume fraction of the conductive fillers, P_c is the volume fraction of conductive filler at the percolation threshold. The first equation is valid only very near to the percolation threshold. Following the normalized percolation equation proposed by Mamunya et al. (2002b), the variation of electrical conductivity with the filler volume fraction can be described by Equation 3.4 to Equation 3.6 below.

$$\sigma = \sigma_c + (\sigma_m - \sigma_c) \cdot \left(\frac{\phi - \phi_c}{F - \phi_c} \right)^k \quad (3.4)$$

$$K = A - B\gamma_{pf} \quad (3.5)$$

$$k = \frac{K\Phi}{(\phi - \phi_c)^{0.75}} \quad (3.6)$$

When the volume filler fraction σ reaches a critical value σ_c (percolation threshold), an infinite conductive cluster (IC) is formed and, consequently, the composite becomes conductive. One of the most important characteristics of the filler polymer composite is the filler packing factor F . The value of F depends on the particle shape and on the possibility of the skeleton or chained structure formation. The parameter F is a limit of system filling and equal to the highest possible filler volume fraction at a given type of packing as given in Equation 3.7.

$$F = V_f / (V_f + V_p) \quad (3.7)$$

where V_f is the volume occupied by the filler particles at the highest possible filler fraction and V_p the volume occupied by the polymer (space among filler particles). For statistically packed monodispersed spherical particles of any size, F is equal to 0.64.

This model fits well with the experimental value and experimental data for polymer carbon black, however not extended to include other types of filler.

Mamunya et al. (2002b) showed that the percolation threshold value depends on the particle shape and on the kind of the spatial distribution of the particles and it's connected to F . Due to absence of polymer-filler interactions, a linear relationship is observed between the percolation threshold and the packing factor, $\phi_c = X_c F$. The critical parameter X_c was found experimentally to be $X_c = 0.17$. Pressing the mixture of polymer and metallic powders having particle sizes D and d , respectively (assuming $D \gg d$), allows the formation of a shell structure having a low percolation threshold value.

Geometrical percolation models explain the system with conductive particles which was dry mixed and/or sintered. Model predicts the insulating material forms regular cubic particles where the conductive particles locate in a regular arrangement on the surface of the polymeric material. The main parameter was diameter of the conductive particles (Lux, 1993; Clingerman, 2001).

McLachlan model was statistically predicts the conductivity well also include some parameters implies the geometry size and shape of the conductive particles. And this model can accurately predict the conductivity for a wide range of systems and is valid for all volume fractions.

Structure oriented model was based on, the composite mixture which was prepared by compression moulding technique. This preparation technique was one achieves the lack of an inhomogeneity in distribution of conductive phase. Nielsen was proposed a model based on structure oriented percolation; and development accounts for the geometry of the filler particles and provides good predictions of thermal conductivity at higher volume fractions of the filler loading. However this theory has been shown to be invalid for predicting the electrical conductivity of polymer-metal composites. This is due to difference in two conductivity mechanism (thermal-electrical). Electrical conductivity is related with the flow of free electrons and requires a continuous path (Bigg, 1977).

Pal (2007) was developed a new model to understand the particulate filled materials electrical behavior which the filler have nearly isomeric (same dimensions in all direction). The existed equations fail to predict the right behavior when $\Phi \rightarrow \Phi_m$ where Φ_m is the maximum packing volume fraction of the particles where the particles touch each other. When λ (electrical conductivity of filler / electrical conductivity of matrix) $\rightarrow \infty$ the electrical conductivity of a composite is expected to approach infinity at $\Phi \rightarrow \Phi_m$. Maxwell prediction for infinitely dilute composites was given in Equation 3.8.

$$\frac{\sigma}{\sigma_m} = 1 + 3\alpha \left(\frac{\sigma_d - \sigma_m}{\sigma_d + 2\sigma_m} \right) \Phi \quad (3.8)$$

where; α is a correction factor, σ , σ_m , and σ_d were the electrical conductivities of composites, matrix and filler respectively and Φ is the volume fraction.

Maxwell equation cannot be applied at finite concentration of particles. To extend the applicability to concentrated system effective medium theory was used. According to effective medium theory a concentrated composites was considered to be obtained by the addition of small quantities of particles to the system until the final volume fraction of the filler was reached.

According to the Maxwell equation the incremental change in the conductivity can be explained by the addition of infinitesimally small quantity of particles $d\Phi$. Pal (2007) described the model to the assumption of all the volume of the existing composite, is available as free volume to the new particles. When differential quantities of new particles were added to the composite the actual volume fraction of the dispersed

phase was larger than $d\Phi$. The increase in the volume fraction of the dispersed phase called as “crowding effect” caused by packing difficulties of particles and the equation was derived for concentrated suspension as given in Equation 3.9;

$$\left(\frac{\sigma}{\sigma_m}\right)^{1/3} \left(\frac{\sigma_d - \sigma_m}{\sigma_d - \sigma}\right) = \left(1 - \frac{\phi}{\phi_m}\right)^{-\alpha\phi_m} \quad (3.9)$$

For conducting particles dispersed in conducting matrix such that $\lambda \rightarrow \infty$ given in Equation 3.10.

$$\sigma_r = \left(1 - \frac{\phi}{\phi_m}\right)^{3\alpha\phi_m} \quad (3.10)$$

For insulating particles dispersed in conducting matrix such that $\lambda \rightarrow 0$ given in Equation 3.11 (Pal; 2007).

$$\sigma_r = \left(1 - \frac{\phi}{\phi_m}\right)^{3\alpha\phi_m/2} \quad (3.11)$$

Pal (2007) studied with 16 different experimental data. Some of them are; aluminum matrix filled with alumina particles, nylon 6 matrix filled with zinc powder, polyethylene matrix filled with graphite particles. All the experimental data sets can be described well using the α values in the range of 0.867-1.03.

3.2. Thermal Conductivity and Thermal Conductivity in Polymer Composites

Thermal conductivity can be defined as the quantity of heat transmitted in unit temperature gradient, and unit time under steady state conditions in a direction normal to a surface of unit area which is a bulk property of material. The heat transfer is the only dependent parameter of heat transfer.

Radiation, convection and conduction are the three mechanisms of heat transfer. The conduction of heat is one of the fundamental property of solids. Equation 3.12 represents the Fourier Law for heat flow under non-uniform temperature explaining the macroscopic view of transporting mechanism (Incropera and De Witt, 1990).

$$h_i = -k_{ij} \frac{\delta T}{\delta x} \quad (3.12)$$

where h_i the heat is transfer, k_{ij} the thermal conductivity and $\frac{\delta T}{\delta x}$ is the temperature gradient defining the rate of heat energy flow per unit area. The thermal conductivity varying with temperature in real is assumed to be constant. Thermal conductivity which was calculated from the equation above did not include the electronic contribution and no net particle flow persisted in the system.

Some of typical thermal conductivity values were 0.2 to 0.4 for polymers, 234 for aluminum, 400 for copper, and 600 for graphite, 418 for silver and 990 for diamond (all values in W/mK) (King et al., 1999). 1.3 to 2 $\text{Wm}^{-1}\text{K}^{-1}$ for mechanical applications and 2 to 4 $\text{Wm}^{-1}\text{K}^{-1}$ for electronic applications was the thermal conductivity in the transverse direction of the plate. (Danes et al., 2003)

The design of power dissipating devices is been effected by semiconductors, like power transistors, solar cells, under strong sunlight diodes. Semiconductors which have low thermal conductivity devices can be used as thermoelectric devices (Srivastova, 2006). Potential applications of thermally conductive polymer composite's are heat sink, such as computer, and transformer housing. Thermal conductivity of 1-30 w/mK is the range of heat sink application polymer composites. (Weber, 2001).

Thermal conduction systems in polymers filled with high conductive particles varing with the volume content of particles are classified with two systems: 1. a system with low content of particles in which dispersed particles hardly touch each other (dispersed system) 2. a system with higher content, in which conductive chains were exponentially formed by particles and contribute to a large increase in thermal conductivity of a composite. Electron transport and lattice vibrations are the two different heat transfer methods existing in solids (Weber, 2001). Electron transport was the dominant mechanism for pure metals where lattice vibration was for dielectric and non metallic materials like polymers. Each atom positioned exactly at its lattice site

when the lattice is at equilibrium, supposing an atom displaced from its equilibrium site by a small amount. The force acting on this atom, affects it to return to its equilibrium position resulting its lattice vibration. Phonon transfer is the quanta of atomic vibrational mode and phonons which do not carry real physical momentum can interact with all particles existing in the system particles such as photons, neutrons and electrons. The reason of not having real physical momentum is the center of mass of the crystal do not change its position under vibrations. The transport energy propagating through the array in a manner similar to phonons by phonons can be simplistically imagined by exciting one or more atoms by twisting, pulling or pushing. (Weber, 2001; Gojny, 2006; Lee et al., 2006).

In crystal potential finite sample size, anharmonicity, static imperfections, and alloying and inhomogeneity provide the main phonon-scattering sources in nonmetallic solids. If a crystal is considered to be infinitely large, pure, has no imperfections, and is characterized by purely harmonic atomic vibrations at all temperatures the thermal conductivity of it is infinite. Thus, phonons of a purely harmonic crystal would transport all heat from the hot end to the cold end on the application of a temperature gradient. In another expression at all temperatures the thermal conductivity of a purely harmonic crystal would be infinite. However, real solids contain defects, are of finite size, and exhibit anharmonicity in atomic vibrations limiting the lifetime of phonons, rendering finite values of thermal conductivity. Experimental measurements are strongly dependent on conductivity. Intrinsic phonon-phonon of anharmonicity at finite temperatures interactions are inelastic in nature, because which makes the concept of phonon lifetime an intrinsically difficult. It could be evaluated theoretically if the concept to comprehend was not impossible. The lifetime of phonons is limited with each mechanism and anharmonicity increases the intrinsic relaxation time, in which other mechanisms produce extrinsic relaxation times (Srivastova, 2006).

Weber (2001) describes the filler/polymer composites thermal conductivity which is path dependent is a bulk property unlike electrical conductivity. In percolation threshold value the electrical conductivity raises about 10 orders of magnitude over a small range of concentration where the fillers get close enough to conduct current with little resistance. Thermal conductivity has a very gentle trend over the same range due to be the bulk property of thermal conductivity. (Weber, 2001).

A material is been affected by several important factor which are constituency (filler and matrix), crystallinity of the polymer, filler size, shape, concentration, degree

of mixing, orientation and bonding between filler and the matrix, defects and vacancies in the filler and conformational defects increasing the thermal conductivity (Kumlutaş and Tavman, 2006; Weber, 2001; Lee, 2006).

According to Lee et al. (2006) phonon scattering is a result of thermal resistance which has to be minimized to increase thermal conductivity. High thermal conductivities of materials can be obtained by fillers intrinsic thermal conductivity value. Despite when the intrinsic thermal conductivity of the filler is greater than 100 times of the polymer no significant improvement in the thermal conductivity could be obtained. The same pronunciation was given by Kumlutaş and Tavman (2006) the thermal conductivity of polypropylene with 30% addition of talc from 0.27 up to 2-5 W/mK. The same matrix material containing the same volume fraction of copper particles had a thermal conductivity of only 1.25 W/mK. However; the thermal conductivity of copper particles were approximately 40 times greater talc particles which is directly due to a complete interconnectivity achieved from talc particles in polypropylene while copper particles show a very poor interconnectivity. Agari and Uno (1985) studied with graphite filled polyethylene composites and found that the thermal conductivity of polyethylene- graphite composite increased forceless than the electrical conductivity, since the heat flows both through the formed conductive graphite chains and the polyethylene itself. Consequently, thermal conductivity was less influenced than the electrical conductivity.

In another point of view; the aspect ratio of the filler is more considerable that dictates the conductivities of a composite. Electron and phonon transfer leading to high conductivities form random bridges or networks from conductive particle facilitates. The properties of the polymer-nanoparticle interface can control thermal transport in the composite material for sufficiently small particles. Interface effects in thermal transport can be captured by effective medium models (Tavman, 1996; Lee et al., 2006).

3.2.1. Thermal Conductivity Models

Thermal conductivity is a bulk property and has similar analogous of viscosity, tensile modulus, and shear modulus. The effective thermal conductivity is an essential parameter that has to be known for designing composites and carrying out the performance analyses. The rule of mixture model and geometric model are two typical models used to predict the thermal conductivity of a unidirectional composite with continuous fibers which the simplest methods would be with the materials arranged in either parallel or series with respect to the heat flow.

According to Taya (2005) formerly an applied heat flux q_0 in the plane of lamellae, or longitudinal direction is considered as shown in Figure 3.7. In this case the temperature gradient in the longitudinal direction in each phase is constant and equal to that of composite seen in Equation 3.13.

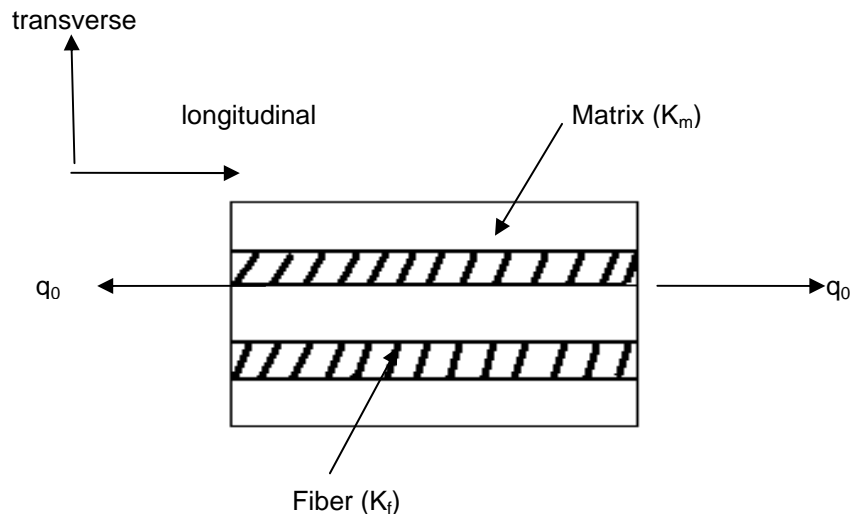


Figure 3.7. One dimensional composite model
(Source: Taya, 2005).

$$\nabla\theta_c = \nabla\theta_m = \nabla\theta_f \quad (3.13)$$

where, $\nabla\theta_i$ is the temperature gradient in the i^{th} phase in the longitudinal direction. For steady state heat conduction valid in each phase is represented in Equations 3.14 a-c.

$$q_o=q_c=k_c\nabla\theta_c \quad (3.14.a)$$

$$q_m=k_m\nabla\theta_m \quad (3.14.b)$$

$$q_f=k_f\nabla\theta_f \quad (3.14.c)$$

where, q_i and k_i are the heat flux and thermal conductivity of the i^{th} phase, respectively. For thermal conduction in the transverse direction, the composite plates transverse temperature gradient (the temperature difference between the top and bottom of the composite divided by the composite thickness) is the sum of the transverse temperature gradient in each phase multiplied by its volume fraction is represented in Equation 3.15 (Taya, 2005).

$$\nabla\theta_c = (1-f)\nabla\theta_m + f\nabla\theta_f \quad (3.15)$$

For two-component composites, the simplest consideration is: “the components are arranged in either parallel or series with respect to heat flow, which give the upper or lower limits of the effective thermal conductivity of composites”. The effective thermal conductivities estimated from the parallel and series models are expressed in Equation 3.16 and Equation 3.17, respectively (Zhang et al., 2005; Zhou et al., 2007).

$$k_e = (1-f)k_m + fk_f \quad (3.16)$$

$$\frac{1}{k_e} = \frac{(1-f)}{k_m} + \frac{f}{k_f} \quad (3.17)$$

where, k_e , k_f and k_m denote the effective thermal conductivity of the composites, thermal conductivity of the particle and the matrix, respectively, and f is the volume fraction of the filled particles. The maximum and minimum estimations for k_e were given with the parallel and series models. According to the volume fraction of each component the thermal conductivity was calculated by the effective thermal

conductivity of the composite, which is regarded as separate phases and neglects interactions between these phases. The minor phase affection is maximized by the separate contribution of the two phases to the thermal conductivity of the composite maximizes leading to an overestimation of the thermal conductivity by this model. Therefore, the thermal conductivity will be got in an upper bound with this model.(Gojny et al., 2006; Taya, 2005).

Filler matrix systems are been proposed with many models. The Maxwell Theoretical model which is the basis one was predicted for spherical, non-interacting particles in a continuous matrix and was not applicable to many systems since it was designed for non-interacting spheres in a homogenous medium for dilute systems. It was assumed that the composites have a periodic structure. Maxwell model is depicted in Equation 3.18. where K is the thermal conductivity of the composite, ϕ is the volume fraction of the matrix and filler. The Subscripts 1 and 2 indicate pure polymer and filler, respectively (Zhang et al., 2005; Tavman, 1996; Zhou et al., 2007).

$$K = k_1 \left[\frac{k_2 + 2k_1 + 2\phi_2(k_2 - k_1)}{k_2 + 2k_1 - \phi_2(k_2 - k_1)} \right] \quad (3.18)$$

Thermal conductivity of a two phase system calculated from Nielsen Model gives more accurate results in the literature which is predicted for polymer and a filler. Equation 3.19.a-c represents the Nielsen model (Nielsen, 1974).

$$\frac{K}{k_2} = \frac{1 + A.B.\phi_2}{1 - B.\psi.\phi_2} \quad (3.19.a)$$

$$B = \frac{\frac{k_2}{k_1} - 1}{\frac{k_2}{k_1} + A} \quad (3.19.b)$$

$$\psi \cong 1 + \frac{1 - \phi_m}{\phi_m^2} \cdot \phi_2 \quad (3.19.c)$$

In Equation 3.19 a-c K is the thermal conductivity of the composite and k_i is the thermal conductivity of an individual component. The subscript 1 and 2 represents

polymer and filler, respectively. “A” takes into account the geometry of the filler; in instance the aspect ratio which can be calculated by “ $A=1+k_e$ ”. k_e is the Einstein coefficient. The constant A related to the shape and orientation of the dispersed particles. ϕ_m is the maximum packing fraction of the dispersed particles. For randomly packed spherical particles $A=1.5$ and $\phi_m=0.637$, whereas for randomly packed aggregates of spheres or for randomly packed, irregularly shaped particles $A=3$ and $\phi_m=0.637$ (Tavman, 2003; Nielsen, 1974; Bigg, 1977). McGee and McCullough (1981) studied with Nielsen model for natural silica and epoxy resins and the correlation of the results were determined for modulus by developing the “ ψ ” equation with modification of the Nielsen model instead of thermal conductivity and is given in Equation 3.20.

$$\psi = 1 + \frac{\phi_1}{\phi_m} (\phi_m * \phi_2 + (1 - \phi_m) * \phi_1) \quad (3.20)$$

where, ψ is the volume resistivity of the composite and Φ is volume fraction for subscript m denotes to the maximum packing fraction 1 and 2 denotes to polymer and filler fractions, respectively.

CHAPTER 4

OPTICAL PROPERTIES OF ZINC OXIDE AND POLYMER COMPOSITES

Light is a form of energy that exhibits both wave-like and particle-like properties. In other words, a photon is simultaneously both a wave and a particle. It is a form of electromagnetic radiation, with properties that arise from the electric and magnetic waves oscillating sinusoidally at right angles to each other. Figure 4.1 shows different photon energies expressed as wavelength in a spectrum. The waves clearly have a 'wavelength'. Light in the visible region of the spectrum is also characterized by its color, which is a straight forward function of its wavelength (Monk, 2004).

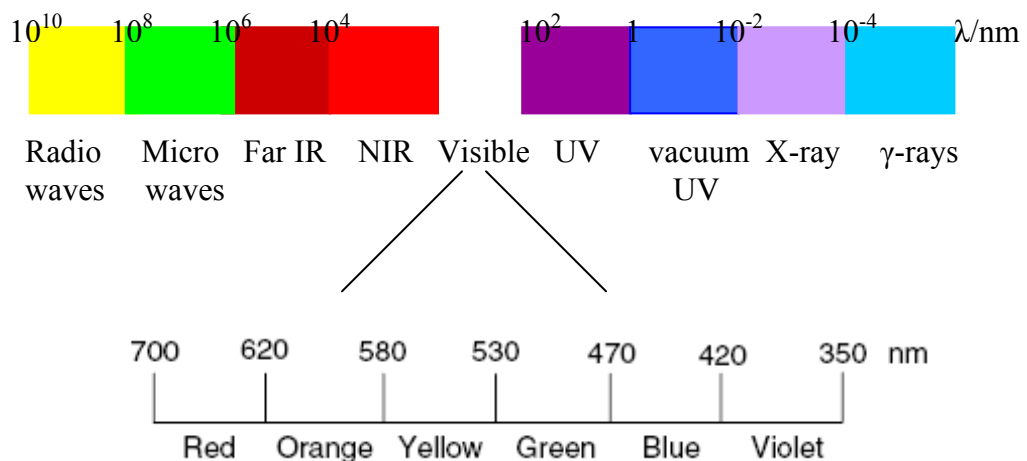


Figure 4.1. A continuum of photon energies exists from radio waves through to γ -rays (Source: Monk, 2004).

A photon is absorption of a particle of light and a photochemical process occur during absorption which is; a particle of electromagnetic radiation (light), causing

excitation of electrons of a material from ground state to one of the several energy states.

“Photoluminescence (PL) is spontaneous emission of light from a material under optical excitation.” PL spectroscopy is a selective and extremely sensitive probe of discrete electronic states and provides electrical characterization, of the material. The intensity of the PL signal provides information on the quality of the surfaces and interfaces. The characteristics of the emission spectrum can be used to identify surface, interface, impurity levels, and where discrete defect and impurity states surfaces abound (Gfroerer; 2000). PL is a simple, versatile, and nondestructive method which required for ordinary PL work is an optical source and an optical power meter or spectrophotometer. Because the measurement does not rely on electrical excitation or detection, sample preparation is minimal. This property makes PL spectroscopy particularly attractive for systems having poor conductivity or undeveloped contact/junction technology. Having absorbed energy and reached one of the higher vibrational levels of an excited state, the molecule rapidly loses its excess of vibrational energy by collision and falls to the lowest vibrational level of the excited state (Dijken et al., 2000; Li et al., 2008).

Luminescence includes both Fluorescence and phosphorescence. When the light of electromagnetic radiation is emitted by a molecule (or group on a molecule) it relaxes from an excited singlet state to the ground state of electronic energy level. Such a process usually occurs within nanoseconds of excitation and the spectral characteristics of the emission often possess a mirror image relationship to the absorption spectrum occurring at a longer wavelength. When the molecule of the primary excited state undergoes some changes to create a triplet state, the radiation was emitted when the molecule returns to a singlet ground state and named as phosphorescence. Such a radiative transition is theoretically “forbidden”. Phosphorescence is usually weaker than fluorescence, and occurs at much longer times (milliseconds to seconds) after excitation. In addition, since the excited triplet state is of lower energy than the excited singlet of the same molecule, phosphorescence occurs at longer wavelengths than fluorescence. These excited state “lifetimes” (nanoseconds for fluorescence, milliseconds for phosphorescence) are important since they determine the time scales of the processes which can be observed using luminescent techniques (Lacowicz, 2006).

The existence of shells and energy levels improve observations of light emitted by the elements since the kinds of light that interact with atoms indicate the energy

differences between shells and energy differences in atom. Not all atoms in a sample will absorb or to be excited exactly at the same shell level. For example hydrogen in the ground state has the electron in the n:1 shell. The electron in some hydrogen atoms may be excited into the n:2 shell level. Other hydrogen atom can have electron excited into n:4 shell. This means; different elements emit different emission spectra when they are excited because each type of element has a unique energy level system. Each element has a different set of emission colors because they have different energy level spacing (Lacowicz, 2006).

4.1 Optical Properties of Zinc Oxide

Transition metal oxides (TiO₂, and ZnO) are highly photoactive materials with photostability. ZnO is a semiconductor with wide band gap (3.2–3.5 eV) that makes it a promising material for photonics and optical applications since can absorb UV-light and blue region of the electromagnetic spectrum. The high exciton-binding energy (60 meV) allows efficient excitonic emission even at room temperature. The electroluminescence generates UV and visible light from ZnO. Many narrow band gap materials like metals are susceptible to photodegradation and thus reducing the life time of photo devices (Lahiri and Batzill, 2008, Lima et al., 2007, Ammala et al., 2002).

ZnO is probably the richest family of nanostructures among all semiconductive materials. ZnO can exhibits (at room temperature) unique optical, photocatalytic, piezoelectric and pyroelectric properties, produces an efficient blue-green luminescence, and displays excitonic ultraviolet (UV) laser action. ZnO, has a relatively high absorption band starting at 385 nm and extending into the far-UV. In addition to its excellent UV absorption characteristics, ZnO has several other advantages as a UV-emitting additive material, it does not migrate, not degraded by absorbed light and in many cases may improve mechanical, optical and electrical properties of the bulk polymer. Recently; ZnO nanoparticles have attracted much attention due to the ability to decompose harmful bacteria or toxic gases in the environment due to the particles with dimensions well below the wavelength of light materials that have negligible loss of light by scattering.

ZnO powders can find potential application areas; like UV-light emitting diodes, transparent UV-protection coatings, luminescent device, laser emitters, fluorescent marker, piezoelectric devices, screening material etc. (Lin et al., 2009, Lü et al., 2007, Fangli et al., 2003; Ammala et al., 2002). Semiconductor ZnO can be used for detection of UV-A (300-400 nm) radiation. By doping with Mg the range can be tuned to the UV-B and UV-C (200-280 nm) regions. Such a wide interval of sensing spectra makes the material UV detectors to be used in many applications such as solar UV radiation monitoring, ultra-high temperature flame detection, and airborne missile warning systems. (Nickel and Terukov, 2004).

Generally, ZnO shows four photoluminescence (PL) emissions; (a) near band edge emission at around 390 nm (UV emission), explained as to free-exciton recombination (b) blue emission at around 460 nm is because of intrinsic defects such as oxygen and zinc interstitials (c) green emission at around 540 nm is known to be a deep level emission caused by impurities, structural defects in the crystal such as oxygen vacancies, zinc interstitials and (d) red emission at around 630 nm due to oxygen and zinc anti-sites. ZnO nanoparticles excited at 325 nm exhibited 4 emission PL bands at around 390, 411 nm, 471 nm and 517 nm. The PL peak at 411 is attributed to zinc vacancies which are intense and sharp when excited at 304 nm. This showed that the probability of trapping and giving the PL emission by zinc vacancies at the excitation of 304 nm is more as compared to 325 nm excitation. The peak around 470 nm i.e. blue emissions is attributed to intrinsic defects such as oxygen and zinc interstitials. This blue emission is common for all excitation wavelengths, but for 322 and 325 nm excitation blue emission is superior. The green band emission corresponds to the singly ionized oxygen vacancy in ZnO in the bulk of nanoparticles and excess oxygen on the surface, which might be in the form of OH^- ions and results from the recombination of photo-generated hole with single ionized charge state of this defect. The weak green emission also implies that there are few surface defects in ZnO nanoparticles. (Singh et al., 2009; Yu and Yu, 2009).

Bohr radius of the ZnO is 19 nm and a powder below that value, resulted to change its properties. Much of the research on the luminescence of ZnO is performed on single crystalline powders or single crystals. Two emission bands are usually found. A relatively weak and narrow UV emission band is observed around 380 nm (3.25 eV), just below the onset of absorption. This band is due to the radiative annihilation of excitons. The lifetime of this exciton emission is very short, of the order of several tens

to hundreds of picoseconds. A much stronger and broader emission band is situated in the green part of the visible spectrum, with a maximum between 500 and 530 nm (2.50 eV) (Dijken et. al; 2000).

When the particle size is reduced below 6 nm, a shift in the emission spectrum to shorter wavelengths due to the quantum behavior of electrons and holes in the particles occurs. ZnO emits a broad luminescence emission in the green-yellow region, and, as a result, it is a potential material for use in white light sources. The peak for the emission spectrum is located in the blue region for particle sizes smaller than about 3 nm. Very large ZnO particles show an emission spectrum that peaks at a wavelength of around 550 nm, i.e., a green-yellow color. If ZnO nanoparticles could be produced in a range of sizes from about 3 nm up to around 10 nm, a variety of emission peaks could be produced. Abdullah et al., 2004 studied ZnO colloids that have been aged for different times. Composites containing a specific size of ZnO were produced by aging. The excitation and emission luminescence spectral positions of ZnO are dependent on particle size, (shift to blue region with reducing particle size), composites that emit a specific color can be produced using this method. In this study they have been produced composites that emit colors from blue (460 nm) up to yellow-green (550 nm). (Abdullah et al., 2004).

Bhat et al. (2009) studied thin films of colloidal ZnO nanoparticles. The PL spectra of ZnO nanoparticles show an absorption peak at 350 nm, which is blue shifted compared to that of bulk ZnO (370 nm), due to quantum confinement. The PL spectra of the prepared nanoparticles show an intense defects-related band centered at 560 nm (green) and a weak band edge luminescence centered at 373 nm (UV). The green luminescence has been attributed to defects such as oxygen vacancies, zinc vacancies as well as donor-acceptor pairs. In the case of colloidal ZnO nanoparticles, this may be due to the surface defects. According to Bhat et al. (2009) reported that in optical quality, as well as the dark and the photocurrents of the thin films are strongly dependent on the annealing temperature (Bhat et al., 2009).

In another study, zinc oxide nanoparticles coated with a zinc aluminate layer have been prepared by carrying out basic carbonate of aluminium precipitate on the precursor of zinc oxide. It is expected that a homogeneous layer coating of zinc aluminate would form and retard the oxidation and photocatalytic activity of the zinc oxide. The structures of the coated surface have been characterized. The oxidation and photocatalytic activity and also the optical properties of coated zinc oxide nanoparticles

have been investigated. Zinc oxide powders coated with zinc aluminate show excellent UV blocking properties. Furthermore, it helps to change the pale yellow color of zinc oxide powders to white (Fangli et al; 2003).

Thermoluminescence (TL) glow curves recorded on ZnO nano-needle arrays have shown a broad peak at about 360 °C similar to that observed in ZnO polycrystalline powder. A very strong TL peak at about 325 °C superimposed on a broad one has been observed in a ZnO film-type sample. TL was tentatively attributed to the recombination of charge carriers released from the surface states associated with the oxygen related defects, mainly interstitial oxygen ion centre; these surface states are also responsible for the 585 nm PL band. (Secu and Sima, 2009).

Viswanothamurthi et al. (2004) studied zinc oxide in the form of nanofibres by an electrospinning method. Figure 4.2 shows the photoluminescence spectrum of ZnO fibres after calcination at 600 °C. The narrow UV band at 3.13 eV (395 nm in wavelength) and a broad green band at 2.21 eV (560 nm in wavelength) are observed in the photoluminescence spectrum. The UV emission band can be explained by a near band-edge transition of wide band gap ZnO nanowires, namely the recombination of free excitons through an exciton-exciton collision process. The green band emission results from the radial recombination of a photogenerated hole with an electron that belongs to a singly ionized oxygen vacancy.

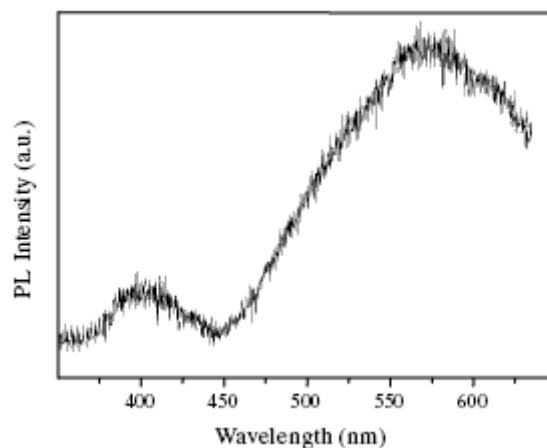


Figure 4.2. A photoluminescence spectrum of ZnO fibres calcined at 600 °C (Source: Viswanothamurthi et al.; 2004).

Li et. al. (2008) reported synthesis of ZnO nanorods doped with Mn, Cr, and Co by a hydrothermal method from aqueous solutions of zinc nitrate hydrate, TM (TM, Mn, Cr, Co) nitrate hydrate, and hexamethylenetetramine. The properties of doped nanostructures were explained by photoluminescence spectra given in Figure 4.3. The characteristic ZnO weak UV emission and strong defect (yellow) emission, which is characteristic for ZnO prepared by a hydrothermal method. It can also be observed that the UV emission peak position was at slightly different position for different samples, which could be due to different native defect and free carrier concentrations in different samples.

According to Behera and Acharya (2008); doping with Al introduces aggregation of crystallites to form micro-size clusters affecting the smoothness of the film surface. Al³⁺ ion was found to promote chemisorption of oxygen into the film, which in turn affects the roughness of the sample. Six photoluminescence bands were observed at 390, 419, 449, 480, 525 and 574 nm in the emission spectra. Excitation spectra of ZnO film showed bands at 200, 217, 232 and 328 nm, whereas bands at 200, 235, 257 and 267 nm were observed for ZnO:Al film. In luminescence process, vacancies and interstitials play a key role. In semiconducting ZnO system, majority of donors are oxygen vacancies (VO) and zinc interstitials (Zni), although there are other defect states present in the system.

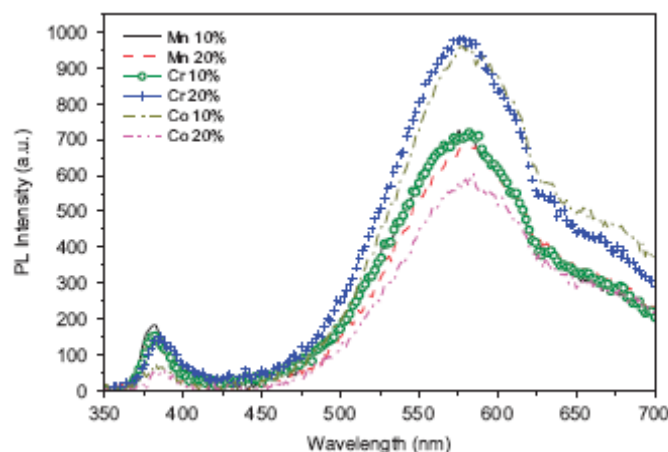


Figure 4.3. Photoluminescence of ZnO rods with different dopants (Source: Li et al., 2008).

UV photoconductivity of Zinc Oxide is governed by surface related and bulk related process. The surface related process is primarily governed by the adsorption and desorption of the chemisorbed oxygen at the surface of the ZnO, which is exploited for gas sensing applications. The process becomes important in nanocrystalline films, where the surface area is large. In the bulk relate process, oxygen molecules in the grain boundaries contribute to photoconductivity. The bulk related process is however considered to be faster in comparison to the surface related process (Bhat et al., 2009). Table 4.1 is prepared to define a general view about the luminescence effect of different zinc oxides.

As given in the Table 4.1 the emission spectra of the zinc oxide generally resemble with each other although, the luminescence behavior of the powder depends on the particle size. Also the emission spectrum was independent of excitation wavelength.

Table 4.1. The luminescence effect of Zinc oxide from literature.

ZnO type	Excitation	Emission	Application Area	Reference
ZnO nanocrystals	3.5 eV	3.32 -2.21 eV	Photoconductive	Bhat et al., 2009
ZnO nano rods doped Mn, Cr, Co	-	2.13- 3.22 eV	Hydrothermal growth optimization	Li et al., 2008
ZnO nanofibre	-	2.21-3.13 eV	Optoelectronic	Viswanothamu rthi et al., 2004
ZnO nano particle	-	3.26- 2.48-2.33 eV	-	Dijken et al., 2000
Single crystal	-	2.4-3.35-3.36 eV	Hall effect measurement	Look et al., 2003a

4.2. Optical Properties of Zinc Oxide-Polymer Composites

Due to the unique luminescence properties of inorganic nano materials and the good processability of their dispersions in polymer solutions or monomers, inorganic/polymer nanocomposites are promising materials for different lighting and display devices.

According to Leguenza et al. (2002) subjecting a polymer to UV radiation -C-C- and -C-H bonding breakage may occur. In both cases chain-end radicals may be produced in the presence of oxygen, this phenomenon involve two competitive processes: polymer and hydrogen radicals formation and formation of cross-linking which can also occur in the absence of oxygen. The photoluminescence studies including PP and PE related with degradation of these polymers under UV irradiation. According to Ito et al. (2004) for PP and PE due to the irradiation of UV photons, PL peak at 3.6 - 4.0 eV in PE originates from the same chemical groups as the PL around 4.0 eV observed in PP. The PL intensity around 4 eV changed probably due to the decrease in the number of the chemical group. There are at least two possible candidates. One is unsaturated ketone, which is present in a typical impurity in organic polymers. The other candidate is benzene ring present in a typical antioxidant. It is known that the two chemical groups have the PL component around 4 eV and that they are decomposed by the irradiation of photons or by capturing radicals induced in polymers (Ito et al., 2004, Ohki et al., 2000).

The fluorescence and phosphorescence emission properties of polymers may be classified into two types A and B. A type includes polyalkanes, synth rubbers, aliphatic polyamides and typically the chromophores present in these polymers are carbonyl and α , β unsaturated carbonyl compounds or groups and unsaturation and some aromatic and polyaromatics. The second type includes aromatic polyesters, aromatic polyamides and so on, these polymers luminescence by virtue of the intrinsic nature of the polymer. In polymers intermolecular energy transfer may involve the transfer of energy from small molecule chromophores to those on a polymer and chain from a chromophores on a small molecule polymer chain (Soutar, 1991, Vollath et al., 2004, Rozenberg, 2008).

The integration of inorganic nanoparticles into polymers has been used for the functionalization of polymer materials with great success. Inorganic nanocrystals often

possess organophobic surface characteristics, and significant phase segregation through direct mixing, such as melt compounding and this hinders some of the commercial applications. Nanoparticles allow one to functionalize transparent polymers if the formation of aggregates or agglomerates is avoided. The particles must be integrated in a way leading to isolated primary particles inside the matrix. The physical properties of polymer matrices, such as thermal stability, may be significantly improved by increasing interfacial areas between nanocrystals and polymer matrices via good dispersion of nanocrystals. It should be noted that highly aggregated nanocrystals in polymers fatefully cause substantial light scattering due to their size and refractive index mismatch, which impedes polymer nano composites for optical applications. In nanocomposites the particle dimensions are small enough for the production of highly transparent composites (Sun et al., 2009; Althues et al., 2007).

Lü et al. (2007) prepared, nano-ZnO/polymer composite films with different concentration of ZnO. Nano ZnO was put into monomer mixtures of urethane-methacrylate oligomer and 2-hydroxyethyl methacrylate, followed by ultraviolet (UV) radiation-initiated polymerization. The colloidal ZnO nanoparticles with a diameter of 3–5nm were synthesized from zinc acetate and lithium hydroxide in ethanol via a wet chemical method. The ZnO nanoparticles were uniformly dispersed in the polymer matrix no aggregation was observed, which contributed to the high transparency of the nanocomposites. And the researchers found that, these composite film materials have the potential to be used as UV absorber and luminescent films in the design of optical coatings (Lü et al., 2007).

Sun et al. (2009) studied monodisperse ZnO quantum dots (QD) with a diameter of 5.0 nm. They have synthesized ZnO through a simple colloidal method without addition of organic capping agents. After purification, the monodisperse ZnO QDs are well dispersed in epoxy by addition of exfoliated nanoplates. The epoxy hybrid nanocomposites are highly transparent and show UV-absorption properties and strong UV emission, as well (Sun et al., 2009).

According to review of the Althues et al., (2007) particle diameters below 40 nm are essential to obtain transparent nanocomposites. The reason is the steeply increasing intensity of scattered light with increasing particle diameter. Decreasing the particle size furthermore allows a much more homogeneous distribution of a material and leads to a drastic increase of the polymer/particle interfacial area. The high specific surface area of

small nanoparticles may induce their aggregation. Aggregates also lower the homogeneity of particle distribution.

Guo et al. (2000) studied the optical properties of ZnO nanoparticles capping by poly (vinylpyrrolidone) polymer molecule. The absorption and photoluminescence spectra of none modified and modified ZnO is given in Figure 4.4. ZnO nanoparticle samples exhibit exciton absorption peak wavelengths of both capped and noncapped nanoparticles (300 nm); that are substantially blueshifted relative to that of the bulk ZnO (373 nm) due to the strong restriction effect. For example, the excitonic absorption peak of the PVP-capped ZnO nanoparticles was at a shorter wavelength ~ 303 nm than that of the noncapped ones ~ 312 nm. This might be attributed to the smaller size of the PVP capped ZnO nanoparticles. Another difference between the two absorption spectra was the appearance of a bump at; 260 nm for the noncapped ZnO nanoparticles, which was absent for the PVP-capped ZnO nanoparticles. It was unlikely that this was due to higher-energy exciton absorption in nanoparticles of the average size (Guo et al., 2000).

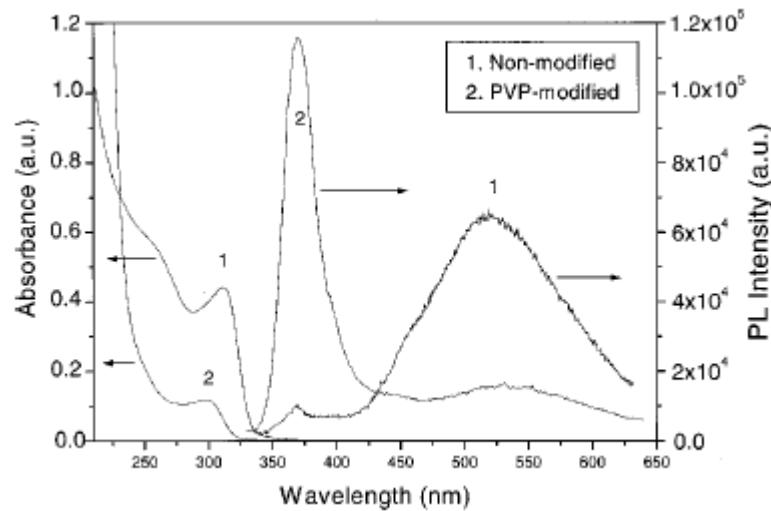


Figure 4.4. Optical absorption and photoluminescence spectra of non modified ZnO and poly(vinylpyrrolidone) capped ZnO nanoparticle (Source: Guo et al., 2000).

Honk et al., (2009) studied polystyrene which was grafted onto ZnO nanoparticles; the dispersion and the photocatalytic activity of the ZnO were investigated. To see the photocatalytic effect methylene orange (MeOr) solution was used as a degradation material. The photocatalytic degradation of MeOr solution after UV radiation using only ZnO polystyrene capped ZnO was taken using Uv-Vis

spectrometer. The photocatalytic degradation of bare ZnO and polystyrene grafted ZnO nanoparticles were entirely different under the same condition, and the photocatalytic activity of ZnO nanoparticles greatly reduced after coating with polystyrene (Honk et al., 2009).

Polymers are generally used for outdoor applications and the more commonly known degradation reason is UV light. Rate of the outdoor used polymers degradation do not only depend on UV, also depends on exposure conditions; such as sunlight intensity, temperature, relative humidity, structure of polymers and impurities in the polymeric material. In the degradation of polymers, there are two main processes photocatalytic degradation and photo oxidation processes. Photolysis involves the UV region above 280 nm which causes to the release of the sufficient energy to cause bond scission resulting formation of radicals or initiate photo oxidation.

Ito et al. (2001) studied degradation behavior of polypropylene (PP) and polyethylene (PE) by Ultraviolet Laser Irradiation (UV). 50 micron thick PP sheets and 500 micron thick low density PE sheets were taken containing only saturated C-C and C-H bands which were not chromophores. In these polymers luminescent additive chromophores should be seen easily due to the degradation. After UV irradiation the luminescence component around 3.6 - 4 eV decreases with an increase in irradiation time irrespective of the irradiation atmosphere. This is probably due to the decomposition of unsaturated ketone or benzene ring present in polymer as an impurity or antioxidant. Photochemical reactions are responsible from surface oxidizing and bond scission of PP and PE which was induced by the irradiation of the ultraviolet rays (Ito et al., 2001, Ohki et al., 2000, Ammala et al., 2002, Uthirakumar et al., 2006).

Ammala et al. (2002), studied to improve the UV stability of polypropylene and high density polyethylene (HDPE) loaded with ZnO nanoparticles. The UV degradation of polymers only manifests itself as a change in the physical characteristic of polymer such as yellowing, embrittlement, cracking and hazing. Loading 2 wt% of nano particles zinc oxide effectively stabilizes the PP and HDPE plaques for one year outdoor exposure. The UV stabilizer performance of ZnO was found better than organic ingredient stabilizer (Ammala et al., 2002).

Zhao and Li (2006) aimed to study the photo-degradation characteristics for zinc oxide (ZnO) nanoparticle filled polypropylene (PP) nanocomposites. It has been observed that UV irradiation caused significant photo-degradation for unfilled PP. Results from this research study indicate that the incorporation of ZnO nanoparticles

into PP matrix can impart significant improvements on the photo-degradation resistance of PP to UV-irradiation. This is due to the superior UV light screening effects offered by the ZnO nanoparticles. After UV-irradiation treatment, surface cracks were formed on the surface of all the investigated systems. Results from surface profile measurements supported that the surface cracking was more severe in unfilled PP, and the extent of surface cracking was found to reduce with increasing ZnO nanoparticle content (Zhao and Li; 2006).

CHAPTER 5

MATERIALS AND METHODS

5.1. ZnO Powder Preparation

Analytical grade chemicals, zinc chloride-ZnCl₂ (98%; Aldrich), potassium hydroxide-KOH (85%; Pancreac) and triethylamine-TEA (C₆H₁₅N, Merck), were used for the preparation of zinc oxide powders throughout the experimental study. Milipore ultrapure fresh water (18 ohm-cm) was used in all steps of the synthesis.

100 cm³ aliquot containing 0.2 M KOH and 0.02 M surfactant, triethylamine (TEA), were mixed with 100 cm³ 0.1 M ZnCl₂ solution. Ultrasonic treatment was applied to the mixture (Elma; Transsonic 660/H) at approximately 30 °C for 30 min as shown in Figure 5.1. The solid and liquid phases were separated by centrifuge (Hettich, Rotofix 32). The solid phase was then washed for three times with water, dried at 50 °C for 15 h and at 190 °C for 24 hours in a vacuum oven.

5.1.1. Al-doped ZnO Powder Preparation

Al (NO₃)₃.9H₂O (Al:Zn=0.5 mol) were used as an Al³⁺ source and dissolved in 100 cm³ water with zinc chloride (0.1 M). The precipitant solution (KOH (0.2 M) and TEA (0.02 M)) was added into the ZnCl₂ solution and mixed for 30 minutes in ultrasonic bath. The centrifuged and washed powders were dried at 50 °C for 15 h. The dried powder was calcined at 900 °C for 3 hours in air and 700 °C for 4 hours under N₂ atmosphere.

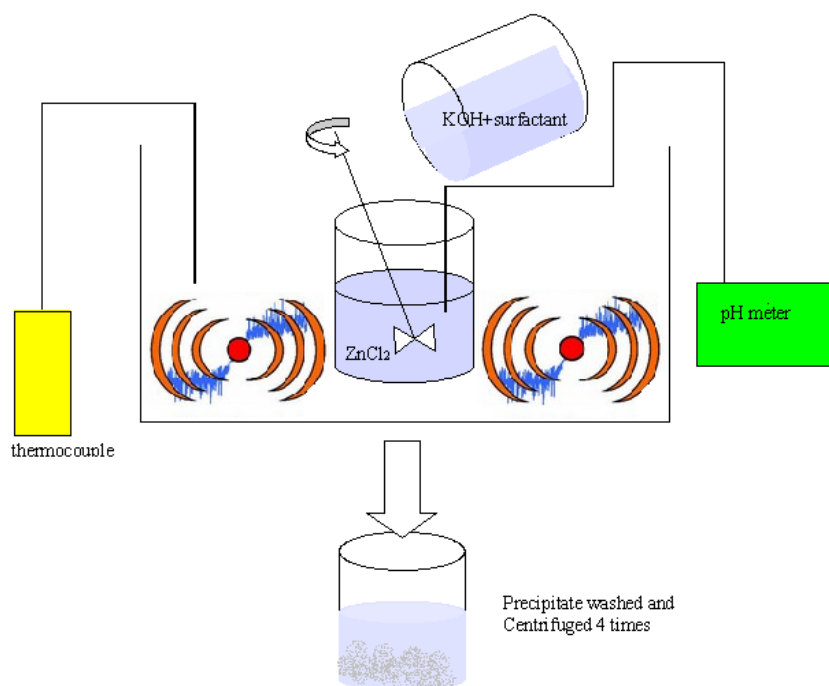


Figure 5.1. Experimental set-up of zinc oxide synthesis.

5.1.2. Specifications of Materials

Three commercial ZnO powders with different particle sizes were supplied by Ege Kimya Co. and Aldrich. The particle size of the powders supplied from Aldrich was in the sub micron (sZnO) and nanometer (nZnO) ranges while powders supplied from Ege Kimya Co. (eZnO) was in micrometer range. The synthesized ZnO powders were coded as synZnO and AlZnO. The properties of commercial powders are given in Table 5.1.

Polypropylene (PP) and low density polyethylene (PE) (Aldrich) were used as a matrix material. However, eZnO loaded composites were prepared by using PE (F2-12) and PP (MH-418) supplied by Petkim Petrokimya Co. which were only used for thermal characterization (TGA and DSC). The properties of PE (F2-12) and PP (MH-418) are given in Table 5.2. In the production of polypropylene composites maleic anhydride (Clariant) was used as a compatibilizer and added to the system at a level of 2 wt% of PP .

Table 5.1. Reported Properties of Commercial ZnO powders by the Suppliers.

Zinc Oxide Powder	Supplier	Appearance	Density g/cm ³	Particle Size	Assay
Ege Kimya A.Ş. (eZnO)	Ege Kimya Co	White/powder	5.56	2 micron	99%
Submicron Powder (sZnO)	Aldrich	White/powder	5.61	< 1 micron	99.99 %
Nano Powder (nZnO)	Aldrich	White/powder Fluffy	5.61	< 100 nm	99 %

Table 5.2. Properties of Polypropylene and Polyethylene.

Matrix	Supplier	Density (g/cm ³)	Radiation resistance	Refractive index	Resistance to Ultra-violet	Volume resistivity (Ohm.cm)
Polypropylene (PP)	Aldrich	0.9	Fair	1.49	Poor	10 ¹⁶ -10 ¹⁸
Polypropylene (PP)	Petkim Co.	0.9	-	-	Poor	10 ¹⁶ -10 ¹⁸
Polyethylene (PE)	Aldrich	0.92	Fair	1.51	Poor	10 ¹⁵ -10 ¹⁸
Polyethylene (PE)	Petkim Co.	0.91	-	-	Poor	10 ¹⁵ -10 ¹⁸

5.1.3. Characterization of ZnO Powders

The phase identification and crystal size of ZnO powders were conducted by X-Ray diffractometer (Philips X'Pert diffractometer , Cu-K_α radiation). The powder morphology and impurities in the ZnO powders were determined by SEM (Philips XL-30S FEG) and FTIR spectra (Shimadzu FTIR-8201), respectively. Thermal

behavior of the powders was determined by TGA (Shimadzu TGA-51) and DTA (Shimadzu DTA-50) with a heating rate of 10 °C/min up to 1000 °C. The particle size of the powders was determined by ZetaSizer (Malvern Instruments 3000 HSA) and Sedigraph (Micromeritics-5100, 50 w/w % water-glycerol suspension).

The volumetric resistivity of the ZnO powders were determined by applying 50 V potential and I-V data was recorded on a Voltage source (Keithley 2420). The I-V data were obtained by the aid of silver contacts which were formed by thermal evaporation on the pellet's surface (about 2.5 cm in diameter, 2-3 mm in thickness).

ZnO powders were dry pressed, sintered at 1100 °C and polished to determine the contact angle of water (Krüs-G10 goniometer). Surface roughness of the sintered pellets and the polymers (PE and PP) were determined by Mitutoyo Surface Profilometer, SJ-301. Helium pycnometer (Quantachrome Co. Ultrapycnometer 1000) was used to determine the powder densities. The N₂ adsorption/desorption analysis were performed to determine the surface area of the powders (ASAP Micromeritics 2000).

Reflection and absorption spectra of pellets were obtained by using UV-Vis spectrometer (Perkin Elmer Lambda 45). The Fluorescence spectra were determined by using fluorescence spectrometer (Varian Cary Eclipse) and samples were excited at 380 nm and/or 350 nm, data were recorded in the 390 and 600 nm range.

5.2. Surface Modification of ZnO Powders

The surface modification of powders was performed with 3-aminopropyl-triethoxysilane (AMPTES) (Fluka) and PEG 4000 (Aldrich) in 1:1 ethyl alcohol solution for 2 hour with a constant stirring rate and drying was carried out at 50 °C for 15 hour.

5.3. Preparation of Composites

ZnO and polymer mixing process was performed in torque rheometer (Haake Polydrive Rheomixer R600/610) with 50 rpm speed at 190 °C for polypropylene and at 160 °C for polyethylene composites and the mixing time was 20 minutes. The blended materials were then uniaxially pressed and well shaped (15x15x0.1 cm) at 6800 kg force at 180 °C and 150 °C for PP and PE composites respectively, with a 10 minute hold in (Carver) hot press. Haake Rheomixer and Carver hot press used in this work are shown in Figure 5.2 and Figure 5.3 respectively.

eZnO and sZnO-polymer composites were prepared in vol % of 5, 10, 15 and 20 by using PP and PE as a matrix material as well as neat PP and PE sheets. For PP composites, maleic anhydride was grafted into polypropylene at 2 wt%. Polymeric composites were prepared by using nZnO, synZnO and AlZnO powders in 5, 10 and 15 vol% by using only PE matrix. Composites with PE matrix containing 20 vol% eZnO, sZnO and 15 vol% ZnO, synZnO were prepared by using surface modified powders.

5.3.1 Characterization of Composites

Polymer composites crystallinity were determined by X-Ray diffractometer (Philips X'Pert diffractometer with Cu-K_α radiation). The morphology of composites were characterized by using SEM (Philips XL-30S FEG), the elemental distribution were determined by EDX and 5000X magnification was used for mapping analysis of composites. Composites were broken after immersing in liquid N₂ (77 K) and fracture surfaces were examined using SEM. Density of the composites was measured by using density kit apparatus (Sartorius).

Melting and degradation behavior of composites were determined by TGA (Shimadzu TGA-51) and DSC (Shimadzu DSC-50) with a heating rate of 10 °C/min up to 600 °C for DSC, and up to 1000 °C for TGA.



Figure 5.2. Haake Polydrive Rheomixer R600/610.



Figure 5.3. Carver hot press.

Hot wire method (KEM QTM-500) was used to determine the thermal conductivity of the composites which was generally used for materials with low thermal conductivity. The measuring probe is given in Figure 5.4 consist of a single heater wire and a thermocouple. When an electric current is passed through the wire, heat is generated per unit length of wire per unit time. A constant power was supplied to the heater element and temperature increase of the heating wire was measured by a thermocouple and for short heating intervals data was recorded with respect to time. The thermal conductivity (k) of the sample was calculated from temperature–time data and power input according to Equation 5.1 (Source: QTM 500 Handbook, 2007).



Figure 5.4. Hot wire probe
(Source: QTM 500 Handbook, 2009).

$$k = \frac{q \ln(t_2 / t_1)}{4\pi(T_2 - T_1)} \quad (5.1)$$

k : Thermal conductivity of the sample (W/mK)

g : Generated heat per unit length of sample/time (W/m)

$t_{i,j}$: Measured time length (sec)

$T_{i,j}$: Temperature at $t_{i,j}$ (K)

Keithley 6517A Electrometer/High Resistance meter was used for determination of the electrical resistivity of the composites connected to 8009 Resistivity Text Fixture sample holder. Keithley 6524 test software was used for data

recording and analysis was performed at constant polarity of 50 V. The resistivity was measured according to ASTM D257.

Volume resistivity is defined as the electrical resistance through a cube of insulating material. Volume resistivity is measured by applying a voltage potential across opposite sides of the insulator sample and measuring the resultant current through the sample as shown in Figure 5.5. The Model 6517-A automatically performs the calculation using Equation 5.2 and displays the volume resistivity data at an applied voltage potential (Keithley 6517-A manual, 2004). The characteristic data obtained from Keithley 6517-A as shown in Figure 5.6.

$$\rho_v = \frac{K_v}{\tau} R \quad (5.2)$$

ρ_v = Volume resistivity

K_v = The effective area of the guarded electrode for particular electrode arrangement employed

τ = Average thickness of the sample (mm)

R = Measured resistance in ohms (V/I)

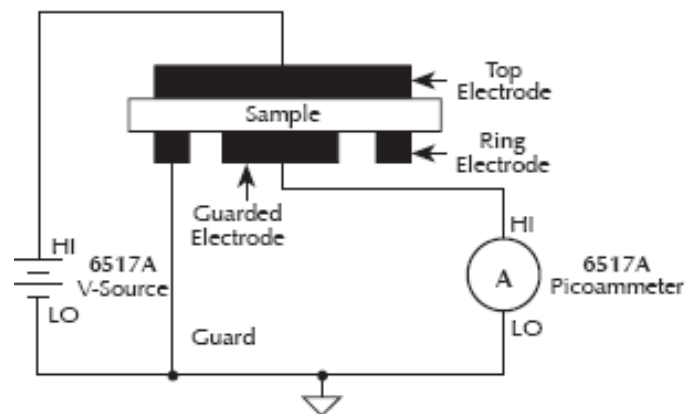


Figure 5.5. Volume resistivity measurement technique (Source:Keithley 6517-A manual, 2003).

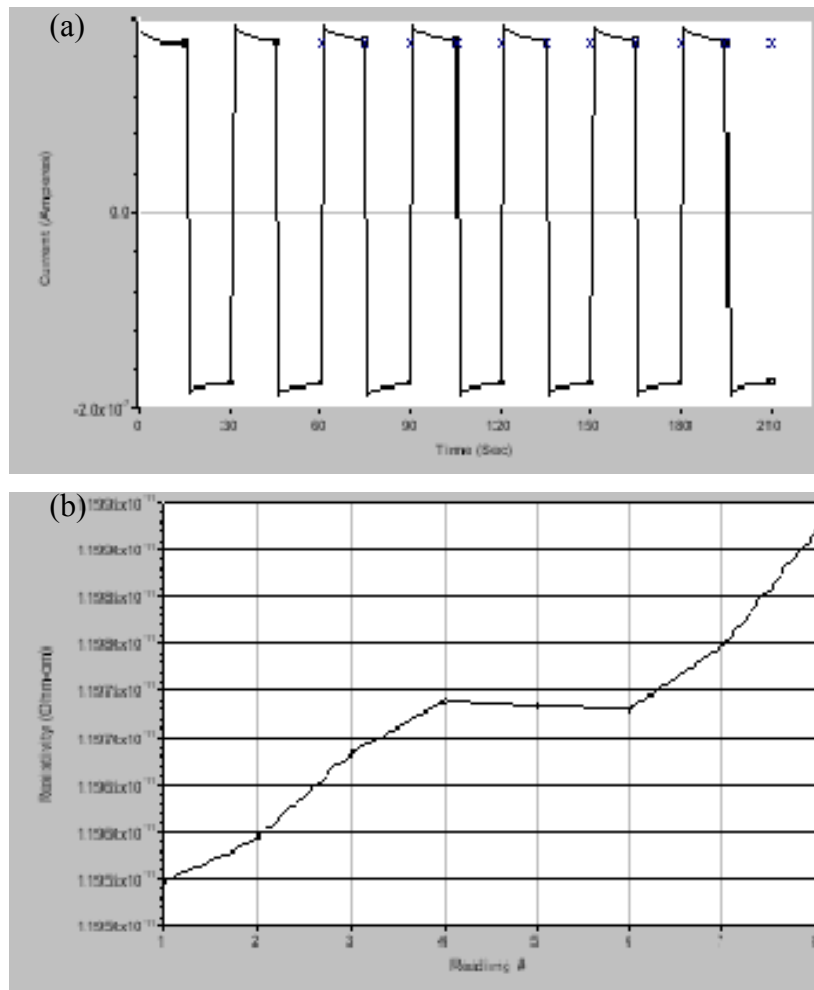


Figure 5.6. High resistivity test data sheet taken from Keithley 6517-A a) Current-time b) Volume Resistivity-Number of Reading.

The direct current (DC) high resistivity data for current-time graph shown in Figure 5.6-a indicates the accuracy of the experiment and a typical alternative current-time graph is shown in Figure 5.6-a. The volume resistivity versus number of reading is given in Figure 5.6-b. Among the eleven readings, first three of them were discarded and rest was used to calculate the average volume resistivity. The current and resistivity through the composites were measured after the system reaches steady state conditions (approximately in 1 hour).

Absorption and reflection spectra of ZnO-PP and ZnO-PE composites were recorded by UV-visible spectrophotometer (Perkin Elmer lambda 45). Fluorescence spectrometer (Varian Cary Eclipse) was used to characterize the optical properties of composites with 380 and 350 nm light as an excitation and emission between 390 and 600 nm spectrum was recorded.

The tensile tests of the samples were conducted by Shimadzu AG-I 250kN using 5 mm/min and 50 mm/min stretching rate at room temperature according to ASTM standard 638 for PP and PE matrix composites, respectively. Dogbone samples were cut from composite plates by using Ceast Automatic hollow die punch for the determination of mechanical properties of the composites.

CHAPTER 6

RESULTS AND DISCUSSION

6.1. Characterization of ZnO Powders

Zinc oxide is a white and fluffy powder with a very high bulk density which is insoluble in water and alcohol but soluble in acid and alkali. The SEM micrograph of the commercial ZnO coded as eZnO, sZnO and nZnO which was used as filler is given in Figure 6.1.

The SEM micrograph of eZnO shows a heterogeneous distribution of particle which some of the crystals were needle, tripod, and rod shaped depicted in Figure 6.1-a. The particle size distribution of eZnO powder determined from Sedigraph is given in Figure 6.2. The mean particle size of eZnO powders was found 3.86 μm with 98.6% under 10 μm , 82.2% under 5 μm , 28.1% under 2 μm and 16% under 1.5 μm . The surface area of eZnO was found 1.57 m^2/g (BET specific surface area).

The SEM micrograph of sZnO powder crystals were, polydispersed and mostly bar shaped seen in Figure 6.1-b with a mean particle size of 752 nanometer determined by Zetaizer. The surface area of sZnO powder was 10.1 m^2/g (BET surface area).

The nZnO powders have a nonuniform distribution of particle morphology. Most of the particles were in bar shaped seen in SEM micrograph 6.1-c. Mean particle size of this powder was 378 nm established by using ZetaSizer. The particle size of the powder was found to be greater than 100 nm since the supplier reported it to be smaller than 100 nm. The sample preparation method of ZetaSizer could differ the results since the nano powder could not dispersed well in the water. The surface area of the powder was 15-25 m^2/g . The L/D ratios of sub micron and nano sized powders were low. The XRD pattern of the commercial zinc oxide powders are given in Figure 6.3.

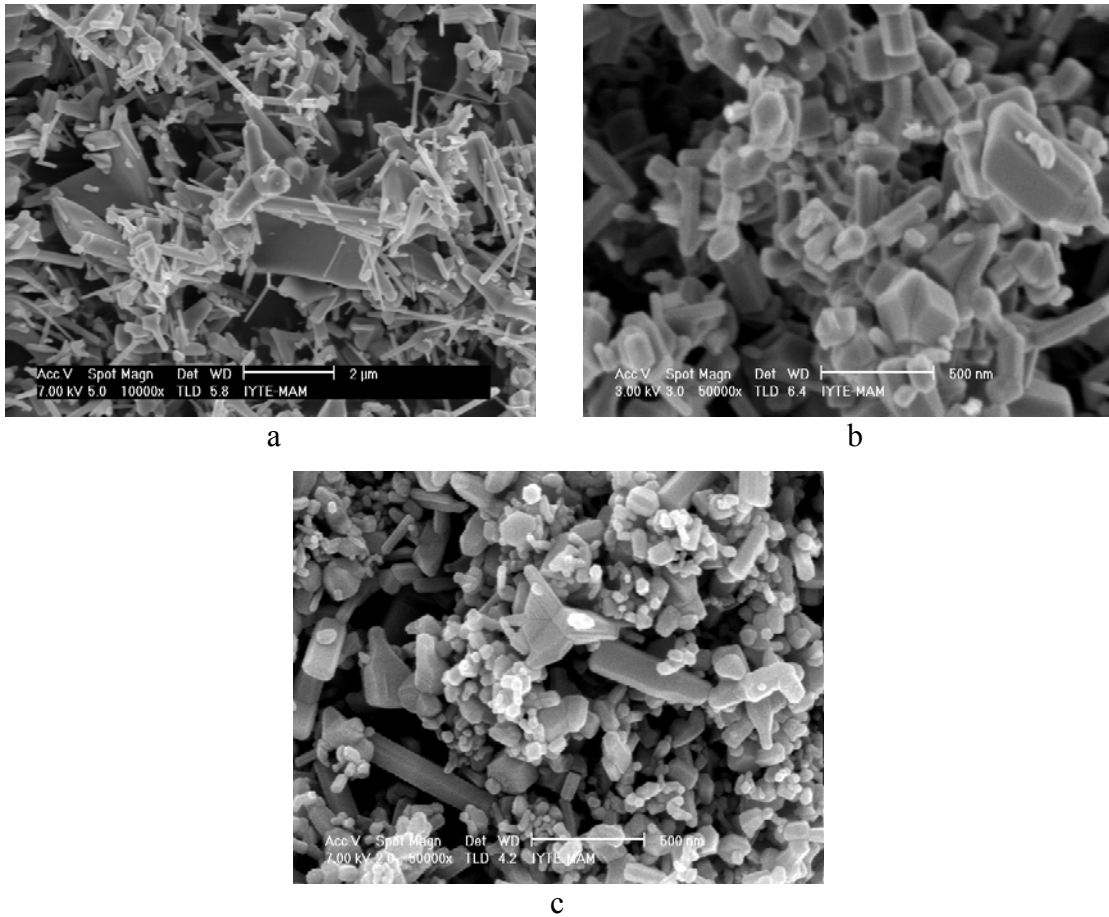


Figure 6.1. SEM micrographs of Zinc oxide powders a) eZnO powder b) sZnO powder c) nZnO powder.

Diffraction patterns of ZnO powders corresponding to (100), (101), (102), (110), (103) and (112) planes in agreement with the typical wurtzite structure of bulk ZnO given in the literature were nearly similar and 2θ values of main peaks were 31.9° , 34.5° , 36.2° , 47.5° , 56.5° , 62.8° , 67.9° , and 69.3° respectively (Ohara et al., 2004). The crystallite sizes were estimated with Scherrer formula given in Equation 6.1 using the software of the X'Pert Plus.

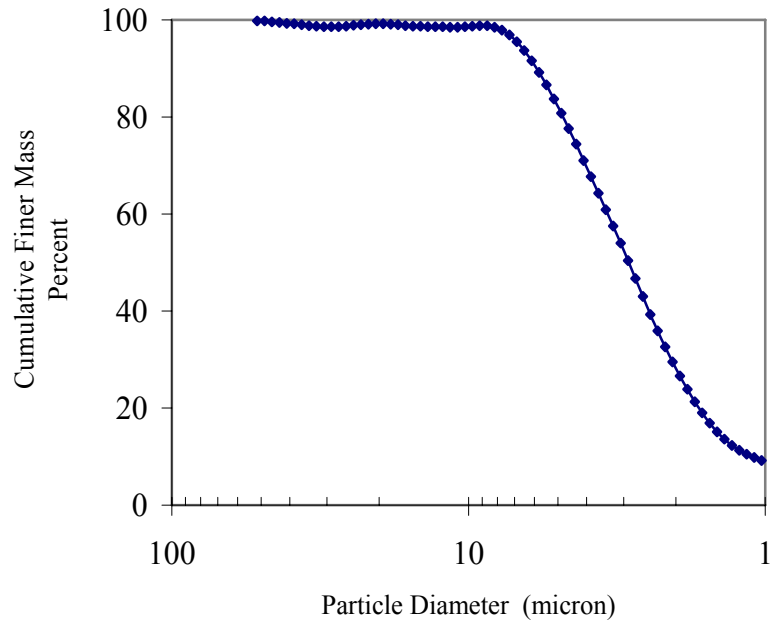


Figure 6.2. Particle size distribution of eZnO powder.

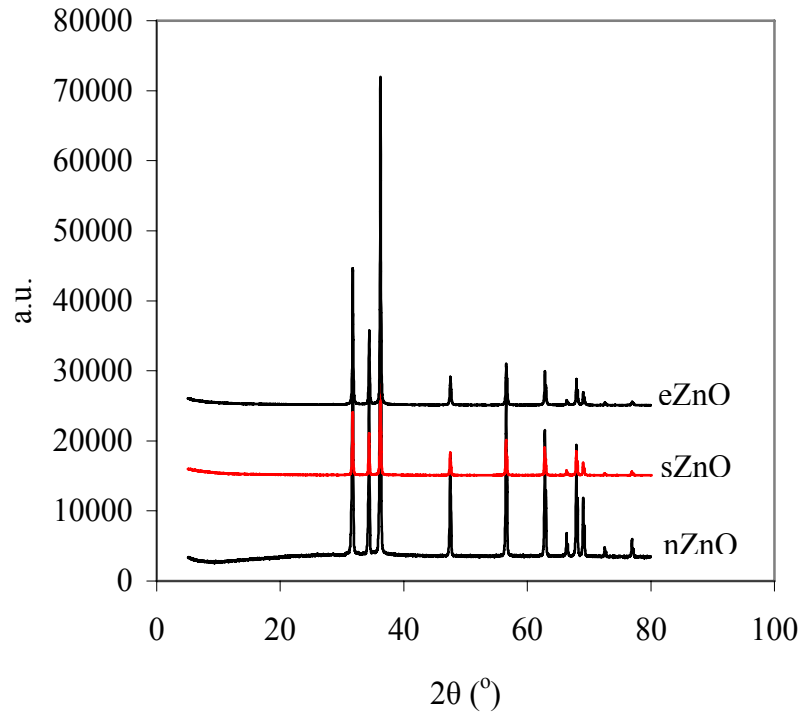


Figure 6.3. XRD pattern of commercial zinc oxide powders.

$$D = \frac{0.9\lambda}{\beta \cos \theta} \quad (6.1)$$

where, λ is the X-ray wavelength, θ is the Bragg's angle and β is the peak full width of the diffraction line at the half of the maximum intensity. The crystalite sizes were calculated for 34.4° 2θ value as, 415.8 nm, 237.6 nm and 202.8 nm for eZnO, sZnO and nZnO respectively.

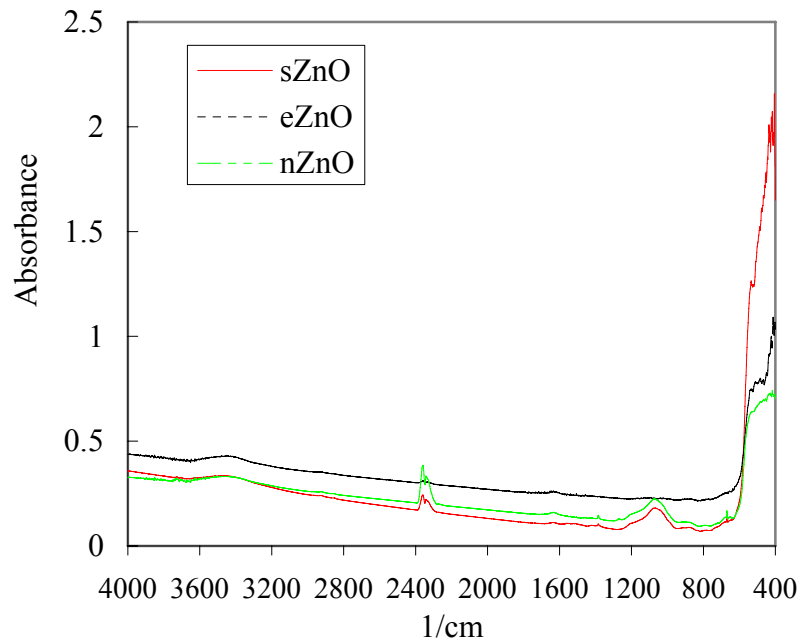


Figure 6.4. FTIR spectra of commercial zinc oxides.

The FTIR spectra of the three commercial ZnO powders are given in Figure 6.4. The FTIR spectra of all zinc oxide powders have characteristic Zn-O vibration peaks at 473 cm^{-1} and 532 cm^{-1} .

6.1.1. Characterization of Prepared ZnO Powder

The particle size of the ZnO nano powders was prepared with TEA as a surfactant by optimizing the effects of temperature, mixing speed, time, and washing parameters. The optimum temperature and reaction time was found to be 30 °C and 30 min under ultrasonic treatment and mechanical mixing with rapid addition of the precursor materials. The precipitate obtained from the reaction was washed three times to remove the impurities. The nano zinc oxide particles, which were dried at 50 °C for 24 hours were characterized to understand the properties of the powder. BET surface area of the synthesized ZnO (synZnO) powder was 21.2 m²/g. The X-ray diffraction pattern of the synZnO powder is shown in Figure 6.5 and the SEM micrographs of the powders are given in Figure 6.6.

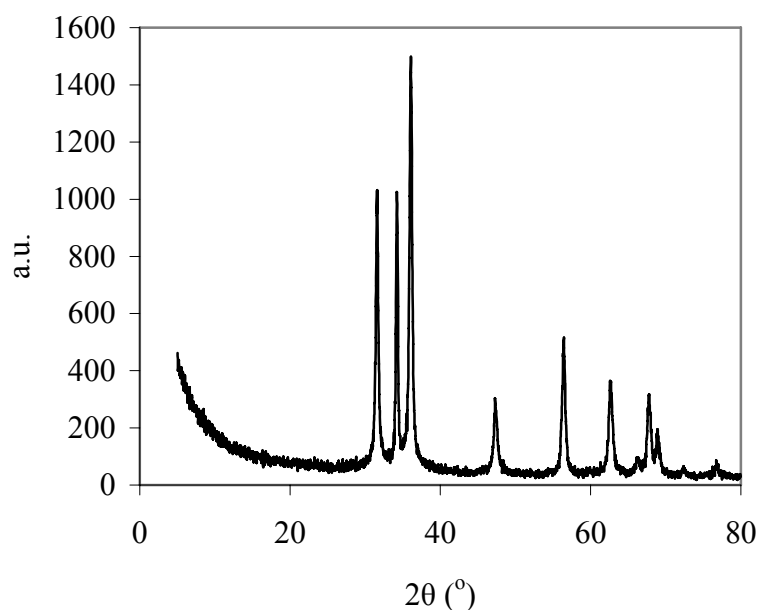


Figure 6.5. X-ray diffraction pattern of synZnO.

In the literature nine peaks appear at 2theta values for ZnO powders at 31.7 °, 34.4 °, 36.3 °, 47.5 °, 56.6 °, 62.3 °, 66.5 °, 67.9 °, and 69.1 ° (Ohara et al., 2004, Music et al., 2000). synZnO particles possess a high crystallinity as depicted in Figure 6.5, since

all peaks were very sharp. The synZnO powder 2theta values taken from XRD were 31.6° , 34.26° , 36.1° , 47.35° , 56.4° , 62.66° , 66.2° , 67.76° , 68.86° , 72.2° and 76.78° . The crystallite size for 34.25° 2 theta value was 68.1 nm determined with Scherrer Equation 6.1.

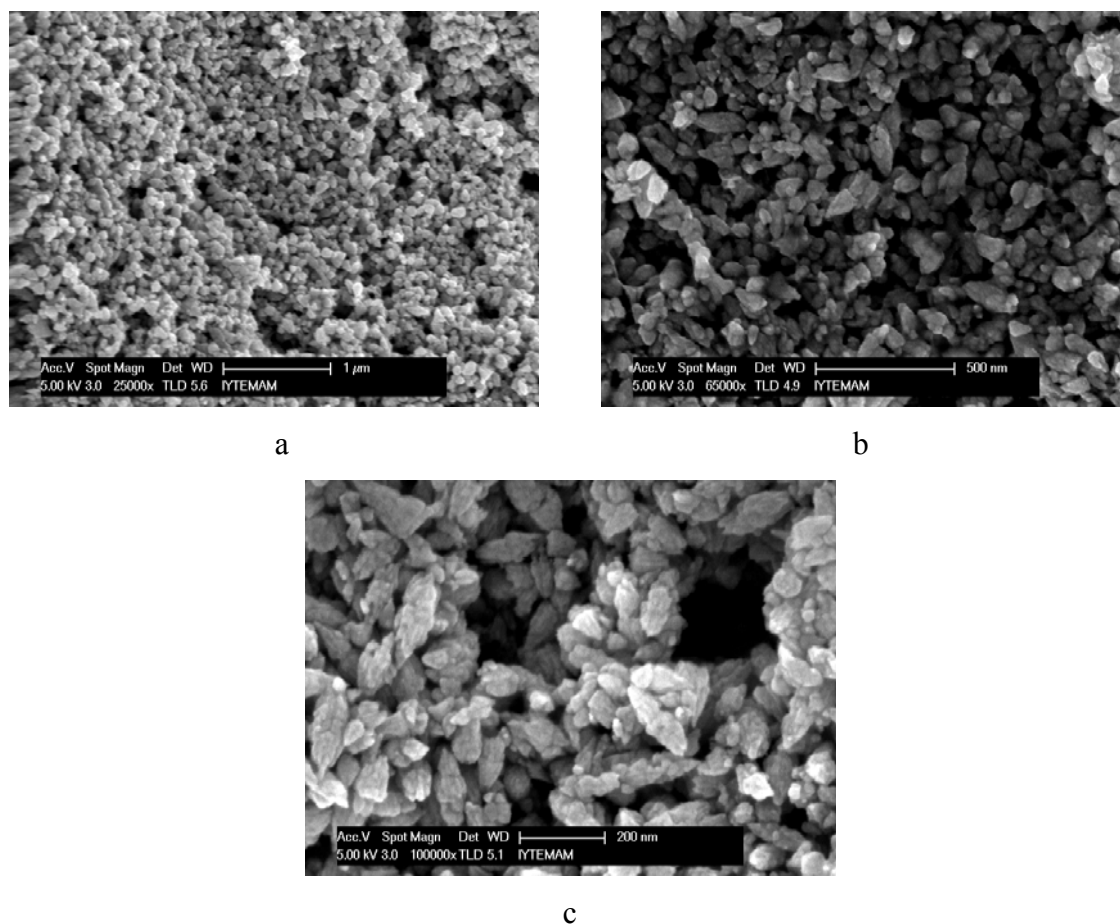


Figure 6.6. SEM micrographs of the synZnO powder of different magnifications a) 25000X b) 65000X and c) 100000X.

The SEM micrographs of the synZnO powder were nearly ellipsoidal in shape and were generally smaller than 100 nm in size (Figure 6.6-b), but there were some aggregates which increased the size of the particles seen in Figure 6.6-c. Energy dispersive X-ray spectroscopy (EDX) method was performed to make a rough estimation about the elemental analysis and chemical composition. The elemental analysis showed that 81.39 wt% zinc, 13.56 wt% oxygen and 5 wt% carbon structured the synZnO powder. The FTIR spectrum of the synZnO powder is shown in Figure 6.7.

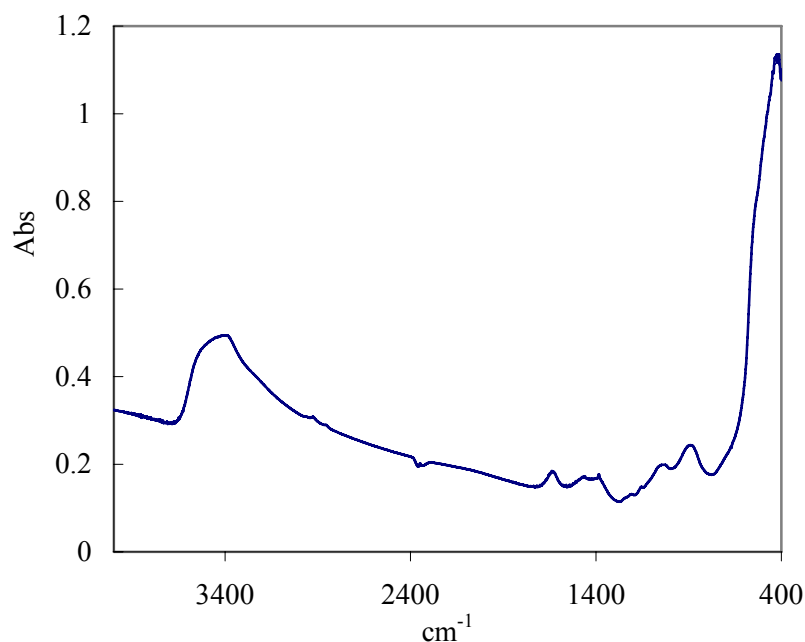


Figure 6.7. FTIR spectrum of the synZnO powder dried at 50 °C.

Zinc oxide showed a fairly simple, effective bonding between Zn-O (473cm^{-1} , 532 cm^{-1}) and was discussed in part 6.1 as well. Furthermore peaks were obtained at 1660 cm^{-1} corresponding to bending vibration of H_2O and peaks at 908 cm^{-1} , 707 cm^{-1} belonged to OH group which may due to $\text{Zn}(\text{OH})_2$. The thermal characterization of the 50 °C dried synZnO powder given in Figure 6.8 and Figure 6.9 was determined with TGA and DTA.

The DTA plot presents three maximum endothermic peaks at 59 °C, ~430 °C, and 940 °C, which induces to the release of water (loosely bond water and crystal water), dehydration of $\text{Zn}(\text{OH})_2$ and melting of the other impurities in the powder respectively. $\text{Zn}(\text{OH})_2$ detected from the spectroscopic results (FTIR) and DTA explaining the TGA data was due to the dehydration of $\text{Zn}(\text{OH})_2$ and water. The mass loss of the synZnO powder was 5.2%.

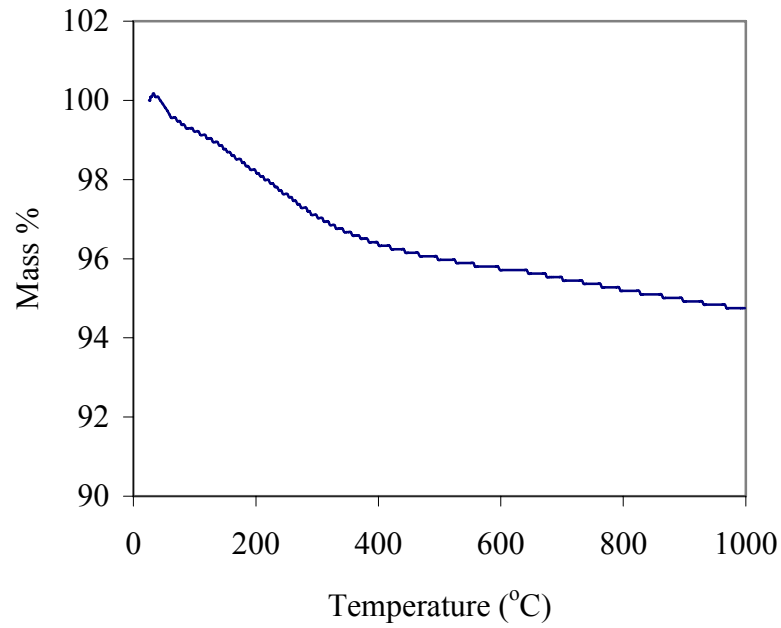


Figure 6.8. TGA curve of synZnO dried at 50 °C.

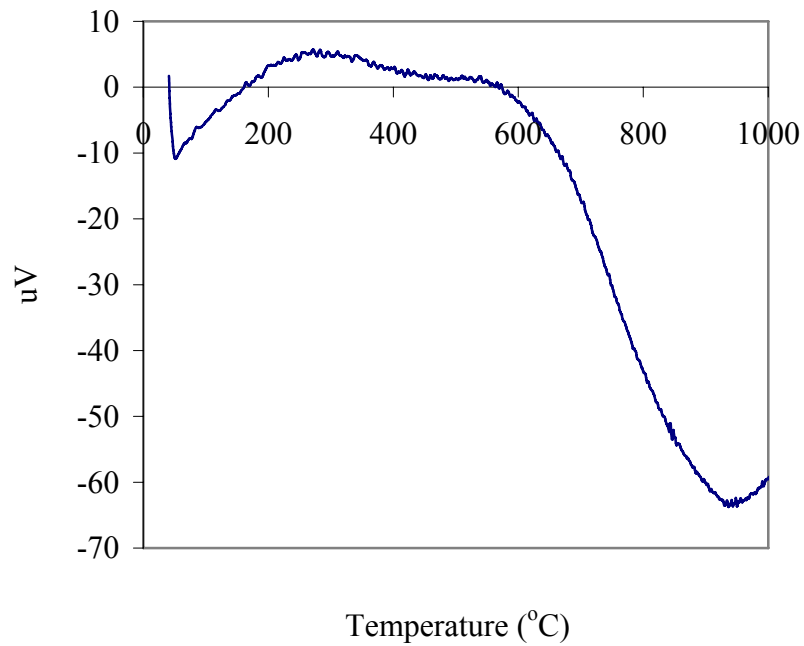


Figure 6.9. DTA curve of synZnO dried at 50 °C.

The powder mentioned above was dried at 50 °C while the polymer composite production was achieved at 170-190 °C. The powder was dried at 200 °C for 24 h under vacuum to enhance some problems like air bubbles in polymer composite production

caused by water and Zn(OH)_2 seen in 50 °C dried synZnO powder TGA results. The mean particle size of synZnO powder dried at 200°C given in Figure 6.10 was found 169 nm. The mean particle size (169 nm) does not confirm the XRD data (68 nm) since the crystals were small however big aggregates were obtained during precipitation and drying process.

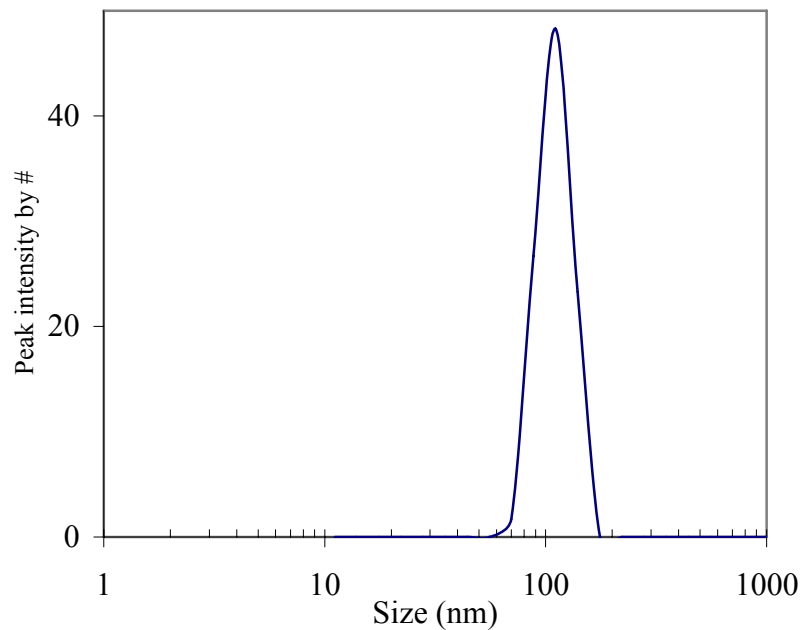


Figure 6.10. Particle size distribution of synZnO powder dried at 200 °C.

6.1.2. Characterization of Al doped ZnO Powder

ZnO is a semiconductive material. In order to improve the electrical properties of the ZnO powder (reduce the resistivity) one important method is introducing III-VA group elements such as boron, aluminum, gallium and indium to the powder. In this part of the study Al doped to improve the conductivity of ZnO powder was prepared by hydrothermal precipitation. Figure 6.11 shows the XRD pattern of the Al-doped powder.

In order to determine the phase transformation and orientation of the nano crystals XRD measurements were carried out. The 2theta values of the main peaks of AlZnO powder were at 11.01°, 22.4°, 31.54°, 33.9°, 34.14°, 36.044°, 47.38°, 56.36°, 62.6°, 66.1°, 68.8° and 72.3°. The XRD pattern shows a peak along the c-axis (002) corresponding to the orientation of the wurtzite structure at 34.14° 2theta. Depending on the Al-doping level, the maximum of the (002) peak decreases while the peak width broadens. An estimation of the nanocrystallite size was calculated by using the Scherrer formula (Equation 6.1). The crystal size calculated from 34.14° 2theta value was found 50.7 nm. A shrinking was obtained although the estimation of the particle size at the highest doping level is less accurate due to the low peak intensity and the large peak width, the tendency of a decreasing crystallite size with increasing extrinsic doping level is clearly visible. The 34.25° 2theta peak departed slightly to 34.14° with Al doping as Wan et al. (2008) indicated. The SEM micrographs of the powder are shown in Figure 6.12.

In Figure 6.12 Al-doped powders are polydispersed with some impurities coming from the ineffective washing of the precipitate. Although, the particles are small there are some big agglomerates due to heterogeneous phases in the structure. Back scattering detector of the microscope was used to detect the metallic Al in AlZnO powder. Since the doping was seen in the atomic level it could not be observed in the SEM micrograph due to the undetectable size of metallic Al and Zn. EDX elemental analysis of AlZnO powder resulted as 79.82 wt% zinc, 10.82 wt% oxygen, 2.22 wt% aluminum and 7.14 wt% carbon. As a consequence, 6% of Zn atoms were substituted with Al atom.

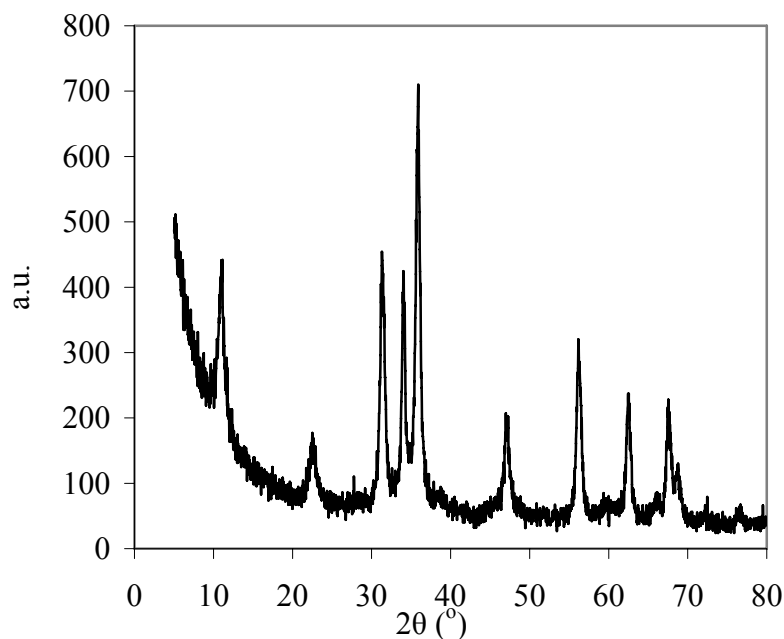


Figure 6.11. XRD pattern of the AlZnO powder dried at room temperature.

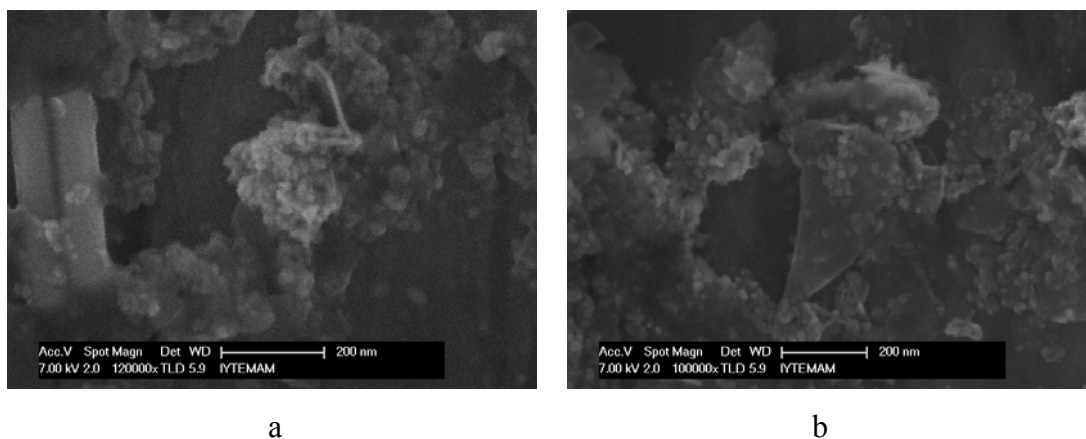


Figure 6.12. SEM micrographs of AlZnO powder for different magnifications dried at room temperature a) 120000X b) 100000X.

The FTIR spectrum of the Al-doped powder is given in Figure 6.13. The main vibration peaks for room temperature dried powder are assigned as follows: a shoulder at 740 cm^{-1} and 930 cm^{-1} (Wan et al., 2008) belong to vibration of Al-O units; the band at 450 cm^{-1} and 560 cm^{-1} corresponds to vibration of Zn-O bond; and the bands at 1640 cm^{-1} and 3500 cm^{-1} corresponds to H_2O bending and OH stretching respectively. The peak around 1400 cm^{-1} could correspond to NO_3^- peak. After calcination and annealing

process the peaks which correspond to NO_3^- , OH^- and H_2O disappear. The FTIR spectrum of the powder change and the peaks which were pertaining to ZnO shifted, 450 cm^{-1} peak to 520 cm^{-1} , 520 cm^{-1} shifted to 560 cm^{-1} and 720 cm^{-1} shifted to 742 cm^{-1} . Since the peak at 700 cm^{-1} corresponds to Al-O, FTIR results showed that Al ions incorporate into ZnO lattice.

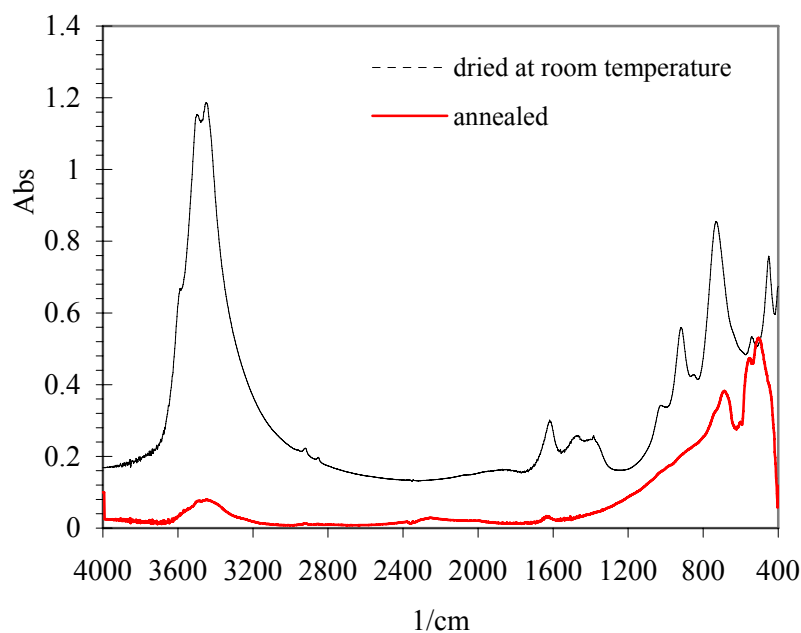


Figure 6.13. FTIR spectrum of Al doped ZnO powder.

The particle size distribution of Al- doped powder is given in Figure 6.14. The particle size distribution of the powder was analyzed by number; and for room temperature dried powder it was found that, the 97% of the powder was in mean diameter of 122 nm and 3% of the powder was in mean diameter 508 nm. This difference is due to big agglomerates of the powder. The mean particle size of annealed AlZnO powder was found 820 nm. The calcination and annealing process lead to increase in the crystal size and for the reason that the particle size increases. TGA and DTA curves of AlZnO powder are given in Figure 6.15 and Figure 6.16 respectively.

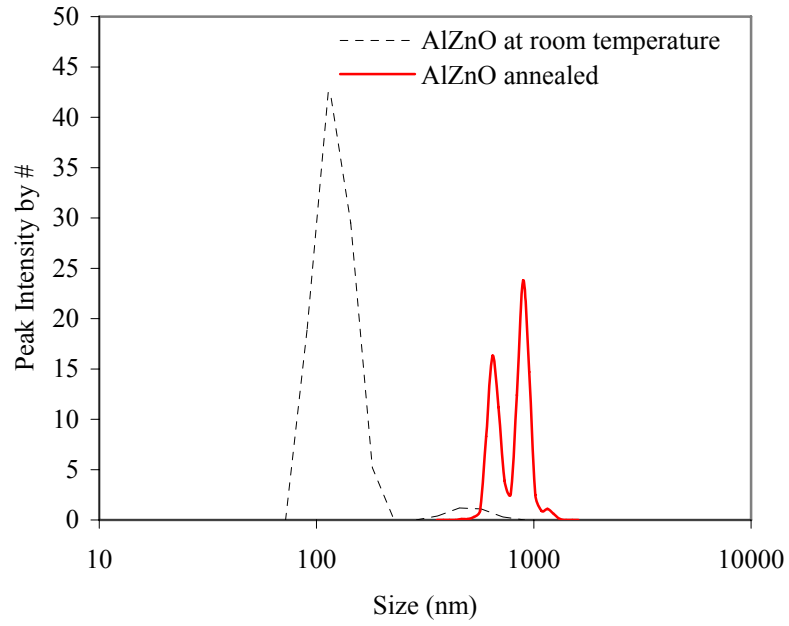


Figure 6.14. Particle size distribution of AlZnO.

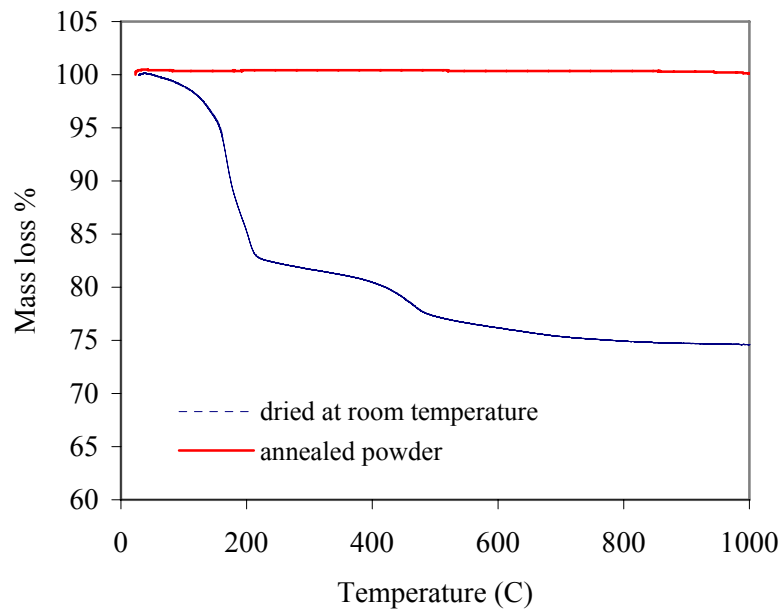


Figure 6.15. TGA curve AlZnO powder.

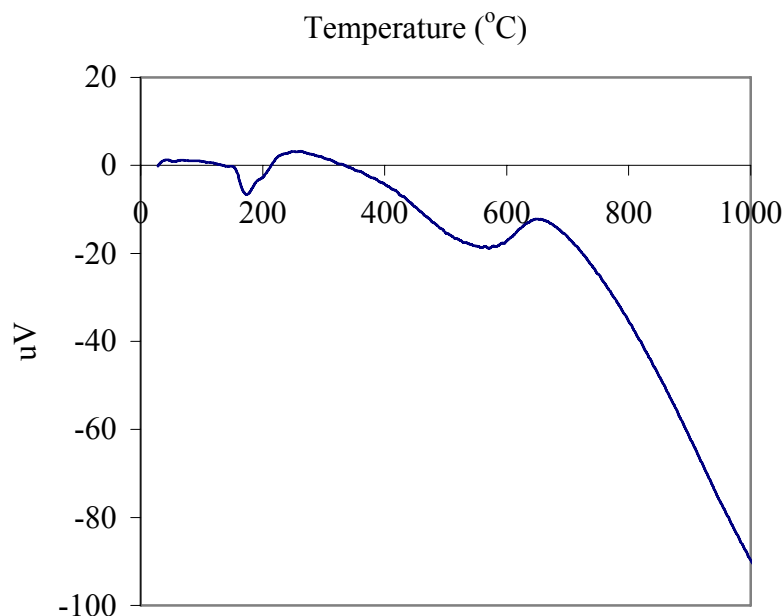


Figure 6.16. DTA curves of Al doped-zinc oxide dried at room temperature.

TGA curves exhibit two distinct weight loss steps for room temperature dried powders and the DTA curves indicating one weak and one significant exothermic and endothermic peak. The former weight loss depending on the loss of water is caused by rising up the temperature from room temperature to 200 °C. The latter weight loss at 200–450 °C, accompanied by a weak exothermic peak around 450 °C in the DTA curve, might be the result of the decomposition of the organic intermediates and dehydration of water. The third weight loss at 450–600 °C and the significant exothermic peak around 630 °C in the DTA curve, could be attributed to the formation of Al phase. Annealed AlZnO powder TGA analysis showed zero mass loss as given in Figure 6.15. All impurities and water were degraded during calcination and annealing processes. To improve the electrical properties of the Al-doped powder; the powder calcined to 900 °C under atmospheric air and then annealed 2 hours under N₂ atmosphere. Calcination process supplied to remove the impurities and to reduce Zn(OH)₂ to ZnO at 900 °C. ZnO powder and Al⁺³ tend to be unstable at 900 °C, and this temperature helped metallic Al to interfere to the material. N₂ gas was passed through the powder at 700°C to obtain a stable powder containing metallic Al. The XRD pattern and the SEM micrographs is given in Figure 6.17 and Figure 6.18, respectively.

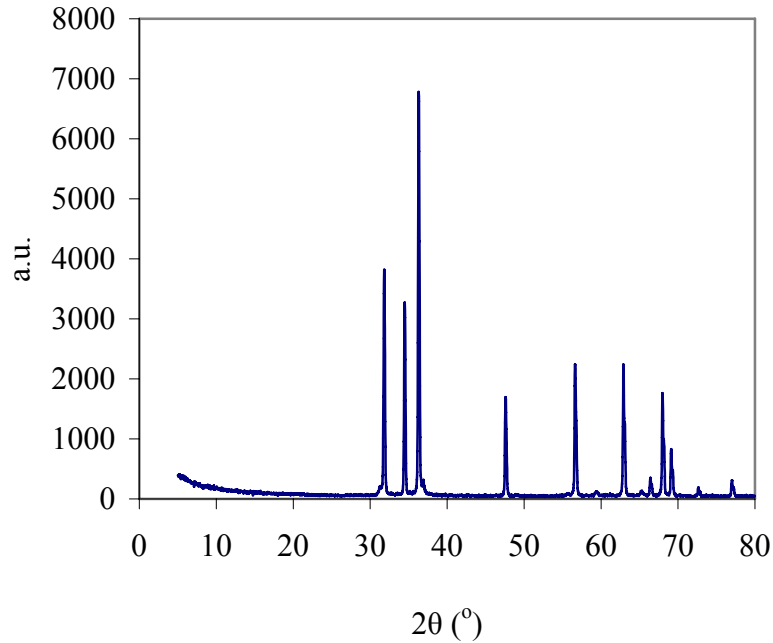


Figure 6.17. XRD pattern of Al doped annealed ZnO powder.

The crystal size calculated from 34.32° 2theta value was found to be 176.9 nm from Scherrer equation. The crystals enlarged due to calcination, which could be supported by SEM micrographs as well. The last micrograph was taken by using back scattering detector. The brighter parts correspond to zinc and the dark parts to aluminum. However 5 mol% Al was added during the preparation of AlZnO powder, 3.2 mol% Al was detected by EDX analysis.

According to Serier et al. (2009) lower Al-doping levels of ZnO samples than expected could due to the incorporation of higher Al⁺³ percentages of precursor, or the excess aluminum could be in noncrystallized form i.e not detectable by XRD. Serier et al. (2009) found that introduction of Al⁺³ dopant inside ZnO lattice was difficult, with steric, electronic and geometric conditions. According to XRD investigations Al⁺³ doping is in low level owing to very low solubility limit (under 0.3 mol %),.

Many semiconducting oxides display n-type conductivity. One of the reason is the formation of cation interstitials (donors) is easier than the formation of anion interstitials (acceptors) (van de Krol and Tuller, 2002). The Zn atoms are tetrahedrally coordinated to four O atoms, where the Zn d-electrons hybridize with the O p-electrons.

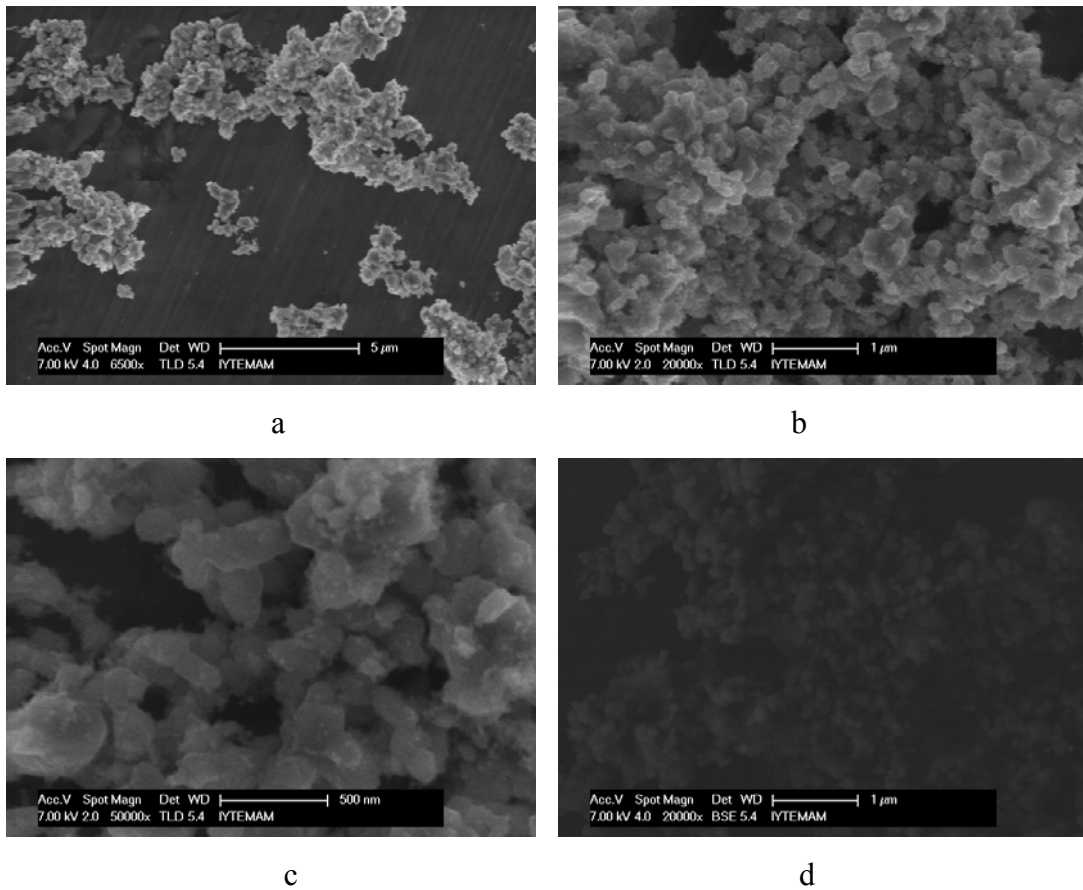


Figure 6.18. SEM micrographs of Al doped annealed ZnO powder for different magnifications annealed at 900 °C a) 6500X b) 20000X c) 50000X d) BSE 20000X.

6.1.3. Surface Modification of ZnO

A PP/PE-ZnO composites property was to improve by enhancing the interphase between polymer and ZnO powder. For this purpose ZnO was treated with two different types of modifier: aminopropyltrimethoxy silane (AMPTES) and polyethylene glycol 4000 (PEG 4000).

There are a lot of different methods which can be used to investigate the treatment of the surface modifier onto ZnO which one of them is measuring the contact angle. To make the polymer and ZnO surface incompatible the hydrophilic ZnO surface was modified with an organic compound to make the ZnO surface hydrophobic. The contact angles of the polyethylene and polypropylene determined by using contact angle

of water and were found; 76° and 56° respectively. The contact angle of the ZnO powder was obtained (water contact angle) as 47° , 38° , and 45° for eZnO, nZnO and sZnO pellets, respectively. The contact angles of the polymers were expected to be higher than 90° , since both PP and PE were hydrophobic materials. In PP and PE composites the migration of ZnO to the surface may cause low contact angles which induces errors. In order to understand, if there was an error in contact angle measurements coming from the surface roughness of the materials; the surface roughness of composite films were measured. Roughness of the composites (PE and PP) was found $0.09\ \mu\text{m}$ and $0.29\ \mu\text{m}$, respectively. For the sintered ZnO powder it was found; $0.02\ \mu\text{m}$, $0.07\ \mu\text{m}$, and $0.2\ \mu\text{m}$ for eZnO, sZnO and nZnO powder, respectively. There should be no error coming from the roughness of the materials already they were found to be very low.

The modification of ZnO powders were characterized with FTIR spectroscopy. The FTIR spectra of the PEG 4000 modified nZnO powders and AMPTES modified nZnO powders are given in Figure 6.19 and Figure 6.20 and others are attributed in Appendix A.

Characteristic peaks of (Zn-O) 473cm^{-1} , $532\ \text{cm}^{-1}$ were seen in the FTIR spectra. Figure 6.19 observes the characteristic Zn-O peaks. Organic peaks seen in the FTIR spectra instead of characteristic ZnO peaks were attributed to polyethylene glycol. The $2800\ \text{cm}^{-1}$ C-H stretching, $1100\ \text{cm}^{-1}$ C-O-C stretching, $1300\ \text{cm}^{-1}$ CH_2 bending and $1200\ \text{cm}^{-1}$ CH_2 twisting vibration, are the peaks related with PEG 4000 (Derosa et al., 2002). Two different modifier (PEG 4000 and AMPTES) weight percentages (1 wt% and 2 wt%) were used for the modification of ZnO powders and the quantitative analysis carried out with FTIR data confirmed experimental weight percentages. The characteristic peaks of Zn-O peaks were observed and silane coupling agents characteristic peak was at $1591\ \text{cm}^{-1}$ belonging to amine in AMPTES is given in Figure 6.20. Other peaks were related with Si-O- C_2H_5 group at $1030\ \text{cm}^{-1}$ bond and silylester of AMPTES at $1132\ \text{cm}^{-1}$ (Metin, 2002).

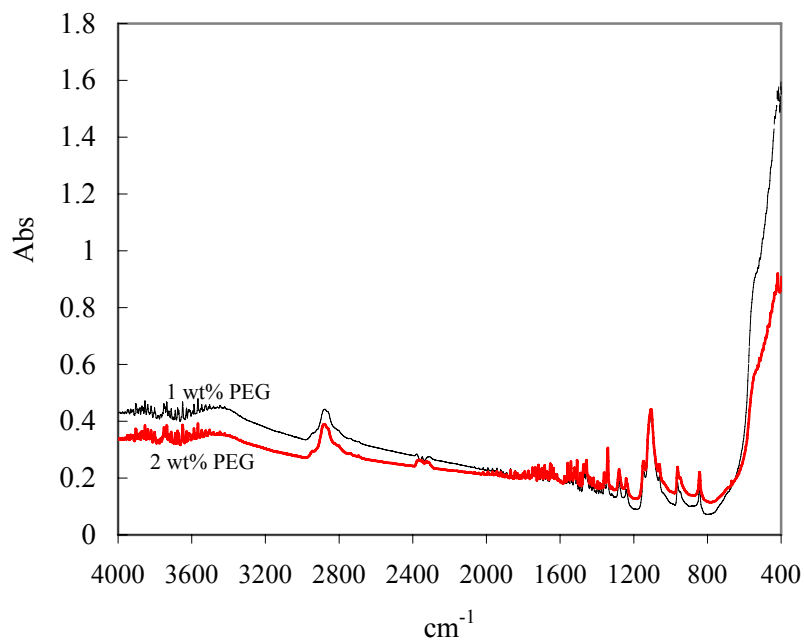


Figure 6.19. FTIR spectra of PEG 4000 modified nZnO powder.

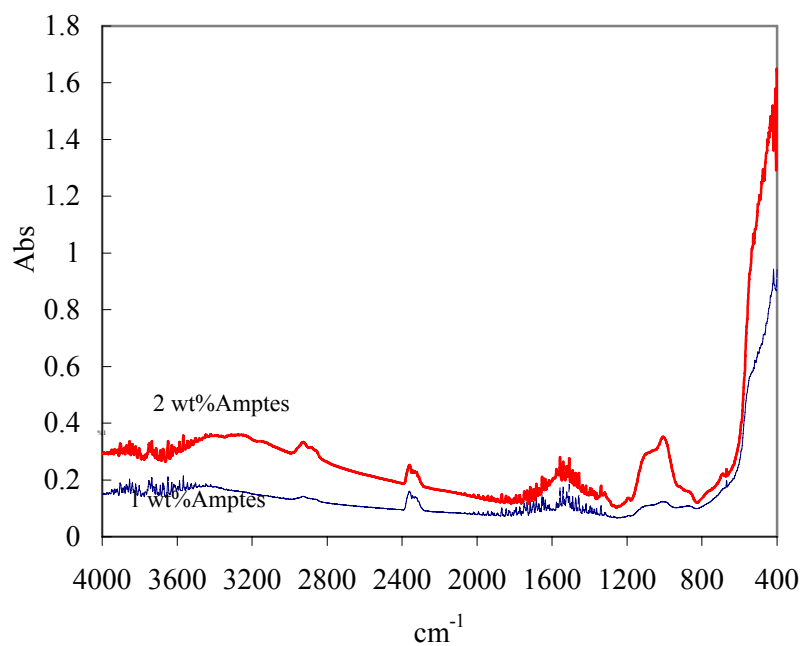


Figure 6.20. FTIR spectra of AMPTES modified nZnO powder.

6.1.4. The Electrical Properties of ZnO Powder

The volume resistivity values of zinc oxide powders were measured by preparing pellets of zinc oxide and taking contact points by thermal evaporation method with silver. Figure 6.21 gives the sweeping voltage versus current for synZnO. I-V (Current, I; Voltage, V) curves of other ZnO powders are given in Appendix B. The resistivity values were calculated according to ohm's law, the curve was linearized with a very high "0.9984" correlation coefficient. The resistivity values were calculated using the reverse slope of the I-V line. The volumetric resistivity calculations were done by multiplying the area/thickness of the pellets. The calculated volumetric resistivity were found 1.5×10^6 , 1.5×10^9 , 1.7×10^8 , and 1.3×10^7 ohm-cm for eZnO, sZnO, nZnO and synZnO, respectively.

Non-ohmic devices are generally electronic ceramic materials. These non-ohmic ceramic devices were also known as "metal-oxide" varistors (variable resistors). These types of materials show a highly nonlinear current-voltage (I-V) characteristic with a highly resistive state in the pre-breakdown region as given in Figure 6.22 (Bueno et al., 2008). In a diode characteristic material I-V curve shows typically a diode characteristic peak as seen in Figure 6.23.

As given in the characteristic diode curve (Figure 6.22), very small changes in voltage can cause very large changes in current. The breakdown process depends upon the applied electric field, so by changing the thickness of the layer to which the voltage is applied under the influence of the applied electric field can be accelerated enough. I-V curve (Figure 6.23) of Al-doped ZnO powders was not suitable for resistivity calculations determined with ohm's law. If a calculation has to be carried out with ohms law the curve was divided into two part which were between 0-20 V and 20-35 V resulting with resistivity's of around 10^5 ohm-cm and 10^4 ohm-cm, respectively.

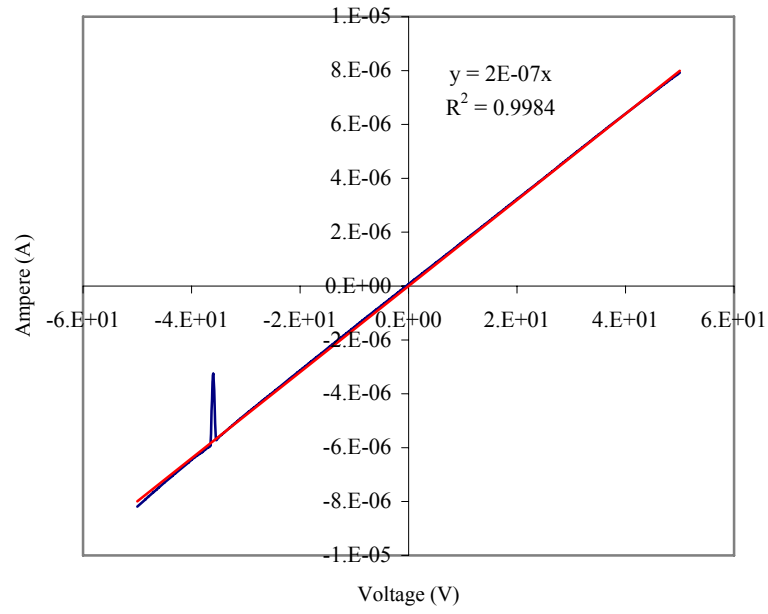


Figure 6.21. Sweeping voltage versus current values for synZnO.

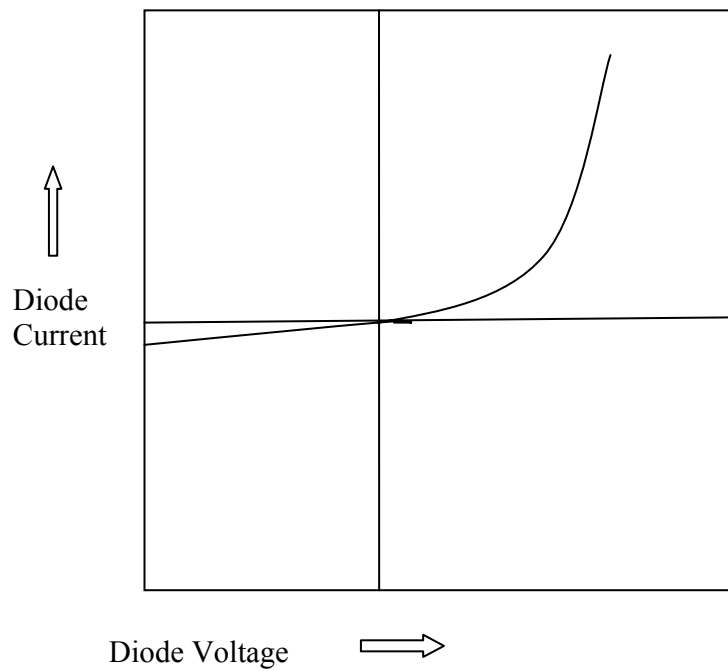


Figure 6.22. Typical diode curve
(Source : Bueno et al., 2008).

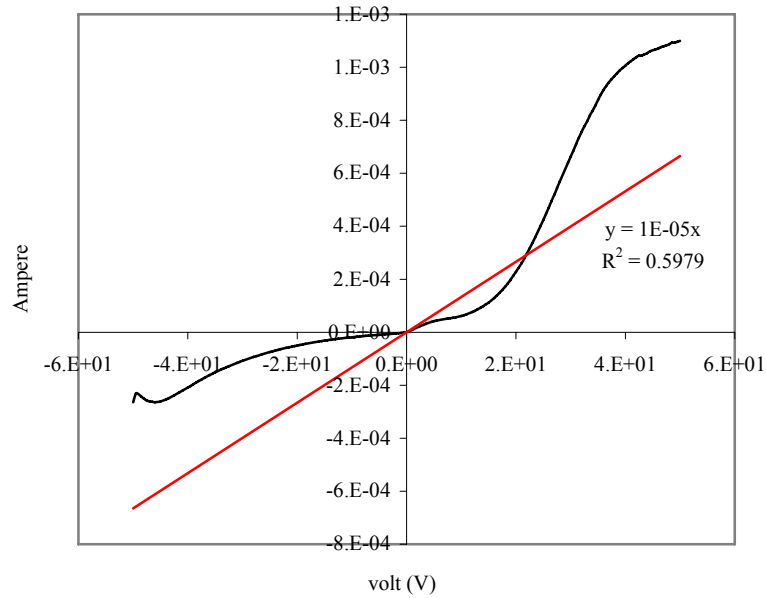


Figure 6.23. Sweeping voltage versus current values for annealed Al doped ZnO.

Serier et al. (2009) explained the doping mechanism by two different ways given in Figure 6.24.

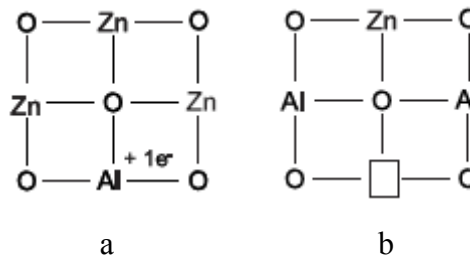


Figure 6.24 a-Creation of free electrons b- formation of vacancies (Source: Serier, 2009).

In Figure 6.24-a Zn^{+2} cation was replaced with an Al^{+3} cation paired up with a free electron, so the conductivity of the material was predicted to increase. In Figure 6.24-b three Zn^{+2} cations were replaced by two Al^{+3} cations, due of neutral defects acting as electron traps, no electrical conductivity was expected (Serier, 2009). Al doped powder was prepared to have a higher electrical conductivity than undoped ZnO powders since the conduction of ZnO powder tend to increase with presence of metallic Al ions. Annealing was important for having highly conductive materials in doped

systems. After precipitation of AlZnO powders by hydrothermal synthesis (at 30°C), the Al ions which were not in metallic form was presented on the surface of the ZnO powder. The aim of the annealing procedure was to diffuse the Al ions into the interior of the ZnO and partially replace the Al ion by the Zn ions rapidly while the temperature is increased. The powder was heated until 900 °C under oxygen atmosphere and all of the impurities were removed resulting unstable zinc and aluminum ions. The flow of the air was cut and an inert gas (N₂) was given to the system to terminate the reactions and Al ions got to the interior of the zinc oxide. According to Wan et al. (2008) the increase of resistivity might be due to the oxygen vacancies which have been taken up by Al ions and as the temperature further increased, Zn ions were substituted by Al ions and the carrier concentration increased. Therefore, the resistivity of ZnO reduced rapidly. AlZnO powder was prepared intending to increase the number of free charge carriers for this semiconductor, decrease the particle size of the powders and increase the possibility of obtaining conductive network. However decreasing crystal size increased the band gap energies of the materials.

6.1.5. Optical Properties of ZnO Powders

The optical properties of ZnO, were investigated by reflection, absorption and fluorescence spectrum analysis. A well known UV blocking material ZnO takes considerable attention, especially in UV-A region. UV-irradiation is a frequently encountered factor that can induce photo-degradation of polymers. “Severe molecular chain degradation in PP can be induced when it is irradiated within the active wavelength range of 310–350 nm, which means that photo-degradation can occur easily in PP based materials.” (Zhao and Li, 2006). The reflection spectra of the commercial ZnO powders taken by dry pressing and are given in Figure 6.25 to understand the effect of light on visible and UV regions.

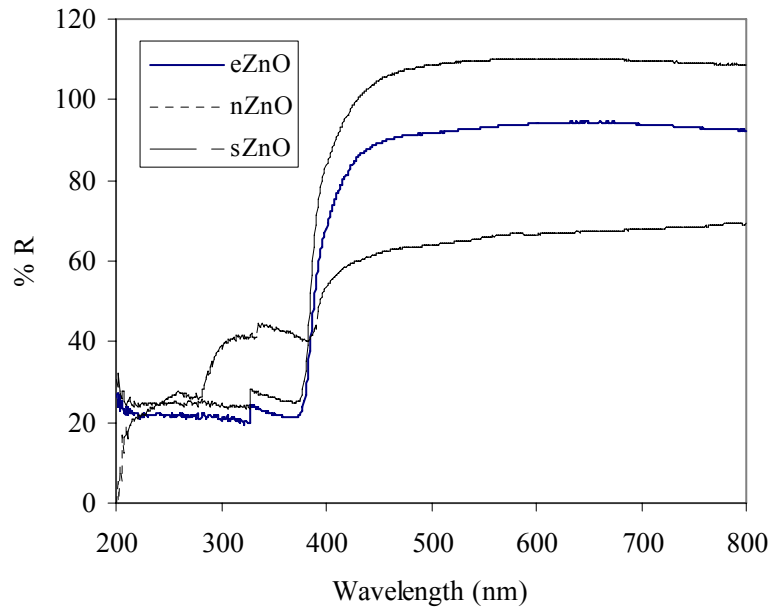


Figure 6.25. Reflection spectra of zinc oxide powders.

Reflection spectra of zinc oxide powders were about the same for eZnO and sZnO powders. Until 476 nm the sZnO reflects the light at about 100 % and in the UV region absorbs the 80% of the light. For eZnO powder except in visible region 90 % of the light reflected and about 10% was absorbed. nZnO powder, 60% of the visible light was reflected in 400-700 nm, in the UV region between 280-400 nm 60% of the light was absorbed and below 280 nm nearly %100 of the light was absorbed. In reflection spectra of the powder low reflectance value indicate high absorption in the corresponding wavelength region. In the visible region the powders were opaque and white. Simultaneously, composites did not absorb the visible light; however in the UV-region the light was absorbed.

The absorption spectra of the commercial and prepared powder are given in Figure 6.26 and Figure 6.27, respectively. They were spectra of very dilute aqueous solution of the powders.

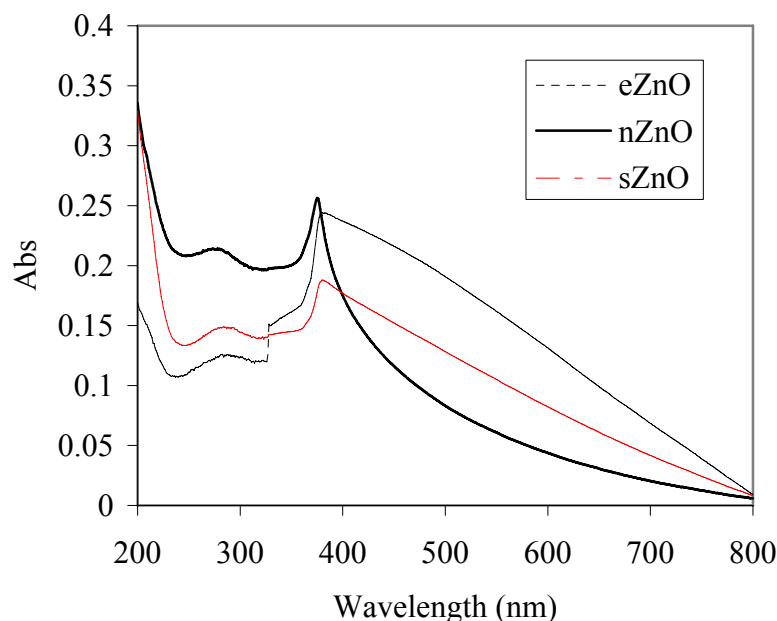


Figure 6.26. Absorption spectra of commercial powders.

The absorption spectra of the commercial zinc oxide powders observed peak maxima. The absorption of the powder started in visible region and increased in UV light region. However it was not expected, haziness of the suspension could effect on starting the absorption in the visible light region. The peak maxima values of eZnO, sZnO, nZnO and synZnO powders as given in Figure 6.26 and Figure 6.27 were found 378 nm, 376 nm, 373 nm and 353 nm, respectively. As a consequence UV-A light absorbed by the ZnO powders the band gap energy was justified by following the crystal size of the powders. The peak maximum of AlZnO powder as given in Figure 6.27 was found at 328 nm and this powder also absorbs light in the visible region.

The fluorescence spectra of the ZnO powders were taken by dry pressing and given in Figure 6.28 to Figure 6.33 for eZnO, sZnO, nZnO, synZnO and AlZnO powders, respectively. It is difficult to compare the PL spectra (fluorescence spectra) of samples resulting with different directly emission intensities, because neither the fabrication of powders nor the quantity of the samples were same. However the peak positions can be compared. A blue–green emission, centered at around 500 nm in wavelength, has been explained within the context of transitions involving self activated centers formed by a doubly ionized zinc vacancy and an ionized interstitial Zn, oxygen

vacancies, donor–acceptor pair recombination involving an impurity acceptor, and/or interstitial O.

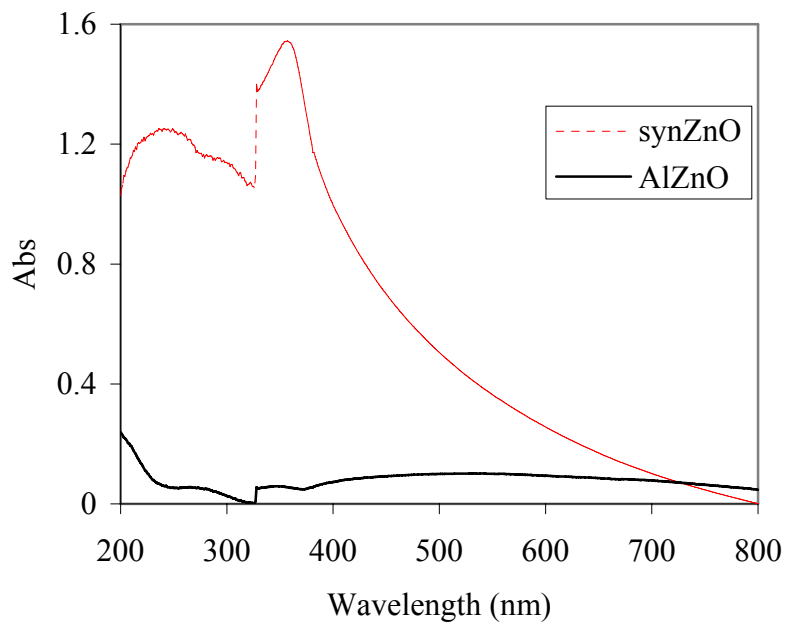


Figure 6.27. Absorption spectra of prepared powders.

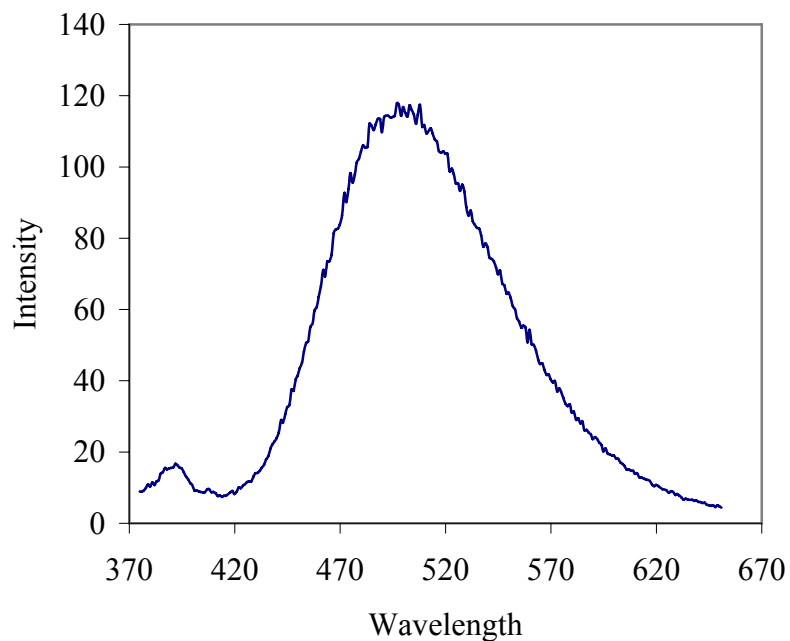


Figure 6.28. Fluorescence spectrum of eZnO.

eZnO shows a weak narrow UV band around 380 nm due to radiative annihilation of exciton and a broader band in the green part of the spectrum with a maximum at 500 nm due to the defects in the sample caused by doubly ionized zinc or oxygen vacancy.

The PL spectrum of sZnO powder shows peaks at 421 nm, 480 nm, 510 nm and 530 nm. The PL spectrum was slightly different from eZnO since there was no peak observed in the UV region but there were a lot of peaks in green and yellow regions exhibiting the different defects in the system. The same occasion is observed for nZnO powder as seen in Figure 6.30. The PL spectra of eZnO and other powders showed different defects and light emissions. Since eZnO is a commercial material and the defects are greater than the powders which are produced only for R&D studies.

In synZnO two peaks are observed. The peak at 391 nm corresponds to free exciton or bound exciton of ZnO in the UV region. The zinc vacancy attributed a blue luminescence at 405 nm. However the green and yellow luminescence which was mentioned for complex defects did not occurred for this powder.

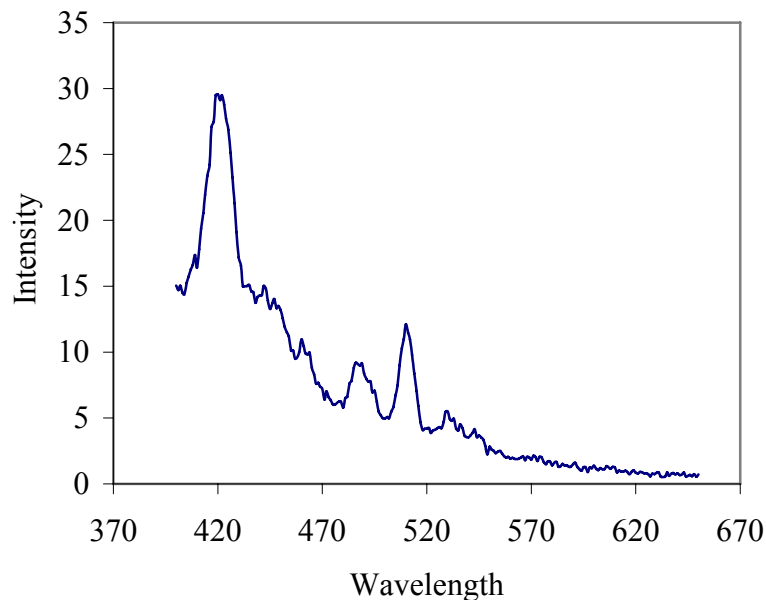


Figure 6.29. Fluorescence spectrum of sZnO.

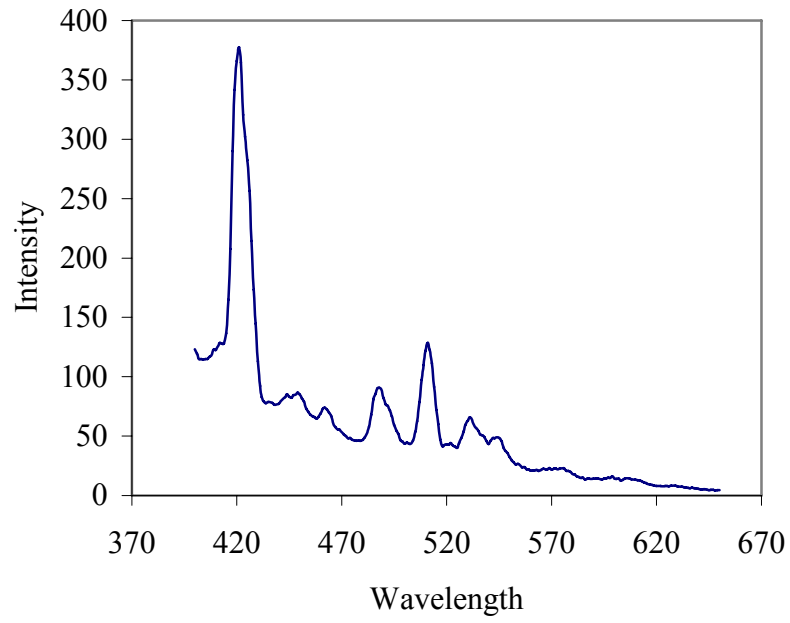


Figure 6.30. Fluorescence spectrum of nZnO.

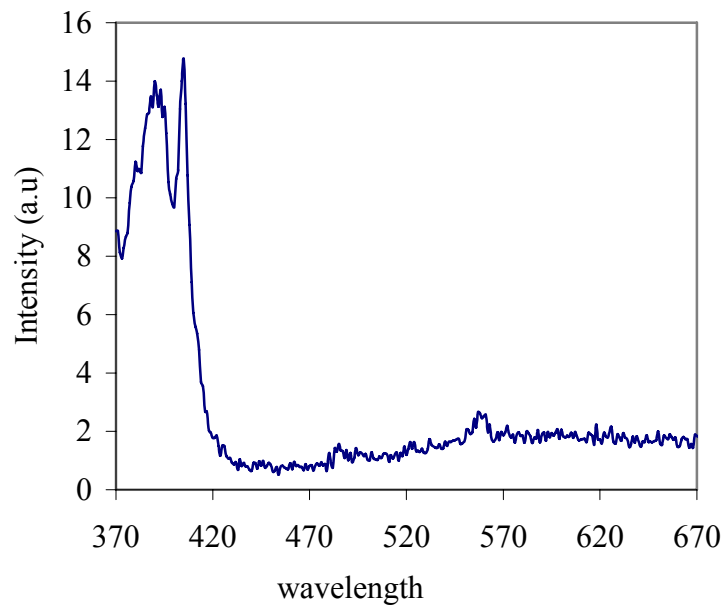


Figure 6.31. Fluorescence spectrum of synZnO.

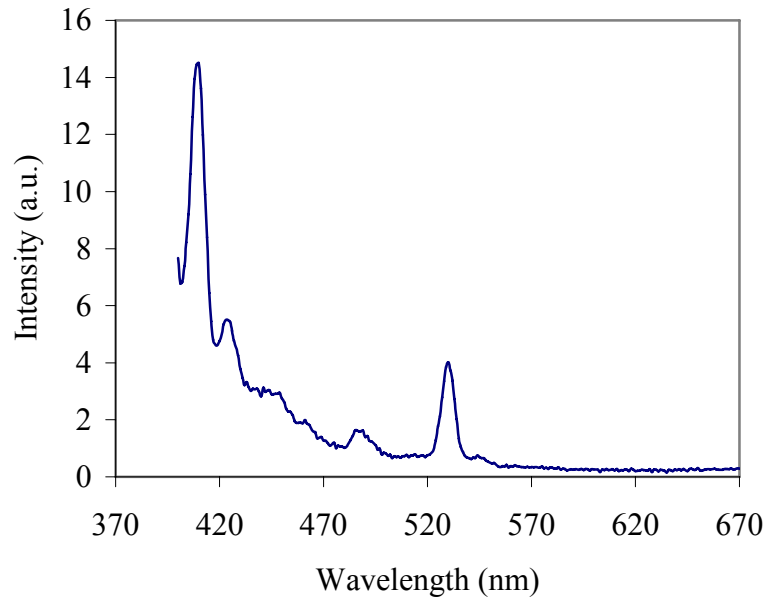


Figure 6.32. Fluorescence spectrum of AlZnO.

The doping of the fluorescence spectrum of the powder was expected to be changed with the acceptor-donor relation. Figure 6.32 shows the fluorescence spectrum of AlZnO powder. AlZnO powder peaks were observed at 411, 425, 465, 490 and 531 nm wavelength. There was a green emission at 530 nm pointing out the presence of defects due to acceptor donor relation. The peak at 425 nm attributed to interstitial zinc. Blue emission at 410 nm was observed in ZnO that might be due to possible existence of cubic ZnO. Again oxygen and zinc vacancies or interstitial or their complexes, gave an emission peak at 460 nm.

Table 6.1 clearly represents the absorption and emission peaks of zinc oxides. The particle size effect was not seen in the emission spectra of the powders but the defects were generally obtained due to zinc or oxygen vacancy except synZnO powder. In this powder there was an emission peak due to exciton of ZnO in UV region and a small defect due to zinc vacancy. As a conclusion, the synZnO which was prepared in laboratory was a defect free powder compared with other powders.

Table 6.1. The absorption and emission spectrum results of zinc oxide powders.

ZnO	Absorption peaks (nm)	Emission Peaks (nm)
eZnO	378	380, 500
sZnO	376	421, 480, 510, 530
nZnO	373	421, 480, 510, 530
synZnO	353	391, 405
AlZnO	328	411, 425, 465, 490, 531

6.2. Characterization of Polymer Composites

The mechanism of electrical and thermal conductivity of the composites could be explained by understanding the interface and morphological relation between polymer and ZnO powders. Morphological, structural and thermal characterization methods were applied to characterize the polymer composites.

6.2.1. Structural and Morphological Characterization of Polymer Composite

The appearance of ZnO filled PP matrix composites was white, opaque, smooth, bright and brittle. The physical properties of PE matrix filled composites were suitable for PP matrix filled composites; however PE matrix composites were more elastic. The dispersion of ZnO particle appeared homogenous (naked eye) for both PE and PP matrix composites. The filler dispersion into polymer matrix was investigated by SEM. These analyses were performed on the fracture surface of the composites. The composites dipped in the liquid nitrogen and the fractured surfaces elemental analyses for composites were taken using SEM and SEM-EDX module. The morphologies of sZnO-PE composites and sZnO-PP composites are given in Figure 6.33 and 6.34, respectively.

Particles of metal oxide appear as white features against dark background due to the polymer as seen in Figure 6.33. As seen in the figure, almost all particles were distributed in the continuous phase (PE phase) or nearby the interfaces between continuous phase and dispersed phase. Figure 6.33-a-d observes the concentration difference of the zinc oxide particles. In Figures 6.33-a, b and c the particles of zinc oxide are far from each other. However, in some of the regions there were spaces obtained between the powder and polymer. This attributes to the adhesion problem in the interface between polymer and filler or they may be formed during fracturing of the composites. In Figure 6.33-d there is a view like spider's web formed by plastic deformation of polymer phase during fracture. sZnO loaded PP matrix composites SEM micrographs shown in Figure 6.34 with increasing filler concentrations depicted a same trend (adhesion and wetting problem) with PE matrix composites.

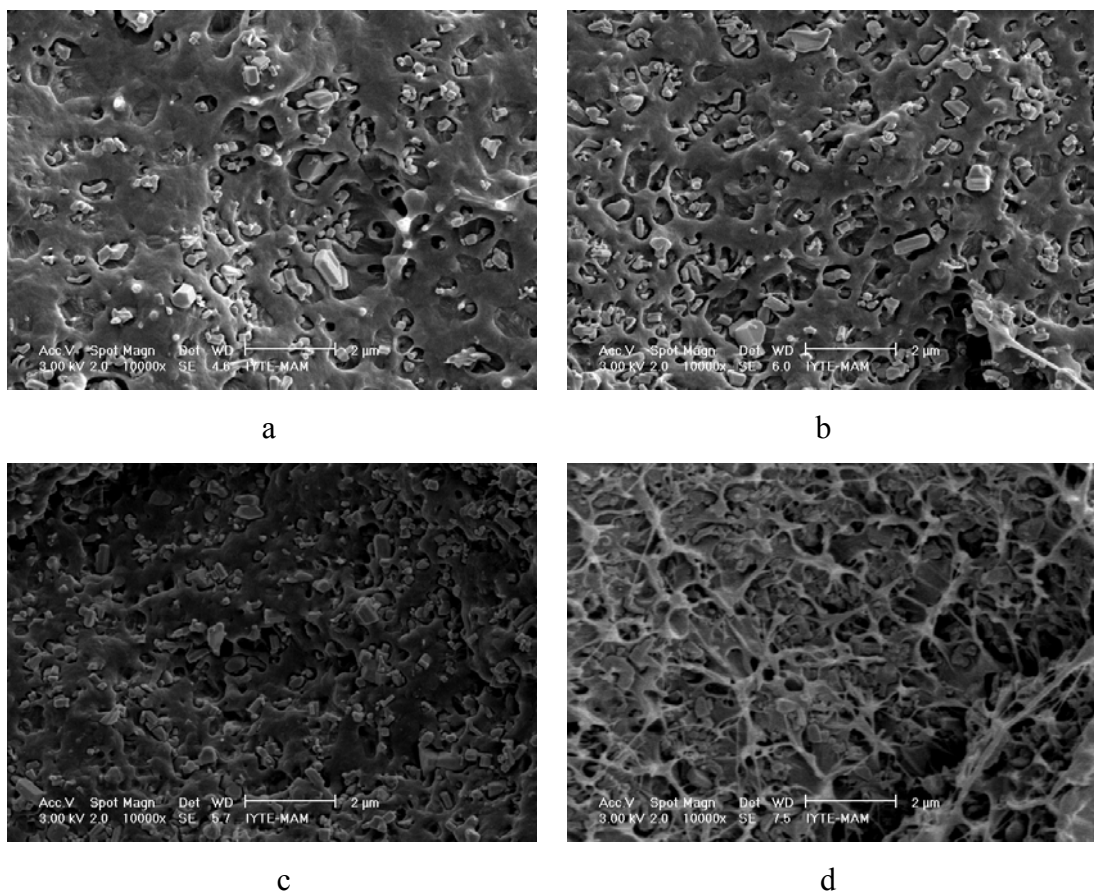


Figure 6.33. sZnO –PE composite SEM micrographs a) 5vol% sZnO-PE, b) 10vol% sZnO-PE, c) 15vol% sZnO-PE, d) 20vol% sZnO-PE.

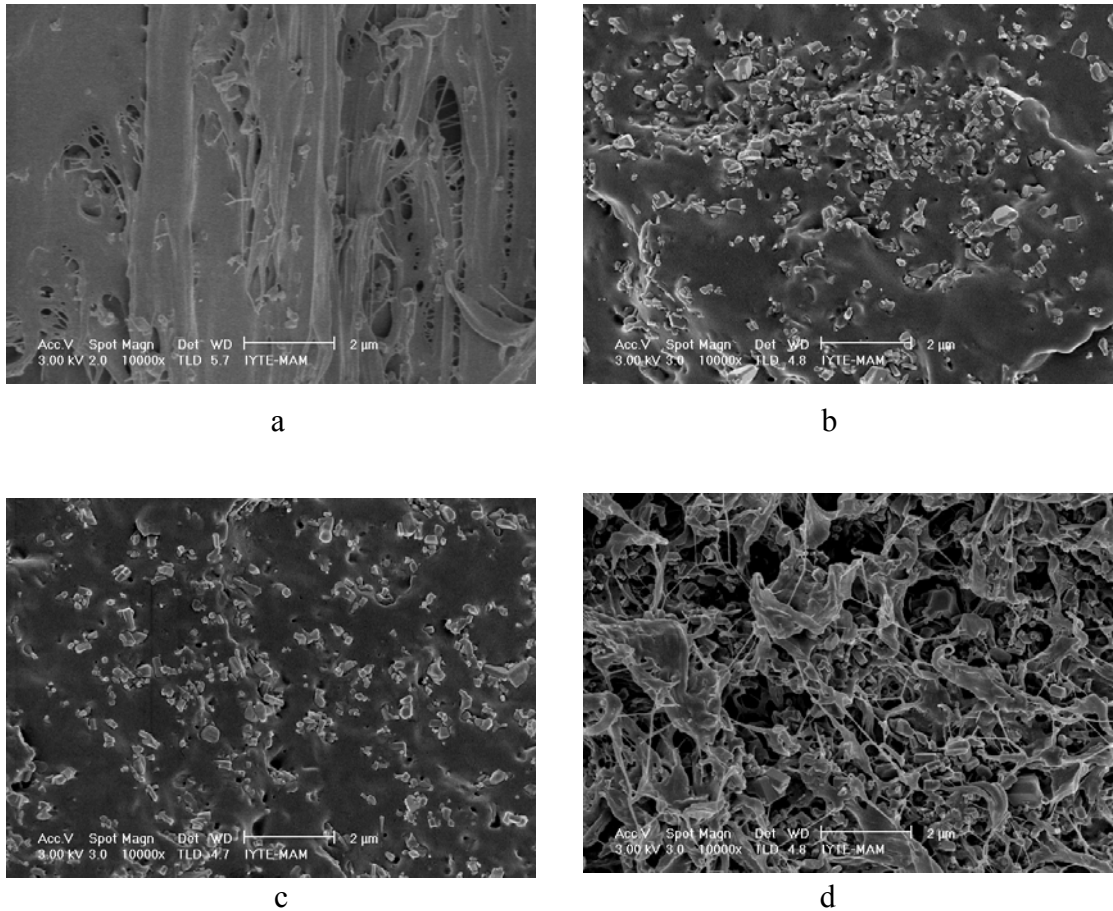


Figure 6.34. sZnO-PP composites SEM micrographs a) 5vol% sZnO-PP, b) 10vol% sZnO-PP, c) 15vol% sZnO-PP, d) 20vol% sZnO-PP.

To overview if there is a serious wetting and adhesion problem observed for all of the prepared composites (eZnO-PE, nZnO-PE, synZnO-PE and AlZnO-PE) the SEM micrographs were taken for the highest loaded ZnO-PE composites and given in Figure 6.35.

eZnO-PE matrix composites look well dispersed in Figure 6.35-a however they look like over loaded. In the highest filler loaded sZnO-PE, the particles of the filler did not agglomerate, but the polymer could not wet the filler efficiently because of the overloading of ZnO powder. In nZnO powder loaded composites, adhesion problem did not obtain but the particles were getting larger because of the agglomerations. Some of the agglomerate sizes were about 1 μm . 15 vol% nZnO-PE composites could be prepared from nanosized ZnO powder since the 20 vol% nZnO-PE composites could not be prepared due to the wetting problem between polymer and filler. It is known that inorganic materials are not easily dispersed in most of the polymers because of their

preferred face-to-face stacking in agglomerated tactoids, which make them incompatible with hydrophobic polymers. It is necessary to consider the coupling agent to enhance the adhesion and overcome the wetting problem. In synZnO loaded composite and AlZnO loaded composite some of the particles were well dispersed and some were agglomerated. Especially in AlZnO loaded composite, the particle size enlarged about 1-2 μm . On the other hand air gaps were obtained during the production of the composite what would negatively affect the conductivity and mechanical properties of the composites. Filler distribution in continuum polymer matrix is very important; since the electrical and thermal conductivity mechanisms are changing. To understand, if there was a conductive path obtained in the composites (homogenous dispersion), maps of the elements (Zn and C) were determined by using SEM-EDX mode and given in Figure 6.36 for eZnO-PE/PP, sZnO-PE/PP and nZnO-PE-PP composites.

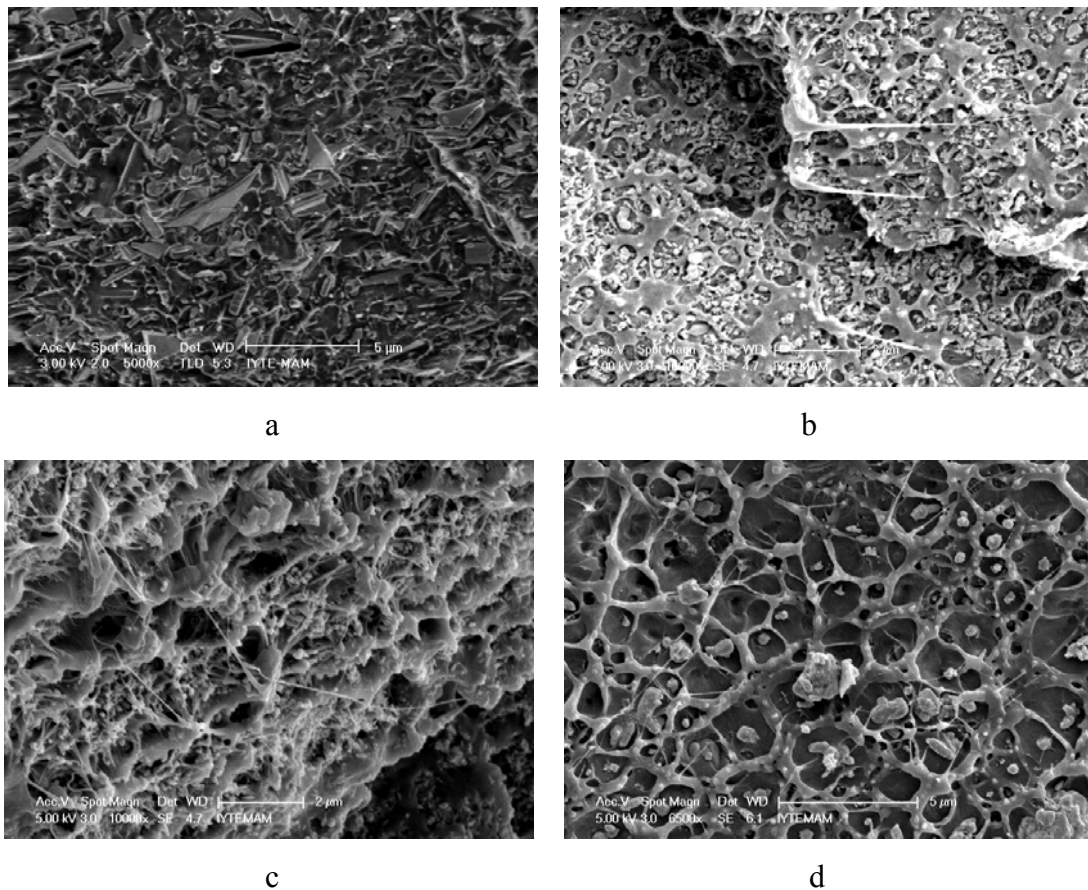


Figure 6.35. SEM micrograph of composites a) 20 vol%eZnO-PE, b) 15 vol% nZnO PE, c) 15 vol% synZnO-PE, d) 15 vol%AlZnO-PE.

The eZnO, nZnO and synZnO-PE composites SEM micrographs and Zn map of modified ZnO-polymer composites (SEM-EDX) are given in Appendix C.

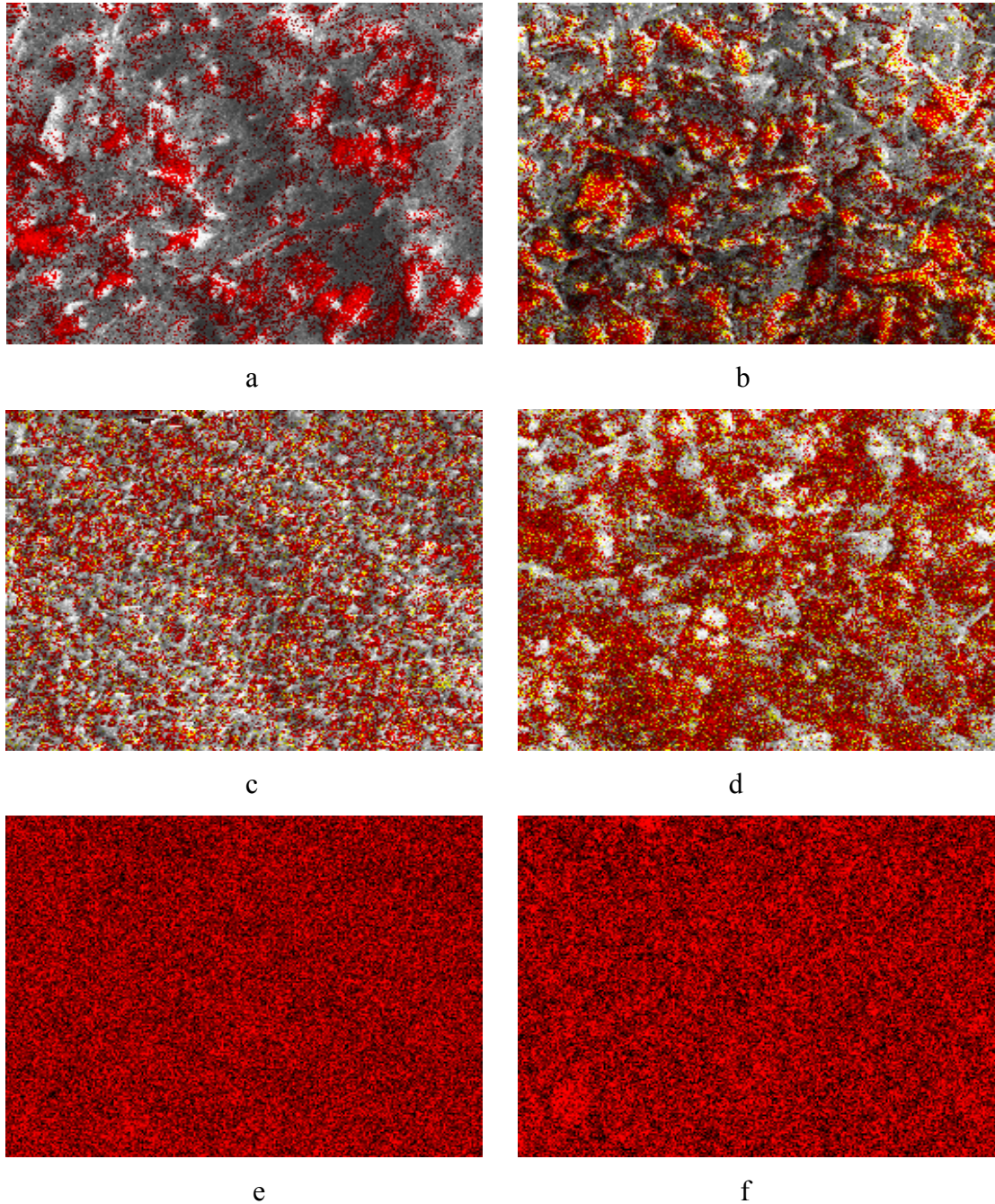


Figure 6.36. Map of elemental Zinc in EDX a) 20 vol% eZnO-PE b) 20 vol% 10 eZnO-PP c) 20 vol% sZnO-PE d) 20vol% sZnO-PP e) 15 vol% nZnO-PE f) 15 vol% nZnO-PP. Red colors indicate zinc, black color indicates polymer matrix.

In the elemental map analysis of the polymeric composites the red colors indicate Zn element and black colors indicate C element as depicted in Figure 6.36. There is no conductive path observed for eZnO-PE matrix composites as seen in Figure 6.36-a and zinc oxide is agglomerated as well. Due to maleic anhydride was added to the PP matrix composites system filler distribution (Figure 6.36-b) became more homogenous than PE composites. sZnO-PE and sZnO-PP composites Zn map are given in Figure 6.36-c and d. ZnO powders for each composite tend to contact each other and form a conductive path. However the continuity of the path is not observed. In PP composite agglomeration of ZnO powders is more than PE composites. The maleic anhydride addition to PP composites prevented the adhesion problem between polymer and filler since maleic anhydride is a good compatibilizer and coupling agent. According to EDX analysis (Figure 6.36-e and f) of nZnO-PE and nZnO-PP composites, ZnO particles are dispersed homogeneously and the conductive path is obtained. As a consequence, the change in the particle size (micron to nano) of filler in the composites would result a conductive path due to increasing surface area. Obtaining a well dispersed and conductive path in the composites could increase the electrical conductivity and enhance the mechanical properties of the composites. Furthermore a serious adhesion and wetting problems occurred in the composites, there may be some voids obtained between two materials as seen in SEM micrographs which would affect the conductivities (electrical and thermal) and mechanical properties of the composites negatively. The reason of the voids (seen in the SEM images) could be formed during formation of fracture surface as well.

Degree of crystallinity is an important parameter for improving the conductivity (electrical and thermal) and mechanical property of the composites. Higher degree of crystallinity and more uniform crystalline structure of polymer matrix increase the possibility of conduction in the composites. Inorganic nanoparticles (ZnO) affect the crystallization behavior of PP and PE matrix and the influence of zinc oxide, on crystallinity of polymer was studied by using XRD and DSC. It is expected to fulfilling the two results with each other. The XRD pattern of eZnO-PP and eZnO-PE are given in Figure 6.37 and Figure 6.38, respectively.

PP (isotactic) yields reflections at the following Bragg angles and corresponding Miller indices; 14.18° (110), 16.8° (040), 18.68° (130), 21.18° (111), 21.88° (131) and (041) (Tang et al., 2004). The XRD pattern of PE had one dominant fairly sharp peak at 21.4° , a weak broad peak at 23.6° and a weak broad third peak centered on 19.5° . The

dominant peaks (21.4° and 23.6°) and a small broad peak (19.5°) arose from crystalline and amorphous regions in PE. It was clearly understood from the relative areas under these crystalline peaks that the polymer sample produced in plate form after solidification (from the melt) becomes highly crystalline. The typical diffraction peaks of ZnO powders were observed at 31.9° , 34.5° , 36.2° , 47.5° , 56.5° , 62.8° , 67.9° , and 69.3° 2θ and all diffraction peaks were in agreement with the wurtzite structure. The composites possess typical crystal peaks of ZnO (wurtzite) and also increasing ZnO content increases the intensity of the peaks as shown in Figure 6.37 and Figure 6.38. The following procedure was adopted to calculate the total crystalline fraction and contributions from each crystalline phase. From the iterative peak-fit procedure, the crystalline peak, and the amorphous background curve were extracted. Total crystallinity of various samples was calculated by using the Equation 6.2 (He et al., 2007).

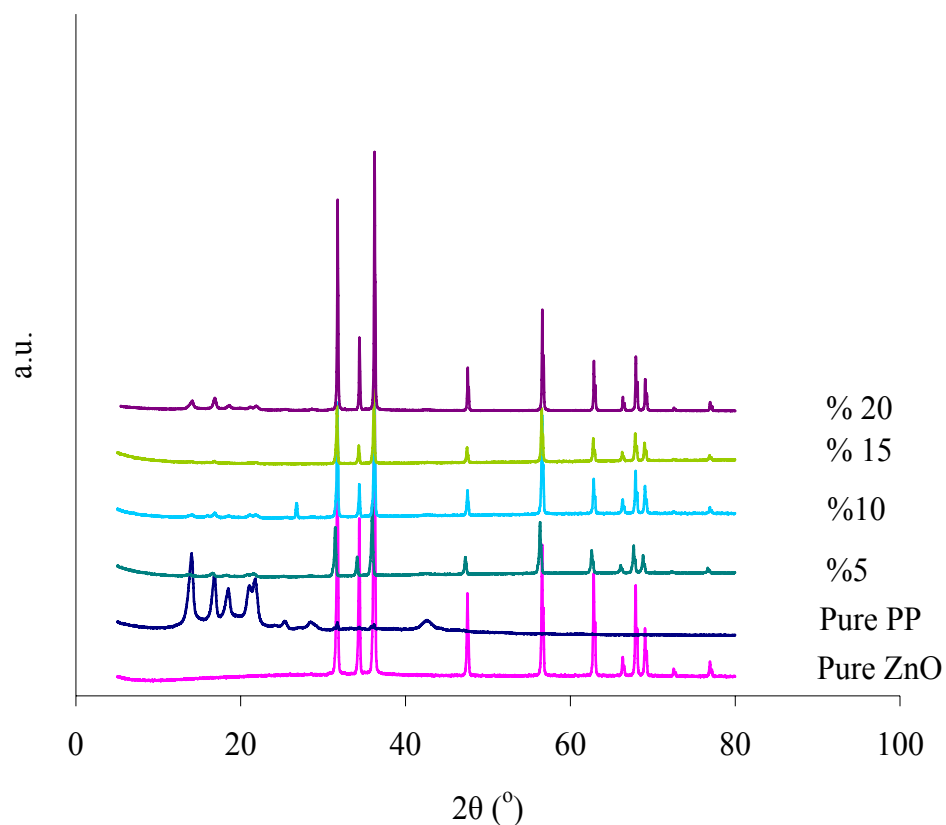


Figure 6.37. XRD pattern of eZnO-PP composites.

$$\% \text{ crystallinity} = W_c / (W_c + W_a) 100 \quad (6.2)$$

where, W_c is the integral area of peaks of crystalline phase, W_a is the integral area of peaks of amorphous phase. The crystallinities of the eZnO-PP/PE and sZnO-PP/PE composites found from XRD data are given in Table 6.2 and Table 6.3, respectively.

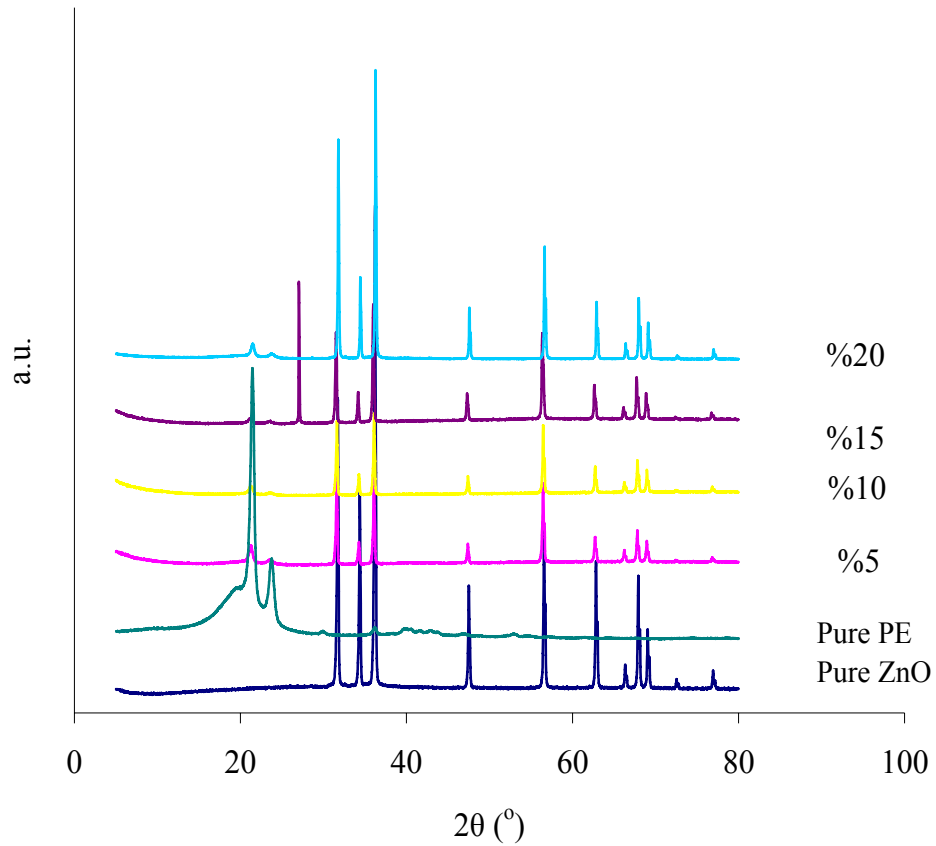


Figure 6.38. XRD pattern of eZnO-PE composites.

Table 6.2. % crystallinity of eZnO-PP/PE composites calculated from XRD.

Polymer-Composites	% crystallinity	Polymer-Composites	% crystallinity
Pure PP	55.8	Pure PE	44.2
5 vol% eZnO-PP	64.5	5 vol% eZnO-PE	45.8
10 vol% eZnO-PP	60.1	10 vol eZnO-PE	45.0
15 vol% eZnO-PP	64.0	15 vol% eZnO-PE	49.0
20 vol% eZnO-PP	68.1	20 vol% eZnO-PE	59.8

Table 6.3. % crystallinity of sZnO-PP/PE composites calculated from XRD.

Polymer-Composites	% crystallinity	Polymer-Composites	% crystallinity
Pure PP	55.8	Pure PE	44.2
5 vol% sZnO-PP	67.2	5 vol% sZnO-PE	42.0
10 vol% sZnO-PP	64.0	10 vol% sZnO-PE	44.8
15 vol% sZnO-PP	67.3	15 vol% sZnO-PE	54.0
20 vol% sZnO-PP	64.9	20 vol% sZnO-PE	53.9

Crystallinity of the PP and PE matrix were essentially affected by ZnO powder addition. Addition of ZnO powder increased the crystallinity of composites by increasing ZnO content for PP and PE composites. Crystallinity value of the composites increased about ~22% after the addition of 15 and 20 vol% of ZnO addition to the system. Behind finding the XRD pattern of the composites it was aimed to search the particle size effect on crystallinity of the polymer composite. Tang et al. (2004) found crystal structure of PP was unaffected by ZnO addition and the largest spherulites were observed for pure PP. Both micro and nanoparticles of ZnO reduced spherulite size in PP, but smaller spherulites were observed when the inorganic nanoparticles (40-150 nm) were loaded to the polymer composite relative to micron-size particles. In this study, the particle size difference did not have an affect on crystallinity of polymer matrix materials.

Isotactic polypropylene is a polymorphic material with form of α (monoclinic), β (hexagonal), and γ (triclinic) crystals. X-ray diffraction patterns are produced with α phase diffracting strongly in 110 and 040 planes. According to Cook and Harper (1998); the orientation of polypropylene α and β phases can be obtained by taking the ratio of the intensity of PP 110 planes to the 040 plane. If the ratio is less than 1.3 the b axis lies predominantly parallel to the surface under analysis. If the ratio is greater than 1.5, the a-axis is parallel to the surface under analysis. If the ratio lies between 1.3 and 1.5, then there is an isotropic mixture of crystallites. Orientation of sZnO-PP composites was calculated as 1.5, 0.9, 0.6, 1.1 and 0.9 for pure PP, 5 vol%, 10vol%, 15vol % and 20vol%, respectively. For eZnO-PP composites the ratio was found as 1.5, 0.97, 0.9, 0.9, and 0.85 for pure PP, 5 vol%,10 vol%,15 vol% and 20vol% respectively. Pure PP

was an isotropic mixture of crystallites and other composites were oriented with b-axis lies parallel to the surface.

6.2.2. Thermal Characterization of Polymer Composites

The effect of ZnO powders on thermal behavior of polymer composites were investigated by TGA and DSC. ZnO addition could affect (increase/decrease) the processing temperature. Representative TGA thermograms and DSC curves for eZnO loaded composites are given for PP composites in Figure 6.39 and Figure 6.40 respectively. To understand the particle size effect of ZnO powder on composites only eZnO-PE/PP (micron sized ZnO) and sZnO-PE/PP (submicron sized ZnO) composites were studied. The representative composites degradation temperature, weight loss at 1000°C, melting and decomposition peak temperatures are given in Table 6.4 to Table 6.7 for eZnO loaded PP and PE and for sZnO loaded PP and PE composites, respectively.

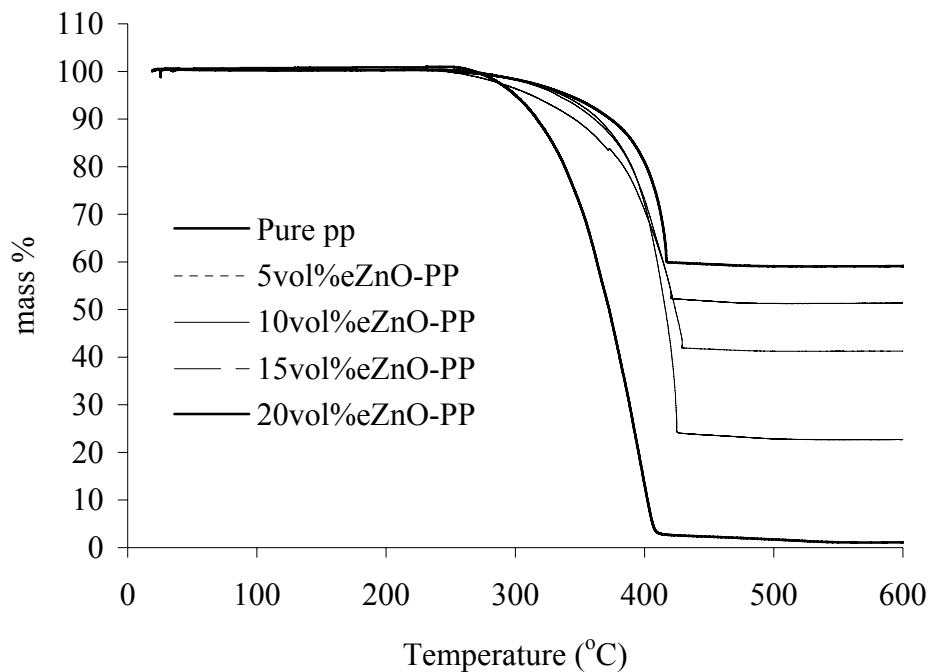


Figure 6.39. TGA curve of eZnO-PP composites.

Figure 6.39 represents the onset temperature of the thermal decomposition for composites and PP matrix which is about the same value and found at 273 °C. The degradation temperature increased with increasing ZnO loading as depicted in Table 6.4. At the end of the TGA analysis (at 1000°C) the remained mass (in the cell of TGA) was expected to give the loading percentage of ZnO powder. The composites were prepared in volume percentages of 5, 10, 15 and 20 with respect to ZnO powder loading and according to the weight percentages the ZnO loadings were 25, 40, 53 and 61. For pure polymers the mass remained at 1000°C indicating carbonization of the polymeric material. The remained mass % of composites at 1000°C was found, 25, 42, 70, and 60 wt% for sZnO-PE composites and was inconsistent with the theoretical loading of ZnO powder. According to DSC curve the melting and degradation temperature of the composites did not change by the addition of ZnO loading as seen in Figure 6.40. The degradation behavior of pure PP, 5vol% sZnO-PP and 10vol% sZnO-PP was exothermic but at 15 and 20vol% sZnO-PP its behavior turned to endothermic.

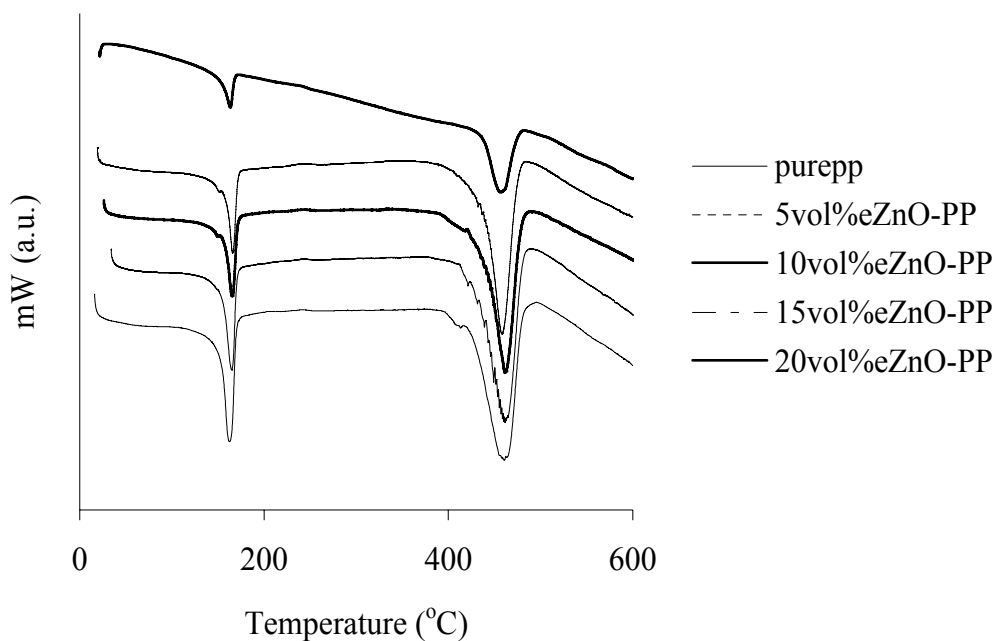


Figure 6.40. DSC curve of eZnO-PP composites.

Crystallinity of the composites was calculated by using pure isotactic polypropylene heat of melting value of 209 J/g and pure polyethylene heat of melting value of 288.4 J/g as depicted in Equation 6.3. X_c , is the crystallinity of the composite, W_f is the weight fraction of polymer in composite, ΔH_1 is the melting heat of composite and ΔH_2 is the melting heat of 100% crystalline polymer.

$$X_c = \frac{\Delta H_1}{\Delta H_2} \frac{1}{W_f} \quad (6.3)$$

Table 6.4 to Table 6.7 reports the weight loss taken from TGA results at 1000 °C which were consistent with the weight loss due to polymer matrix material. As seen in Figure 6.41, mass loss at 1000 °C versus ZnO content of the composites is represented by a straight line with slope nearly 1.

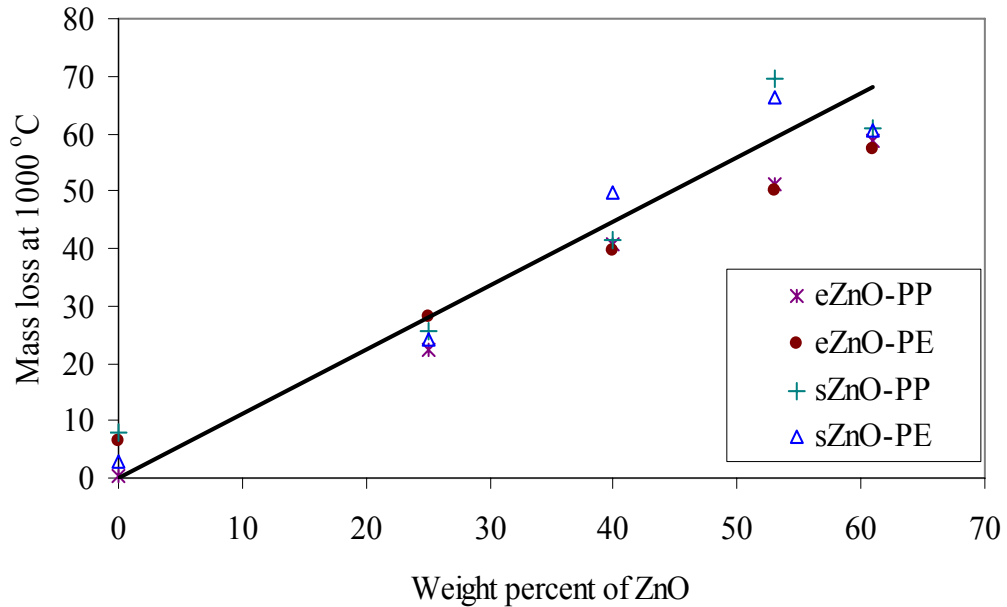


Figure 6.41. Weight loss at 1000°C versus weight % of ZnO in composites.

Table 6.4. eZnO-PP composites thermal analysis results.

Vol % ZnO	TGA results		DSC results		% Crystallinity
	Wt % loss at 1000° C	Degradation Temp. (start) (°C)	Melting Peak Max. Heat/ Temp (J/g) (°C)	Decomposition Peak Max. Heat / Temp (J/g) / (°C)	
0	99.8	256.5	-67.8 / 165.2	-247.6 / 466	32.4
5	77.8	245.2	-58.5 / 166.9	-257.8 / 465.8	37.3
10	59.1	249.9	-49.2 / 167.2	-231.8 / 464.6	39.2
15	48.9	242.4	-40.1 / 167.5	-175.2 / 461	40.8
20	41.2	237.3	-42.2/155.8	-127.9/ 454.1	51.5

Table 6.5. eZnO-PE composites thermal analysis results.

ZnO Vol %	TGA results		DSC results		% Crystallinity
	Wt % Loss at 1000°C	Degradation Temp. (start) (°C)	Melting Peak Max. Heat / Temp (J/g) / (°C)	Decomposition Peak Max. Heat / Temp (J/g) / (°C)	
0	93.6	264.9	-96.9 / 111.8	-276.3 / 478.9	33.6
5	71.9	275.2	-50.7 / 110.9	-294.1 / 473.6	23.4
10	60.2	269.5	-70.1 / 111.7	-220.8 / 473.4	40.5
15	49.9	270.9	-75.1 / 110.8	-183.4 / 471.7	55.4
20	42.8	280.8	-75.0/109.8	-137.1/470.4	66.8

eZnO addition to PP matrix caused to decrease the starting point of degradation and end point of degradation about 15-20 °C as given in Table 6.4 which means that ZnO powder addition influences the polymers degradation negatively. In the melting and degradation temperature of eZnO-PP composites no change were obtained from DSC results. The starting point of degradation temperature shifts about 10-15 °C higher by the addition of eZnO resulting more stable polymer composites. However this temperature rise had no significant effect on processing temperature of composite. From DSC analysis, the melting point of eZnO loaded PE composites did not changed (108-

111°C); however the heat of melting decreased (from 96.9 to 50 J/g) by ZnO addition. The TGA results of sZnO composites were found in the same manner with the eZnO loaded composites even “sZnO powder” has smaller particle size and there were no relation obtained between particle size of the powder and thermal properties of the composites. The starting degradation temperature decreased for PP matrix composites about 5-25 °C and for PE matrix composites increased about 8-33 °C. However the changes in the degradation temperature had not significantly affected the processing temperature.

Table 6.6. sZnO-PP composites thermal analysis results.

ZnO Vol %	TGA results		DSC results		% Crystallinity
	Wt % loss at 1000°C	Degradation Temp (start) (°C)	Melting Peak Max. Heat/Temp (J/g) / (°C)	Decomposition Peak Max Heat/Temp (J/g) (°C)	
0	92.11	265.2	-64.3/ 167.0	110.9/237.7 6850 / 404.1	30.8
5	74.24	240.3	- -56.8/165.8	5620/420.7	36.3
10	58.71	240.3	- -54.6/164.1	4880/432.7	43.5
15	30.34	255.9	- -53.4/175.2	-114.2/459.2	54.5
20	39.09	260.5	- -44.9/164.7	-133.5/459.9	55.1

Crystallinity % of the polymer composites were calculated from the melting heats (heat of fusion) of the composites using DSC results. For the crystallinity calculations heat of melting values for pure PP (209 J/g) and PE (288.4 J/g) were used as stated before. According to crystallinity percentages ZnO addition caused to have more crystalline materials. In section 6.2.1 the crystallinity % of the composites were calculated from XRD results to compare the crystallinity results which were found from

DSC and XRD. ZnO loading versus crystallinity results were drawn in Figure 6.42 and Figure 6.43 for PP and PE composites respectively.

Table 6.7 sZnO-PE composites thermal analysis results.

ZnO Vol %	TGA results		DSC results		% Crystallinity
	Wt % Loss at 1000°C	Degradation Temp (start) (°C)	Melting Peak Max. Heat/Temp (J/g)/(C)	Decomposition Peak Max. Heat/Temp (J/g)/(C)	
0	97.15	243.4	- -128.6/121.2	1770/438.1 510.2/ 485.6	44.6
5	75.79	276.1	- -102.9/122.5	-246.7/470.6	47.6
10	50.35	276.1	- -97.7/121.5	-302.4/475.1	56.5
15	33.78	268.8	- -52.1/121.9	85.3/222.2 3690/435.1	22.9
20	39.59	251.2	- -38.7/120.3	67.2/218.0 3250/483.9	27.7

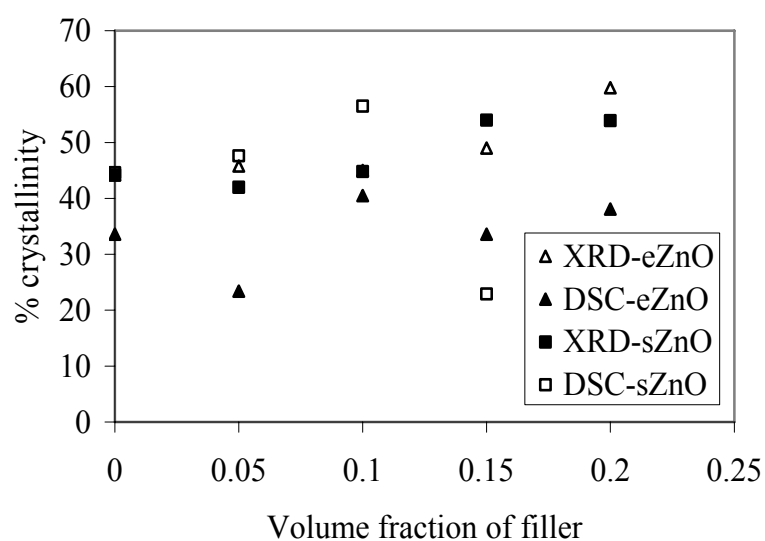


Figure 6.42. Crystallinity values found from XRD and DSC for PP composites.

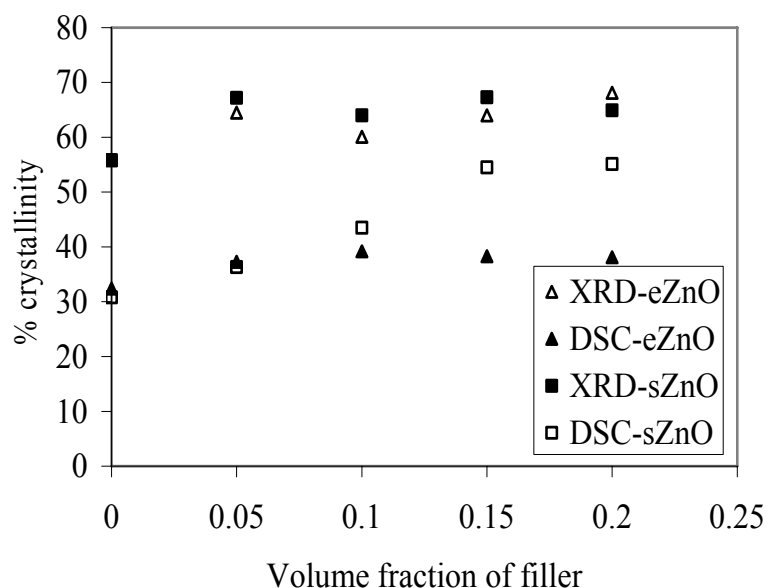


Figure 6.43. Crystallinity values found from XRD and DSC for PE composites.

The crystallinity values which were found from DSC were lower than XRD while DSC measures the energy absorbed during melting of the polymer and crystallites, and XRD measures the order in crystals. This may be the cause of the difference between crystallinities obtained by two methods.

The crystallinity ratio calculated from two separate methods increased with increasing zinc oxide addition. For PE the crystallinity ratio which was calculated from XRD found at about 60% and for DSC it was calculated about 40%. The huge difference might be related with composites preparation method. The shapeless mixture of the polymer filler composites was well shaped in hot press at 180 °C for PP and 150 °C for PE at 6800 kg pressure while the samples were cooled to room temperature by circulating tap water die. The cooling rate changed depending on the temperature and flow rate of tap water. Sometimes due to different cooling rates, composites could be cooled faster or slower so the crystal percentage of the polymer would also change. Furthermore, especially highly loaded ZnO powders tend to agglomerate in the composites causing heterogeneous dispersion from place to place and might present big agglomerates. So, the analysis carried out from certain samples, differs XRD and DSC results.

6.2.3. Morphological Characterization of Surface Modified Composites

Surface modified powders were used only for the highest loading (15 vol% and/or 20 vol%) of ZnO-PE composites to enhance the adhesion and wetting properties. Effects of modification was detected by SEM micrograph as shown in Figure 6.44 of 20vol% loaded sZnO-PE composites which was modified by 1wt% PEG4000, 2wt% PEG4000, 1wt% AMPTES, and 2wt% AMPTES.

Wetting and adhesion problem for modified composites between polymer and the filler was got better than unmodified composites. SEM micrograph of PEG modified ZnO-PE composites is given in Figure 6.44-a and c. The ZnO powders are in chain like arrangement, and are connected to each other as seen in the composite. According to Liufu et al. (2004), PEG macromolecules bond to the solid surface of ZnO from the -OH group and the adsorption of PEG macromolecules causes to hydrogen bonding between PEG and ZnO molecule. When polymer was melted the chemical bond between PEG and ZnO causing long chain like arrangement since the tail of PEG molecule had no chemical attraction to polymer. Chemicals were mixed in the presence of alcohol and water in the experimental procedure of the modification part and then the slurry (mixture) was dried. During the drying process particles might started to agglomerate. In the preparation of composite, firstly the powders were ground in the agat mortar and no extra grinding (ball milling) was applied to the powders before the preparation of composite. The reason of the agglomeration in the composite should be the poor grinding method of ZnO powders since the agglomerates could not disperse in the composite during the processing of the composite. The long chain like arrangement of ZnO powder in the polymer composite could cause to increase in the electrical conductivity of the composite since there would be a conductive path obtained. From the SEM micrograph the air gaps between polymer and filler decreases after modification of the filler. However the adhesion problem could not be solved.

AMPTES modified ZnO powders in polymer matrix are well dispersed as seen in Figure 6.44-b and d. However, in Figure 6.44-d microvoids are seen in the structure of composite material. These microvoids might be obtained only in the fracture surface of the material (not in the interior) since the composite was dropped to the liquid N₂ (77K) for obtaining fracture. Composites were broken at about glass temperature of the

polymeric material and this tends to elongation in the surface of the material. To understand if microvoids were formed in the composite, the densities of the composites should be determined and the porosity should be calculated.

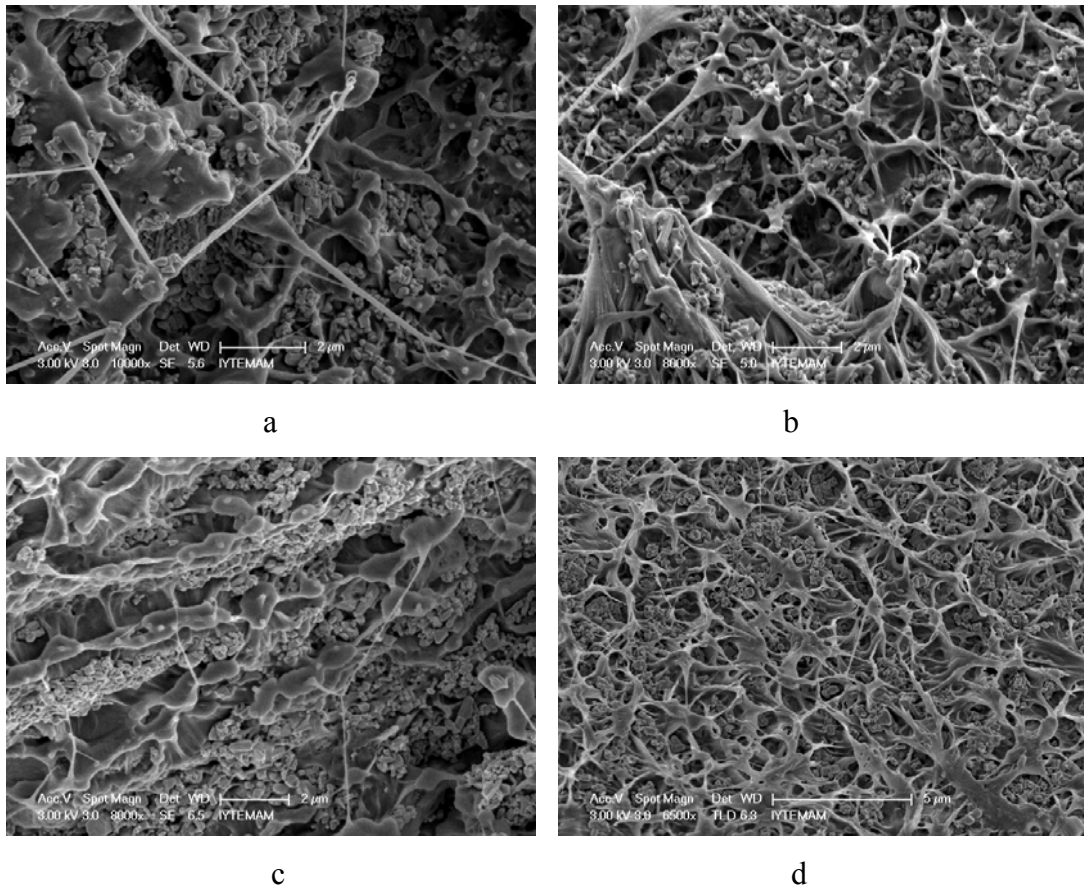


Figure 6.44. SEM micrograph of a) 1%PEG4000 b) 1% AMPTES c) 2% PEG4000 d) 2% AMPTES modified, 20vol % sZnO-PE composites.

6.2.4. Density of the Polymer Composites

Theoretical density of the composites were calculated by using density given in the Table 5.1 and Table 5.2 for ZnO powders (5.6 g/cm^3) and PP (0.89 g/cm^3) and PE (0.92 g/cm^3) matrix materials. synZnO and AlZnO powder densities were found using mercury pycnometer as 4.8 and 5.2 g/cm^3 , respectively. The theoretical density calculation of composites was made using Equation 6.4. In Equation 6.4 volume fractions of the filler and polymer were taken into consideration.

$$\rho_{Theoretical} = \rho_{PE}(1 - \Phi) + \rho_{ZnO}\Phi r \quad (6.4)$$

In Equation 6.4 Φ is the volume fraction of the filler, ρ is the density of the individual materials. The density of the composite was used to find out the pore volume since it explains the air gaps (microvoids) in the composite. In the equation the density of eZnO loaded PE composite, sZnO and nZnO loaded PE composites is given in Table 6.8, 6.9 and 6.10 respectively. Density of PE changed with degree of crystallinity of PE. Thus 0.88 g/cm³ density, corresponds to 100% amorph and 1.00 g/cm³ density, corresponds to 100% crystal polyethylene.

Table 6.8. Density of eZnO-PE composites.

ZnO Loading or modification	Theoretical (g/cm ³)	Archimed (g/cm ³)	Porosity %
Pure PE	0.92	0.88	4.3
5 vol%	1.16	1.10	5.2
10 vol%	1.38	1.32	4.3
15 vol%	1.65	1.51	8.5
20 vol%	1.88	1.76	6.4
1wt%PEG 4000	1.88	1.66	11.7
2wt%PEG 4000	1.88	1.56	17.0
1wt%AMPTES	1.88	1.78	5.3
2wt%AMPTES	1.88	1.80	4.2

For commercial ZnO filled composite the pore volume did not significantly increase by the addition of ZnO. Microvoids might be the reason of porous structure. Microvoids formed firstly in the interface of ZnO-PE composite. The weak interfacial interaction was the first reason of microvoids between polymer and filler. Another reason should be the melting temperature where the mass density of a polymeric melt decreased with increasing shear rate. The volume of the polymeric material increased after melting, during the processing of the composite.

Table 6.9. Density of sZnO-PE composites.

ZnO Loading or modification	Theoretical (g/cm ³)	Archimed (g/cm ³)	Porosity %
Pure PE	0.92	0.88	4.3
5 vol%	1.16	1.13	2.8
10 vol%	1.38	1.38	0.1
15 vol%	1.65	1.58	4.3
20 vol%	1.88	1.52	19.0
1wt%PEG 4000	1.65	1.55	6.1
2wt%PEG 4000	1.65	1.68	-
1wt%AMPTES	1.65	1.71	-
2wt%AMPTES	1.65	1.51	8.5

Table 6.10. Density of nZnO-PE composites.

ZnO Loading or modification	Theoretical (g/cm ³)	Archimed (g/cm ³)	Porosity %
Pure PE	0.92	0.88	4.35
5 vol%	1.16	1.13	2.84
10 vol%	1.38	1.27	8.10
15 vol%	1.65	1.55	6.15
1wt%PEG 4000	1.65	1.40	14.9
2wt%PEG 4000	1.65	1.49	9.8
1wt%AMPTES	1.65	1.52	7.9
2wt%AMPTES	1.65	1.51	8.6

For PEG 4000 modified composites, the porosity increased with increasing weight percentage of modifier. Density and porosity results were inconsistent with the SEM micrographs given in Figure 6.44-a and Figure 6.44-c. For PEG 4000 modified ZnO, there were long chains side by side arranging ZnO and voiding in the polymer

network. These voids should be obtained due to insufficient modifier-polymer chemical bonds. PEG modified composites were expected to be more conductive composites since the electrical conductivity of composites obtaining a conductive path was important. AMPTES modified ZnO-PE composites porosity values were found nearly the same with the unmodified samples. Since, the organic and inorganic tails of modifiers provided stable bonds between polymer and filler which obtained again some microvoids. They could be due to the volume difference between melt and solid form of polymeric material. Table 6.11 and 6.12 gives the density and porosity results of the synZnO and AlZnO composites, respectively.

Table 6.11 Density of synZnO-PE composites.

ZnO Loading	Theoretical (g/cm ³)	Archimed (g/cm ³)	Porosity %
Pure PE	0.92	0.88	4.35
5 vol%	1.15	1.14	0
10 vol%	1.36	1.32	2.9
15 vol%	1.61	1.54	4.3

Table 6.12 Density of AlZnO-PE composites.

ZnO Loading	Theoretical (g/cm ³)	Archimed (g/cm ³)	Porosity %
Pure PE	0.92	0.88	4.35
5 vol%	1.16	1.45	-
10 vol%	1.37	1.15	15.3
15 vol%	1.63	1.58	3.1

For synZnO and AlZnO loaded composites the porosity did not change significantly by the addition of ZnO except 10 vol% AlZnO-PE composite. In this composite the higher porosity should be coming during the hot pressing of the material since this is an experimental error.

As a consequence, electrical conductivity, thermal conductivity, and mechanical strength of the composites expected to affect from the porosity of the composites negatively. Since air gaps could drop the electrical and thermal conductivity. The optical properties of the composites could affect as well, since the air gaps differs the refractive index of the materials and prevents the continuity of the composite materials.

6.3. Electrical Conductivity of Polymer Composites

Volume resistivity of the composites was measured by using High-Resistivity Test apparatus to determine the electrical properties of composites. The confidence of the test was obtained from the applied current and time values of the composites. Alternative voltage was applied to the sample; the (+, -) current polarity frequency should be the same; and the peak to peak interval between first volume resistivity value and the last one should be below 1. At the end of the test, (8 readings) an average data was given as a resistivity value. The volume resistivity values of composites are given in Figure 6.45 and Figure 6.46 for PP and PE composites, respectively and tables of the volume resistivity values are given in Appendix D.

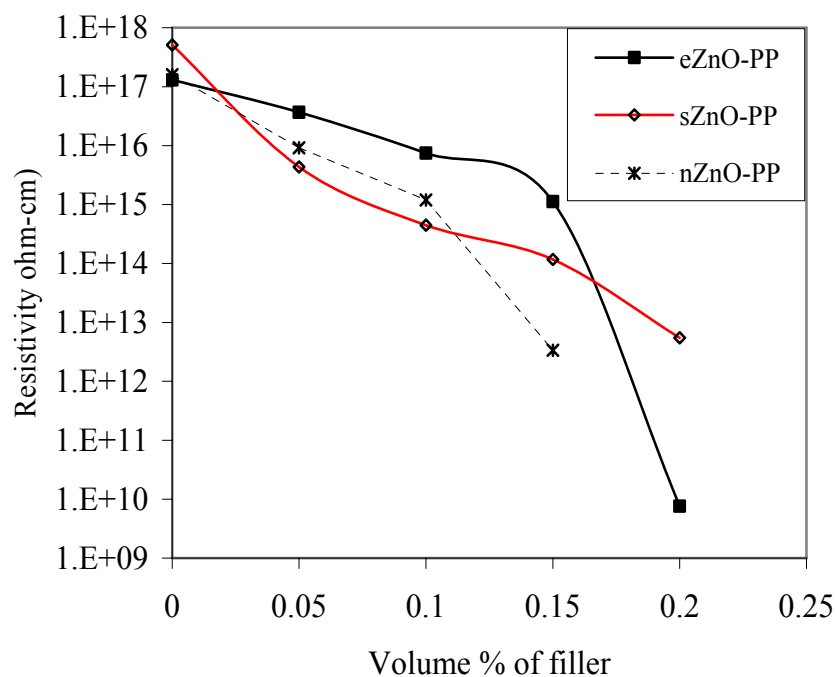


Figure 6.45. Volume resistivity values of PP composites.

The volume resistivity of PP was found about 10^{17} ohm-cm. For the addition of 15 vol% eZnO to the polymer the volume resistivity value dropped to 10^9 ohm-cm. Besides, sZnO and nZnO added composites resistivity value dropped to 10^{12} ohm-cm for 20 vol% and 15 vol% loaded zinc oxide, respectively. Electrical conductivity of PE was about 10^{17} ohm-cm and for 20 vol% filler added composites it changed to 10^9 for eZnO and 10^{12} ohm-cm for sZnO loading. In 15 vol% nZnO added composites the conductivity value was found to be 10^{12} ohm-cm. In order the composite materials used for conductive applications, the materials should have an electrical conductivity in the range of 10^{-12} and 10^{-8} S/cm for ESD applications, 10^{-8} and 10^{-2} S/cm for moderately conductive applications, 10^{-2} S/cm and higher for shielding applications. According to this information the composites which were prepared from nZnO, sZnO and eZnO could be used in ESD application loading 20 vol% sZnO and eZnO powder and 15 vol% for nZnO powder. Especially eZnO powder found 100 times conductive than other powders at 20 and 15 vol% loading composites.

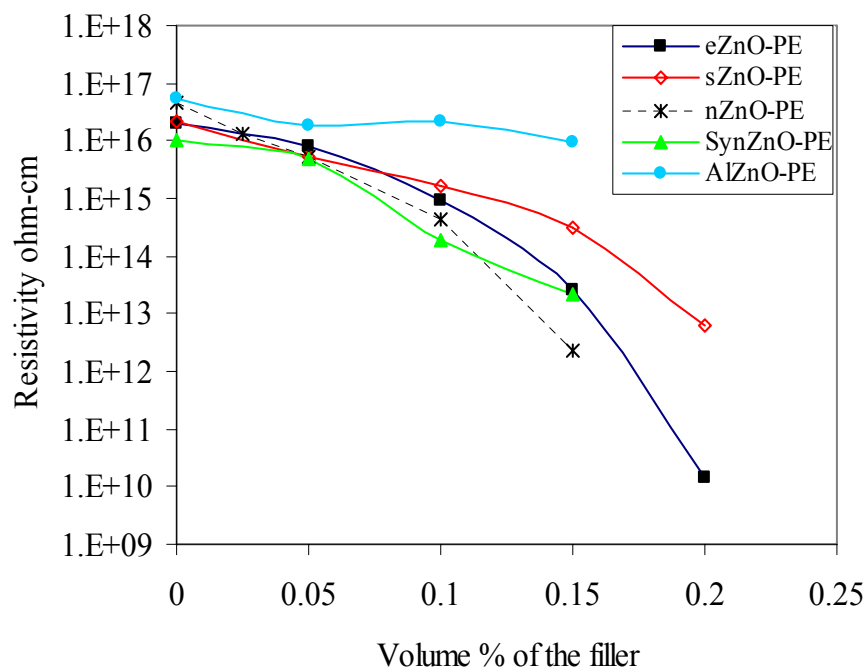


Figure 6.46. Volume resistivity values of PE composites.

The volume resistivity of ZnO powders were found to be $1.5 \cdot 10^6$, $1.5 \cdot 10^9$, $1.7 \cdot 10^8$, and $1.3 \cdot 10^7$ ohm-cm for eZnO, sZnO, nZnO and synZnO, respectively. On the other hand for the highest loading the resistivity values were found in the order of eZnO, nZnO, sZnO, synZnO and AlZnO PE matrix composites. Theoretically, increasing the surface area might increase the probability of particle touches. According to general effective media theory the conductor-insulator relation was explained by percolation. The charge carrying process in the percolation theory can be explained by hopping or tunneling effect. In these composites the tunneling effect was pointed at issue, because hoping effect is usable for more conductive fillers, like carbon fiber or some metallic loadings. In the tunneling effect there should be a conductive path which was based on zinc oxide. When the concentration is loaded at or above the percolation threshold value the resistivity of the composites will drop dramatically. However, both in Figure 6.45 or Figure 6.46 only eZnO loaded composites resistivity value dropped dramatically but others did not. This could be due to the low conductivities of the powders which were not as high as ought to be. eZnO powder has the highest average particle size and the electrical conductivity. The electrical resistivity of 20 vol% loaded eZnO was found $1.4 \cdot 10^{10}$ ohm-cm with the seen anticipated result. Second expectation

on the highest electrical conductivity was synZnO powder since the mean particle size was about 110 nm but the electrical conductivity found for 15 vol% loading was 2.1×10^{13} ohm-cm. This could be due to serious adhesion and wetting problem between the polymer and the filler. The polymer could not wet the powder because of the high surface area and the powders were agglomerated as well because only mechanical grinding was performed on the powder with agat mortar. From the SEM micrograph (Figure 6.35-c) of the synZnO-PE composites some air gaps are obtained. This should also take a serious effect on lowering the conductivity of the composite.

15 vol% nZnO powder loaded composites resistivity dropped to the value of 2.3×10^{12} ohm-cm which was a satisfactory result. However the resistivity should decrease more than that value because the particles of the powder were very small (according to Aldrich below 100 nm) and the surface area was between 15-25 m²/g. Even the wettability and adhesion problem might affect the system. In sZnO loaded composites the highest loading dropped the resistivity to 6.2×10^{12} ohm-cm. The powders resistivity was in the order of 10^9 ohm-cm and the composites resistivity was in an expected value.

Electrical resistivity of AlZnO powder addition to the polymer did not change the volume resistivity of polymer composite significantly (10^{16} to 10^{15} ohm-cm). The expectation was getting lower electrical resistivity after the addition of AlZnO powder rather than undoped powder addition to the polymer matrix. However the volume resistivity did not decrease as expected. It could be due to the doping mechanism which was taken place at 900 °C. Serier et al. (2009) explained two possible mechanisms about doping system. First one was, the Zn⁺² cation might replace with Al⁺³ cation and there will be a free electron in the medium so the conductivity could increase. If three Zn⁺² cation replaced by two Al⁺³ cation, no electrical conductivity was expected since of neutral defects was acting as electron traps. For AlZnO powder, the second mechanism might be worked and the resistivity of the powder could not drop. In the fluorescent spectrum of the AlZnO powder, at 460 nm there was a peak which corresponds to oxygen and zinc vacancy. The spectrum result supports the probability of second mechanism as well.

In another point of view, the AlZnO powder might be very conductive. Generally Al doped ZnO powders absorbed/desorbed water vapor and used as humidity sensor. During processing of polymer composites (170°C) dehydration of water could obtain air gaps and resistivity of the composites influences from these air gaps negatively. However in Table 6.12 the porosity % of AlZnO added powder composites

did not found as high as to obtaining huge air gaps. As a consequence, AlZnO powder volume resistivity was not decreased by doping Al to the ZnO powder.

Using a coupling agent to change the surface properties of filler is needed to improve the adhesion and wetting problem between polymer and filler. Other important properties affecting the conductivity of the composites were the crystallinity of the polymer matrix material. More crystalline, defect and orientation free matrix has better conductivity. The cooling process of the polymer is important for the crystallinity of the polymer. However in our system the flow rate of cooling water could not be controlled after the hot pressing mechanism. These processing differences could get some deficiencies in the resistivity of the polymeric matrix due to crystallinity.

Surface properties of the powders were changed by using two different coupling agents in two different concentrations as followed: 1wt% and 2 wt%, AMPTES and PEG 4000 respectively. Surface modified powders were prepared only for the highest volume percentages. The synZnO were modified only with 2 wt% PEG4000 because of the low amount of powder and AlZnO powder could not modified since it takes long time to prepare efficient amount of powder. PE matrix composites were prepared by the surface modified powders and the resistivity values are given in Table 6.13.

Table 6.13. Volume resistivity of modified composites.

Composites	Volume Resistivity of Composites (ohm-cm)				
	Unmodified	AMPTES 1 wt%	AMPTES 2 wt%	PEG 4000 1 wt%	PEG 4000 2 wt%
eZnO 20 vol%-PE	$1.4 \cdot 10^{10}$	$7.9 \cdot 10^{13}$	$6.1 \cdot 10^{13}$	$6.2 \cdot 10^{10}$	$1.35 \cdot 10^{11}$
sZnO 20 vol%-PE	$6.2 \cdot 10^{12}$	$1.2 \cdot 10^{15}$	$3.8 \cdot 10^{14}$	$7.1 \cdot 10^9$	$3.1 \cdot 10^8$
nZnO 15 vol%-PE	$2.3 \cdot 10^{12}$	$4.4 \cdot 10^{14}$	$6.3 \cdot 10^{14}$	$5.6 \cdot 10^8$	$2.5 \cdot 10^{10}$
synZnO 15 vol%-PE	$2.1 \cdot 10^{13}$	-	-	-	$4.01 \cdot 10^{10}$

For all of the composites the AMPTES modifier did not have a significant affect on composites volume resistivity value. However PEG 4000 modified ZnO loaded composites volume resistivity decreased significantly. Serious difference between resistivity values of silane (AMPTES) coupled zinc oxide composites and PEG 4000 modified zinc oxide composites were due to the difference in the surface characteristic of the coupling agents. Polyethylene glycol (PEG) is a family of long chain polymers made up of ethylene glycol subunits and the chemical formula is HO-(CH₂-CH₂-O)-n-H. Silane (AMPTES) coupling agents are silicon-based chemicals that contain two types of reactivity “inorganic and organic” in the same molecule. A typical structure is (RO)₃SiCH₂CH₂CH₂-X, where RO is a hydrolyzable group. In order to explain the mechanism in the electrical resistivity point of view the silane coupling agent is a well dispersant and it is inorganic and organic tail was well coupled to the inorganic and organic parts of the composites (Tang et al., 2007, Athues et al., 2007). In our composites, as it was mentioned before in the morphology part of the study, the dispersion of the filler was homogenous when AMPTES modifier was used as a coupling agent. According to percolation theory there were no conductive path was obtained due to homogenous dispersion of the filler in the composite as a consequence the resistivity could not dropped.

Interparticle distance between particles was calculated using Equation 3.1. The assumptions for using this equation was, homogeneously dispersed, uniformly distributed spherical particles dispersed in a polymeric network. Table 6.14 gives the interparticle distance according volume fraction of ZnO.

Table 6.14. Interparticle distance for the PE-ZnO composites.

Zinc Oxide	Particle Size (nm)	Volume Fraction of Filler (%)			
		5	10	15	20
		Interparticle Distance (nm)			
eZnO	3860	4584.9	2842.8	1995.4	1459.9
sZnO	752	893.2	553.8	388.7	284.4
nZnO	378	448.9	278.4	195.4	142.9
synZnO	170	201.9	125.2	87.9	64.3
AlZnO	820	974	603.9	423.9	310.15

Table 6.14 shows the interparticle distance decreases with increasing the zinc oxide content and decreasing the particle size of the filler. Although the expectations was on increasing the electrical resistivity by the decreasing interparticle distance as given in the literature, the related results obtained from the study has no direct relation between interparticle distance. In the case of ZnO having different particle size with identical electrical resistivity, it would be comparable according to the interparticle distance. However, the ZnO powders electrical resistivity values were individually different from each other so the relation could not observe. The assumptions about the particle shape and uniform size distribution could not make since the particle shapes were generally polydisperse and there were no uniform distribution of particle obtained.

In chapter 3.1.2 the electrical resistivity values of the related research were given by Hong et al. (2006) and Tjong et al. (2006) found that 10^9 ohm-cm, after 30 vol% addition of ZnO and 10^{13} ohm-cm, after the addition of 60 vol% ZnO addition respectively. If the results were compared with the related papers, in our study the highest electrical resistivity were found in 20 vol% added ZnO-PE composites at a volume resistivity of 10^8 ohm-cm. As a consequence, the electrical resistivity of the ZnO-PE and PP matrix composites were improved in this thesis.

PEG 4000 has a (-OH) group in surface and these -OH groups tends to conduct electricity. In this research, one of our aim was producing, low electrical resistivity materials so, PEG 4000 modified zinc oxide were chosen as a proper coupling agent material. eZnO-PE composites electrical resistivity was in the range of 10^{10} ohm-cm and after modification with AMPTES the resistivity increases to 10^{13} ohm-cm and modification with PEG 4000 has no significant effect. For sZnO, nZnO and synZnO powder loaded composites, surface modification with PEG 4000 worked very well and the composites volume resistivity value drops to 10^{10} - 10^8 ohm-cm. These composites could find an application area as an antistatic material or in moderately conductive electronic applications.

To compare the compatibility between volume resistivity of theoretical models and experimental (volume resistivity) value, Mc Lachlan model was performed. Mc Lachlan proposed this model for conductive particles in an insulating matrix, which was the type of the system studied here. McLachlan model was proposed in Equation 3.2 (section 3.1.4). The model calculations include factors related with; the conductivity of the constituent materials, the percolation threshold value and a critical exponent. Critical exponent had a typical value ranges between 1.5 and 3.1 for most of the

composite system. Therefore, for the parametric study of this model, the value of t varied within this range in order to determine the sensitivity of the model calculations to change with this parameter. The result of this portion of the study is given in Figure 6.47.

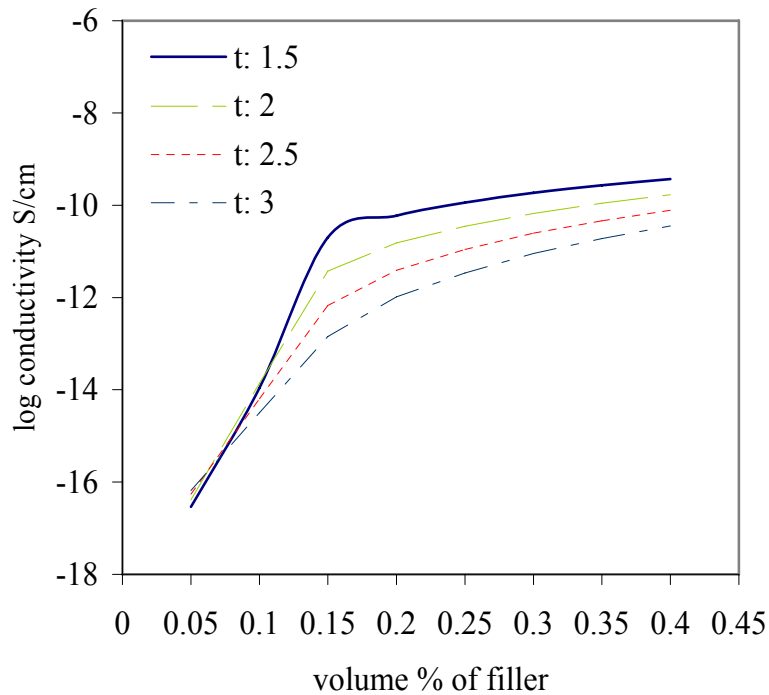


Figure 6.47. Effect of critical exponent (McLachlan model) on volume resistivity of nZnO-PE composites.

As t increased, the calculated conductivity is decreased by up to several orders of magnitude in some portions of the curve as given in Figure 6.47. This indicates the importance of this parameter to the application of this model. In order to accurately predict the conductivity using this model, its important to pick the correct value of t otherwise this lead significant differences between expected conductivity values those actually obtained through experimentation. The critical exponent was chosen as 2.5, 3, 1.5 and 3 for eZnO, sZnO, nZnO and synZnO composites, respectively. The conductivity of the composites was found using the Microsoft excel solver. Figure 6.48 to Figure 6.51 shows the resistivity results using Mc Lachlan equation compared to experimental data for eZnO-PE, sZnO-PE, nZnO-PE and synZnO-PE composites.

McLachlan model could not apply to the AlZnO-PE composites, since the resistivity of the powder is not known.

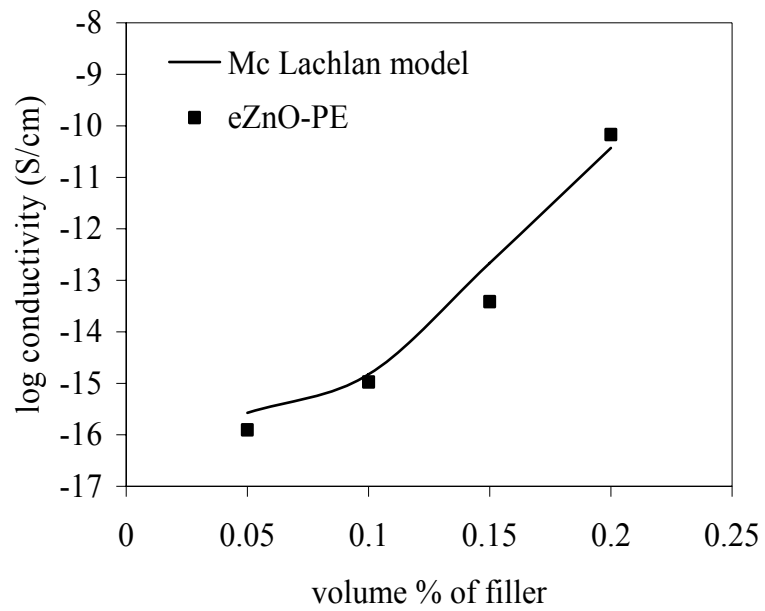


Figure 6.48. Experimental resistivity values of eZnO-PE and McLachlan model.

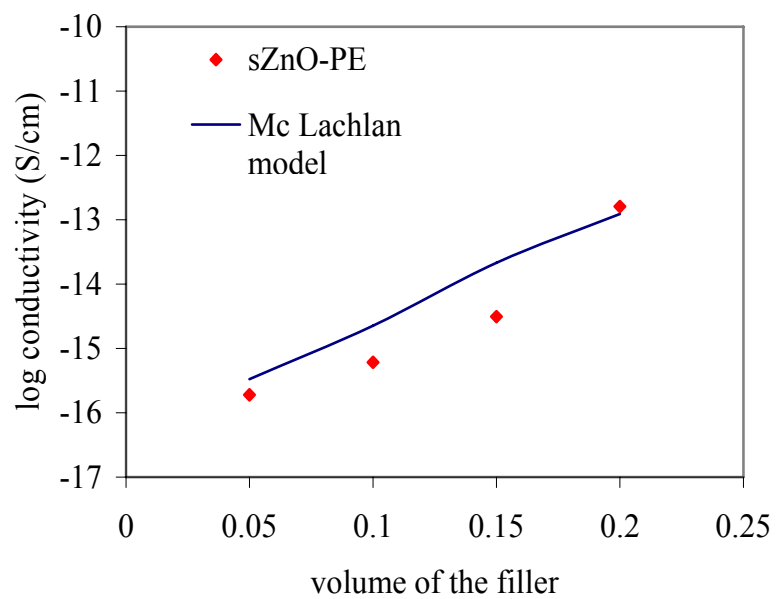


Figure 6.49. Experimental resistivity values of sZnO-PE and McLachlan model.

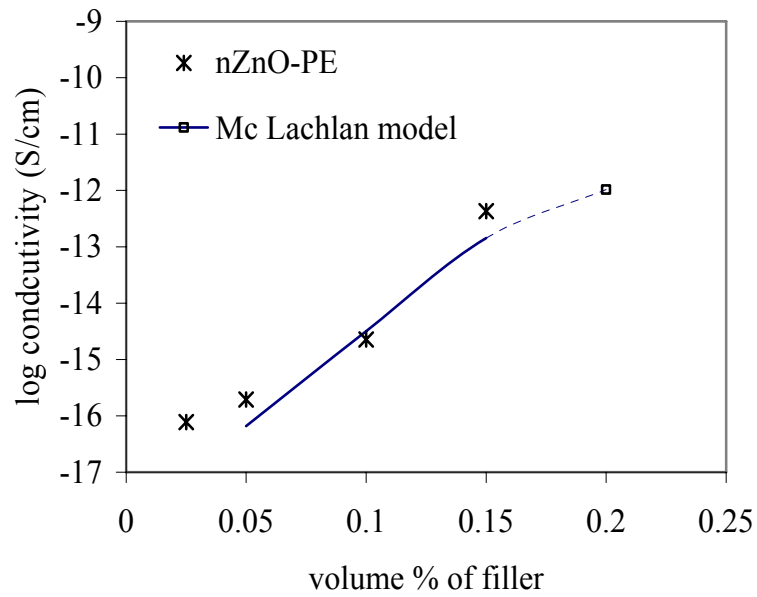


Figure 6.50. Experimental resistivity values of nZnO-PE and McLachlan model.

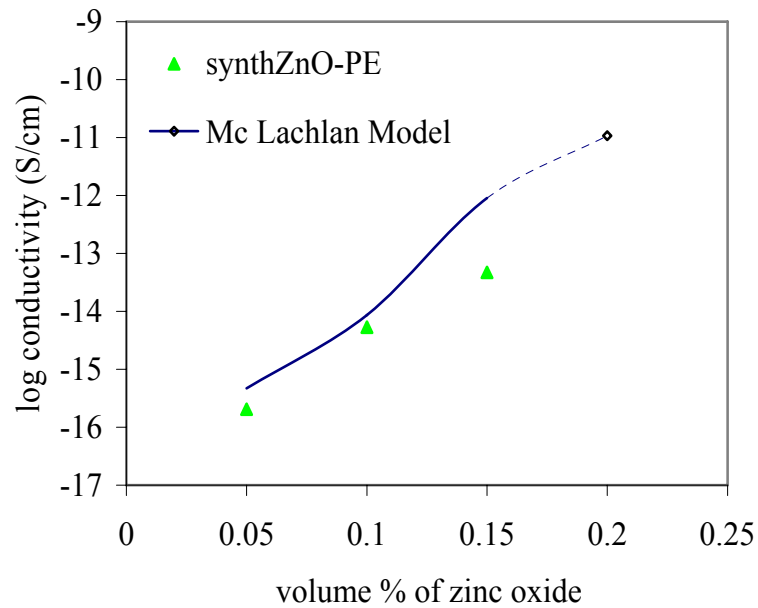


Figure 6.51. Experimental resistivity values of synthZnO-PE and McLachlan model.

Figure 6.48 to Figure 6.51 shows that, the McLachlan model predicts well the resistivity data. McLachlan model fits better to eZnO composites, because this powder had crystals with high aspect ratio.

6.4. Thermal Conductivity of Polymer Composites

Hot wire method which is a quick measuring method including a probe which consists of single heater wire and thermocouple was used to measure the thermal conductivity of the composites. When constant electric power was applied to the heater (by choosing appropriate current) temperature of the wire rose up in exponential progression and the thermal conductivity was read. The measuring temperature of the composites ranged in between 33-40 °C. The difference in the thermal conductivity was neglected due to the difference in the temperature, since there should be no significant effect obtained in composites conductivity values between these ΔT . Thermal conductivity of the composites were measured and given in Figure 6.52 and Figure 6.53 for PE and PP composites, respectively and the thermal conductivity values for composites are given in Table 6.15 and Table 6.16, respectively.

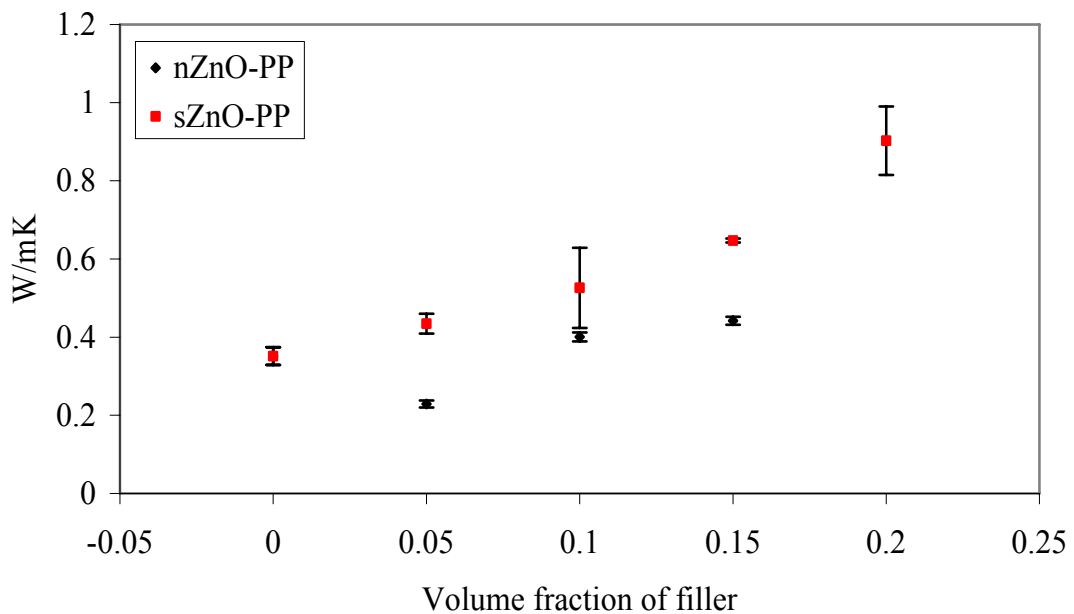


Figure 6.52. Thermal conductivity values of PP composites (“0” corresponds to Pure PP).

A much larger effect was obtained from sZnO addition to the PP matrix on thermal conductivity at the same loading than the nZnO loaded composites, where the expected result was just the opposite, since the surface area of nZnO was greater than sZnO and the probability of phonon transfer should be greater depicted in Figure 6.52. However, according to these results the aspect ratio should be the main parameter since the aspect ratio of sZnO powder was greater than nZnO.

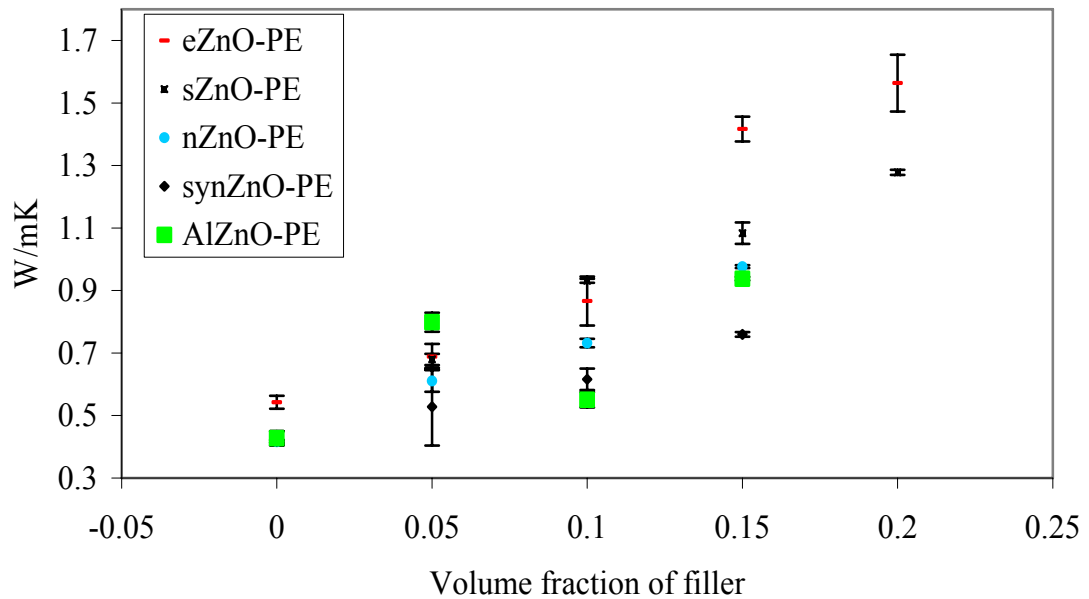


Figure 6.53. Thermal conductivity values of PE composites.

Thermal conductivity of the composites increased with increasing zinc oxide content as seen in the Figure 6.53. At the same loading level the conductivity values of PE composites were in order of the highest to lowest levels as eZnO, sZnO, nZnO, AlZnO and synZnO. There were some exceptions, in instance at 10 vol% AlZnO added composites thermal conductivity decreased; which might be due to un-homogenous dispersion of the particles in the polymer matrix. Thermal conductivity models providing a good description of systems with micro-meter or larger-size particles, failed to describe thermal transport in nanocomposites. Interfaces between materials become increasingly important on small length scales. For sufficiently small particles, the properties of the polymer/particle interface control the thermal transport in the composite as well. However in this study the expectation failed because of the

particulate and fiber like loading materials. The surface area affect could not be seen because of the big agglomerates obtained in the composites during the processing.

Table 6.15. Thermal conductivity (W/mK) values of the PE composites.

ZnO Type	Filler Loading (vol %)				
	0	5	10	15	20
eZnO-PE	0.55	0.69	0.87	1.41	1.56
sZnO-PE	0.43	0.68	0.93	1.08	1.28
nZnO-PE	0.41	0.61	0.73	0.98	-
synZnO-PE	0.42	0.53	0.62	0.76	-
AlZnO-PE	0.43	0.80	0.55	0.94	-

Table 6.16. Thermal conductivity values of the PP composites.

ZnO Type	Filler Loading (vol%)				
	0	5	10	15	20
sZnO-PP	0.35	0.44	0.53	0.65	0.90
nZnO-PP	0.35	0.23	0.40	0.44	-

Both PP and PE are dielectric materials; therefore, the thermal conduction is transported but by phonons. The semi-crystalline polymer allowed better phonon conduction with less scattering incidents than that of an amorphous material so

crystallinity of the polymer was very important. The results showed that; thermal conductivity of the PE matrix composites was higher than that of the PP matrix composites. The crystalline% of the PE composites might be higher than PP composites where the crystallinity results confirmed with that of DSC results given in Table 6.4. 20 vol% loaded eZnO composites had the highest electrical conductivity. It could be due to the aspect ratio of the filler since the transport mechanism explained by phonons exciting one or more atoms by twisting, pulling or pushing will be easily propagate the transportation of energy. The conductivity was affected most by the addition of 20 vol% of eZnO and sZnO to PE composites and it was found about 1.56 and 1.26 W/mK, respectively. The conductivity of the composites increased about 2.5-3 times for the highest loading compared with polymer thermal conductivity. The sZnO and eZnO loaded composites can be used in heat sink applications.

AlZnO loaded composites thermal conductivity value was greater than synZnO loaded composites as given in Table 6.15. It was expected to have the same results since these two powders were prepared by using the same procedure (hydrothermal). However there were two transport mechanisms obtained for the solids; phonon transport (lattice vibrations) and electron transport mechanism. Although, phonon transport was the dominant mechanism for this system, the Al doping in the powder should affect the electron transport and increase the thermal conductivity of the material.

The theoretical model calculations were made using four different methods. Nielsen model, modified Nielsen model, rule of mixture and geometric rule of mixtures models were applied to predict the thermal conductivities. To compare the compatibility between theoretical and experimental values the model calculations were performed and given in Figure 6.54 to Figure 6.60 for eZnO-PE, sZnO-PE, sZnO-PP, nZnO-PE, nZnO-PP, synZnO-PE, and AlZnO-PE composites, respectively. Thermal conductivities of eZnO, sZnO, nZnO, synZnO and AlZnO powder were assumed as 5, 4.5, 4.2, 3.5 and 3.5 W/mK in the model calculations, respectively. In the Nielsen, and modified Nielsen models given in Equations 3.18 and 3.19 the shape factor “A” and maximum packing factor were chosen as 4.98 and 0.637 for irregular particles respectively (Nielsen, 1974).

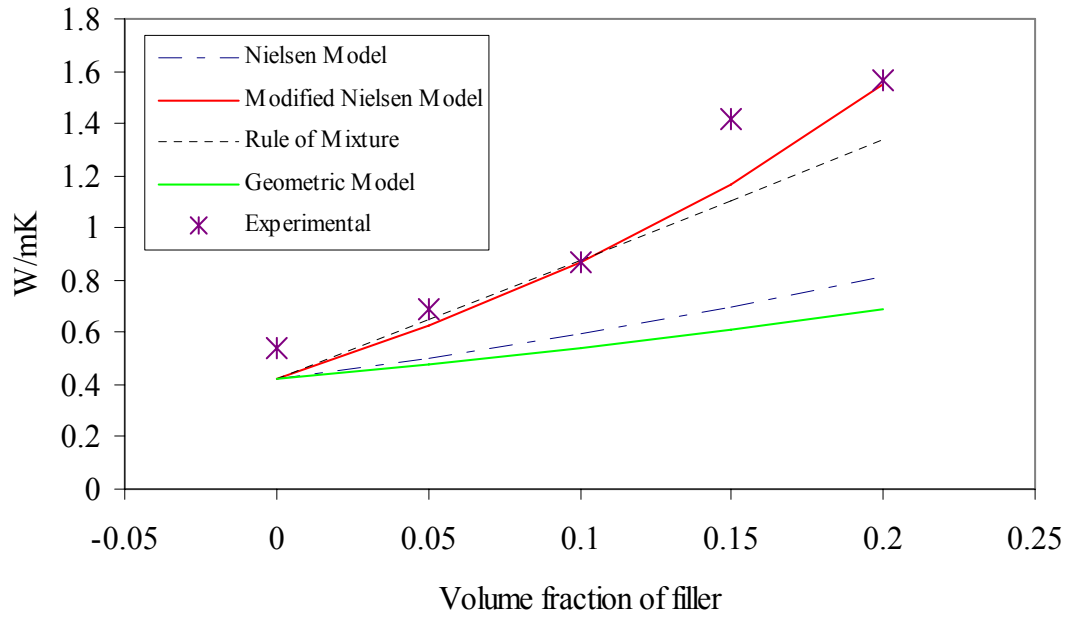


Figure 6.54. Comparison of the experimental and predicted thermal conductivity values for eZnO-PE composite from theoretical models.

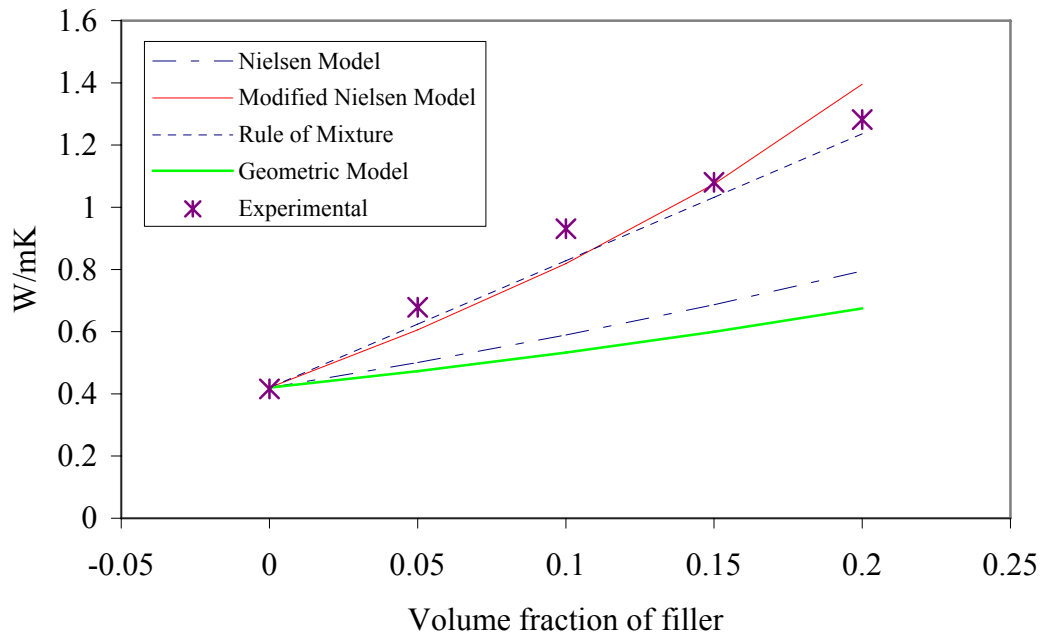


Figure 6.55. Comparison of the experimental and predicted thermal conductivity values for sZnO-PE composite from theoretical models.

The thermal conductivity of the composite was underestimated in all models for all particle contents except 20 vol% loading as seen Figure 6.54. However, the modified Nielsen model fairly predicted the experimental value.

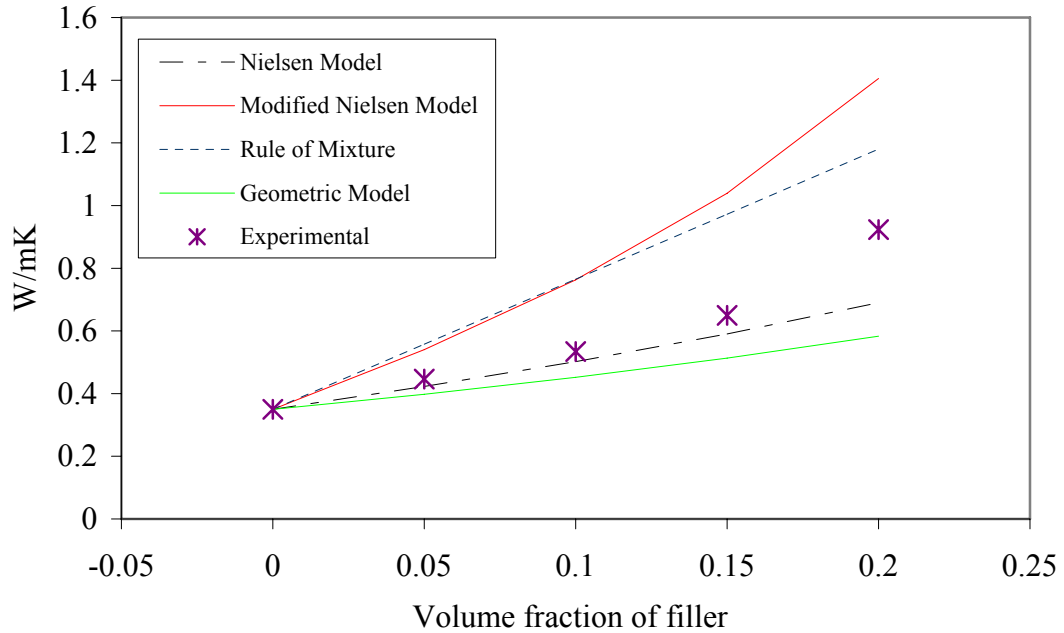


Figure 6.56. Comparison of the experimental and predicted thermal conductivity values for sZnO-PP composite from theoretical models.

sZnO-PE composites predicts well with the modified Nielsen model as depicted in Figure 6.55. Nevertheless, sZnO-PP composites with low loading levels the Nielsen model fairly predicts with the experimental data but with high loading it starts to deviate as seen in Figure6.56. Any of the theoretical model predicting the thermal conductivity of sZnO-PP composite deviates. The models could not predict the value since the non-homogeneous distribution of the ZnO particles concentration into polymer matrix during the preparation of the specimen could be high.

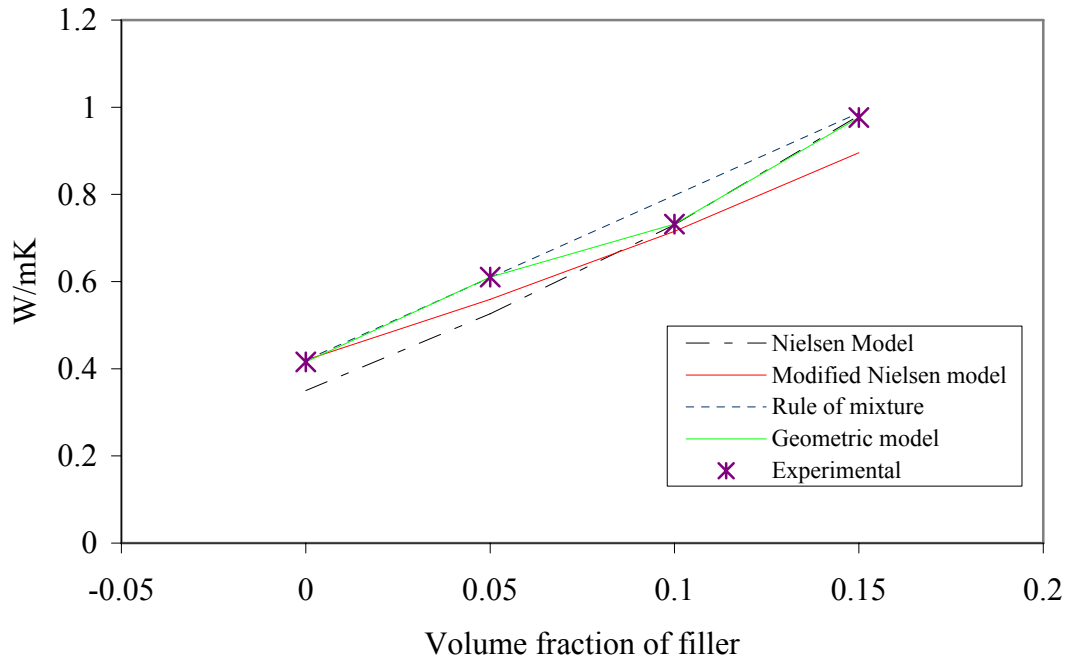


Figure 6.57. Comparison of the experimental and predicted thermal conductivity values for nZnO-PE composite from theoretical models.

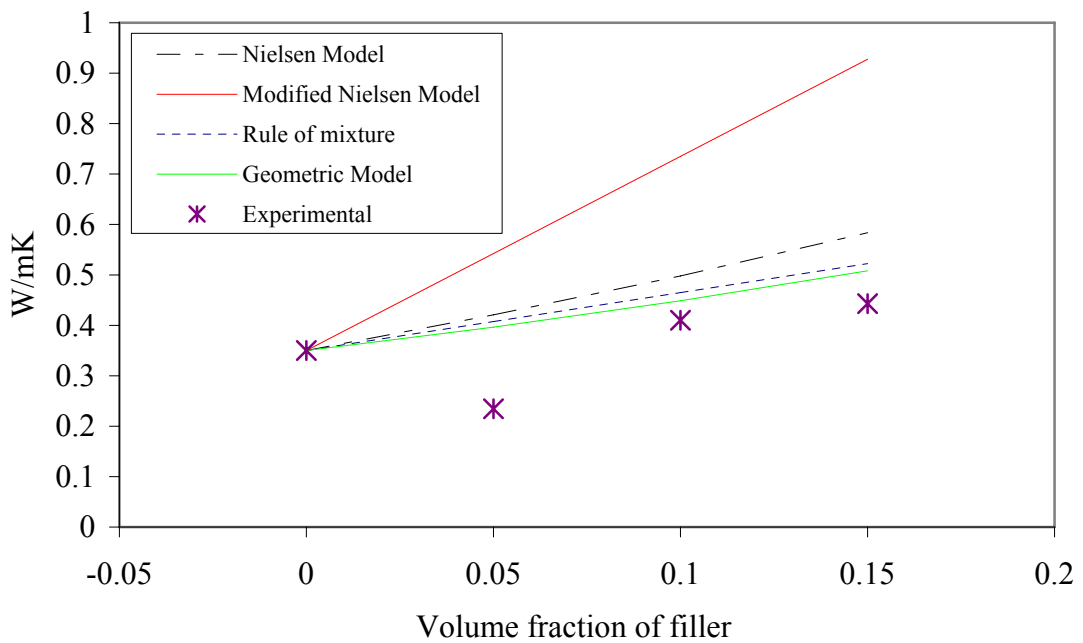


Figure 6.58. Comparison of the experimental and predicted thermal conductivity values for nZnO-PP composite from theoretical models.

For nZnO-PE composites the rule of mixture predicted the experimental data as seen in Figure 6.57, but for nZnO-PP composites theoretical models overestimated the experimental data (Figure 6.58). This might be due to big agglomerates obtained in the nZnO particles and the particles behave like a micron sized powder (however it was nanoscale) in the matrix but could not interact to each other (conduct the energy by phonon) and decreased in thermal conductivity value.

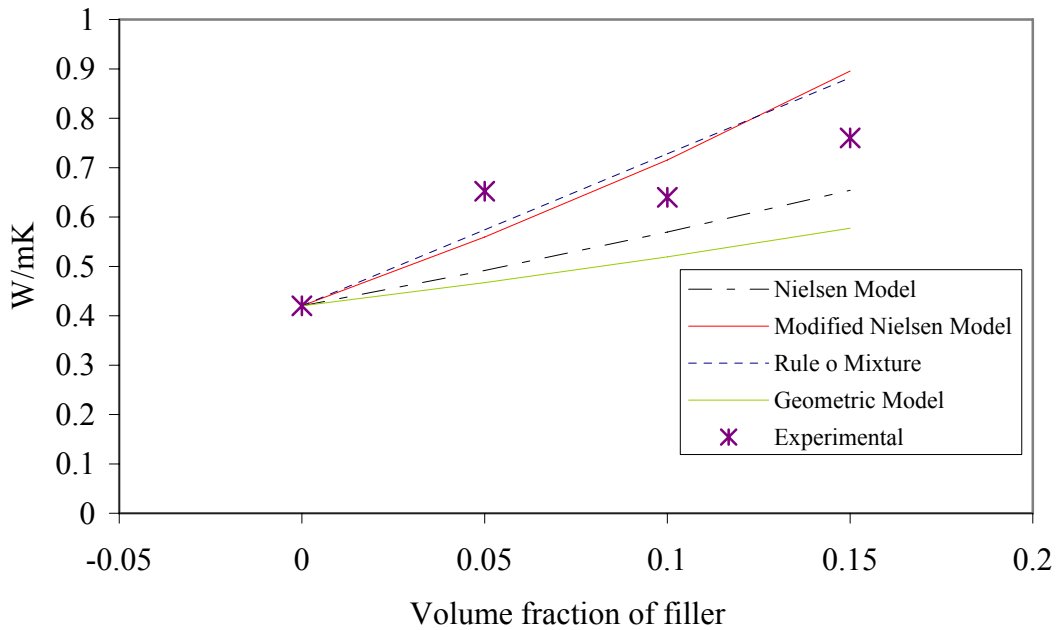


Figure 6.59. Comparison of the experimental and predicted thermal conductivity values for synZnO-PE composite from theoretical models.

For synZnO and AlZnO loaded composites Modified Nielsen and Rule of mixture models predicted quite well of the composites in the whole range as given in Figure 6.59 and Figure 6.60. For the ZnO-PE/PP composites modified Nielsen model predicted well than other models.

To understand the thermal conductivity of composites and mixtures equations were derived from continuum-level phenomenological formulations that typically incorporate only the particle shape and volume fraction as variables. Diffusive heat transport is assumed in both phases and no effects of interfaces or particle mobility were taken into account. This approach, while providing a good description of systems with

micro-meter or larger-size particles, failed to describe thermal transport in nanocomposites. Interfaces between materials become increasingly important on small length scales.

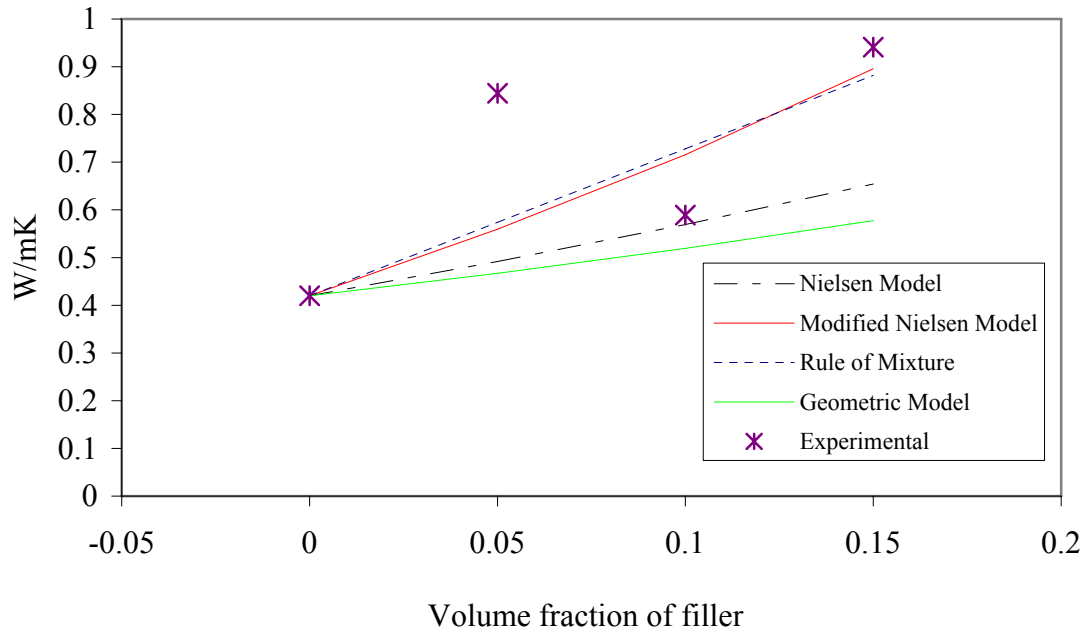


Figure 6.60. Comparison of the experimental and predicted thermal conductivity values for AlZnO-PE composite from theoretical models.

6.5. Optical Properties of Polymer Composites

In the industrial applications PP and PE are the commonly used thermoplastic polymers. However UV irradiation, light or other high energy radiation systems, stress loading, biological sources and so forth causes degradation of these polymers on a time of period. Especially UV-irradiation is a frequently encountered factor that can affect photo-degradation of polymers. ZnO powders absorbed nearly 100% of in the UV region. As a result, the ZnO addition influenced the photo-degradation of PP and PE since below 370 nm the UV light was absorbed by ZnO. Zhao and Li (2006) found chain degradation in PP can be induced when it was irradiated within the active wavelength range of 310–350 nm, which means that photo-degradation can occur easily

in PP based materials. According to Ito et al. (2001) due to unsaturated ketone or benzene ring presented in the antioxidant around 4 eV (310 nm) started to decompose by the irradiation of photons or by capturing radicals induced in polymers. The composites optical properties were investigated if composites possess the ZnO optical properties of powders. ZnO is a luminescent material that can emit light in different regions of electromagnetic spectrum when electrically excited. Also it's a chemically stable, inexpensive and environmental friendly material. Its luminescent property can be useful to construct solid-state lamps for illumination or as UV emitter.

Polymer matrix materials have luminescence spectra shown in Figure 6.61. They show a peak at 425 nm due to the decrease of its chemical groups. The visible light emission was studied to understand the luminescence in composites. Fluorescence spectra of eZnO filled PE and PP composites are given in Figure 6.62 and Figure 6.63 respectively.

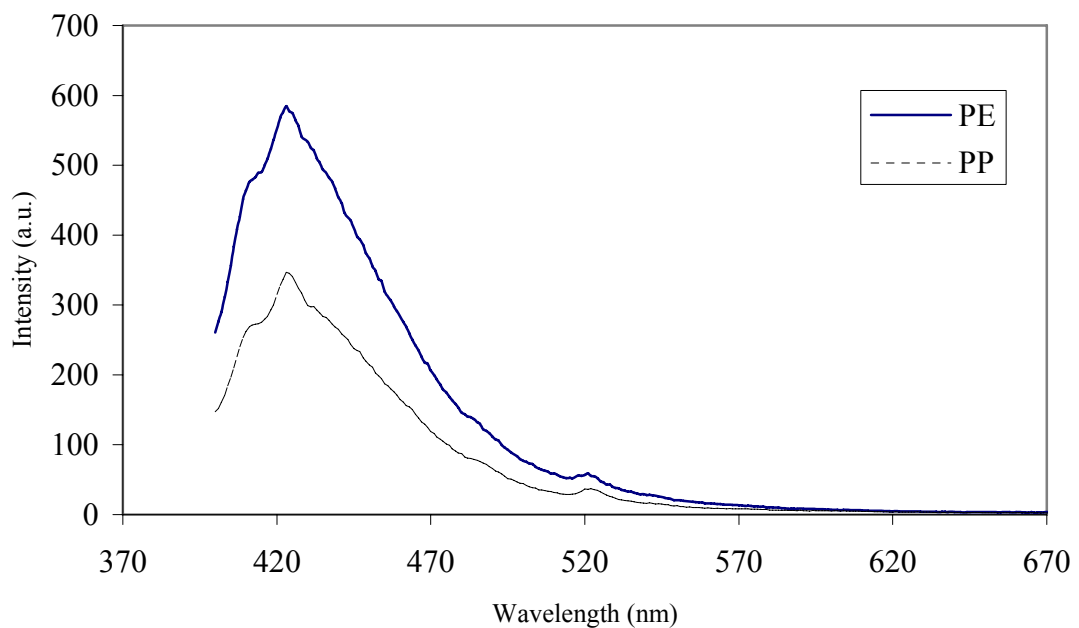


Figure 6.61. Fluorescence spectra of PE and PP matrix.

In the optical perspective of ZnO-polymer composites system, ZnO absorbed light in UV region and it screened the polymer matrix from the affect of UV light and the light could penetrate into the polymer matrix. Thus, ZnO fluorescence spectra rather

than the fluorescence spectra of polymer became important. As seen in Figure 6.62 to Figure 6.70 all ZnO-polymer composites and those of their ZnO (filler) spectra were nearly similar with each other.

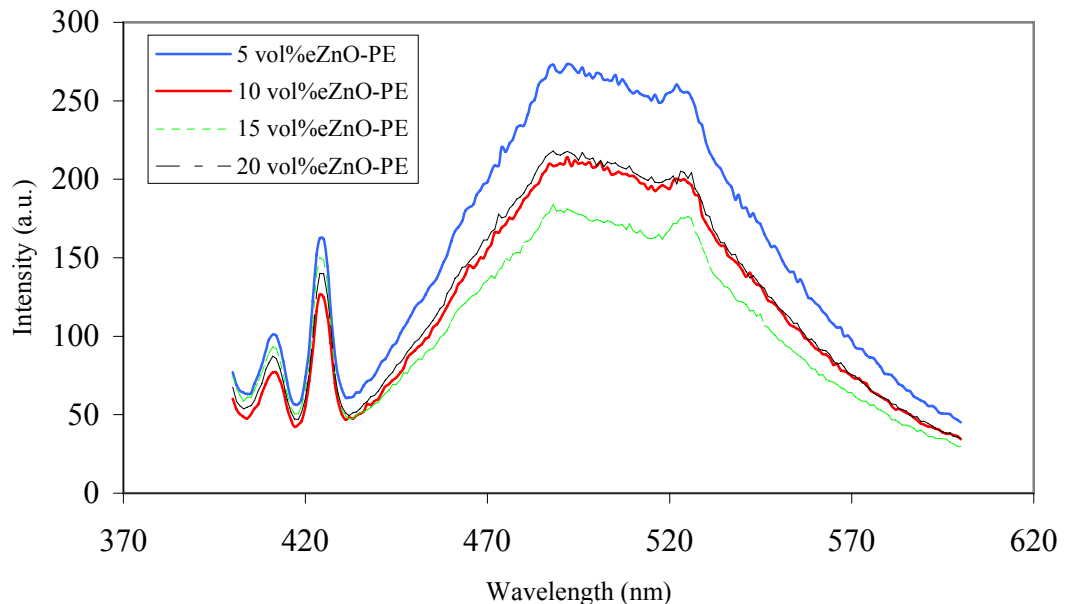


Figure 6.62. Fluorescence spectra of eZnO loaded PE composites.

Pure eZnO shows a weak narrow UV band around 380 nm due to exciton and a broader band at 500 nm due to defects in the sample as represented in Figure 6.62. Interestingly after being incorporated into PE, ZnO exhibit complete UV emission. Composites were excited at 370 nm where the first peak came at 400 nm. PE composites showed two narrow peaks at 410 nm and 425 nm and a broader band in the green part of the visible spectrum with a maximum between 480-525 nm. As a conclusion, the PE matrix influences the optical properties of composites in these spectra have a great importance due to the affect of polymer matrix on the luminescence spectra. The emission peak of 380 nm shifts to 400 nm under the influence of PE. When the electron in the valence band was excited to the conduction band it could be trapped in a shallow level and then recombined with the hole left in the valence band, this process gave a rise of the band centered at 420 nm (Lima et al., 2007, Chen et al, 2009).

The emission peak at 425 nm can be attributed to electron hole plasma recombination emission of ZnO particles as from the Figure 6.62. The broad peak around 480-530 nm corresponds to green and blue shifts of composite. For PP composites 20 vol% filled composites, the PP addition significantly affected the luminescence behavior of the composite as given in Figure 6.63 which was like the PE matrix composites. However the 5, 10 and 15 vol% composites did not show a maximum broad peak between 480-525 nm, they have two small peaks at 488 nm and 525 nm which were attributed to the defects coming from zinc oxide and responsible of green emission. The intensities of the peaks in PL spectra did not increased with concentration of zinc oxide in the composites which might be due to un-homogeneity in the composites.

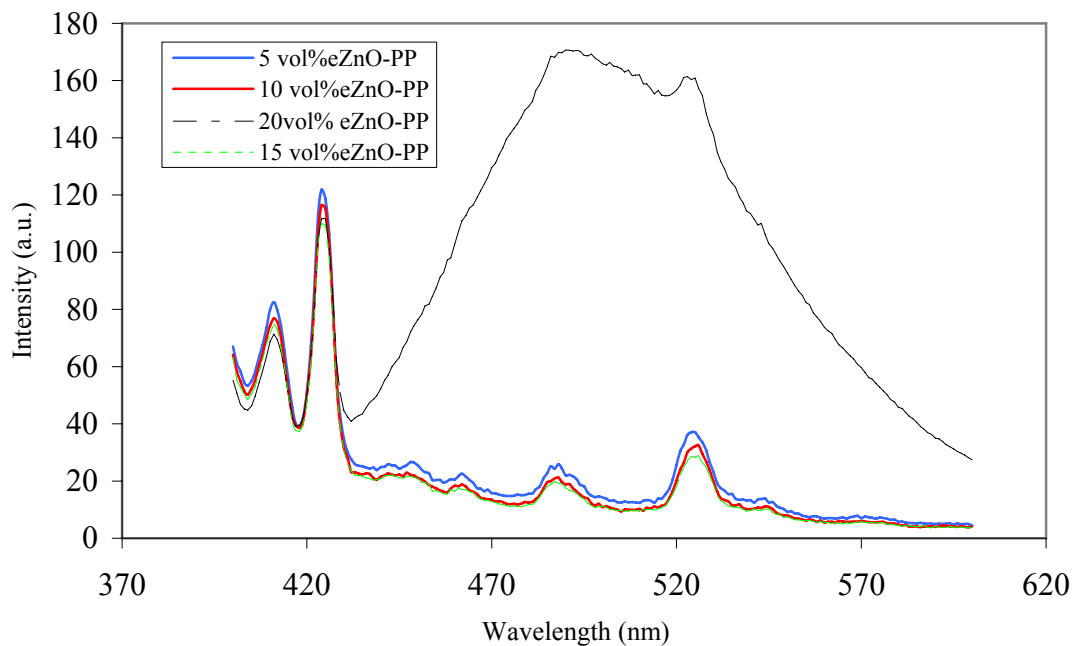


Figure 6.63. Fluorescence spectra of eZnO loaded PP composites.

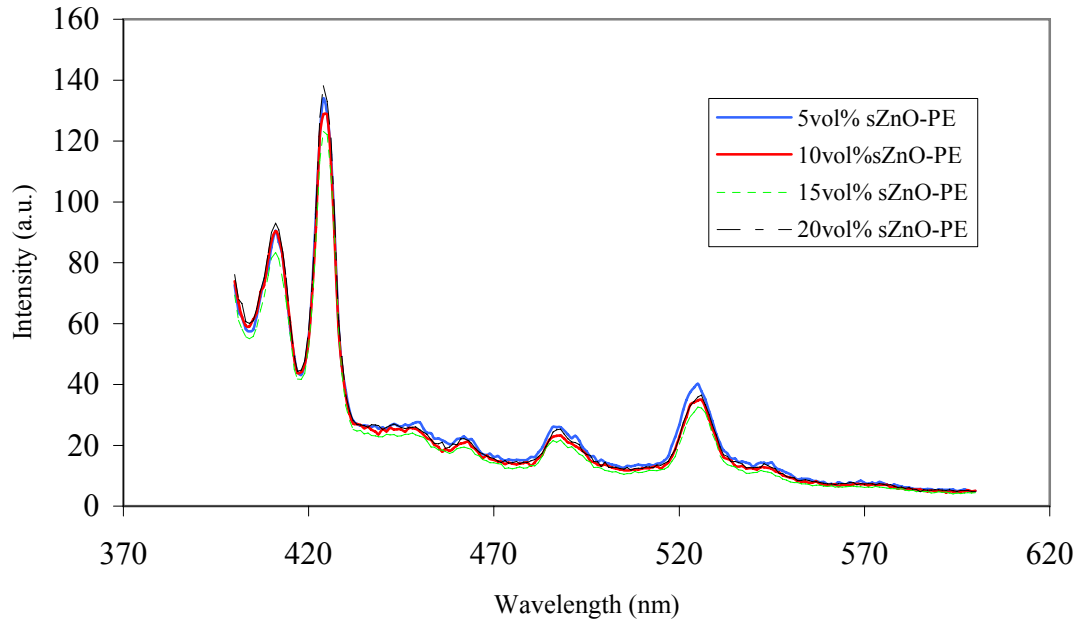


Figure 6.64. Fluorescence spectra of sZnO loaded PE composites.

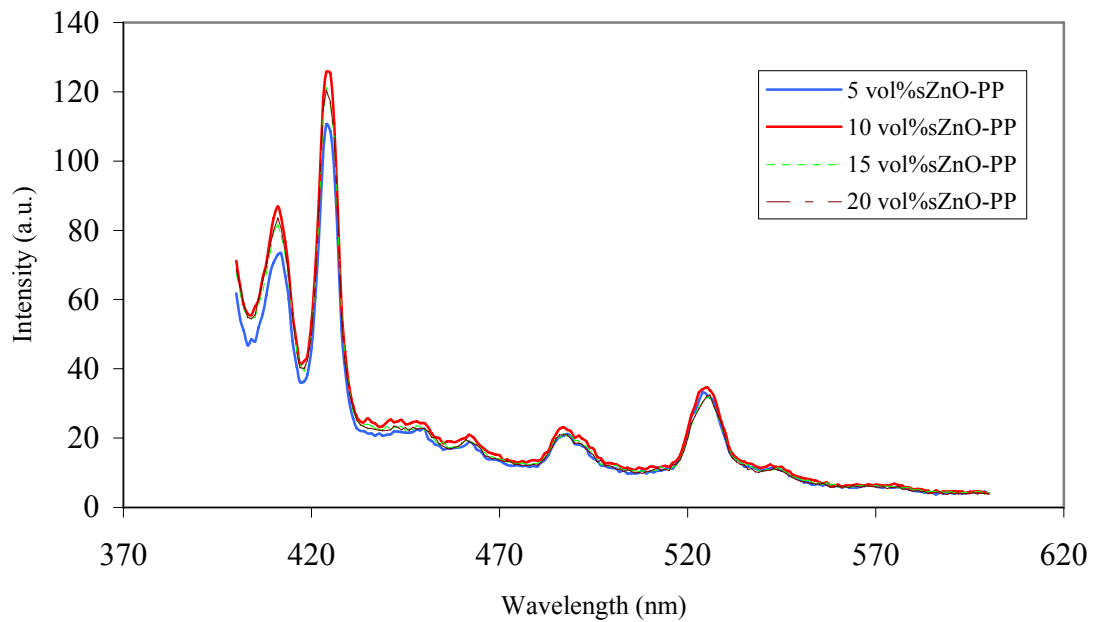


Figure 6.65. Fluorescence spectra of sZnO loaded PP composites.

sZnO-PE and PP composites fluorescence spectra are given in Figure 6.64 and Figure 6.65, respectively. The PL spectrum of pure sZnO composites show peaks at 421 nm, 480 nm, 510 nm and 530 nm. The composites for both PE and PP show the same peaks with pure ZnO powder. Only two peaks at 410 and 510 nm were added to photoluminescence spectra, due to the influence of the polymer to the luminescence behavior of zinc oxide. The peak at 410 nm probably corresponded to the shift in the level of the oxygen vacancies. The 510 nm green-emission band was attributed to paramagnetic isolated oxygen vacancies in the ZnO powders (Vanheusden et al., 1997). The PE and PP composites, gave blue and green emissions under 380 nm excitation wavelength.

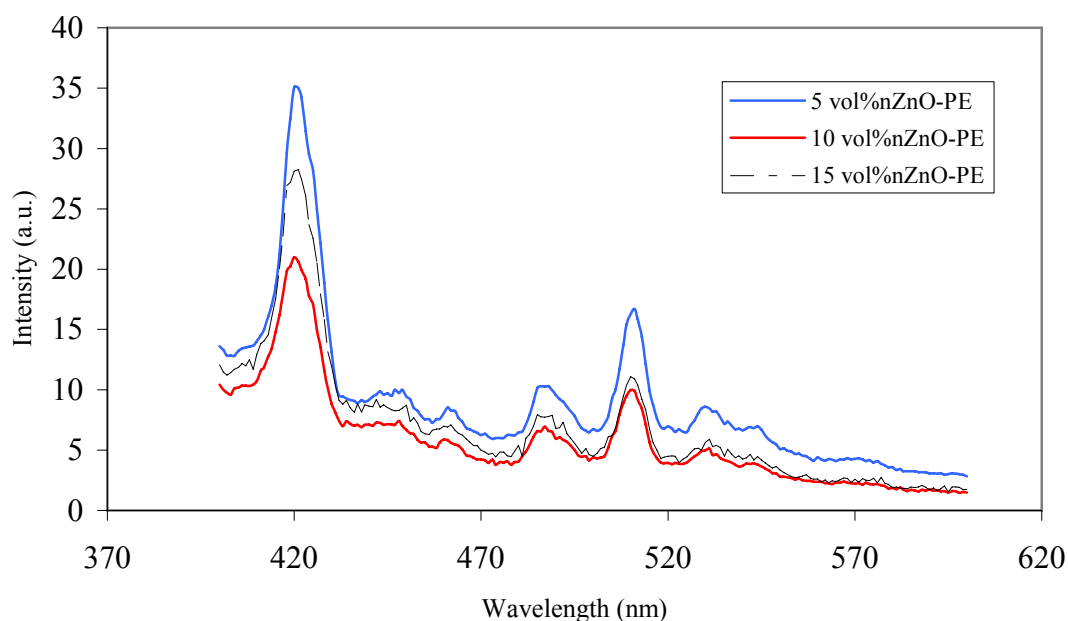


Figure 6.66. Fluorescence spectra of nZnO loaded PE composites.

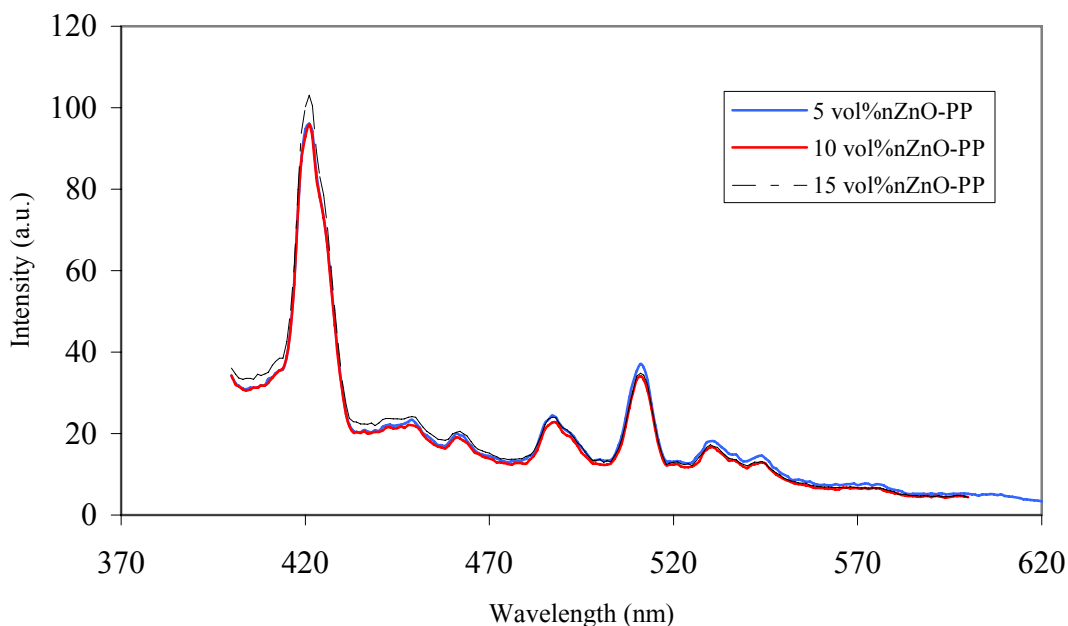


Figure 6.67. Fluorescence spectra of nZnO loaded PP composites.

Figure 6.66 and Figure 6.67 shows the nZnO filled PE and PP composites fluorescent spectra, respectively. For nano zinc oxide filled composites the same characteristic peaks previously mentioned for sZnO filled composites were observed. PL spectra PP and PE matrix composites and the PL spectra for pure zinc oxide powders exhibited the same behavior. As a consequence, composites shift blue and green emission. Figure 6.68 gives the fluorescence spectra of synZnO loaded composites. Figure 6.68 shows the evolution of intensities of exciton emission and green defect band. The exciton band intensities and the peak maximum values of the peaks shifted due to the influence of the polymer. At 405 nm there is another peak which was attributed to blue luminescence due to zinc vacancy.

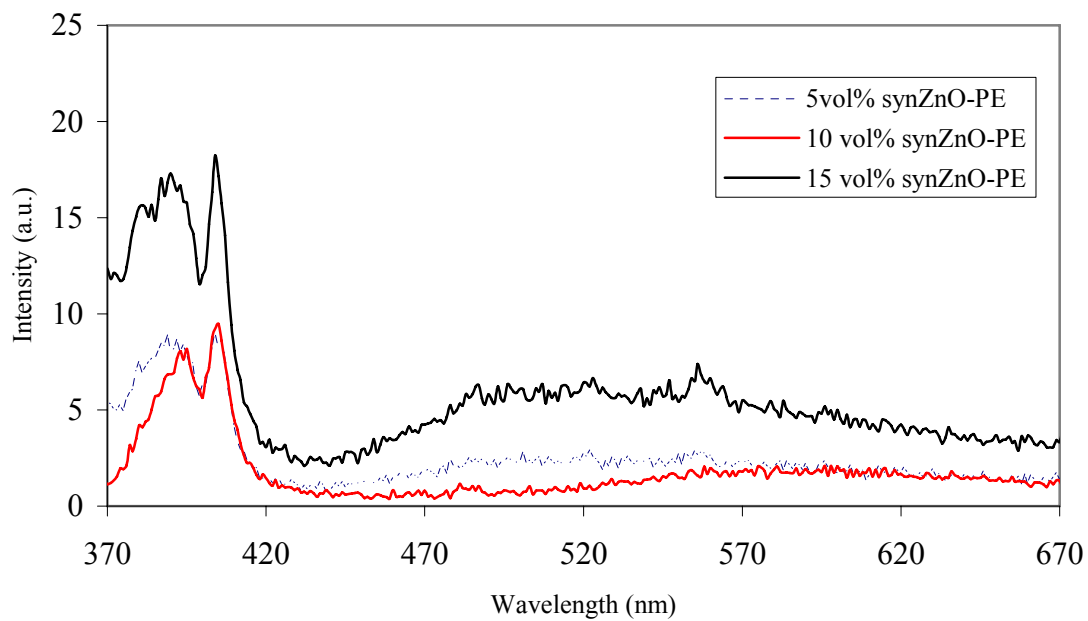


Figure 6.68. Fluorescence spectra of synZnO loaded PE composites.

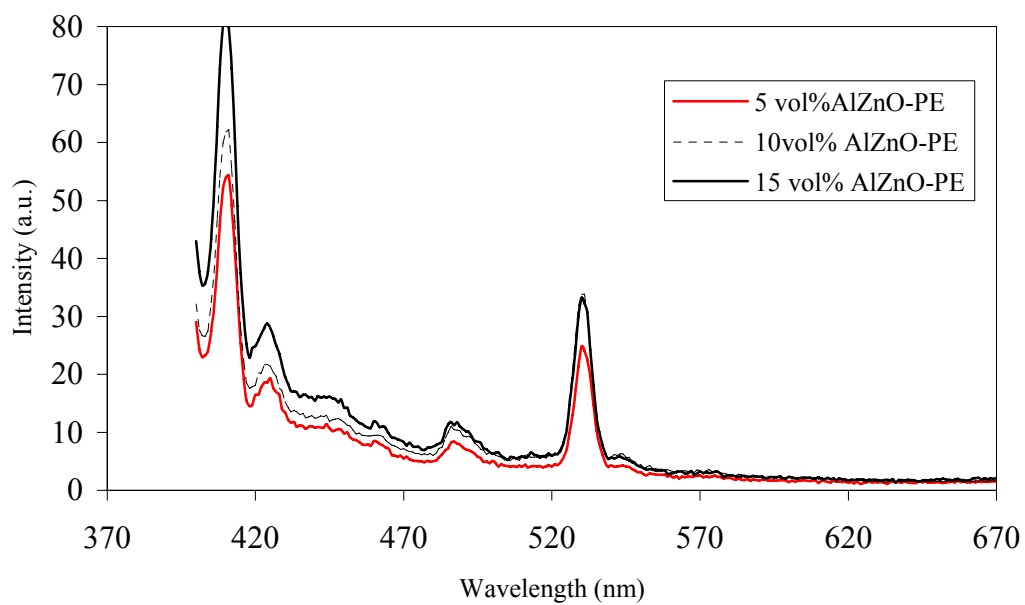


Figure 6.69. Fluorescence spectra of AlZnO loaded PE composites.

Figure 6.69 gives the AlZnO filled composites fluorescence spectrum. AlZnO loaded composites spectrum was not influenced from polymer matrix. The excitation wavelength of the Al doped ZnO powder was found 380 nm so the same value was observed for the composites. Emission spectrum has peaks at 530 nm, 490 nm, 448 nm, 426 nm and 408 nm which was attributed to the defects coming from zinc oxide (zinc or oxygen vacancies), and emitted light in green and blue regions.

Figure 6.70 shows the modified zinc oxide (sZnO) loaded composites fluorescence spectra. The modified composites shows roughly the same fluorescence spectra, only AMPTES modified composites peak maximum values are shifted slightly. The composite emitted light in blue and green regions. Table 6.17 and Table 6.18 represents the optical data for PE and PP composites.

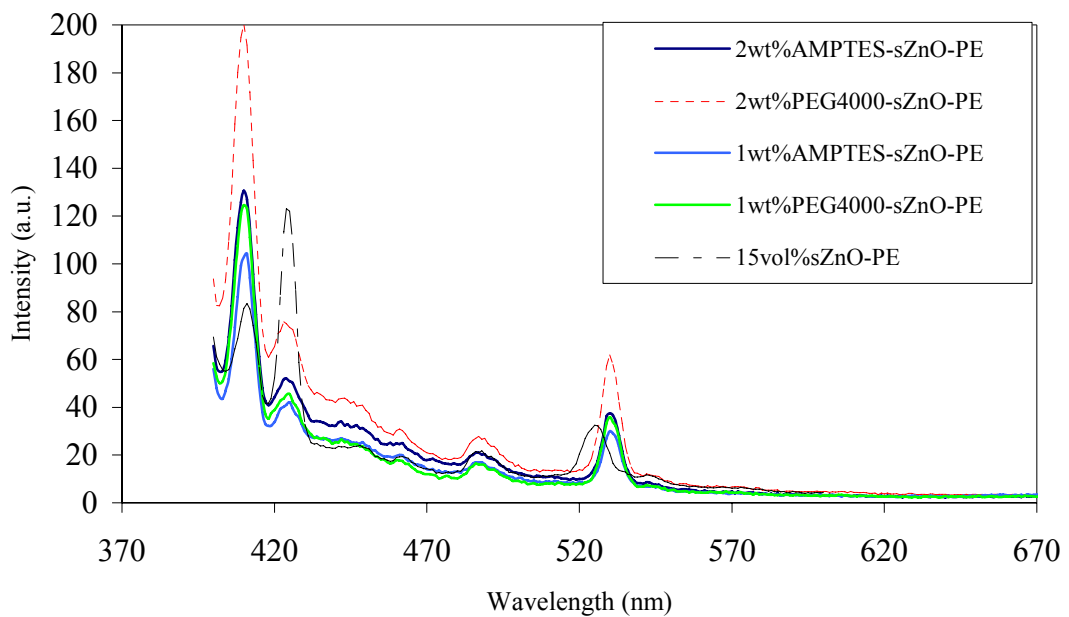


Figure 6.70. Fluorescence spectra of modified sZnO loaded PE composites and unmodified composite.

Table 6.17. Fluorescence Spectra results of PE composites.

Composites	Excitation (nm)	Emission (nm)
eZnO-PE	380	411, 425, 488-523
sZnO-PE	380	411, 425, 488, 525
nZnO-PE	380	421, 448-461, 488, 511
synZnO-PE	350	380, 390, 404, 480-570
AlZnO-PE	380	408, 426, 448, 490, 530

Table 6.18. Fluorescence Spectra results of PP composites.

Composites	Excitation (nm)	Emission (nm)
eZnO-PP	380	411, 425, 488-525
sZnO-PP	380	411, 425, 488-525
nZnO-PP	380	421, 451-463, 490, 511,545

Optical properties of ZnO-polymer composites were intended to investigate for possession probability of the optical properties of ZnO to the composite, since zinc oxide is an luminescent material that can emit light in different regions of electromagnetic spectrum when electrically excited. The affect of polymer matrix on the luminescence spectra was of great importance. Finally, the PE and PP matrix influences the optical properties of composites. For example, in the eZnO loaded composites there was a big emission peak ranging between 420-620 nm. In the polymer composite the spectra of the broad peak changed to 435-590 nm scale. However this change in the broadening did not affect the luminescence property so much. The composite showed luminescence in the green and yellow regions as previously reported. In the composites the emission peak of 380 nm shifts to 400 nm under the influence of PE. The emission peak at 425 nm can be attributed to electron hole plasma recombination emission of ZnO particles. In conclusion, the composites show the same effect like zinc oxide in all of the composites. Generally emits light in blue, green and yellow regions. The particle size effect difference was obtained in the synZnO powder loaded composites since defect free and more stable optical properties were obtained. The porous structure

seemed not to affect the property of the polymer composite but homogeneity problem in the composite brought huge changes in the intensity of the spectrum.

6.6. Mechanical Characterization of Polymer Composites

The stress-strain behavior of a particulate (or small L/D fibers) filled composite was determined by the polymer, the filler concentration and the particle size of ZnO powder (eZnO and nZnO). The mechanical characterization of the composites was performed by tensile test given as force-stroke curve shown in Figure 6.71. Instead of stress-strain curve, force-stroke curve was used to see the elongation affect by the addition of zinc oxide filler.

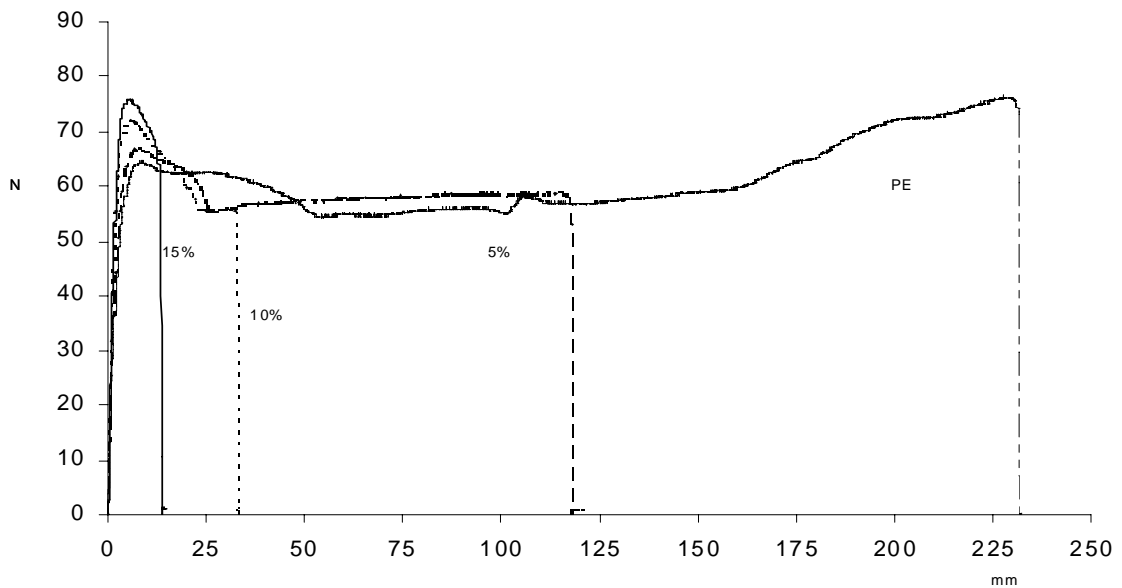


Figure 6.71. Force-Stroke diagram for eZnO loaded PE.

As clearly shown in Figure 6.71, zinc oxide addition decreased the elongation, tensile strength, and yield stress. The average of three samples was used for each composite. The mechanical properties of nZnO, eZnO and their modified forms of composites are reported in Table 6.19 through to Table 6.23 .

Table 6.19. eZnO-PE composites mechanical behavior.

Sample Name	Elastic Modulus (N/mm ²)	Yield stress (N/mm ²)	Yield Strain %	Tensile Strength (N/mm ²)	Elongation at break (mm)
Pure PE	80.3	8.3	8.7	23	232.6
5 vol % eZnO-PE	110.8	8.4	6.9	6.6	120.1
10 vol% eZnO-PE	165.3	8.6	5.2	7.0	34.0
15 vol% eZnO-PE	182.7	8.8	4.9	7.4	14.9

Table 6.20. 15 vol% Modified eZnO loaded PE composites mechanical behavior.

Sample Name	Elastic Modulus (N/mm ²)	Yield stress (N/mm ²)	Yield Strain %	Tensile Strength (N/mm ²)	Elongation at break (mm)
Unmodified	182.7	8.8	4.9	7.4	14.9
%1 AMPTES	192.6	3.5	1.7	5.4	6.0
%2 AMPTES	222.9	3.4	1.2	5.3	6.7
%1 PEG4000	140.2	4.7	7.5	4.2	33.5
%2 PEG 4000	182.9	5.7	5.3	6.9	241

PE matrix composites are flexible and ductile plastics which tend to be tough and resist deformation. The mechanical properties of composites significantly influenced by the addition of ZnO powder since the elastic modulus of the composites

increased while yield strain decreased. The maximum force applied to the composites might be lowered by addition of zinc oxide, as well. As a consequence, ZnO addition to the polymer matrix decreased the toughness, increased the brittleness and stiffness. As seen in Table 6.18, the Young modulus of the composites increased. The ultimate elongation of pure PE was very high, but with the addition of ZnO to the composite the elongation decreased.

Improving the filler polymer interface might be positive effect on elongation of particle filled-polymer composites due to the chemical structure of PE. When the chains are orientated, they start to form orientation in the crystallinity, which evokes an increase in the strength of PE sample. Incorporating particles to the PE matrix reduces chains mobility which leads to a rapid decrease in elongation at break, and introduces discontinuity in stress transfer to the filler-polymer interface in the composites structure (Zhou et al., 2009).

As reported in Table 6.20, AMPTES modified composites had positive effect on stiffness. However, the yield strain increased for PEG 4000 modified composites. In 2 wt% PEG 4000 modified composite the elongation at break increased up to 241 mm. This extraordinary elongation might be due to the well dispersed powders in the composites with void free structures. In general tensile properties of materials are largely determined by imperfections and micro cracks in the composites. When a tensile stress was applied to composite debonding was observed between the ZnO particles and polymer matrix. The debonding is created at low stress level and gets bigger until interruption of load transfer to the matrix. The elongation increased due to good interfacial adhesion between polymer and filler. However, the non-homogeneity in the dispersion and void formation during the production negatively affected the mechanical behavior.

Table 6.21. eZnO-PP composites mechanical behavior.

Sample Name	Elastic Modulus (N/mm ²)	Yield stress (N/mm ²)	Yield Strain %	Tensile Strength (N/mm ²)	Elongation at break (mm)
Pure PP	812.1	19.2	2.6	19.7	5.4
5vol% eZnO-PP	1153.7	25.2	2.5	20.7	2.7
10 vol% eZnO-PP	1024.6	26.9	3.0	21.4	2.4
15 vol% eZnO-PP	1247.9	18.8	1.7	21.4	1.9

The PP matrix composites are rigid, tough, hard and brittle plastics which tend to be strong and resist deformation. ZnO addition decreased the toughness, increased the brittleness and stiffness. As seen in Table 6.21 the Young modulus of the composites increased but there is no order with respect to filler volume fraction. This might be caused by the failures or micro fractures (voids) on the composites when loading were applied. In PE and PP composites the same mechanical behavior was obtained which were stiffer but brittle.

Table 6.22. nZnO-PE composites mechanical behavior.

Sample Name	Elastic Modulus (N/mm ²)	Yield stress (N/mm ²)	Yield Strain %	Tensile Strength (N/mm ²)	Elongation at break (mm)
Pure PE	80.3	8.3	8.7	23	232.6
5vol% ZnO-PE	190.8	6.3	6.9	6.8	217.6
10 vol% nZnO-PE	234.6	6.4	9.4	6.6	186
15vol% nZnO-PE	220.4	5.2	3.3	7.2	6.3

Table 6.23. 15 vol% modified nZnO loaded PE composites mechanical behavior.

Sample Name	Elastic Modulus (N/mm ²)	Yield stress (N/mm ²)	Yield Strain %	Tensile Strength (N/mm ²)	Elongation at break (mm)
Unmodified	220.4	5.2	3.3	7.2	6.3
%1 AMPTES	221.6	6.9	4.2	7.5	15
%2 AMPTES	221.4	4.6	2.1	5.9	5.4
%1 PEG4000	162.5	4.0	2.9	4.6	15.5
%2 PEG 4000	209.8	4.0	1.7	5.5	5.2

As reported in Table 6.22 for nZnO loaded composites the elastic modulus increased, therefore increasing the stiffness decreased the tensile strength which could affect the applied load to the composites. However, the composites exhibit lower tensile strength even at low ZnO content compared with pure PE. This may attributed to poor interaction between polymer and ZnO powder interface which should be enhanced. The modified composites showed higher stiffness but lower tensile strength as seen in Table 6.17. Only 1wt% PEG 4000 loaded composite showed higher elongation value.

It is known that, the interface adhesion influences the mechanical behavior of particulate filled polymer composite. Microfillers (eZnO) commonly increase the stiffness but on the other hand, they may have a harmful effect on the strain at break. The flexural strength of microparticle-filled composites may also be reduced with increasing filler content especially in the case when the load transfer between matrix and particles is insufficient and the interface is weak. This is also true for composites which contain particle agglomerates. nZnO composites did not show “nano-size particle effect” due to the formation of large agglomerates as given in Figure 6.35-b. The size of the particles determines the shape of voids that were formed at the debonding of particles from the matrix. This structural weakness that would have been expected from the agglomeration behavior of the nanoparticles and this could be fully eliminated by the modification of chains of the individual particle and polymer.

It can be concluded that, the tensile properties of the composites can be purposely adjusted. Young's modulus shows another aspect by the point of modified polymer composites view. The increase in stiffness of the nanocomposites is obviously

a result of the high modulus of the particulate fillers. Figure 6.72 and Figure 6.73 gives the Young's modulus and yield stress relation between two different composites.

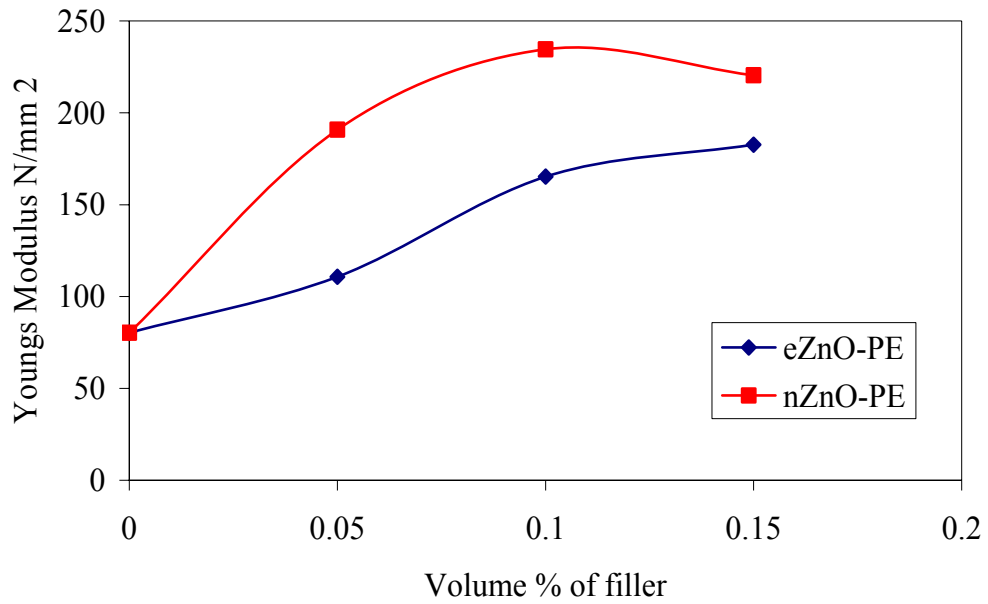


Figure 6.72. Youngs modulus of eZnO and nZnO-PE composites.

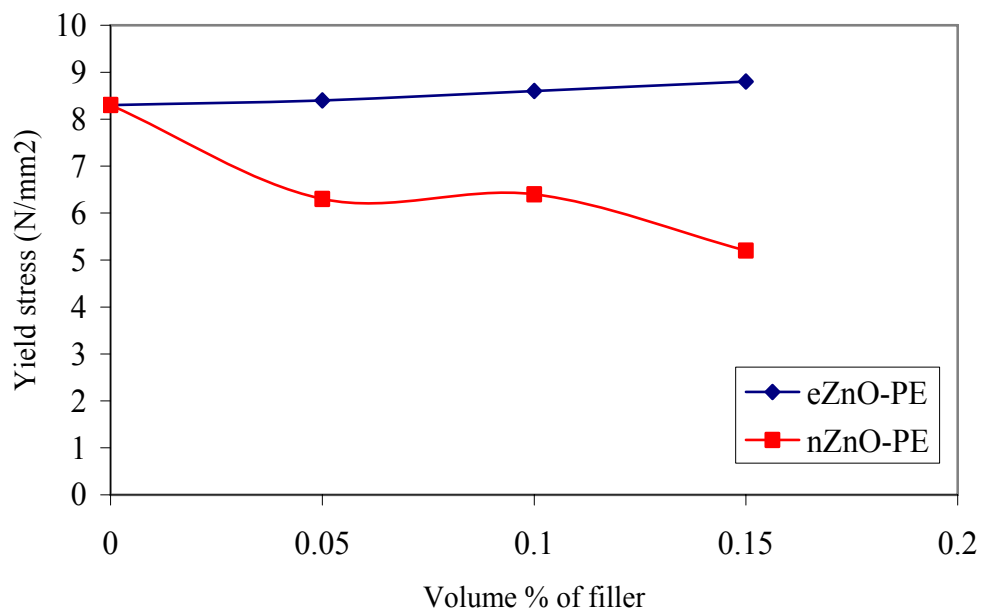


Figure 6.73. Yield stress of eZnO and nZnO-PE composites.

Figure 6.72 shows the effect of volume % filler on Young modulus. As the volume % of the filler increases the young modulus of the nZnO composites increases higher than eZnO composites. Stiffness of the composites prepared by nZnO with nano particle size increased compared to composites prepared by eZnO with micron particle size. Yield stress is an important parameter for engineering applications hence, when a polymer matrix is deformed the stress-strain behavior change. By increasing the filler content, changes for nZnO loaded composite were obtained from plastic deformation to brittle structure of composite as seen in Figure 6.73. This might be due to the poor adhesion between polymer and filler since the yield stress was decreased. For eZnO loaded composite the yield stress was independent of filler content due to good adhesion between polymer and filler.

6.7. Properties of ZnO Powders and Composites

ZnO is an important electronic and photonic material. ZnO-PE and ZnO-PP composites could be economic, weight saving, chemically resistive, flexible and conductive materials which possess the properties of zinc oxide, as well. It was aimed to investigate how ZnO with different particle size would affect the electrical, thermal conductivity and optical properties of PE and PP composites. Moreover, enhancement of the interphase between polymer and ZnO (surface modification) on electrical and mechanical properties of the composites was investigated. Table 6.24 gives an overview of the properties of powders.

Table 6.24. Properties of ZnO Powders.

ZnO	Particle Size (nm)	Surface Area (m ² /g)	Crystal Size (nm)	Resistivity (ohm.cm)	Max. Emmision Peak Wavelength (nm)	Density (g/cm ³)
e-ZnO	3860	1.57	415	1.5x10 ⁶	500	5.6
s-ZnO	752	10.11	237	1.5x10 ⁹	430	5.6
n-ZnO	378	20.00	203	1.7x10 ⁷	421	5.6
synZnO	169	21.2	68	1.3x10 ⁷	405	4.8
AlZnO	820	-	190	-	411	5.2

Electrical resistivity of ZnO powders having different particle size was found with a resistivity in the range of 10⁶-10⁹ ohm-cm. Although, it was expected to have, nearly the same electrical resistivity of ZnO powders with changing particle size, the significant difference in the electrical resistivity of the powders was observed. Powders particle size has an indirect effect on the electrical resistivity. Since aggregated crystals were formed during powder preparation the crystal size calculated from Scherrer Equation was found smaller than mean particle size of the powders as shown in Table 6.24. Surface area of the powders was increased as the particle and crystal size of powders decreased as expected. There were some defects observed in ZnO powders which influenced its optical properties generally be due to zinc/oxygen vacancy or interstitial. eZnO showed peak maximum at 500 nm and emitted light in green region. sZnO, nZnO, synZnO and AlZnO had peak maxima in the range 405 nm-430 nm and emitted light in blue region.

The change in the properties of composites were observed caused either by the introduction of nanoparticle fillers or by the dispersion state of the powders in the polymer matrix. Dispersion of nano powders in the polymeric system have great importance on the processing of polymer nanocomposites because the agglomeration limits the improvements of the properties of nanoparticles.

Non-homogenous filler distribution is required to improve the electrical properties in the composite since it is a higher field dependent property. In this manner, thermal conductivity of the material should be improved by homogenous dispersion of

particles since it depends on the bulk property of the composite. Table 6.25 gives the properties of 15 vol% ZnO loaded PE composites.

Table 6.25. 15 vol% loaded-PE composites properties.

Composites	Volume resistivity (ohm-cm)	Thermal Conductivity (W/mK)	Maximum Emmission Peak (nm)	Density (g/cm ³)	Mechanical
					Yield Stres (N/mm ²)
eZnO-PE	2.60E+13	1.41	488	1.5	8.8
sZnO-PE	3.20E+14	1.08	425	1.6	-
nZnO-PE	2.34E+12	0.98	421	1.6	5.2
synZnO-PE	2.13E+13	0.76	404	1.1	-
AlZnO-PE	9.60E+15	0.94	408	1.6	-

Table 6.25 shows the effect of particle size of ZnO powders on the volume resistivity of composites. There was an indirect relation with electrical resistivity and particle size of ZnO powders. The same result is true for thermal conductivity since the highest thermal conductivity corresponds to the ZnO having the highest particle size. The optical properties of composites showed the same properties with ZnO powders. eZnO-PE composites emit light in green regions while sZnO, nZnO, synZnO and AlZnO-PE composites emit light in blue region. It is generally expected that a decrease in the particle size causes an increase in the yield stress. However, as the particle size of ZnO powders were decreased from micron-size (eZnO) to nano-size (nZnO) the contrary results were found for composites. Decreasing yield stress might be due to the agglomeration of the nanoparticles in the composites during the processing. In spite of having relatively low yield stress, both composites can be used as an engineering material since they can safely be loaded by 4 MPa and 2.5 MPa force for eZnO-PE and nZnO-PE, respectively.

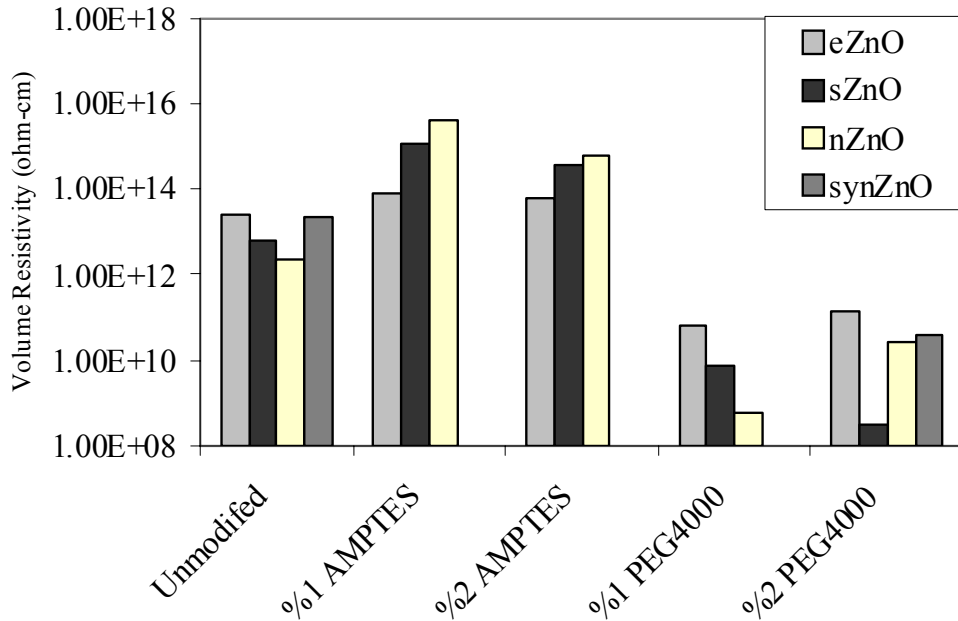


Figure 6.74. Electrical resistivities of 15 vol% ZnO-PE composites prepared from unmodified and modified zinc oxide powders.

Electrical resistivity of composites with 15 vol% ZnO-PE prepared with unmodified and modified zinc oxide powders were changed as shown in Figure 6.74. AMPTES modified composites have higher electrical resistivities than unmodified composites. AMPTES is a good modifier and make chemical bonds with both polymer and filler therefore adaptations of two different surfaces tend to disperse particles homogenously. The composites could not conduct the electricity due to the high interparticle distance. In PEG modified composites the electrical resistivity drops until 10^8 ohm-cm and can be used in the elimination of static electricity and in moderately conductive applications. Conductivity increases because of strong hydrogen bonding between ZnO and PEG molecules. The modification may cause bonding ZnO molecules with each other that can make an alignment in the polymeric network therefore a conductive network could be obtained. Modification did not affect the thermal conductivity, yield stress and optical properties of composites properties.

CHAPTER 7

CONCLUSION AND RECOMMENDATION

Zinc oxide powder was used as an alternative material to improve the electrical and thermal conductivity of the polypropylene and polyethylene matrix composites. Luminescence properties of ZnO have another advantage on polymeric composite to possess optical properties as well.

The synZnO powder was synthesized under mechanical stirring and ultrasonic treatment simultaneously at 30 °C. The crystals of the powder were elipsoidally shaped and the crystal size was calculated as 681 nm from Scherrer equation. The XRD pattern and FTIR spectrum gave the characteristic peaks of ZnO however there were some peaks related with Zn(OH)₂.

The AlZnO powder was in polydispersed crystal structure and crystal size was calculated as 176.9 nm. 3.2 mol% Al was found in the structure by EDX analysis. Characteristic ZnO peak of (002) plane at 34.25° shifted to 34.14° in XRD diagram of AlZnO. This departure helps to verify the Al⁺³ doping onto ZnO powder after annealing.

The particle size of ZnO powders were 3.86 μm, 752 nm, 378 nm, 110 nm, and 820 nm for eZnO, sZnO, nZnO, synZnO and AlZnO powders, respectively. The eZnO powder crystals were needle, tripot and rod shaped and the crystal size was found 415.8 nm. sZnO crystals were polydispersed but mostly bar shaped and the crystal size was found as 237 nm while nZnO powder was bar shaped with small L/D ratio particles having crystal size of 202 nm.

To enhance the interface between ZnO and polymer matrix, two different modifier AMPTES and PEG 4000 were used in two different weight percentages (1 wt%, 2wt%). The modification was confirmed by FTIR spectra having the bands corresponding to organic structure.

The electrical resistivity values of the pellets prepared from eZnO, sZnO, nZnO and synZnO powders were found as $1.5 \cdot 10^6$ ohm-cm, $1.5 \cdot 10^9$ ohm-cm, $1.7 \cdot 10^8$ ohm-cm

and 1.3×10^7 ohm-cm, respectively. Although the expectation was finding approximately the same resistivity value for all powders, they were found significantly different from each other. The electrical resistivity of Al-doped powder could not be determined since the Ohm's law could not be applied to its I-V curve with diode characteristic.

The absorption spectra of ZnO powder gave absorption in UV-A and UV-B region of light. The luminescence properties of powders were generally in blue and green regions of visible light.

A rheometer was used to obtain well dispersed polymer composite materials. Nonuniformly distributed composites were observed. Especially for highly loaded composites serious adhesion and wetting problems existed between polymer and filler. The highest particle sized filler (eZnO) 20 vol% resulted in overload therefore, nZnO, synZnO and AlZnO loaded composites were prepared only for 15 vol%. Microvoids detected in the composites due to adhesion and wetting problems existed between organic and inorganic materials.

Degree of crystallinity is an important parameter by means of conductivity. The crystallinity of the polymer in composites increases from 0.30 to 0.55 by the addition of ZnO. Higher crystallinity could increase the conductivity of the composite, as well.

Thermal characterization of the composites was done to understand the changes in melting, degradation temperatures and heats by the addition of ZnO. The melting point did not change for composites but heat of melting and degradation decreased. eZnO loading caused an increase while sZnO loading a decrease in the starting temperature of degradation however these variations in the degradation temperature did not significantly influence the processing.

The electrical conductivity of the composites were measured by using Keithley 6517-A fixed with a test fixture of 8009 apparatus for the measurement, to prevent errors coming from the contact points. The volumetric resistivity was found as 10^{17} ohm-cm for PP and drops to 10^9 ohm-cm after the addition of 20 vol% eZnO filler. For PE matrix the resistivity value was 10^{16} ohm-cm and drops to 10^{10} ohm-cm after addition of 20 vol% eZnO filler. Generally the highest loadings had also the highest conductivity in the composite. PEG 4000 modified ZnO-PE composites had the lowest resistivity about 10^8 ohm-cm. ZnO particles and PEG molecules make hydrogen bonding and long chain like arrangements in the polymer matrix which create a conductive path and decrease the electrical resistivity of the composite. Although the air gaps were present in the structure of composites for 20 vol% loaded sZnO and eZnO

composites which can find an application area due to their electrostatic dissipation (ESD) property. PEG 4000 modified 15 vol% loaded composites could be used on ESD and on moderate conductive applications. AMPTES modified ZnO powders did not enhance the electrical properties of composite. Good dispersion was obtained with organic and inorganic tails of modifier which provided stable bonds between polymer and filler. The interparticle distance between powder particles was not sufficient for electrical conduction by hopping or tunneling so the properties did not change. However, Al⁺³ doped ZnO powder did not significantly change the electrical resistivity of composite; the main reason might be the porosity.

It was expected to decrease the electrical resistivity of composites by using five different powders having different particle sizes. The resistivity should be lower, the smaller are the particles.

No direct relation between particle size and composites resistivity was obtained. Mc Lachlan model was used to predict the electrical resistivity theoretically and this model predicts well with the resistivity data of the composites. On the other hand McLachlan model fits to eZnO composite better than the others because eZnO has high aspect ratio. Thermal conductivity measurements were carried out with hot wire method, which is the quickest one and gives error in the range of 5%. Thermal conductivity of the composites increased by increasing the ZnO content and after addition of 15 or 20 vol% of ZnO the conductivity increases to 1.56, 1.28, 0.98, 0.76 and 0.74 W/mK for eZnO, sZnO, nZnO, synZnO and AlZnO loaded composites, respectively. The relation of the particle size and the thermal conductivity was expected as, the smaller particle size due to increase in the surface area should increase the probability of the phonon scattering and increase in the thermal conductivity. However the presence of the big agglomerates in the composite the nano affect was not observed and also the aspect ratio of the particles was another parameter of disorder of particle size in the relation of thermal conductivity. Irrespectively, the highly loaded composites can be used in heat sinks applications.

Four different models were applied to the composites to predict the correct thermal conductivity. Generally modified Nielsen model predicts well with the experimental data but porous structure of the composites avoids the model prediction well. The continuum level of the phenomenological formulations that thermal conductivity follows typically should not include only particle shape and volume fraction of variables and should also assume heat transport in both phases, the interface

and particle mobility should also taken into account. Under these approaches better predictions will be done.

One other aim of composite preparation was to give the optical properties of ZnO to composite, since ZnO is a luminescent material that can emit light in different regions of electromagnetic spectrum when electrically excited or excited by UV light. As a conclusion, all the composites showed the same luminescence behavior of their ZnO. They emit light in blue and green regions of visible spectrum when excited under UV light. The porous structure seems not to affect the luminescence of the polymer composites but homogeneity problem obtained huge changes in the intensity of the spectrum.

It is known that the interface adhesion influences the mechanical behavior of particulate filled polymer composite. Microfillers (eZnO) commonly increase the stiffness on the one hand, but on the other hand, they may have a detrimental effect on the strain at break. However composites prepared in this study had sufficient mechanical strength for engineering applications. The size of the particles determines the shape of voids that were formed at the debonding of particles from the matrix. That is, a structural weakness that would have been expected from the agglomerating behavior of the nanoparticles could be fully eliminated by the modifying of chains onto the individual particle and polymer. It can be concluded that, the size affect for Youngs modulus was seen. Having nanosized particle composite is stiffer than micron sized particles and both of the composites can be used as an engineering material since they can load safely, 4.0 MPa and 2.5 MPa for eZnO-PE and nZnO-PE respectively.

If compared to the modified and unmodified case, it can be stated that, the mechanical loading seems to be more effectively transferred from the matrix to the filler particles owing to the interfacial bonding effect of the polymers and increase elongation. The decrease in tensile strength can be explained by a change in the disperse state of the fillers and increase in the porosity.

As a consequence, the composites can be used in ESD and moderately electrical conductivity applications in the field of electrical conductivity, as a heat sink in the field of thermal conductivity and as a solid state lamp because of the luminescence properties as well. Stiffness of the composites was very high when compared with neat polymer. However, recent studies on a polymer composite should be focused on the homogenous dispersion and void free particulate composites. Preparation of void free composites by dispersing powder in a liquid organic media using good dispersants for air release is

recommended to understand the particle-polymer relation and finding better electrical, thermal and optical properties.

REFERENCES

- Abdullah, M.; Shibamoto, S.; Okuyama, K., Synthesis Of ZnO/SiO₂ Nanocomposites Emitting Specific Luminescence Colors. *Optical Materials*, **2004**, 26, 95–100.
- Agari, Y.; Uno T. Thermal Conductivity of Polymer Filled with Carbon Materials: Effect of Conductive Particle Chains on Thermal Conductivity. *Journal of Applied Polymer Science* **1985**, 30, 2225-2235.
- Althues, H.; Henle, J.; Kaskel, S., Functional Inorganic Nanofillers for Transparent Polymers. *Chem. Soc. Rev.*, **2007**, 36, 1454–1465.
- Ammala, A.; Hill, A.J.; Meakin, P.; Pas S.J.; Turney, T.W. Degradation Studies of Polyolefins Incorporating Transparent Nanoparticulate Zinc Oxide UV Stabilizers, *Journal of Nanoparticle Research*, **2002**, 4,167–174.
- Andrés-Vergés, M.; Martínez-Gallego, M.; Lozano-Vila1, A.; Díaz-Álvarez J. Microscopy Techniques Applied to the Study of Zinc Oxide Microcrystalline Powders Synthesis. *Current Issues on Multidisciplinary Microscopy Research and Education*, **2005**, 283-288.
- Avella, M.; Cosco, S.; Volpe, G. D.; Errico, M. E. Crystallization Behavior and Properties of Exfoliated Isotactic Polypropylene/Organoclay Nanocomposites. *Advances in Polymer Technology*, **2005**, 24, 2, 132–144.
- Bangal, M.; Ashtapure, S.; Marathe, S.; Ethiraj, A.; Hebalkar, N., Gosavi, S.W.; Urban, J.; Kulkarni, S. K. Semiconductor Nanoparticles. *Hyperfine Interactions*, **2005**, 160, 81–94.
- Behera, D.; Acharya, B.S. Nano-Star Formation in Al-Doped ZnO Thin Film Deposited by Dip-Dry Method And Its Characterization Using Atomic Force Microscopy, Electron Probe Microscopy, Photoluminescence and Laser Raman Spectroscopy. *Journal of Luminescence*, **2008**, 128, 1577–1586.
- Beyler, C. L., Hirschler, *SFPE Handbook of Fire Protection Engineering*, M.M., *Thermal Decomposition of Polymer*, Section One, Chapter 7 , 120-140.
- Bhargava S.; Temperature And Gas Sensing Characteristics of Graphite/Polymer (PEO) Based Composite Structures, University of Cincinnati MSc Thesis; March 2006.
- Bhat, S.V. Vivekchand, ; S.R.C.; Govindaraj A.; Rao C.N.R. Photoluminescence and Photoconducting Properties of ZnO Nanoparticles, *Solid State Communications*, **2009**,149 510-514.

- Bigg, D. M.; Conductive Polymeric Compositions. *Polymer Engineering and Science*, **1977**, 17 (12), 842-847.
- Boiteux, G.; Fournieri, J.; Issotier, D.; Seytre, G.; Marichy, G. Conductive Thermoset Composites: PTC Effect. *Synthetic Metals*, **1999**, 102, 1234-1235.
- Bueno, P. R.; Varela, J. A.; Longo, E., SnO₂, ZnO and Related Polycrystalline Compound Semiconductors: An Overview and Review on the Voltage-Dependent Resistance (Non-Ohmic) Feature. *Journal of the European Ceramic Society*, **2008**, 28, 505–529.
- Cai, W-Z.; Tu, S-T.; Gong, J-M. A Physically Based Percolation Model of the Effective Electrical Conductivity of Particle Filled Composites, *Journal of Composite Materials*, **2006**, 40 (23), 2131-2142.
- Celzard, A.; McRaet, E.; Mareche, J. F.; Furdin, G.; Duforts, M.; Deleuzes, C. Composites Based on Micron-Sized Exfoliated Graphite Particles: Electrical Conduction, Critical Exponents And Anisotropy. *J. Phy. Chem. Solids*, **1996**, 57 (6-8), 715-718.
- Celzard, A.; McRae, E. Critical Concentration in Percolating Systems Containing a High-Aspect-Ratio Filler. *Physical Review B*, **1996-II**, 53 (10), 6209-6214.
- Celzard, A; McRae, E; Furdin, G; Marêch'e, J F. Conduction Mechanisms in Some Graphite–Polymer Composites: The Effect of a Direct-Current Electric Field. *J. Phys.: Condens. Matter*, **1997**, 9, 2225–2237.
- Ceylan Ö.; Electrochemically-Aided Control Of Solid Phase Micro-Extraction (Easpm) Using Conducting Polymer Coated Fiber. PhD thesis, Department of Chemistry of the College of Arts and Sciences, University of Cincinnati. May 2003.
- Chipara, M.; Lozano, K.; Hernandez, A.; Chipara, M. TGA Analysis of Polypropyleneecarbon Nanofibers Composites. *Polymer Degradation and Stability*, **2008**, 93, 871-876.
- Chow, W. S.; Tham. W. L. Thermal and Antistatic Properties of Polypropylene/Organo Montmorillonite Nanocomposites. *Polymer-Plastics Technology and Engineering*, **2009**, 48, 342–350.
- Clingerman M. L. Development and Modeling of Electrically Conductive Composite Materials. PhD Thesis, Bachelor of Science, Michigan Technology University. May 2001.
- Çaglar, M.; Ilican, S.; Caglar, Y.; Yakuphanoglu, F. The Effects of Al Doping on the Optical Constants Of ZnO Thin Films Prepared by Spray Pyrolysis Method. *J. Mater Sci: Mater. Electron*, **2008**, 19,704–708.

- Danes, F.; Garnier, B.; Dupuis, T. Predicting, Measuring, and Tailoring the Transverse Thermal Conductivity of Composites from Polymer Matrix and Metal Filler. *International Journal of Thermophysics*, **2003**, 24(3), 771-774.
- Deng, H. M.; Ding, J.; Shi, Y.; Liu, X. Y.; Wang, J. Ultrafine Zinc Oxide Powders Prepared By Precipitation/Mechanical Milling. *Journal Of Materials Science*, **2001**, 36, 3273– 3276.
- Dijken, A. V.; Meulenkamp, E.A.; Vanmaekelbergh, D.; Meijerink, A. The Luminescence of Nanocrystalline ZnO Particles: the Mechanism of the Ultraviolet and Visible Emission. *Journal of Luminescence*, **2000**, 87-89, 454-456.
- Djurisic, A. B. ; Choy, W. C. H. ; Roy, V. A. L. ; Leung, Y. H. ; Kwong, C.Y.; Cheah, K. W.; Rao, T. K. G., Chani W. K.; Lui H. F.; Surya C. Photoluminescence and Electron Paramagnetic Resonance Of ZnO Tetrapot Structures. *Advanced Functional Materials*, **2004**, 14 (9), 856-864.
- Dow Corning Silicones-Dow Corning Home page.
<http://www.dowcorning.com/default.aspx?bhcp=1> (accessed May 14, 2009)
- Fangli, Y.; Peng, H.; Chunlei, Y.; Shulan, H.; Jinlin, L., Preparation and Properties of Zinc Oxide Nanoparticles Coated With Zinc Aluminatej. *Mater. Chem.*, **2003**, 13, 634–637.
- Fernando, S. S.; Christensen, P. A.; Egerton, T. A.; White, J. R. Humidity Dependence of Carbon Dioxide Generation During Photodegradation of Biaxially Oriented Polypropylene in Oxygen. *Polymer Degradation and Stability*, **2009**, 94, 83–89.
- Flandin, L.; Hiltner, A.; Baer, E. Interrelationships Between Electrical and Mechanical Properties of a Carbon Black-Filled Ethylene–Octene Elastomer. *Polymer*. **2001**, 42, 827–838.
- Fleming, R.J.; Ammala, A., Casey, P.S. and Lang, S.B., Conductivity and Space Charge in LDPE Containing Nano- and Micro-sized ZnO Particles. *IEEE Transaction on Dielectrics and Electrical Insulation*, **2008**,15,1-12.
- Fontana, L.; Vinh, D. Q.; Santoro, M.; Scandolo, S.; Gorelli, F. A.; Bini, R.; Hanfland, M. High-Pressure Crystalline Polyethylene Studied by X-Ray Diffraction and ab Initio Simulations. *Physical ReviewB*, **2007**, 75, 1-11.
- Friedrich, K.; Fakirov, S.; Zhang, Z. *Polymer Composites From Nano- to Macro-Scale*; Springer:NewYork, 2005, pp 45-60 and 170-175.

- Ge J. Interfacial Adhesion in Metal/Polymer Systems For Electronics. PhD Thesis, Department of Electrical and Communication Engineering, Helsinki University of Technology. December 2003.
- Gfroerer, T. H. *Photoluminescence in Analysis of Surfaces and Interfaces*. Encyclopedia of Analytical Chemistry R.A. Meyers (Ed.), 2000, John Wiley & Sons Ltd, Chichester pp. 9209–9231.
- Gojny, F. H.; Wichmann, M.H.G.; Fiedler, B.; Kinloch, I. A.; Bauhofer, W.; Windle, A. H.; Schulte, K. Evaluation and Identification of Electrical and Thermal Conduction Mechanisms in Carbon Nanotube/Epoxy Composites. *Polymer*, **2006**, 47, 2036–2045.
- Grob, M. C.; Minder E. Permanent Antistatic Additives: New Developments. *Plastics Additives & Compounding*, **1999**, 20- 26.
- Gubin, S.P. Metalcontaining Nano-Particles within Polymeric Matrices: Preparation, Structure, and Properties. Colloids and Surfaces. A *Physicochemical and Engineering Aspects*, **2002**, Vol 202, 155–163.
- Guo, L.; Yang, S. Highly Monodisperse Polymer-Capped ZnO Nanoparticles: Preparation and Optical Properties. *Applied Physics Letters*, **2000**, 76 (20), 2901-2903.
- Hammer, M. S.; Rauh, D., Lormann, V.; Deibel, C.; Dyakonov, V. Effect of Doping- and Field-induced Charge Carrier Density on the Electron Transport in Nanocrystalline ZnO. *Nanotechnology*, **2008**, 19. 485701, 1-7.
- Han, W.; Li, Z.; Qin W. Z.; Quan Y. H. Preparation and Mechanical Properties of Polypropylene/ Maleic Anhydride Compatibilized Polypropylene/ Organo-Vermiculite Nanocomposites. *Polymer-Plastics Technology and Engineering*, **2009**, 48, 374–378.
- Hong, J. I.; Schadler;L. S.; Siegel, R. W.; Martensson, E., Rescaled Electrical Properties of ZnO/Low Density Polyethylene Nanocomposites. *Applied Physics Letters*, **2003**, 82, 12, 1956-1958.
- Hong, J.I.; Winberg, P.; Schadler, L.S.; Siegel, R.W.; Dielectric Properties of Zinc Oxide/Low Density Polyethylene Nanocomposites. *Materials Letters*, **2005**, 59, 473–476.
- Hong, R.Y.; Qian J.Z., Cao J.X. Synthesis and Characterization of PMMA Grafted ZnO Nanoparticles. *Powder Technology*, **2006a**, 163, 160–168.

- Hong, J. I., Schadler, A L. S., Siegel, A R. W. A, Ma^ortensson E., Electrical Behavior of Low Density Polyethylene Containing an Inhomogeneous Distribution Of ZnO Nanoparticles. *J Mater Sci*, **2006b**, 41, 5810–5814.
- Hong, R.Y.; Li, J.H.; Chen, L.L.; Liu, D.Q.; Li, H.Z.; Zheng, Y.; Ding, J. Synthesis, Surface Modification And Photocatalytic Property Of ZnO Nanoparticles. *Powder Technology*, **2009**, 189, 426–432.
- Incropera, F.P., De Witt D. P., *Fundamentals Of Heat And Mass Transfer*, John Wiley and Sons, 3rd Edition, 1990, pp 44-53.
- ITO T(Waseda Univ., Tokyo) FUSE N(Waseda Univ., Tokyo) OHKI Y(Waseda Univ., Tokyo), Effects of Additives, Photodegradation, and Water-tree Degradation on the Photoluminescence in Polyethylene and Polypropylene. *Transactions of the Institute of Electrical Engineers of Japan. A*, **2004**, 124 (7), 624-630.
- Ito, T.; Toyoda, T.; &ai, N.; Ohki, Y. Proceeding of the *IEEE 7th International Conference on Solid Dielectrics*, June 25-29,2001, Eindhoven, the Netherlands.
- Junior, J.A.J. Ultrasonic Decrosslinking of Crosslinked Poly(ethylene). Master Thesis, University of Akron, May 2007.
- Karain, H. *Handbook of Polpropylene and Polypropylene Composites*, Marcel Dekker, Inc: USA, 1999, pp1-39.
- Klingshirn, C. ZnO: From Basics Towards Applications. *Phys. Stat. Sol.*, **2007**, 244 (9), 3027–3073.
- Krueger, Q. J. Electromagnetic Interference and Radio Frequency Interference Shielding of Carbon-Filled Conductive Resins. Master Thesis, Michigan Technological University, May 2002.
- Kumlutaş, D.; Tavman, I. H., A Numerical and Experimental Study on Thermal Conductivity of Particle Filled Polymer Composites. *Journal of Thermoplastic Composite Materials*, **2006**, 19, 441-455.
- Keithley, Model 6517A Electrometer/High Resistance Meter Getting Started Manual, Keithley Instrument:Ohio, Rev B, 2003.
- Kyoto Electronics, Quick Thermal Conductivity Meter Instruction Manual, http://www.kyoto-kem.com/en/products/heat/qtm_500.html, (accessed July 15, 2009).

- Lahiri, J.; Batzill, M. Surface Functionalization of ZnO Photocatalysts with Monolayer ZnS. *J. Phys. Chem. C* **2008**, *112*, 4304-4307.
- Lakowicz J.R.;, *Principles of Fluorescence Spectroscopy* Third Edition, NewYork, 2006, Springer Science, pp3-25.
- Lee, G.-W.; Park, M.; Kim, J.; Lee, J. I.; Yoon, H. G. Enhanced Thermal Conductivity of Polymer Composites Filled With Hybrid Filler. *Composites: Part A*, **2006**, *37*, 727–734.
- Leguenza, E. L.; Scarpa, P. C. N.; Das-Gupta, D. K. Dielectric Behavior of Aged Polyethylene Under UV Radiation. *IEEE Transactions on Dielectrics and Electrical Insulation*, **2002**, *9* (4), 507-513.
- Li, C.; Liang, T.; Lu, W.; Tang, C.; Hu, X., Improving the Antistatic Ability of Polypropylene Fibers by Inner Antistatic Agent Filled With Carbon Nanotubes. *Composites Science and Technology*. **2004**, *64*, 2089–2096.
- Liang, J.; Yang, Q. Aggregate Structure and Percolation Behavior in Polymer/Carbon Black Conductive Composites. *Journal of Applied Physics*, **2007**, *102*, 083508.
- Lima, S.A.M.; Cremona, M.; Davolos, M.R.; Legnani, C.; Quirino, W.G. Electroluminescence of Zinc Oxide Thin-Films Prepared via Polymeric Precursor and via Sol–Gel Methods, *Thin Solid Films*, **2007**, *516*, 165–169.
- Lin, K.; Tsai, P. Parametric Study on Preparation and Characterization of ZnO:Al Films by Sol–Gel Method for Solar Cells. *Materials Science and Engineering B*, **2007**, *139*, 81–87.
- Lin, H-F.; Liao, S-C.; Hua, C-T A New Approach to Synthesize ZnO Tetrapod-Like Nanoparticles with DC Thermal Plasma Technique, *Journal of Crystal Growth*, **2009**, *311* 1378–1384.
- Liufu, S.; Xiao, H.; Li, Y., Investigation of PEG Adsorption on the Surface of Zinc Oxide Nanoparticles. *Powder Technology*. **2004**, *145*, 20– 24.
- Lo, C. T.; Chou, K.-S.; Chin, W.-K., Effects Of Mixing Procedures on the Volume Fraction of Silver Particles in Conductive Adhesives. *J. Adhesion Sci. Technol.*, **2001**, *15*, (7), 783–792.
- Loh, K. P.; Chua, S. J. *Zinc Oxide Nanorod Arrays: Properties and Hydrothermal Synthesis*, Springer: Berlin, 2007,109, pp 92-117.

- Look, D.C.; Coşkun, C.; Claflin, B.; Farlow, G.C., Electrical and Optical Properties of Defects And Impurities in ZnO. *Physica B*, **2003a**, 340–342, 32–38
- Look, D. C.; Jones, R. L.; Szelove, J. R.; Garces, N. Y.; Giles, N. C.; Halliburton, L. E. The Path to ZnO Devices: Donor And Acceptor Dynamics. *Phys. Stat. Sol.*, **2003b**, 195 (1), 171– 177.
- Looka, D.C.; Skunc, C.C.; Claflin, B.; Farlow G.C. Electrical and Optical Properties of Defects and Impurities in ZnO. *Physica B*, **2003**, 340–342, 32–38.
- Lux, F. Models Proposed to Explain the Electrical Conductivity of Mixtures Made of Conductive and Insulating Materials (Review). *Journal of Materials Science*, **1993**, 28, 285-301.
- Lü, N.; Lü, X.; Jin, X.; Lü, C. Preparation and Characterization Of UV-Curable ZnO/Polymer Nanocomposite Films. *Polym Int.*, **2007**, 56, 138–143.
- Maki, N.; Nakano, S.; Sasaki, H., Development of a Packaging Material Using Non-Bleed-Type Antistatic Ionomer . *Packaging Technology and Science*. **2004**, 17, 249–256.
- Mallick, P.K. *Fiber Reinforced Composites Materials, Manufacturing, and Design*; 3rd Edition, Taylor and Francis Group:Boca Raton, **2007**, pp 33-88.
- Mamunya, Y. P.; Muzychenko, W. V.; Pissis, P.; Lebedev, E. V.; Shut, M.I. Percolation Phenomena in Polymers Containing Dispersed Iron. *Polymer Engineering and Science*, **2002a**, 42 (7), 90-100.
- Mamunya, Y.P.; Davydenko, V.V.; Pissis, P.; Lebedev, E.V., Electrical and Thermal Conductivity of Polymers Filled With Metal Powders. *European Polymer Journal*. **2002b**, 38, 1887–1897
- Manouni, A. El; Manjón, F.J.; Mollar, M.; Marí, B.; Gómez, R.; López, M.C.; Ramos, J.R. Effect Of Aluminium Doping on Zinc Oxide Thin Films Grown by Spray Pyrolysis. *Superlattices and Microstructures*, **2006**, 39, 185–192.
- McGee, S.; McCullough, R. L., Combining Rules for Predicting the Thermoelastic Properties of Particulate Filled Polymers, Polyblends, and Foams. *Polymer Composites*, **1981**, 2, (4), 149-161.
- McLachlan, D.S. An Equation For The Conductivity Of Binary Mixtures with Anisotropic Grain Structures . *J. Phys. C: Solid State Phys*, **1987**, 20, 865-877.

- McLachlan, D.S., Blaszkiewicz, M.; Newnham, R. E., Electrical Resistivity of Composites, *Journal of American Ceramic Society*, **1990**, 73 (8), 2187-2203.
- Metin D. Interfacial Enhancement of Polypropylene Zeolite Composites. MSc Thesis, Department of chemical engineering, İzmir Institute of Technology. July 2001
- Metin, D.; Thmınlıođlu, F.; Balköse, D.; Ülkü, S. The Effect of Interfacial Interactions on the Mechanical Properties of Polypropylene Natural Zeolite Composites. *Composites: Part A*, **2004**, 35, 23-32.
- Meulenkamp, E. Synthesis and Growth of ZnO Nanoparticles. *J. Phys. Chem. B.*, **1998**, 102, 5566-5572.
- Meyer, B.K., Identification of Bound Exciton Complexes in ZnO. *Phys. Stat. Sol.*, **2004**, 241, (3), 607-611.
- Miller, P. H. The Electrical Conductivity of Zinc Oxide. *Physical Review*, **1941**, 60, 890-895.
- Monk, P. *Physical Chemistry Understanding our Chemical World*, John Wiley & Sons:West Sussex, 2004, pp 423-447.
- Mornet, S.; Duguet, E. Surface Modification of Zinc Oxide Nanoparticles by Aminopropyltriethoxysilane. *Journal of Alloys and Compounds*, **2003**, 360, 298-311.
- Music,, S.; Dragcevic D.; Maljkovic, M.; Popovic, S., Influence of Chemical Synthesis on The Crystallization and Properties Of Zinc Oxide. *Materials Chemistry and Physics*, **2002**, 77, 521-530.
- Nickel, N. H.; Terukov, E. *Zinc Oxide-A Material for Micro- and Optoelectronic Applications*. Eds.; VHC: The Netherlands, 2004, pp 1-23.
- Nielsen, L.E. The Thermal and Electrical Conductivity of Two-Phase Systems, *Industrial Engineering Chemical Fundamentals*, **1974**, 13 (1), 17-20.
- Oharaa, S.; Mousavanda, T.; Umetsua, M.; Takamia, S.; Adschiria T.; Kurokib Y.; Takatab M. Hydrothermal Synthesis of Fine Zinc Oxide Particles Under Supercritical Conditions. *Solid State Ionics*, **2004**, 172, 261-264.
- Ohki, Y.; Toyoda, T.; Hama, Y.; Wei, W.; Massines F. Proceedings of *The 6th International Conference on Properties and Applications of Dielectric Materials* June 21-26,2000; Xi'an Jiaotong University, Xi'an.

- Orange, G.; Bomal, Y. *Toughening Effect in Highly Filled Polypropylene Through Multi-Scale Particle Size. Fracture of Polymers, Composites and Adhesives*, Blackman, B.R.K.; Pavan, A.; Williams, J.G. Eds, Elsevier Ltd. and ESIS:NY, 2003, pp 39-50.
- Özgür, Ü.; Alivov, Y. I.; Liu, C.; Teke, A.; Reshchikov, M. A.; Doğan, S.; Avrutin, V.; Cho, S.J.; Morkoç, H. A Comprehensive Review of ZnO Materials and Devices *Journal Of Applied Physics*, **2005**, 98, 041301, 1-103.
- Pal, R. On the Electrical Conductivity of Particulate Composites. *Journal of Composite Materials*, **2007**, 41 (20), 2499-2511.
- Peacock A.J. *Handbook of Polyethylene Structures, Properties and Applications*, Marcel Dekker, Inc.:USA, 2000; pp1-6.
- Pearton, S.J.; Norton, D.P.; Ip, K.; Heo, Y.W.; Steiner, T. Recent Progress in Processing and Properties Of ZnO. *Progress in Materials Science*. **2005**, 50, 293–340.
- Pinto, G.; Jimenez-Martin, A. Conducting Polymer Composites of Zinc-Filled Urea-Formaldehyde. *Polymer Composites*, **2001**, 22 (1), 65-71.
- Psarras, G.C.; Manolakak, E.; Tsangaris, G.M. Dielectric Dispersion and AC Conductivity in-Iron Particles Loaded-Polymer Composites, *Composites: Part A*. **2003**, 34, 1187–1198.
- Rozenberg, B.A.; Tenne, R. Polymer-Assisted Fabrication of Nanoparticles and Nanocomposites, *Progress in Polymer Science*, **2008**, 33, 40–112.
- Secu, C.E.; Sima, M., Photoluminescence and Thermoluminescence of ZnO Nano-Needle Arrays and Films. *Optical Materials*, **2009**, 31, 876–880.
- Serier, H.; Gaudon, M; Me'ne' trier, M. Al-Doped ZnO Powdered Materials: Al Solubility Limit and IR Absorption Properties. *Solid State Sciences*, **2009**, 11 (7), 1192-1197.
- Sethi, R. S.; Goosey, M. T. *Special Polymers for Electronics & Optoelectronics*; Chilton, J. A.; Goosey, M. T., Eds.; Chapman & Hall: London, 1995; pp 14-46.
- Sharma, S.K.; Nayak, S.K. Surface Modified Clay/Polypropylene (PP) Nanocomposites: Effect on Physico-Mechanical, Thermal and Morphological Properties. *Polymer Degradation and Stability*, **2009**, 94, 132–138.

- Singh, A.K.; Viswanath, V.; Janu, V.C. Synthesis, Effect Of Capping Agents, Structural, Optical And Photoluminescence Properties Of ZnO Nanoparticles, *Journal of Luminescence* **2009**, 129 (8), 874-878.
- Sofian N. M.; Rusu M.; Neagu R.; Neagu E., Metal Powder-Filled Polyethylene Composites. V. Thermal Properties. *Journal of Thermoplastic Composite Materials*, **2001** (14), 20-33.
- Soutar, I. The Application of Luminescence Techniques in Polymer Science, *Polymer International* **1991**, 26, 35-49.
- Srivastova, G. P. *High Thermal Conductivity Materials*, Shinde S. L. And Goela, J. S. Eds, Springer Science NewYork, 2006, pp 1-33.
- Strümpfer, R.; Glatz-Reichenbach J. Feature Article Conducting Polymer Composites. *Journal of Electroceramics*. **1999**, 3:4, 329-346.
- Sun, D.; Sue, H.-J.; Miyatake, N., Optical Properties of ZnO Quantum Dots in Epoxy with Controlled Dispersion. *J. Phys. Chem. C*. **2008**, 112, 16002–16010.
- Sue, K., Kimura, K., Murata, K., Arai, K., Effect Of Cations and Anions On Properties of Zinc Oxide Particles Synthesized in Supercritical Water. *J. of Supercritical Fluids*, **2004**, 30, 325–331.
- Sun, X.M; Chen, X.; Deng, Z.X.; Li, Y.D.; A CTAB-Assisted Hydrothermal Orientation Growth of ZnO Nanorods. *Materials Chemistry and Physics*, **2002**, 78, 99–104.
- Tai, W.-P.; Oh, J.-H., Fabrication and Humidity Sensing Properties of Nanostructured TiO₂-SnO₂ Thin Films. *Sensors and Actuators B: Chemical*, **2002**, 85, 1-2, 154-157.
- Tang, E.; Tian, B.; Zheng, E.; Fu, C.; Cheng, G., Preparation of Zinc Oxide Nanoparticle via Uniform Precipitation Method and Its Surface Modification by Methacryloxypropyltrimethoxysilane. *Chem. Eng. Comm.*, **2008**, 195, 479–491.
- Taşdemir, M.; Biltekin, H.; Caneba, G. T., Preparation and Characterization of LDPE and PP—Wood Fiber Composites. *Journal of Applied Polymer Science*, **2009**, 112, 3095–3102.
- Taya M., *Electronic Composites Modeling, Characterization, Processing and Mem Applications*, Cambridge University Press: Cambridge, 2005, pp 1-11.

- Tavman, I. H., Thermal and Mechanical Properties of Aluminum Powder-Filled High-Density Polyethylene Composites. *Journal of Applied Polymer Science*, **1996**, 62, 2161-2167.
- Tchoudakov, W.J.R.; Breier, O.; Narkis, M.; Siegmann, A., Conductive Polymer Blends With Low Carbon Loading: Polypropylene/Polyamide. *Polymer Engineering and Science*, 1996, 36, 1336-1346.
- Tjong, S.C. ; Liang, G.D.; Electrical Properties Of Low-Density Polyethylene/ZnO Nanocomposites. *Materials Chemistry and Physics*, **2006**, 100, 1–5.
- Toker, D.; Azulay, D.; Shimoni, N.; Balberg, I.; Millo, O. Tunneling and Percolation in Metal-Insulator Composite Materials. *Physical Review B*. **2003**, 68, 041403-1-4.
- Triboulet, R.; Sanjosé, V. M.; Zaera, R. T.; Tomas, M.C.M.; Hassani, S., *Zinc Oxide – A Material for Micro- and Optoelectronic Applications; Chapter 1: The Scope of Zinc Oxide Bulk Growth*, Nickel N.H; Terukov E.,Eds.; VCH: Springer: Netherlands, 2005, pp 3–14.
- Tsuiji, K., Nano-Particle Electro-Conductive Zinc Oxide Paset Series. HakuSuitech Co. Ltd. **2003**, 1-7.
- Usui, H., Influence of Surfactant Micelles on Morphology and Photoluminescence of Zinc Oxide Nanorods Prepared by One-Step Chemical Synthesis in Aqueous Solution. *J. Phys. Chem. C.*, **2007**, 111, 9060-9065.
- Uthirakumar, P.; Hong, C-H; Suh, E-K; Lee, Y-S. Novel Fluorescent Polymer/Zinc Oxide Hybrid Particles: Synthesis and Application as a Luminescence Converter for White Light-Emitting Diodes, *Chem. Mater.*, **2006**, 18, 4990-4992.
- van der Werff, H., Tensile Behaviour of Polyethylene and Poly(p-xylyene) Fibers. PhD Thesis, Gröningen University, April 1991.
- van de Krol R. ; Tuller, H.L. Electroceramics—The Role of Interfaces, *Solid State Ionics* **2002**, 150, 167– 179.
- Viswanathamurthi, P.; Bhattarai, N.; Kim, H. Y.; Lee, D., The Photoluminescence Properties of Zinc Oxide Nanofibres Prepared by Electrospinning, *Nanotechnology*, **2004**, 15, 320–323.
- Vollath, D.; Szab’o D.V.; Schlabach, S. Oxide/Polymer Nanocomposites As New Luminescent Materials, *Journal of Nanoparticle Research* **2004**, 6, 181–191.

- Weber, M.; Kamal, M. R., Estimation of the Volume Resistivity of Electrically Conductive Composites. *Polymer Composites*, **1997**, 18 (6), 711-725.
- Wan, C.; Tan, H.; Jin, S.; Yang, H.; Tang, M.; He, J., Highly Conductive Al-doped Tetra-Needle Like ZnO Whiskers Prepared by a Solid State Method. *Materials Science and Engineering B*, **2008**, 150, 203–207.
- Wang, Z. L., Zinc Oxide Nanostructures: Growth, Properties And Applications. *Journal of Physics: Condensed Matter*, **2004**, 16, R829–R858.
- Weber, E. H., Development and Modeling of Thermally Conductive Polymer/Carbon Composites. PhD Thesis, Michigan Technological University, December 2001.
- Wei, Y.; Chang, P., Characteristics of Nano Zinc Oxide Synthesized Under Ultrasonic Condition. *Journal of Physics and Chemistry of Solids*, **2008**, 69, 688–692.
- Wöll, C., The Chemistry and Physics of Zinc Oxide Surfaces. *Progress in Surface Science*, **2007**, 82 (2-3), 55-120.
- Wu, J.; McLachlan, D.S. Percolation Exponents and Thresholds Obtained from The Nearly Ideal Continuum Percolation System Graphite-Boron Nitride, *Physical Review B*, **1997**, 56, 1236–1248.
- Xiao, Q.; Huang, S.; Zhang, J.; Xiao, C.; Tan, X., Sonochemical Synthesis of ZnO Nanosheet. *Journal of Alloys and Compounds*, **2008**, 459, L18–L22.
- Xie, J.; Li, P.; Li, Y.; Wang, Y.; Wie, Y., Solvent-induced Growth of ZnO Particles at Low Temperature. *Materials Letters*, **2008**, 62, 2814–2816.
- Xue, Q.Z., Model for Thermal Conductivity of Carbon Nanotube-Based Composites. *Physica B*. **2005**, 368, 302–307.
- Yu, J.; Yu, X., Hydrothermal Synthesis and Photocatalytic Activity of Zinc Oxide Hollow Spheres. *Environmental Science and Technology*, **2008**, 42, 4902–4907.
- Yuen, S.; Ma, C. M.; Chiang, C.; Teng, C. Morphology and Properties of Aminosilane Grafted MWCNT/Polyimide Nanocomposites. *Journal of Nanomaterials*, **2008**, 1, 1-15.
- Zhang, H.; Ge, X.; Ye, H, Effectiveness of the Heat Conduction Reinforcement of Particle Filled Composites. *Modelling Simul. Mater. Sci. Eng*, **2005**, 13, 401–412.

- Zhang, W.; Yanagisawa, K., Hydrothermal Synthesis of Zinc Hydroxide Chloride Sheets and Their Conversion to ZnO. *Chemical Materials*, **2007**, 19, 2329-2334.
- Zhao, H.; Li, R. K.Y., A study On The Photo-Degradation Of Zinc Oxide (ZnO) Filled Polypropylene Nanocomposites. *Polymer*, **2006**, 47, 3207–3217.
- Zhou, H.; Zhang, S.; Yang M., The Effect of Heat-transfer Passages on the Effective Thermal Conductivity of High Filler Loading Composite Materials. *Composites Science and Technology*, **2007**, 67, 1035–1040.
- Zhou, Z.; Chu, L.; Tang, W.; Gu, L., Studies On The Antistatic Mechanism Of Tetrapod-Shaped Zinc Oxide Whisker. *Journal of Electrostatics*, **2003**, 57, 347–354.
- Zhou, Z.; Deng, H.; Yi, J.; Liu, S., A New Method for Preparation of Zinc Oxide Whiskers. *Materials Research Bulletin*, **1999**, 34, (10-11), 1563–1567.

APPENDICES

APPENDIX A. FTIR SPECTRA of PEG 4000 and AMPTES MODIFIED ZnO

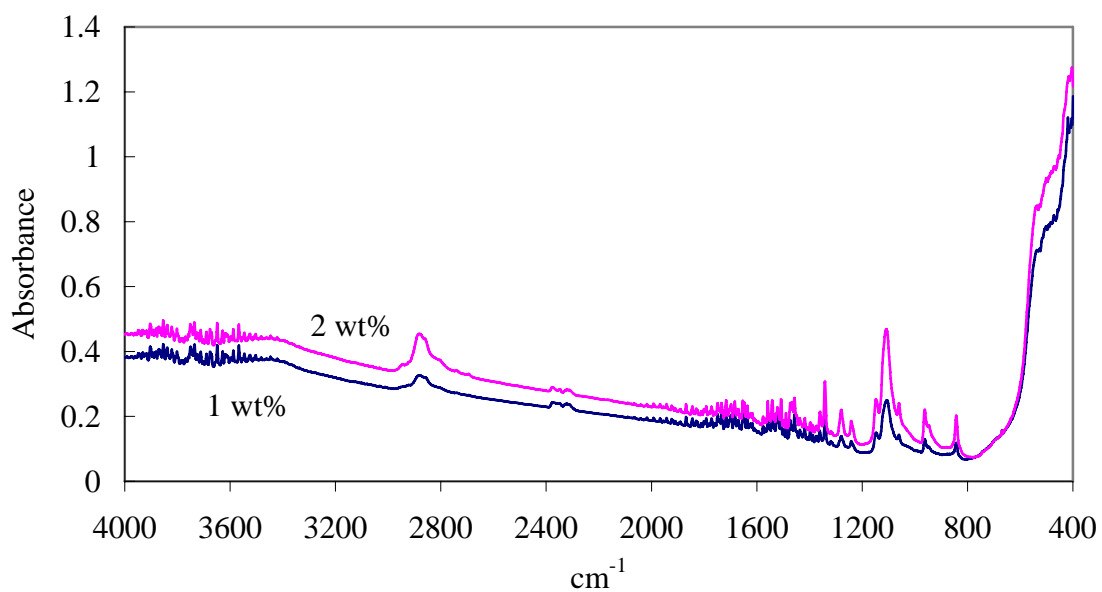


Figure 1. FTIR spectra of PEG 4000 modified eZnO.

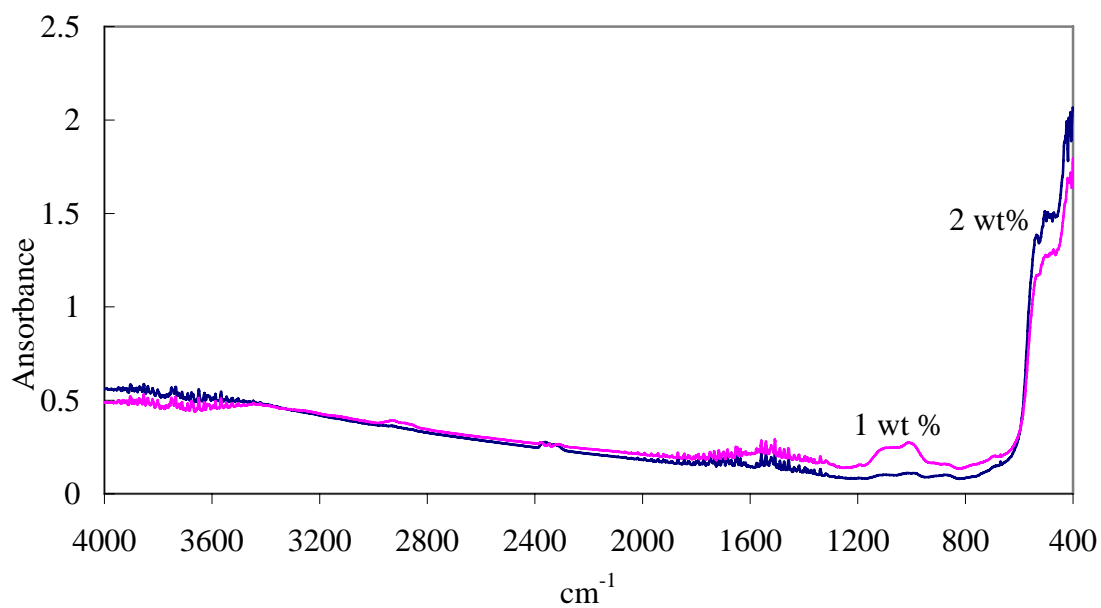


Figure 2. FTIR spectra of AMPTES modified eZnO.

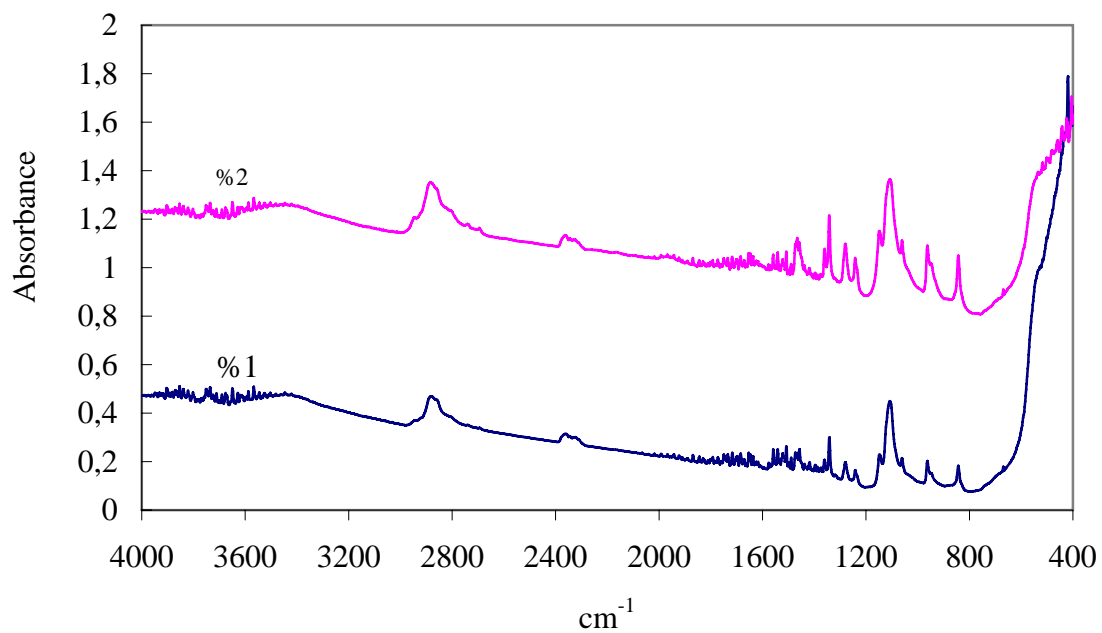


Figure 3. FTIR spectra of PEG 4000 modified sZnO.

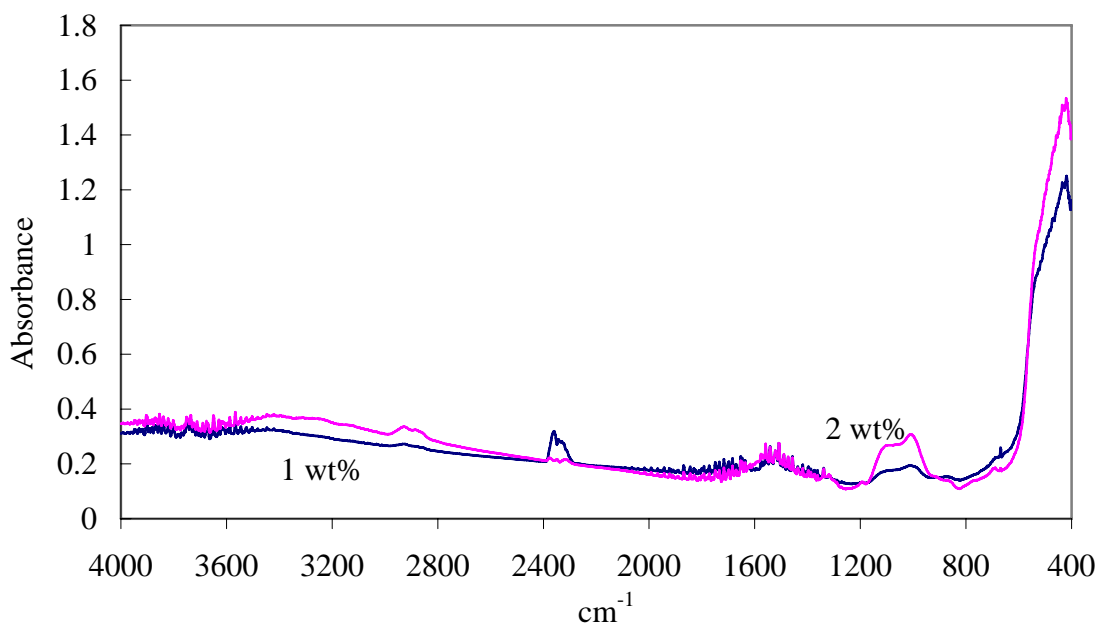


Figure 4. FTIR spectra of AMPTES modified sZnO.

APPENDIX B. I-V CURVES OF POWDERS

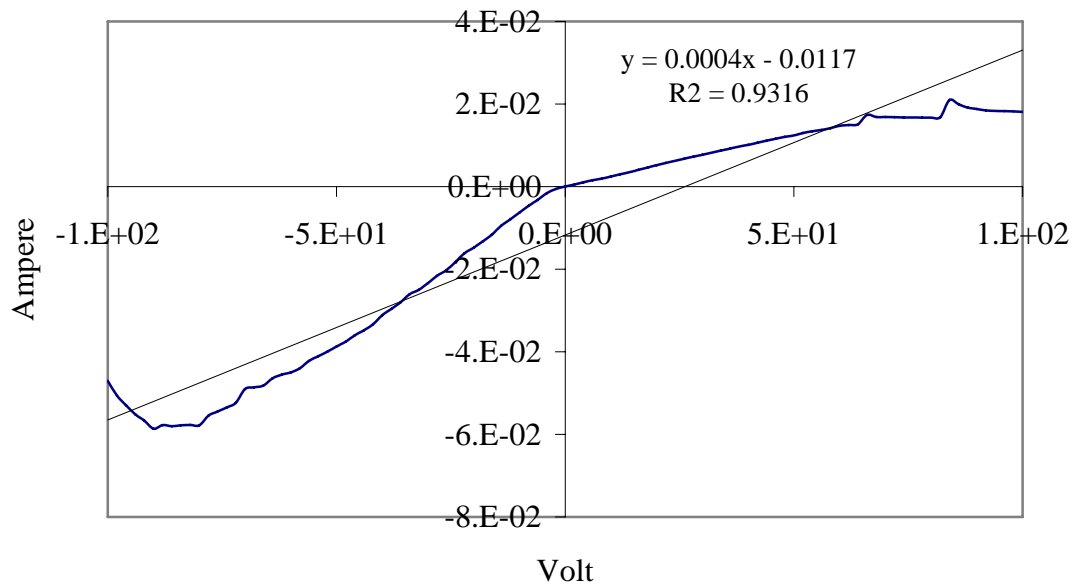


Figure 1. Sweeping voltage versus current values for eZnO.

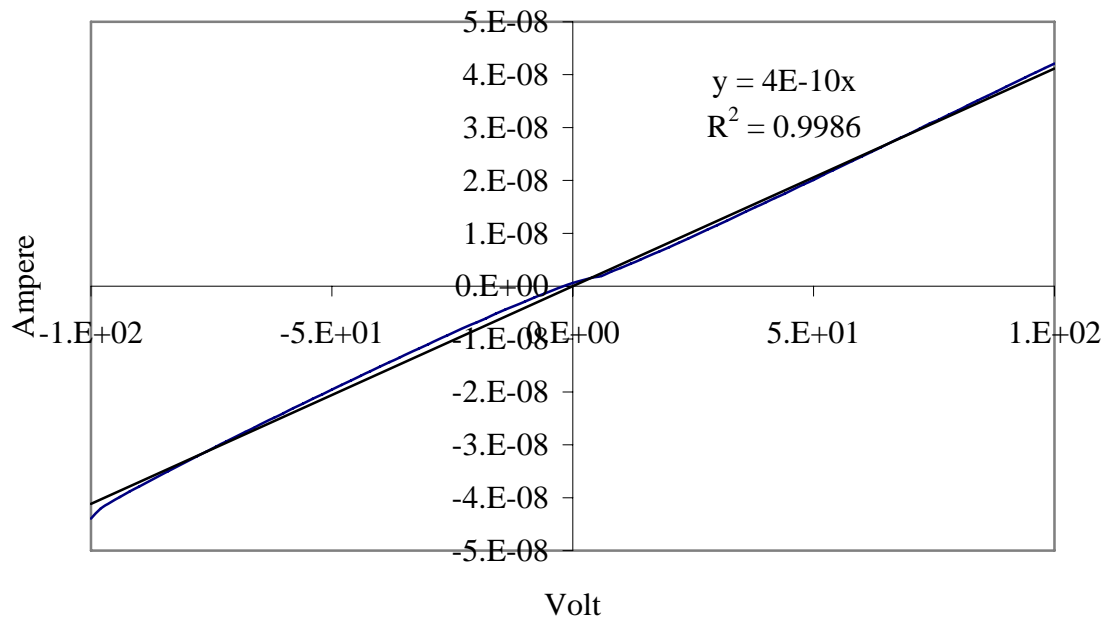


Figure 2. Sweeping voltage versus current values for sZnO.

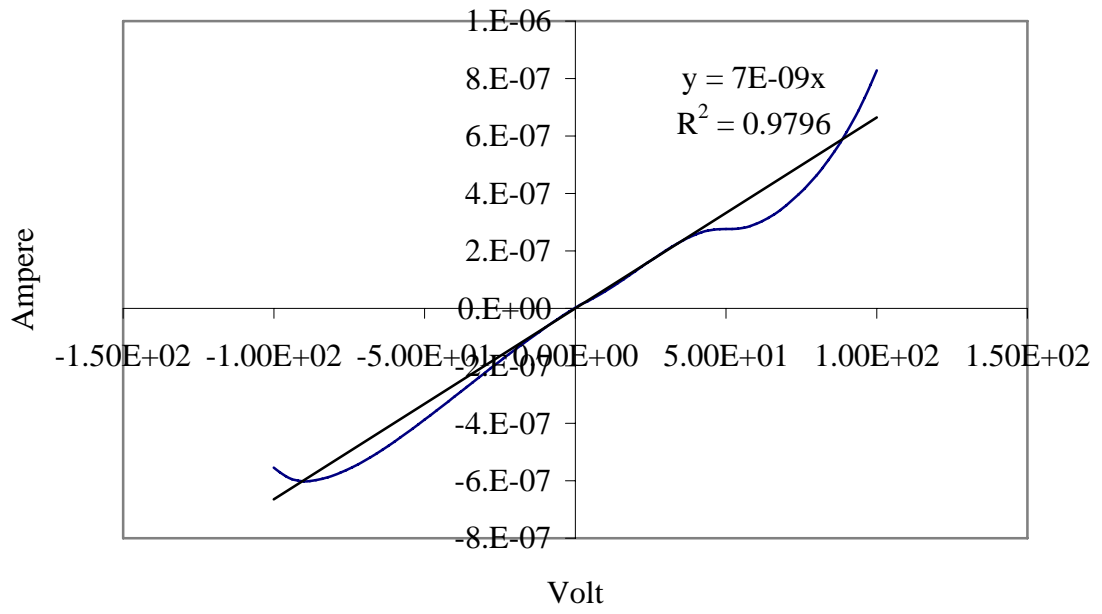
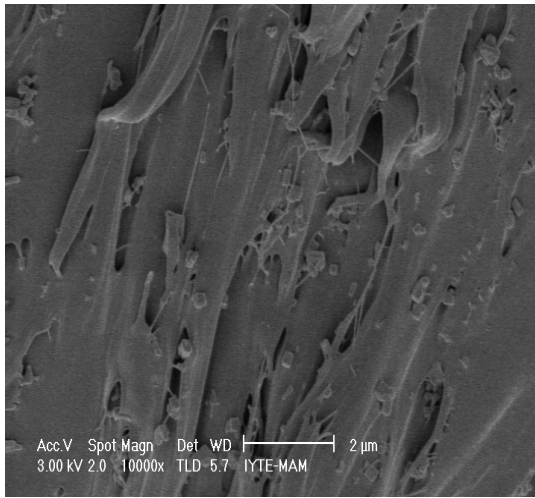
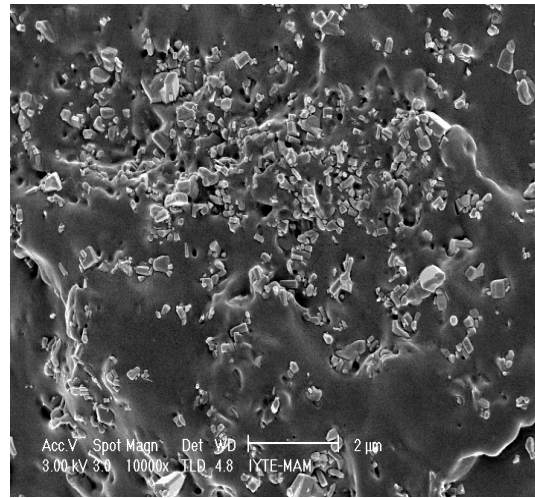


Figure 3. Sweeping voltage versus current values for nZnO.

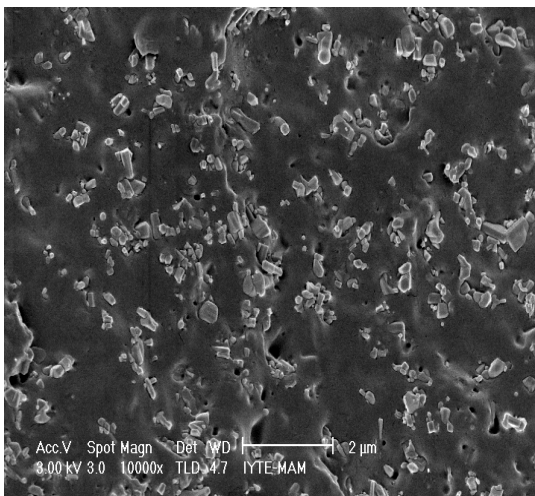
APPENDIX C. SEM MICROGRAPHS AND MAPS OF THE COMPOSITES



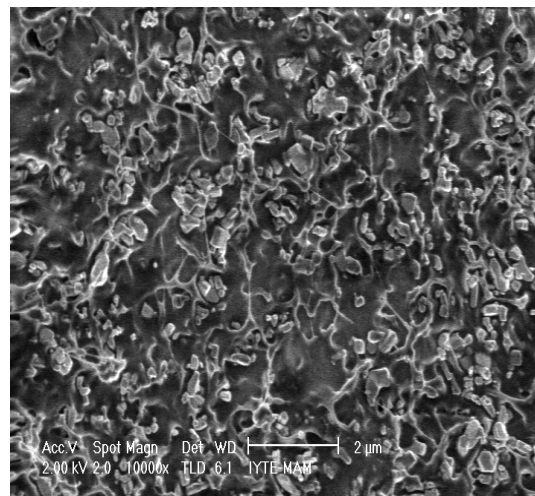
5vol% eZnO-PP



10vol% eZnO-PP

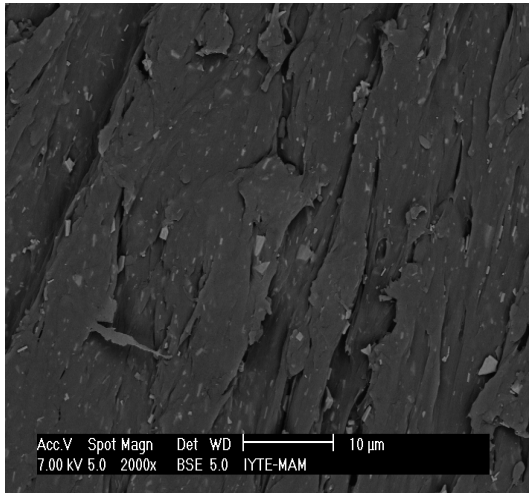


15vol% eZnO-PP

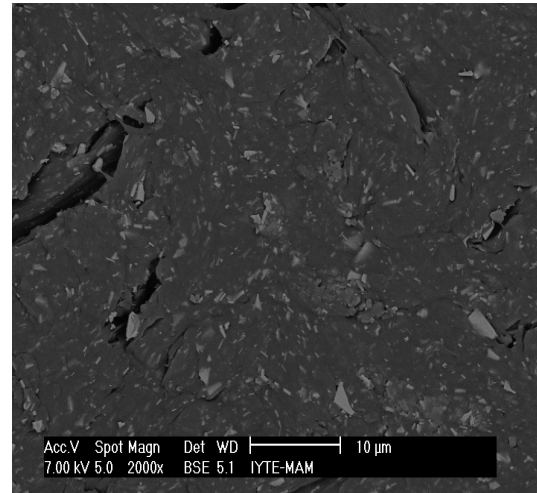


20vol% eZnO-PP

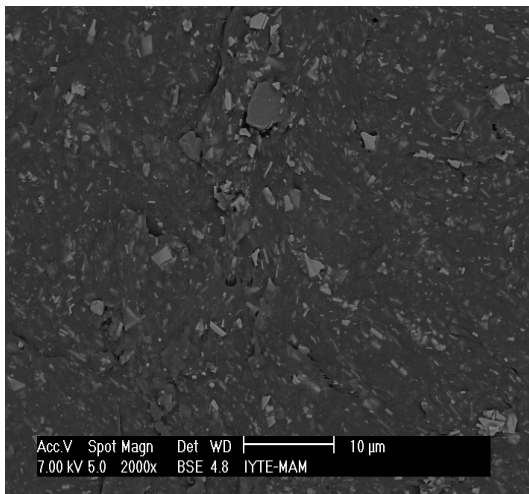
Figure 1. sZnO –PP composite SEM images.



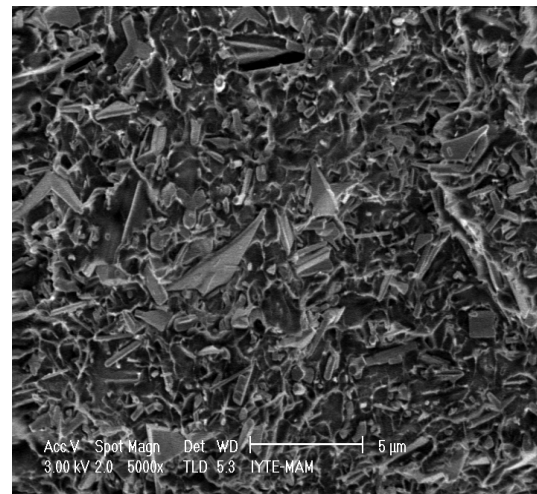
5 vol%eZno-PE



10 vol% eZno-PE

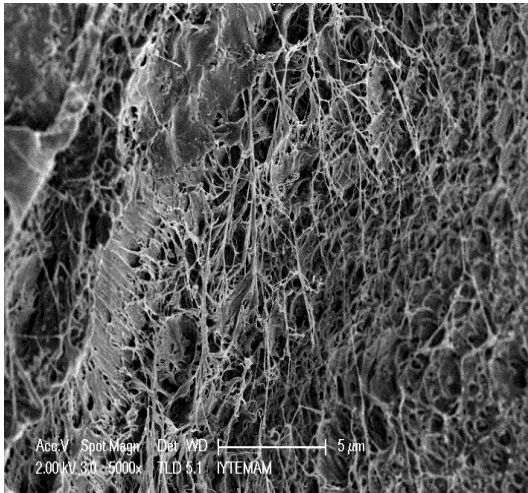


15 vol% eZno-PE

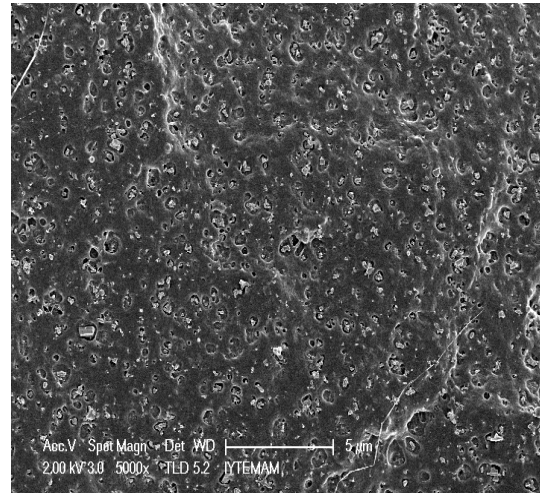


20vol %eZno-PE

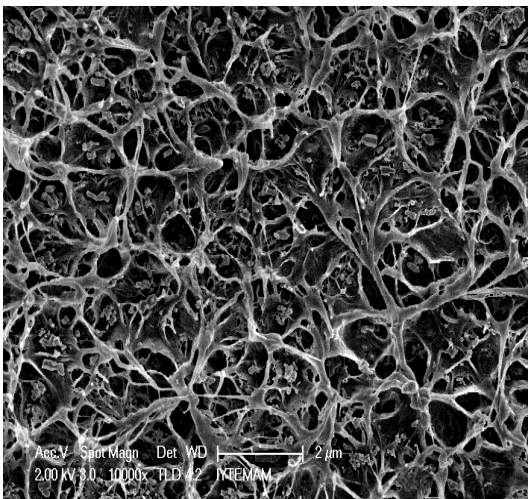
Figure 2. sZnO –PE composite SEM images.



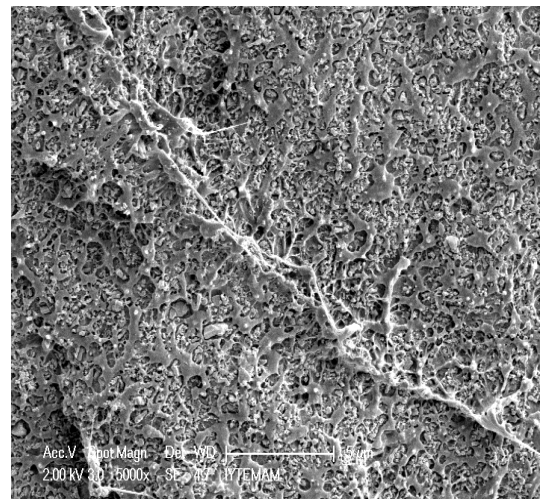
5 vol% nZnO-PE



5 vol% nZnO-PE

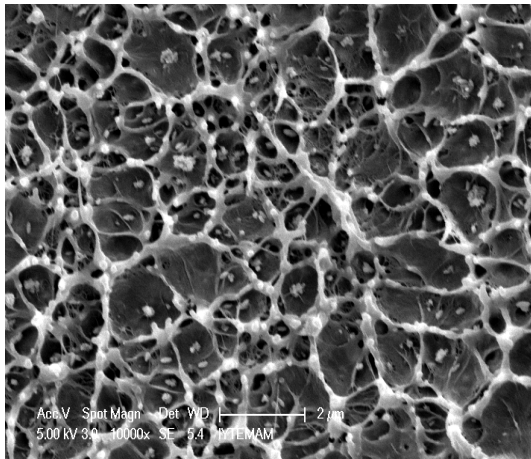


10 vol% nZnO-PE

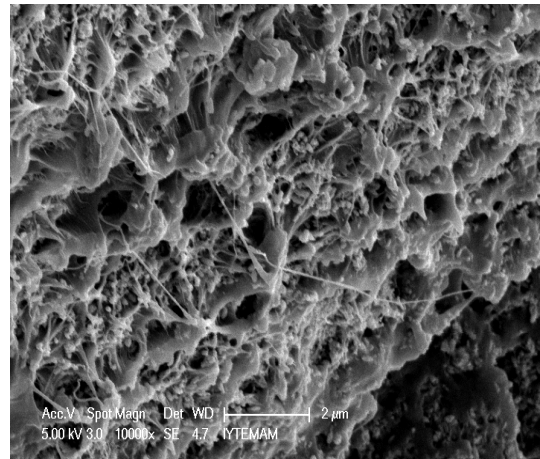


15 vol% nZnO-PE

Figure 3. nZnO –PE composite SEM images.

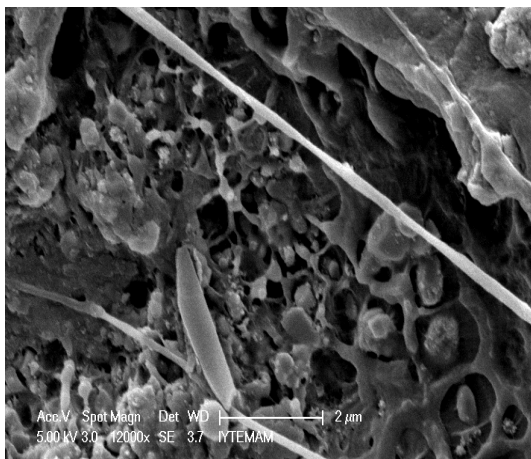


5vol% synZnO-PE

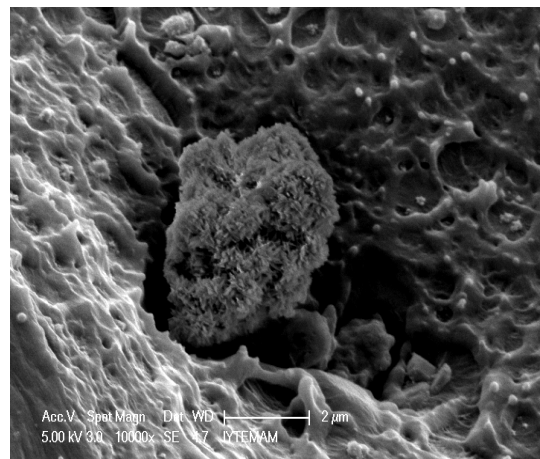


15vol% synZnO-PE

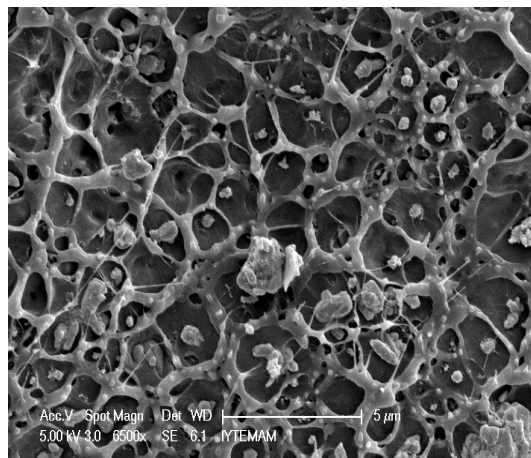
Figure 4. synZnO –PE composite SEM images.



5vol% AlZnO-PE



10vol% AlZnO-PE



15vol% AlZnO-PE

Figure 5. AlZnO –PE composite SEM images.

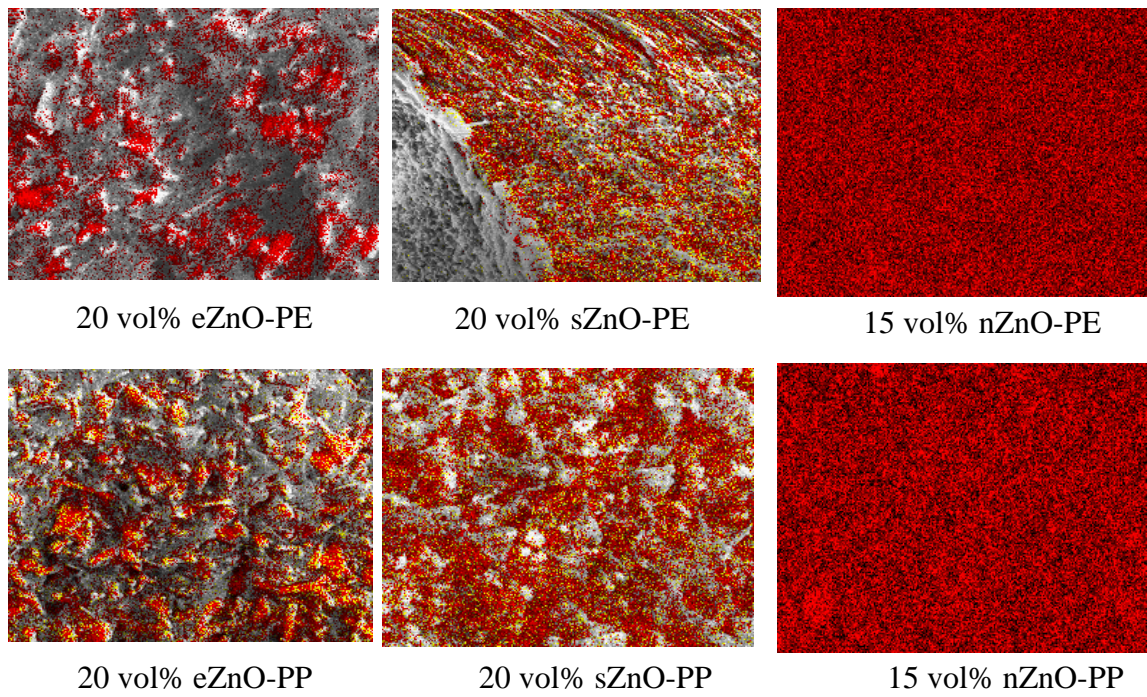


Figure 6. AlZnO –PE composite SEM images.

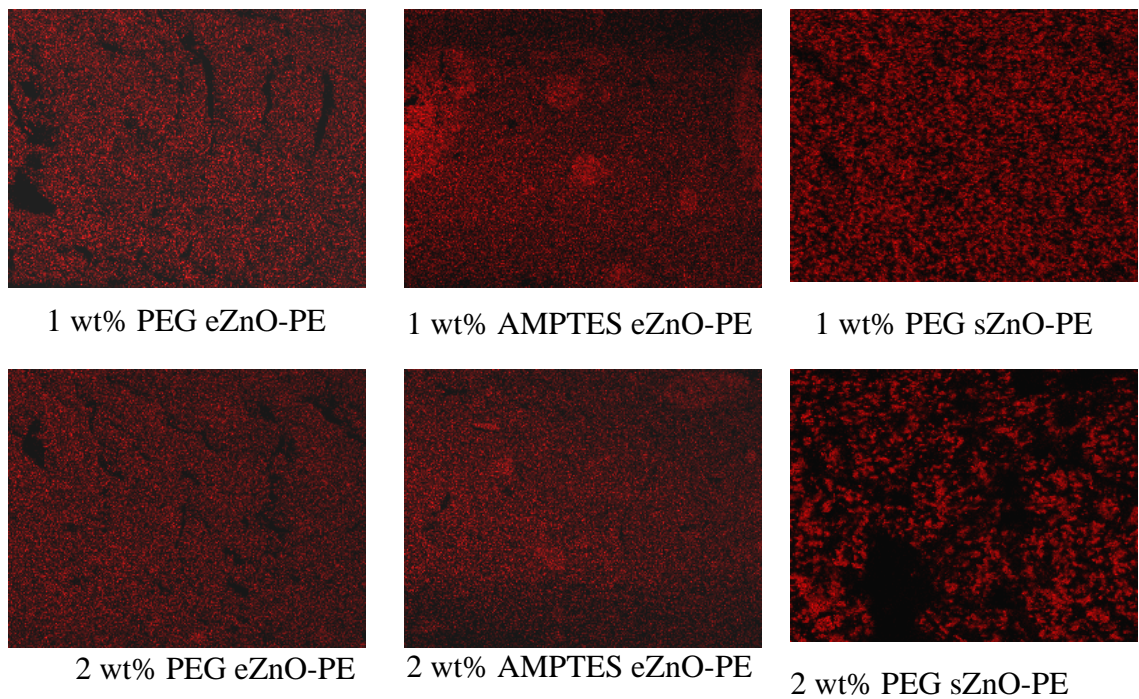


Figure 7. AlZnO –PE composite SEM images.

APPENDIX D. VOLUME RESISTIVITY OF THE COMPOSITES

Table 1. Volume resistivity values of PE composites.

Composites	0 (PE)	5 vol%	10 vol%	15 vol%	20 vol%
eZnO-PE	$1.0 \cdot 10^{17}$	$8.0 \cdot 10^{15}$	$9.4 \cdot 10^{14}$	$2.6 \cdot 10^{13}$	$1.4 \cdot 10^{10}$
sZnO-PE	$1.0 \cdot 10^{17}$	$5.3 \cdot 10^{15}$	$1.6 \cdot 10^{15}$	$3.2 \cdot 10^{14}$	$6.2 \cdot 10^{12}$
nZnO-PE	$1.0 \cdot 10^{17}$	$5.1 \cdot 10^{15}$	$4.4 \cdot 10^{14}$	$2.3 \cdot 10^{12}$	-
synZnO-PE	$1.0 \cdot 10^{17}$	$4.9 \cdot 10^{15}$	$1.9 \cdot 10^{14}$	$2.1 \cdot 10^{13}$	-
AlZnO-PE	$1.0 \cdot 10^{17}$	$1.9 \cdot 10^{16}$	$2.2 \cdot 10^{16}$	$9.6 \cdot 10^{15}$	-

Table 2. Volume Resistivity of PP composites.

Composites	0 (PE)	5 vol%	10 vol%	15 vol%	20 vol%
eZnO-PE	$1.3 \cdot 10^{17}$	$3.7 \cdot 10^{16}$	$7.5 \cdot 10^{15}$	$1.1 \cdot 10^{15}$	$7.63 \cdot 10^9$
sZnO-PE	$5.1 \cdot 10^{17}$	$4.4 \cdot 10^{15}$	$4.5 \cdot 10^{14}$	$1.2 \cdot 10^{14}$	$5.5 \cdot 10^{12}$
nZnO-PE	$1.6 \cdot 10^{17}$	$9.2 \cdot 10^{15}$	$1.2 \cdot 10^{15}$	$3.4 \cdot 10^{12}$	

FİLİZ ÖZMIHÇI ÖMÜRLÜ

Date of Birth : August 08, 1972

Place of Birth : Germany

Citizenship : Turkish

EDUCATION

[1990-1996] B.Sc. (Chemical Engineering)

Ege University

Department of Chemical Engineering, İzmir, Turkey

[1996-1999] M.Sc. (Material Science and Engineering Programme)

İzmir Institute of Technology

Department of Material Science and Engineering, İzmir, Turkey

Dissertation: Natural Zeolite- Polypropylene Composites

Advisor: Prof.Dr.Devrim Balköse

İzmir Institute of Technology

[2002-2009] Ph.D. (Chemical Engineering)

Department of Chemical Engineering, İzmir, Turkey

Dissertation: Enhancement of Thermal, Electrical and Optical Properties of Zinc Oxide Filled Polymer Matrix Nano Composites

Advisor: Prof.Dr. Devrim Balköse

PUBLICATIONS

F. Özmişçi Ömürlü, D. Balköse “Particle Size Effect of Zinc Oxide on the Electrical Conductivity of Polyethylene/ Polypropylene Zinc Oxide Composites” *First International Conference on Multifunctional, Hybrid and Nanomaterials* March (2009), Tours France.

Duvarci, Ö.Ç., Akdeniz, Y., Özmişçi, F., Ülkü, S., Balköse, D., Çiftçioğlu, M. (2007) “Thermal behaviour of a zeolitic tuff” *Ceramic International*, Vol.33 (5) 795-801.

H. Pehlivan, F. Özmişçi, F. Tihminlioğlu, D. Balköse, S. Ülkü “Water and Water Vapor Sorption Studies in Polypropylene- Zeolite Composites” *Journal of Applied Polymer Science*, Vol. 90 (2003): 3069-3075.

F. Özmişçi, D. Balköse, S. Ülkü “Natural Zeolite Polypropylene Composite Preparation and Characterization”, *Journal of Applied Polymer Science*, Vol. 82 (2001): 2913-292.